

DISS. ETH Nr. 30219

Design of modular and responsive hydrogels for drug delivery using supramolecular interactions

A thesis submitted to attain the degree of

DOCTOR OF SCIENCES

(Dr. sc. ETH Zurich)

Presented by

STÉPHANE BERNHARD

M.Sc., EPFL

Born on 23.10.1996

Accepted on the recommendation of

Prof. Dr. Mark W. Tibbitt

Prof. Dr. Owen Fenton

Prof. Dr. Christoph Weder

Dr. Stefan Mommer

2024

*“A little party never killed nobody”
– Fergie*

ACKNOWLEDGEMENTS

I had the chance to perform my PhD thesis at ETH Zürich in the macromolecular engineering laboratory under the supervision of Prof. Mark Tibbitt. At no point in my life did I think I would end up where I am at this precise moment. It is truly when we see the light at the end of the tunnel that we start to wonder how we even got there. In my case, it was all thanks to my friend Charline. When she was looking at job opportunities for herself towards the end of our master's degree, she came across an advertisement for an open PhD position at ETH Zürich. At that time, I was struggling with finishing my master thesis, similarly to how I am wrapping up my PhD thesis. I guess some things never change. She forced me to apply, urging me it was "The" place for me. Thanks to her forcefulness, I applied to the position, and am now finishing one of the best chapters of my life, four and a half years later. Therefore, Charline, I would like to thank you for forcing me to make a decision I have not once regretted.

I would like to thank my advisor, Prof. Mark W. Tibbitt, who has been a mentor and role model to me during these last five years. Mark, I am sorry that you were not the first to be acknowledged, but as you taught me, the story of the paper is what matters. Jokes aside, you are truly one of the best people I have had the chance to meet in this life. When asked about what makes our lab so, you always answer "I don't do anything, you (the members of MEL) make the lab what it is". To correct you, I believe you let us make the lab our own. You show kindness and support, and accept us for who we are, pushing us to be the best version of ourselves, by letting us embrace our inner chaos. I have grown immensely, both on a scientific and a personal level, thanks to your guidance. I am thankful from the bottom of my heart for the unending support you have given me.

Further, I would like to express my gratitude to my co-examiners Prof. Owen Fenton, Prof. Christoph Weder and Dr. Stefan Mommer for travelling to Zurich and taking the time to read the thesis that represents the four and a half last years of my life.

Finishing a PhD would have been possible without the unending support of the members of the MEL lab. Words can't express how I feel towards each member of the lab who laughed with me during the good times and lifted me up during the lows. Thank you, Giovanni, Elia, Oksana, Bruno, Dhanajay, Borte, Lisa and Dalia for welcoming me with arms open and becoming my own little Zurich family. This family has now grown much larger with many new members. Thank you to Lucien, Celine, Lorenza, Florian, Leslie, Tobi, Alex, Yifan, Morris, Stefane, Nika, Gabriela, Jonas, Filippo, Saumithra, Jaimie, Shuo and Ann. I would also like to give a special thanks to Silvia for supporting us for many years.

I would like to thank all my students, without whom, many of the projects I worked on would not have been possible. You not only contributed with great scientific insight but also helped me grow as a person. Thank you, Ines, Wenqing, Marco, Matthias, Max, Camilla, Nika, Nikola, Lauritz, Rea and

Lorena for all the fun we had, in and outside the lab. Further, I want to thank all the other students whom I have crossed paths with during my time at MEL. You brightened my day and life in many ways through your various interests, talents, and cakes.

I would like to thank my friends, without whom I would not be who I am today. You all supported me during the tough times the PhD brought me through and stuck with me when I was at my low points. Thank you to my high school friends Anais and Justine, chemistry friends Charline, Quentin, Remi, Adrian, Pamela, Cecilia, Nancy, Marie, Raph, Riccardo, Francesca, and Camilla, to the DLE Michelle, Sylvain, Anh, Juliette and to the friends I made in Zurich. Thank you to my flatmates who have had to endure me at my best and worst and live with me. A special thanks to Jens for his rizz.

I want to thank my godmother Christine for her constant support and for inspiring me to pursue science. I hope you will forgive me for never parading on the Champs-Élysée.

Finally, I would like to thank my parents for the continuous support you have given me throughout my life. I am not always easy as a person, but you never gave up. Thank you for having been here from the beginning of my life, helping me become who I am and for the future to come.

ABSTRACT

Currently, therapeutics delivery relies heavily on systemic oral or intravenous administration to the patient. To reduce off-site effects and possible premature degradation of the therapeutics, drug delivery platforms are being engineered to enable local, sustained and controlled delivery of therapeutics. Hydrogels have shown their potential as drug delivery platforms because of their biocompatibility, high water content, and ease of therapeutic encapsulation. To allow for simple administration, physical hydrogels leveraging supramolecular interactions as crosslinks are promising. Indeed, the reversible interactions forming the polymer network enable local injection. Of interest, polymer–nanoparticle (PNP) hydrogels are a class of injectable nanocomposite based on reversible interactions between polymer and nanoparticles, which have shown potential drug delivery platforms. Current design of PNP hydrogels is, however, limited to few supramolecular motifs and our understanding of the impact of the crosslinking interactions on the macroscopic properties of the hydrogels is incomplete. In this thesis, we expanded our understanding of how to leverage supramolecular interactions for the rational design of modular nanoparticulate hydrogels by relating molecular interactions, microarchitecture and mechanical properties. We first leveraged a simple supramolecular motif based on α -cyclodextrin (α CD) for the reinforcement of PNP hydrogels. The simple addition of α CD resulted in a concentration dependent increase in mechanical properties through increased polypseudorotaxane formation. Furthermore, the supramolecular motif resulted in increased nanoparticle–nanoparticle interactions, enabling the decoupling of the mechanical properties from the building blocks, allowing the use of interchangeable building blocks from a wide range of biopolymer and nanoparticles. Nonetheless, the origin of the emerging mechanical properties of PNP hydrogel remained poorly described. Building upon this strategy, we engineered a PNP hydrogel using host–guest crosslinks for the investigation of the impact of the supramolecular interactions that form the network on the macroscopic properties of the system. By combining molecular analysis with rheological characterization, we shed light on several underlying mechanisms governing the emergence of the macroscopic properties of PNP hydrogel. Namely, we elucidated the dominant contribution of nanoparticles in network formation, while the polymer mostly provided the required viscosity for gelation. In addition, we leveraged fluorescent and super resolution optical microscopy for the visualization of PNP hydrogel microstructure. We were able to resolve the nanoparticle distribution and investigated the impact of α CD addition on the microarchitecture of the hydrogel. Lastly, we incorporated responsive interactions in the design of a nanogel drug delivery system for the selective delivery of therapeutics upon internalization of the nanocarrier. Through rational chemical design, coupling to protein could be achieved in mild aqueous condition while enabling the chemical-free release of the therapeutic upon exposure to a biological stimulus. Overall, we investigated and leveraged supramolecular and responsive interactions for the design of nanoparticulate-hydrogels targeted to drug delivery application. This work advances the field of supramolecular hydrogel design by creative utilization and extended understanding of the impact of supramolecular interaction on the micro and macro scale properties.

RÉSUMÉ

Actuellement, la prise de médicaments repose en grande partie sur une administration systémique par voie orale ou intraveineuse. Afin de réduire les effets non ciblés et une éventuelle dégradation prématurée des produits thérapeutiques, des biomatériaux sont développés pour permettre une administration locale, soutenue et contrôlée des thérapeutiques. Les hydrogels ont montré leur potentiel pour le relargage de médicaments grâce à leur biocompatibilité, leur teneur élevée en eau et leur facilité à encapsuler les principes actifs. Les hydrogels supramoléculaires exploitant des interactions non covalentes comme point de réticulations, permettent une injection locale et ciblée. Les hydrogels polymère-nanoparticule (PNP) sont une classe de nanocomposites injectables basés sur des interactions réversibles entre polymère et nanoparticules. Ils ont été utilisés pour la conception de plates-formes d'administration de médicaments, de matériaux imprimables en 3D ou pour des applications en ingénierie tissulaire. Cependant, le design des hydrogels PNP reste limité par un nombre restreint de motifs supramoléculaires et par une compréhension limitée de l'impact des structures moléculaires sur les propriétés macroscopiques des hydrogels. Dans cette thèse, nous avons exploité des interactions supramoléculaires pour la conception rationnelle d'hydrogels nanoparticulaires en étudiant les liens entre les interactions moléculaires, la microarchitecture et les propriétés mécaniques. Premièrement, nous avons exploité un motif supramoléculaire basé sur l' α -cyclodextrine (α CD) pour le renforcement des hydrogels PNP. L'addition d' α CD entraîne une augmentation des propriétés mécaniques dépendante de la concentration, via la formation de polypseudorotaxanes. De plus, le motif supramoléculaire renforce les interactions nanoparticules-nanoparticules, permettant le découplage des propriétés mécaniques du choix des éléments constitutifs du système (biopolymères et nanoparticules). Dans le but d'élucider l'origine des propriétés des hydrogels PNP, nous avons conçu un réseau mobilisant des complexes dit « host-guest » comme points de réticulation. En combinant une analyse moléculaire avec une caractérisation rhéologique des hydrogels, nous avons interprété certains des phénomènes gouvernant les propriétés macroscopiques des hydrogels PNP. Nous avons attribué la gélification des réseaux polymériques principalement aux nanoparticules, tandis que le polymère augmente la viscosité de la solution nécessaire à la formation d'un gel. Par ailleurs, nous avons exploité des techniques de microscopie optique (fluorescence et super résolution) pour visualiser la microstructure des hydrogels PNP. Nous avons observé la distribution des nanoparticules dans l'hydrogel et étudié l'impact de l'ajout d' α CD sur la microarchitecture des hydrogels. Enfin, nous avons exploité des liaisons dégradables exclusivement en milieu intracellulaire pour concevoir des nanogels permettant la libération sélective et sans altération de médicaments. En conclusion, nous avons étudié et exploité des interactions supramoléculaires et dégradables pour concevoir des hydrogels nanoparticulaires pouvant servir de plateformes de relargage de médicaments. Cette thèse fait progresser le design des hydrogels supramoléculaires grâce à une utilisation créative et une compréhension approfondie de l'impact des interactions supramoléculaires sur les propriétés des hydrogels aux échelles micro- et macroscopiques.

TABLE OF CONTENTS

ACKNOWLEDGEMENTS	IV
ABSTRACT	VI
RÉSUMÉ.....	VII
TABLE OF CONTENTS	VIII
ABBREVIATIONS.....	XI
INTRODUCTION.....	1
MOTIVATION	1
THESIS OVERVIEW	2
CHAPTER 1.....	4
1.1. INTRODUCTION.....	5
1.2. SUPRAMOLECULAR DESIGN OF HYDROGELS FOR DRUG DELIVERY	7
1.2.1. Supramolecular design to tailor hydrogel mechanical properties	8
1.2.2. Supramolecular binding motifs for hydrogel formation	9
1.2.2.1. Thermogelling and hydrophobic interactions.....	10
1.2.2.2. Hydrogen bonding.....	11
1.2.2.3. Metal–ligand interactions.....	12
1.2.2.4. Host–guest complexes.....	14
1.2.2.5. Nanocomposite hydrogels	17
1.2.2.6. Peptide-based hydrogels and hydrogelators.....	20
1.2.3. Tailoring drug affinity through supramolecular design.....	22
1.2.3.1. Supramolecular binding sites to tailor drug–matrix affinity.....	22
1.2.3.2. Supramolecular integration of drug carriers.....	23
1.2.3.3. Drug as building block	26
1.3. OUTLOOK.....	27
1.4. CONCLUSION.....	27
1.5. ACKNOWLEDGEMENTS	28
CHAPTER 2.....	29
2.1. INTRODUCTION.....	30
2.2. RESULT AND DISCUSSION.....	31

2.2.1.	Supramolecular reinforcement of PNP hydrogel	31
2.2.2.	Supramolecular Bonding Enables Modular Design of CD–PNP Hydrogels	34
2.2.3.	Supramolecular Bonding Enables Modular Design of CD–PNP Hydrogels	35
2.2.4.	Modular Design Enables Tailored Functionality of CD–PNP Hydrogels	37
2.3.	CONCLUSION	39
2.4.	MATERIALS & METHODS	40
2.4.1.	Materials	40
2.4.2.	Instrumentation and characterization	40
2.4.3.	Synthetic procedures	41
2.5.	ACKNOWLEDGEMENTS	47
CHAPTER 3		48
3.1.	INTRODUCTION	49
3.2.	RESULT AND DISCUSSION	50
3.2.1.	Synthesis and Formation of Host–Guest PNP Hydrogels	50
3.2.2.	Mechanical Characterization	53
3.2.3.	Photoreversible Supramolecular PNP hydrogels	56
3.3.	CONCLUSION	58
3.4.	MATERIALS & METHODS	58
3.4.1.	Materials	58
3.4.2.	Instrumentation and methods	58
	<i>Polymer-nanoparticle (PNP) hydrogel formation</i>	59
3.4.3.	Synthetic procedures	60
3.5.	ACKNOWLEDGEMENT	62
CHAPTER 4		63
4.1.	INTRODUCTION	64
4.1.	RESULT AND DISCUSSION	65
4.1.1.	Resolving PNP hydrogel microstructure	65
4.1.1.	Imaging of the hydrogel at various using α CD content	67
4.2.	CONCLUSION	69
4.3.	MATEIRLAS & METHODS	69

X | TABLE OF CONTENTS

4.3.1. Materials	69
4.3.2. Instrumentation and methods	70
<i>PNP hydrogel formation</i>	70
4.3.3. Synthetic procedures	71
4.4. ACKNOWLEDGEMENTS	72
CHAPTER 5	73
5.1. INTRODUCTION	74
RESULT AND DISCUSSION	75
5.1.1. Building block synthesis	75
5.1.2. Self-immolative cleavage	77
5.1.3. Protein coupling	79
5.1.4. Coupling to nanogel and uptake efficiency	80
5.2. CONCLUSION	81
5.3. MATERIALS & METHODS	81
5.3.1. Materials	81
5.3.2. Instrumentation and characterization	82
5.3.3. Synthetic procedures	83
5.3.4. Experimental procedures	86
5.4. ACKNOWLEDGEMENTS	87
CONCLUSION AND OUTLOOK	88
RESULTS OVERVIEW	88
OUTLOOK	89
APPENDIX	91
APPENDIX FOR CHAPTER 2	91
APPENDIX FOR CHAPTER 3	105
APPENDIX FOR CHAPTER 4	112
APPENDIX FOR CHAPTER 5	114
BIBLIOGRAPHY	122
CURRICULUM VITAE	154

ABBREVIATIONS

ACN	Acetonitrile
Ada	Adamantane
AFM	Atomic force microscopy
Alg	Alginate
ATR-FTIR	Attenuated total reflection Fourier-transform infrared spectroscopy
AzB	Azobenzene
BMP7	Bone morphogenetic protein 7
BOP	Benzotriazol-1-yl-oxy- tris- (dimethylamine)-phosphonium-hexafluorophosphate
BSA	Bovine serum albumin
CaCl ₂	Calcium chloride
CB	Cucurbituril
CD	Cyclodextrin
CDCl ₃	Chloroform-d
CDI	1,1'-carbonyldiimidazole
Col	Collagen
CPT	Camptothecin
CuSO ₄	Copper sulfate
D ₂ O	Deuteriumoxide
DCM	Dichloromethane
DF _{eff}	Effective degree of functionalization
DIPEA	N,N-diisopropylethylamine
DLS	Dynamic light scattering
DMEM	Dulbecco's Modified Eagle Medium
DMSO	Dimethylsulfide
DOF	Degree-of-freedom
DOPA	L-3,4-dihydroxyphenylalanine
DOX	Doxorubicin
dSTORM	Direct stochastic optical reconstruction microscopy
EDTA	Ethylenediaminetetraacetic acid
Et ₂ O	Diethyl ether
EtOAc	Ethyl acetate
EtOH	Ethanol
FBS	Fetal bovine serum
FITC-BSA	Albumin-fluorescein isothiocyanate conjugate

XII | ABBREVIATIONS

GRAS	Generally regarded as safe
GSH	Glutathione
H ₂ O	Water
HA	Hyaluronic acid
HA-TBA	Tetrabutylammonium salts of HA
HATU	Hexafluorophosphate azabenzotriazole tetramethyl uronium
Hepes	4-(2-hydroxyethyl)-1-piperazine-ethanesulfonic acid
hMSCs	Primary human mesenchymal stem cells
HPMC	Hydroxypropylmethylcellulose
HRMS	High-resolution mass spectrometry
ITC	Isothermal titration calorimetry
K _D	Equilibrium dissociation constant
Lactide	3,6-dimethyl-1,4-dioxan-2,5-dion
LAP	Lithium phenyl-2,4,6-trimethylbenzoylphosphinate
LED	Light-emitting diode
LVR	Linear-viscoelastic region
MEA	β-mercaptoEthylamine hydrochloride
MeHA	Methacrylated hyaluronic acid
MeOH	Methanol
M _n	Number average molecular weight
M _w	Molecular weight
M _w	Weight average molecular weight
MWCO	Molecular weight cut off
N	Molar ratio
Na ₂ HPO ₄	Sodium phosphate dibasic
Na ₂ SO ₄	Sodium sulfate
NaH ₂ PO ₄	Sodium phosphate monobasic
NaOH	Sodium hydroxide
NH ₄ Cl	Ammonium chloride
NHS	N-Hydroxysuccinimide
NIR	Near-infrared light
NMR	Nuclear magnetic resonance
OR	Oil Red O
OxT	1, 3-oxathiolan-2-one
PBS	Phosphate buffered saline
PDI	Polymer dispersity
PE	Petroleum ether

PEG	Poly(ethylene glycol)
PEI	Poly (ethylene imine)
PLA	Poly(lactic acid)
PNIPAm	Poly(N-isopropylacrylamine)
PNP	Polymer–nanoparticle
PPO	Poly(propylene oxide)
PTFE	Poly (tetrafluoro ethylene)
PyBOP	Benzotriazole-1-yl-oxy-tris-pyrrolidino-phosphonium hexafluorophosphate
RhB	Rhodamine B
RhB-linker	Rhodamine B amine coupled to linker
RhB-NH ₂	Ethylenediamine modified rhodamine B
SEC	Size exclusion chromatography
SEM	Scanning electron microscopy
SnOct ₂	Tin(II)-2-ethylhexanoate
SRM	Super-resolution microscopy
TBAOH	Tetrabutylammonium hydroxide solution
TEM	Transmission electron microscopy
THF	Tetrahydrofuran
TIRF	Total internal reflection fluorescence
UPy	Ureidopyrimidinone
UV	Ultraviolet light
vis	Visible
βCD-HA	βCD modified HA
βCD-HDA	6-(6-aminohexyl)amino-6-deoxy-β-cyclodextrin
βCD-Tos	6-o-monotosyl-6-deoxy-β-cyclodextrin
ΔH	Binding enthalpy

INTRODUCTION

MOTIVATION

A major focus in the field of medicine is the development of new therapeutics to address current challenges in healthcare. As a result, many therapeutics are undergoing clinical trials and progressing toward approval and clinical use.¹ On the other hand, there has been less advances in the administration of commercial therapeutics, where the primary modes of administration remain bolus and systemic application via oral or intravenous administration.^{2,3} As a result, therapeutic efficiency is often impeded by off-target effects and/or early degradation of the therapeutics.³ As such, repeated administration of therapeutics at high dosage can be required to enable sufficient delivery at the site of interest over extended periods of time.⁴ To tackle the current limitation of therapeutic delivery, biomaterials research has focused on the development of delivery platform enabling continuous release and efficient delivery at the site of interest.⁵

Hydrogels are water swollen polymer networks that have been widely used as drug delivery platform due to their high biocompatibility, resemblance to the extracellular matrix, and ease of therapeutic encapsulation.⁶ Indeed, therapeutics can be encapsulated in the hydrogel matrix, enabling controlled and continuous release of the therapeutics in the hydrogel surroundings.⁷ Tuning the polymer network of the hydrogel further enables control over the release of the therapeutics through changes in the release timing and kinetics (e.g., diffusion, degradation).⁸ The use of covalently cross-linked hydrogels however, substantially restrict their administration by requiring surgical implantation of the material to enable local release at the site of interest.

Physical hydrogels based on non-covalent or supramolecular interactions have enabled the design of injectable hydrogels capable of local and minimally invasive administration.⁹ Their injectability relies on the reversible interactions that form the hydrogel network. Upon the application of an external stress the interaction can break—allowing for shear-thinning—and upon release reform—enabling self-healing or elastic recovery.¹⁰ A wide range of supramolecular interaction, such as hydrogen bonding, hydrophobic interactions, host–guest complexation, and electrostatic interactions, have been investigated for the design of injectable hydrogels.^{11–14} Proper tailoring and understanding of the supramolecular interactions enable rational design of hydrogels tailored for select applications.

Polymer–nanoparticle (PNP) hydrogels are a class of nanocomposite hydrogels that are useful as dual drug delivery systems, 3D bioinks, vaccine delivery platforms, and immune cell recruitment platforms.^{15–18} The formation of PNP networks relies on reversible interactions between polymers and nanoparticles. Their current design is however limited to a few, select supramolecular interactions, restricting the pool of building blocks to choose from and the range of accessible mechanical properties available.^{18–20} Further, the current understanding as to how the underlying interactions correlate to the

material microstructure and emergent macroscopic properties remains poor. Expanding our understanding of how to leverage supramolecular interactions for PNP hydrogel design would advance the rational design of the hydrogels for biomedical applications. Further, this work provides a more general insight on supramolecular interactions for hydrogel design through creative utilization and extended understanding of their impact on the micro and macro scale properties.

THESIS OVERVIEW

The goal of this thesis is to investigate how supramolecular and responsive interactions can be leveraged for the design of modular and responsive nanoparticle-based hydrogels targeting drug delivery applications. On the one hand, the thesis focuses mainly on supramolecular interactions as structural components in the hydrogel network formation and, on the other hand, on leveraging responsive interactions to enable triggered release of therapeutics.

Chapter 1 reviews existing strategies for leveraging supramolecular interactions in the design of hydrogels for drug delivery. We first focus on the incorporation of supramolecular interactions as structural components in the hydrogel design to form responsive, self-assembling, and injectable hydrogels. In a second part, we focus our interest on the use of supramolecular interactions for tailoring the drug–matrix affinity to improve control over the drug loading, kinetics, and targeting. This highlights some of the primary chemical strategies and potential of how supramolecular interactions can be used improve current strategies in both material design and drug delivery.

In **Chapter 2**, we describe the supramolecular reinforcement of PNP hydrogels using α -cyclodextrin (α CD) as a supramolecular additive. PNP hydrogels are a promising class of injectable nanocomposite biomaterials relying on reversible interactions between polymers and nanoparticles. Their design is, however, currently limited in the range of attainable mechanical properties and a small pool of building blocks. To tackle those limitations, we leverage α CD as a supramolecular additive for the reinforcement of PNP hydrogel through the formation of polypseudorotaxanes. The addition of the supramolecular host enables concentration-dependent reinforcement of the mechanical properties of the material, while retaining its injectable character. Further, the introduction of the additional supramolecular motif decouples the mechanical properties from the building blocks used. Indeed, the mechanical properties of the material showed non-significant changes with exchange of the polymer or nanoparticle, allowing the use of a range of biopolymers and PEGylated nanoparticles for the design of bioinks, conductive materials, and magnetically responsive hydrogels.

In **Chapter 3**, we aim to elucidate aspects of the underlying mechanisms governing the emergence of the macroscopic mechanical properties of PNP hydrogels. For this purpose, we synthesize a PNP hydrogel using host–guest complexes based on β CD as crosslinking interaction. We analyze the building blocks of the system using isothermal titration calorimetry, showing an increase in binding strength upon functionalization of polymer chains while decreasing the effective number of host or guest molecules available for binding. Using the determined host and guest availability, we relate the viscoelastic

properties, the building block concentration, and the stoichiometry of the host–guest interactions. Overall, this chapter leverages chemical design and characterization of the building block of PNP hydrogel to uncover fundamental relationships between molecular interactions and macroscopic properties in PNP hydrogels.

In **Chapter 4**, we leverage super resolution optical microscopy techniques to resolve the microstructure of PNP hydrogels. Through the integration of fluorescent labels in the nanoparticle formation, the nanoparticle distribution in the sample is resolved, enabling the visualization of a porous network-like distribution of the nanoparticles. Further, the changes in mechanical properties observed upon addition of α CD could be associated to formation of nanoparticle cluster in the network, likely related to increasing jamming and therefore increased mechanical properties. This chapter provides a solution to resolve the microstructure of hydrogels and advance the understanding of structure–property relationships in PNP hydrogels.

Chapter 5 focuses on the design of a redox-responsive nanogel system for the intracellular delivery of therapeutic. For this purpose, we fabricate a nanogel system with covalent attachment of the cargo to the nanogel using a responsive linker with triggered degradation upon internalization by cells. We first design a linker based on self-immolative disulfide bonds that can be reduced in the presence of GSH. The self-immolative character of the linker allows modification-free release of the therapeutic. Further, rational design of the linker enables coupling to proteins in mild phosphate buffer condition. After coupling to the nanogel, the linker provides responsive release of a model protein when exposed to glutathione (GSH) concentrations similar to those in cytosol of liver cells. Overall, in this work we engineer a simple nanocarrier system showing promise as nanocarriers for intracellular drug delivery.

We then conclude the thesis by providing an outlook on the future of PNP hydrogels and future directions of the ongoing projects. In particular, we will further develop the visualization of the hydrogel microstructure and investigate the impact of nanoparticle interactions on the hydrogel mechanical properties. Overall, this Thesis investigates the use of supramolecular and responsive interactions for the design of injectable hydrogels for drug delivery.

CHAPTER 1

SUPRAMOLECULAR ENGINEERING OF HYDROGELS FOR DRUG DELIVERY

SUMMARY *Supramolecular binding motifs are increasingly employed in biomaterials design. The ability to rationally design specific yet reversible associations into polymer networks with supramolecular chemistry enables injectable or sprayable hydrogels that can be applied via minimally invasive administration. Further tailoring select supramolecular binding motifs in the hydrogel matrix enables tuning of the rheological behavior of the materials, such as shear-thinning and self-healing behavior, suitable for application via narrow diameter syringes or catheters. Additionally, the incorporation of therapeutics in the hydrogel and release from the materials can be improved via supramolecular design of drug–matrix affinity.*

This chapter is reproduced with minor changes from: S. Bernhard and M. W. Tibbitt *Adv. Drug Delivery Rev.* **2021**, 171, 240-256 DOI: 10.1016/j.addr.2021.02.002. **AUTHOR CONTRIBUTIONS:** SB and MWT conceived the idea and wrote the manuscript.

1.1. INTRODUCTION

Medical care has advanced with the discovery and development of new therapeutic modalities.²¹ However, a developed therapeutic is not inherently effective—drug efficacy depends on proper administration and use.⁵ Many conventional therapeutics are administered orally or intravenously, which can introduce limits to their efficacy as the molecules have to pass multiple biological barriers and resist degradation in a variety of chemical environments.³ In addition, the high dosage or repeat administration required to achieve therapeutic benefit can result in off-target effects or toxicity.²² Finally, poor adherence to traditional orally-administered therapeutics can also lead to insufficient clinical outcomes.²³ Therefore, efforts have focused on developing strategies to localize therapeutics to the target site and to control their release (or local concentration) over time, with the aim of increasing efficacy while limiting off-target effects.^{24,25}

In recent years, a major focus of targeted therapeutics has been on the development of multifunctional nanotechnologies—including polymeric or lipid nanoparticles, dendrimers, magnetic nanoparticles, and polymersomes / liposomes—that are able to accumulate at or target specific regions of the human body and release therapeutics in a controlled manner.^{24–26} For example, BIND-014, a docetaxel containing polymeric nanoparticle developed to target and treat prostate tumors, recently completed a Phase II clinical trial.²⁷ Despite these advances, precise local administration of therapeutics remains a challenge as most technologies rely on systemic administration and encounter problems, including aggregation in the blood stream, low rates of target accumulation, or unwanted accumulation of the nanocarrier in the liver (mononuclear phagocyte system).^{28–31} One opportunity to extend the scope of local therapy is through the design of injectable or sprayable materials that can be applied directly at the site of interest to form a depot that controls molecule release locally.^{32–34} Within this framework, moldable hydrogels, formed via reversible interactions between associating building blocks, have been explored as platforms for drug delivery, offering minimally invasive administration and compatibility with the local tissue.³⁵

Hydrogels are hydrophilic polymer networks that are swollen with a large volume fraction of water or biological fluid.⁷ Engineered hydrogels have been of specific interest in the biomedical field since their introduction by Wichterle and Lim, as the physical and biochemical properties of hydrogels can be tailored to mimic those of native biological tissues.^{36–39} Throughout the years, macromolecular design and engineering of hydrogels has evolved to enable versatile and tunable properties as well as stimuli-responsive behavior.⁶ Hydrogels are now broadly applied in the biomedical sciences for cell recruitment, wound healing, tissue engineering, and drug delivery.⁴⁰

Traditionally, hydrogels are formed via the formation of covalent bonds between constituent polymer chains or monomers forming permanently cross-linked polymer networks.⁴¹ On account of the fixed network topology, these networks are difficult to process and often cannot be applied after formation without surgical intervention or the use of large diameter needles. In some cases, permanently cross-linked hydrogels have been formulated for less invasive application by generating micron-scale gel

particles or as injectable cryogels.^{42,43} As an alternative, in situ forming hydrogels and moldable hydrogels have been explored as the rheology of these materials enables injection through narrow diameter needles or catheters for minimally invasive administration at the site of interest.⁴⁴ In these cases, the injectable material exists as a depot following application, which can control the release of one or more encapsulated therapeutics.^{45,46} Injectable drug delivery systems have been applied for regeneration of bone, cartilage, and cardiac tissues by delivering therapeutics and/or cells directly to the damaged tissues.^{47,48}

One of the key enabling tools that has accelerated the development of injectable hydrogels for drug delivery applications is the introduction of supramolecular chemistry in hydrogel design. Supramolecular chemistry provides a range of specific yet non-permanent interactions that enable the design of complex materials with tunable and reversible mechanical properties.^{49–51} Indeed, supramolecular chemistry has facilitated the design of advanced biomaterials for a range of biomedical applications.⁵² The creation of supramolecular hydrogels—exploiting transient cross-links for assembly—enable the engineering of self-assembling, moldable, and self-healing materials with stimuli-responsive behavior.

In this review, we discuss how supramolecular chemistry can be harnessed for the design of advanced hydrogels in the field of drug delivery. We maintain a focus on available chemistries and assembly motifs enabled by supramolecular interactions (**Figure 1.1**). The review is not intended as a comprehensive overview of all applications of supramolecular chemistry in drug delivery. Here, we focus on two main areas of active research: *i.* the use of supramolecular binding motifs to engineer the rheology of hydrogels as injectable materials for local drug delivery and *ii.* the use of supramolecular binding motifs to tailor the release of drugs from hydrogels by tuning the affinity between drug and material. For those interested, we refer the reader to comprehensive reviews on the use of supramolecular chemistry in the general design of (bio)materials or nano- and micro-scale drug carriers.^{52,53}

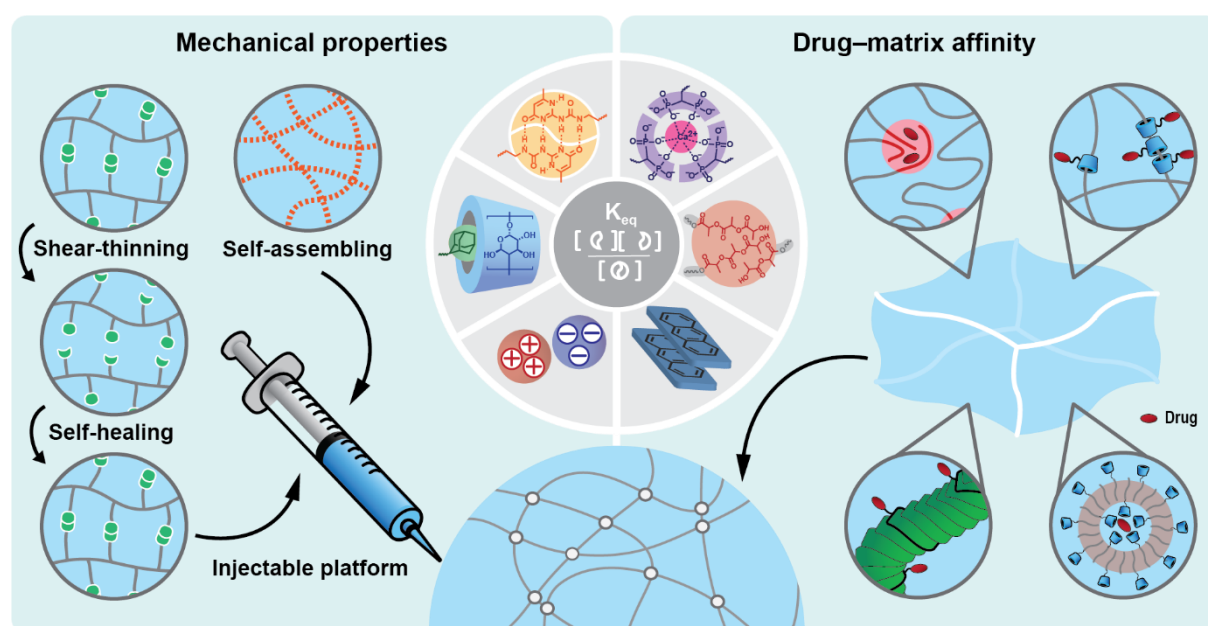


Figure 1.1: Supramolecular binding motifs enable the design of hydrogels for drug delivery applications by enabling control over the mechanical properties and flow behavior as well as methods to tailor the affinity between drug and matrix.

1.2. SUPRAMOLECULAR DESIGN OF HYDROGELS FOR DRUG DELIVERY

The effective design of hydrogels for drug delivery applications must consider several constraints.⁵⁴ First, as the intended use is in the body, the material itself should be composed of building blocks that are compatible with the biological application of interest (commonly referred to as biocompatibility).⁵⁵ That is, they should not elicit a foreign body reaction or non-specific immune activation. A broad range of suitable synthetic and natural polymers are available; however, they must be assembled with safe and non-toxic linking chemistries. Second, the material assembly should proceed in aqueous media and at physiologic pH. Third, the hydrogel should control the release of encapsulated therapeutics through physical constraints to molecular diffusion or via drug–material affinity.

Supramolecular chemistry and design can be applied to address these design constraints. Many of the available supramolecular binding motifs are non-toxic and require minimal chemical modification; several common binding motifs are inspired by natural interactions found in biological systems. As such, the use of these chemistries can provide biocompatible alternatives to cross-linking strategies based on the use of radicals or toxic small molecules. Further, several supramolecular binding motifs proceed in physiologic media making them suitable for biological application. Finally, controlled release can be achieved by tailoring the density, strength, and binding constants of the supramolecular motif or can be used to tune drug–material affinity.

An additional consideration for the design of supramolecular drug delivery vehicles is the potential presence of competitive binders, including proteins or ions, in the physiological environment. Competing interactions can affect the mechanical properties of the supramolecular hydrogel and/or alter the release profile of loaded therapeutics.^{56,57} Selecting interactions with high specificity in the design of supramolecular drug carriers can reduce the chances of having unwanted competitive interactions or materials can be tailored to account for known competitive binders present in a certain biological milieu.

Based on their beneficial features, supramolecular binding motifs have been increasingly explored in the design of biomaterials. Here, we discuss two specific areas where supramolecular chemistry has been leveraged to advance the field of drug delivery through the design of hydrogels. The first focuses on how supramolecular binding motifs can be used to assemble building blocks to engineer the mechanical properties and flow behavior of injectable hydrogels. The mechanics of the formed gels also have a direct influence on the release of encapsulated therapeutics. The second focuses on how supramolecular binding motifs can be used to tune the affinity between drug and material as a secondary method to control the release of therapeutics from supramolecular hydrogels. Throughout, we maintain a focus on the supramolecular binding motifs themselves and highlight how they have been applied in the field of drug delivery when relevant.

1.2.1. Supramolecular design to tailor hydrogel mechanical properties

Supramolecular design is an attractive strategy for designing the mechanical and flow properties of hydrogels as they provide ease of assembly, broad tunability, and stimuli-responsive properties. Importantly, the mechanical and rheological properties of supramolecular hydrogels can be engineered to enable minimally invasive application in the body through narrow diameter needles, which is relevant for many drug delivery applications. In contrast, pre-formed, covalent hydrogels cannot be administered in this manner and often require surgical intervention, and the associated risks, for application.³⁵

The rheology provided by small molecule building blocks or polymer chains that associate through reversible interactions has enabled the design of injectable, sprayable, or in situ gelling materials.⁵⁸ Uniquely, this class of materials facilitates application without significant medical intervention and these moldable materials also have the capacity to adapt to the environment by forming a conformal interface with the available space at the injection site.⁵⁹ These attractive features of moldable hydrogels are directly related to their rheology. In the case of in situ gelling systems, a low viscosity formulation can be prepared that assembles upon application. In the case of injectable or sprayable materials, large changes in viscosity upon application of shear (shear-thinning behavior) allow the materials to be prepared as a solid-like gel that can flow in a liquid-like state upon applied stress.¹⁰ Importantly, these materials reform into a depot that can control the release of encapsulated therapeutics upon cessation of shear. The first condition for an injectable material is its capacity to flow upon applied strain (liquid or shear-thinning material). The second condition is the formation of a solid depot after application that mitigates rapid dispersion of the drug, as occurs in standard bolus injection. This requires quick re-assembly into a gel (in situ gelation or self-healing behavior). Further, the formed material should be sufficiently stable to control drug release over an extended period of time as compared with a bolus injection without controlled release. This can be correlated to the strength or modulus of the network and the capacity of the network to maintain its integrity, as drug release correlates with both the density of the network and the rates of material degradation and erosion.^{60,61}

Therefore, the design of shear-thinning and self-healing properties remains a major interest in the design of injectable drug delivery systems. These properties can be related to the underlying supramolecular chemistry used to assemble the material. The equilibrium binding constant and bond lifetime associated with the reversible interaction dictate the association and dissociation behavior of the network cross-links and, thus, the mechanical properties of the material at rest and the flow behavior under applied stress.⁶²⁻⁶⁵ As the range of supramolecular interactions varies from effectively permanent to highly reversible, the strength of the interaction can be tuned to be in a range that enables robust network formation with shape retention on experimental timescales while enabling flow during injection. The manner in which the reversible interactions are incorporated into the gel structure can also affect the macroscale properties of the hydrogel. For example, in the case of polymer chains cross-linked with grafted supramolecular motifs, the density of cross-links between the polymer chains influenced the shear-thinning behavior of the material.⁶⁶ Here, an increase in cross-linking functionalities (not polymer

chains) resulted in a higher degree of shear-thinning. Additionally, the resulting mechanical properties can be highly sensitive to external stimuli as supramolecular interactions often depend on their local chemical environment. This enables the design of responsive networks for stimuli-triggered release of drugs, but requires special attention during design as the chemical environment at the injection site has to be taken into account during the design of the injectable gel.⁶⁷

The structure and mechanical properties of the hydrogel network will also have an influence on the release kinetics of drugs loaded in the gel. Therapeutics intended for release are commonly encapsulated within hydrogels, resulting in a drug release profile governed by constrained diffusion of the therapeutics through the hydrogel and the rate of erosion of the hydrogel.⁵⁴ In permanently cross-linked hydrogels, several theories based on hydrodynamics, free volume, and polymer chain obstruction have been applied to relate the effective diffusion rate of an encapsulated compound to the molecular structure of the gel.^{68,69} Recently, Axpe et al. introduced a multiscale diffusion model that unifies the main physical theories to describe solute release in covalent hydrogels.⁷⁰ These theories can be instructive in considering the design of supramolecular hydrogels; however, the release behavior in reversible, supramolecular hydrogels is often more complex. In the case of a network with reversible chemistries, the release profile is also influenced by the binding affinity of the reversible cross-links in the hydrogel.⁷¹ In general, the dynamics of the cross-links results in a time-dependent mesh size; therefore, the release profile will depend on the strength of the interaction.⁷² The relationship between network dynamics and release kinetics has yet to be fully understood and should remain the focus of future work to enable the design of supramolecular drug delivery platforms with more precise control over release kinetics.

As the manner in which the building blocks of a network are assembled affects both the network mechanics and the release profile of encapsulated therapeutics, it is necessary to understand how the supramolecular binding motifs influence the structure and dynamics of the network in supramolecular hydrogels. A robust understanding of structure–function relationships in associating polymer networks is an active area of research in the polymer physics and biomaterials community, and this understanding will further advance the rational design of supramolecular hydrogels. In addition, new chemistries are emerging for the design of supramolecular biomaterials that will offer new opportunities to engineer this useful class of materials. In **Section 1.2.2**, we introduce some of the common supramolecular binding motifs used to design the supramolecular biomaterials and highlight how they have been applied in the field of drug delivery. Many of the same chemistries have also been used to tune drug–matrix affinity, as discussed in **Section 1.2.3**.

1.2.2. Supramolecular binding motifs for hydrogel formation

A variety of supramolecular binding motifs exist for the formation of supramolecular hydrogels, including hydrophobic forces, electrostatic interactions, metal–ligand binding, pi–pi stacking, and host–guest interactions (**Figure 1.2a**). Additionally, all of these motifs have been employed for the development of supramolecular materials for biomedical application. However, not all binding motifs

are relevant for the formation of injectable or sprayable drug delivery platforms. As previously mentioned, the strength of the interaction has to enable the formation of a robust network to enable controlled release while exhibiting shear-thinning properties for injection. In this section, we discuss various chemistries that are useful for forming supramolecular hydrogels with a specific emphasis on their relevance for the design of injectable or sprayable drug delivery platforms.

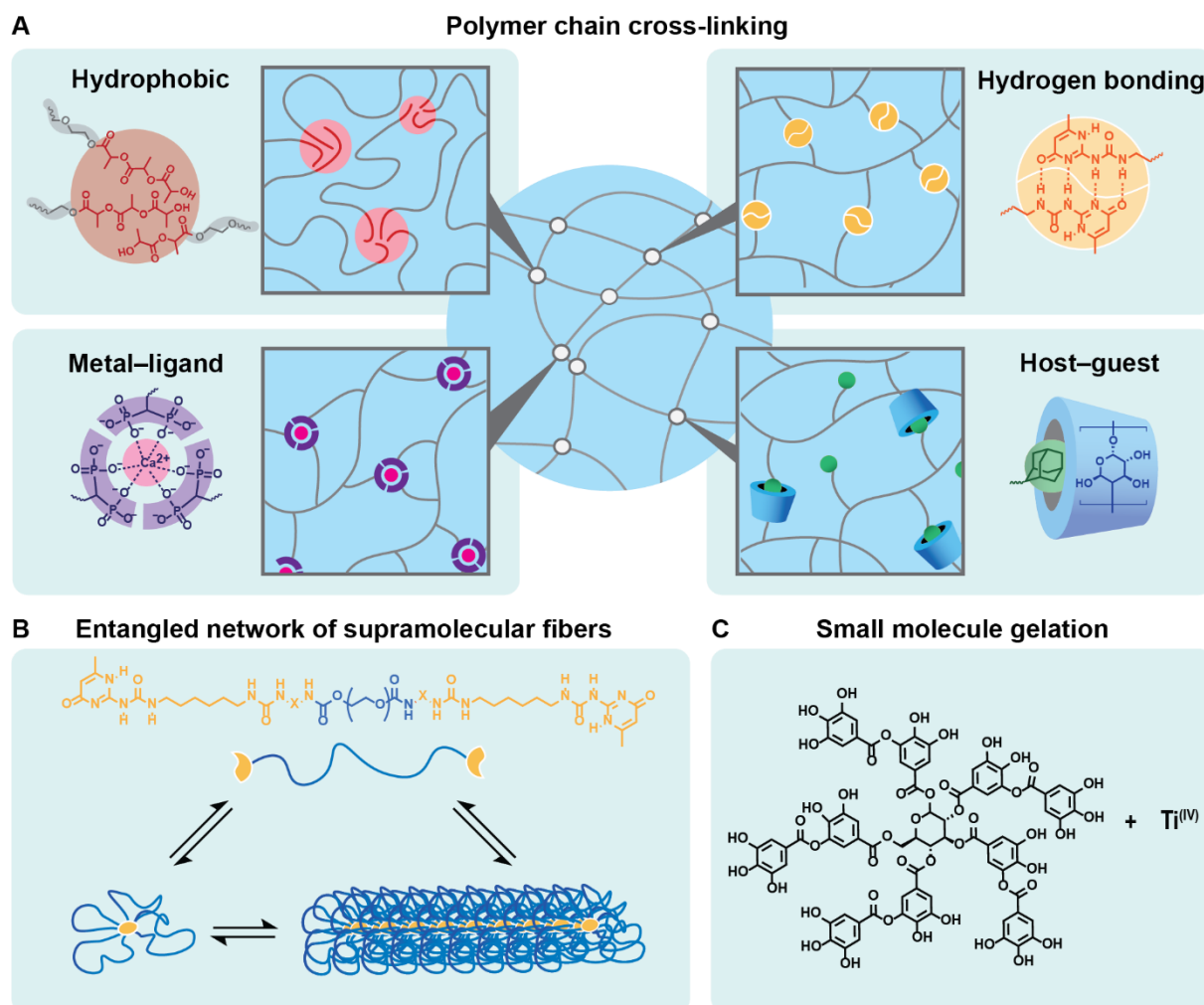


Figure 1.2: Network formation strategies using supramolecular binding motifs. **A.** Polymer chains or other network building blocks can be cross-linked via several classes of supramolecular interaction, including hydrophobic interactions, hydrogen bonding moieties, metal–ligand coordination, and host–guest chemistries. **B.** Hydrogel formation can also proceed via the formation of supramolecular assemblies that can further assemble into networks, such as extended one-dimensional entangled fibers that induce gelation.⁷³ **C.** Supramolecular hydrogels can additionally form via small molecule gelation. For example, polyphenol compounds have been cross-linked with Group IV metal ions, including Ti.⁷⁴

1.2.2.1. Thermogelling and hydrophobic interactions

Some of the first supramolecular hydrogels used as drug delivery platforms were based on thermogelling polymers, which undergo gelation above a threshold temperature related to a change in polymer–solvent interactions. These polymers have been utilized since the 1960s, starting with the synthesis of block

copolymers, such as poly(ethylene glycol)-poly(propylene oxide) (PEG-PPO), which can self-assemble into gels in aqueous media at elevated temperatures via hydrophobic interactions.⁷⁵ As hydrophobic interactions are driven by entropy, their strength is dependent on the temperature of the system, the molecular weight of the interacting blocks, and the polymer concentration. In the case of thermogelling hydrogels, the increase in temperature will strengthen the hydrophobic interaction—the entropic component of the interaction becomes more favorable—and induce the aggregation of the polymer resulting in the formation of a gel. The platform can therefore be injected as a liquid and form a hydrogel upon heating to physiological temperature. Some well-studied systems have been created using block copolymers, such as FDA-approved Pluronics, or thermo-responsive polymers, including poly(*N*-isopropylacrylamine) (PNIPAm).^{76,77}

While this class of hydrogels is attractive for ease of assembly and relatively simple design, the materials can be limited in their tunability. Tuning the properties of thermogelling hydrogels independently is limited as the network is based on non-specific interactions between the polymer chains that serve as building blocks of the material. Tuning the mechanical properties requires an increase in polymer concentration or a change in the structure of the polymer. These modifications can also affect the capacity of the network to encapsulate molecules and the amount of foreign material that needs to be injected into the body. As a strategy to improve the range of mechanics and release profiles enabled by this class of materials, thermogelling systems have been combined with other supramolecular binding motifs, such as hydrogen bonding (**Section 1.2.2.2**) or host-guest interactions (**Section 1.2.2.4**).^{78,79}

1.2.2.2. Hydrogen bonding

Hydrogen bonds are commonly found in natural macromolecular systems. For example, they are a core motif in the binding and assembly of DNA and RNA. Hydrogen bonds are weak diatomic interactions involving an electron poor hydrogen and an electron rich atom, commonly oxygen or nitrogen. Individual hydrogen bonds are relatively low energy ($\sim 40 \text{ kJ mol}^{-1}$) and they are often used in multivalent forms to assemble macromolecular structures.⁸⁰ In this manner, the binding strength of the motif can be tuned by changing the number and organization of the hydrogen bonds, providing a straightforward route to modulate the interaction. This paradigm of weak yet multivalent interactions leading to strong bonding is pervasive in the design and application of supramolecular systems.

A large variety of hydrogen bonding units have been synthesized, covering a wide range of binding strengths.⁸¹ The toolbox of hydrogen bonding motifs has been employed in the design of supramolecular polymeric materials with enhanced mechanical properties, improved processability, and materials with self-healing properties.^{82,83} However, there are fewer instances of hydrogen bonding in the formation of supramolecular hydrogels, as water often competes with hydrogen bond formation.⁸⁴ To enable the formation of supramolecular networks using tailored hydrogen bonding in aqueous media, the binding motif needs to be of sufficient valency, strength, or protected by hydrophobic domains. However, as the strength of the interaction increases, the network can lose its shear-thinning behavior in exchange for a

higher modulus, which can be relevant for application in tissue engineering but makes these materials less suitable as injectable drug delivery platforms.^{85,86} Ureidopyrimidinone (UPy) moieties, a commonly used hydrogen bonding unit for self-assembly, has been incorporated into polymer networks to obtain different types of supramolecular hydrogels. In one case, UPy-functionalized dextran resulted in an injectable supramolecular network, suitable for the growth of cartilage and bone cells.⁵⁹ In another approach, a hydrophobic UPy was incorporated in the structure of a block copolymer to obtain a tough hydrogel; however, the rheology was less suitable for injectable applications.⁸⁵ A thermoreversible, shear-thinning hydrogel was designed by the incorporation of UPy moieties with PNIPAm.⁷⁸ The hydrogel showed promise as a platform for cell therapy as mesenchymal stem cells could be encapsulated and remained viable following injection.

The previously mentioned systems were all formed via the linking of disparate polymer chains through the use of hydrogen bonding units. Dankers et al. harnessed the capacity of hydrogen bonding units to form hydrogels using a different approach.⁷³ Here, UPy units with a hydrophobic spacer induced the formation of polymeric micelles from end-functionalized PEG macromers. The micelles aggregated in elongated and tubular supramolecular structures that entangled to form a hydrogel network (**Figure 1.2b**). Bridging PEG chains between fibers stabilized the network. This hydrogel was used to encapsulate and release bone morphogenetic protein 7 (BMP7), and the release profile of BMP7 was tuned by adjusting the weight percent of fibers in the gel and the ratio between the PEG chains and the hydrophobic units. In vivo studies showed the complete erosion of the material with no apparent damage to the tissues after 7 days, and the bioactive BMP7 acted as an anti-fibrotic agent locally.

Hydrogels based on DNA binding motifs have also been synthesized in recent years, exploiting the intrinsic capacity of the nuclear bases to form pairwise hydrogen bonds. This exciting class of materials has been shown to provide biocompatible materials though the design can be complex, as it requires the rational design of the interacting DNA strands. DNA-based hydrogels are beyond the scope of the present review, and we direct interested readers to another recent review of this topic.⁸⁶

1.2.2.3. Metal–ligand interactions

Metal coordination is another prominent interaction in biological systems, which enables structural integrity and stimuli responsive behavior. For example, iron chelation by hemoglobin and heme has a central importance in the transport and cooperative binding of oxygen in red blood cells (erythrocytes). Metal–ligand interactions occur between a metal ion and one or more ligands and exhibit bond strengths between those of electrostatic and covalent bonds ($\sim 80\text{--}600\text{ kJ mol}^{-1}$). As these interactions can occur via a variety of ligands and metal ions, a variety of complexes with a range of binding strengths have been explored. The strength of the metal–ligand coordination is directly related to the bond kinetics and different bond kinetics result in dramatic changes in the mechanical behavior of the formed hydrogels.^{87,88} Due to the large range of available interactions, it is important to carefully choose which interaction to use for the design of hydrogels for drug delivery. It should also be noted that the use of

metal ions for biomedical applications can be limited as they can be toxic outside of certain concentration windows.

A common approach used to form networks is to functionalize polymer chains with a metal-coordinating ligand, such as L-3,4-dihydroxyphenylalanine (DOPA).⁹¹ Here, the addition of metal ions forms a network by cross-linking DOPA-functionalized polymer chains. Due to the high selectivity of the ligand to metal ions, these interactions have been used for triggered gelation in the presence of select metal ions.⁸⁹ In another example, bisphosphonate was employed as the metal-coordinating ligand to assemble hydrogels by grafting bisphosphonate moieties to hyaluronic acid.⁹⁰ In this example, gelation occurred in the presence of calcium ions, resulting in the formation of shear-thinning and self-healing hydrogels. The mechanical properties of this hydrogel also made it suitable for injection (3D printing) for biomedical applications. Other polymers, including star PEG macromers, have been employed to form similar systems.⁹¹ The use of calcium ions presents the advantage of low toxicity compared with other metal ions, which is attractive for the design of drug delivery platforms.

The formation of hydrogels through metal–ligand coordination is dependent on the amount of available metal ions and ligand.⁹² These concentrations can often be tuned by the pH of the environment—protonating or deprotonating the ligand or shifting the equilibrium of free metal ions.⁸⁸ pH-responsive materials have been engineered using this approach, but this requires the careful design of the hydrogel to ensure stability at neutral pH for biomedical application. Tang et al. designed two different hydrogels with different stability at neutral pH depending on how metal–ligand interactions were used to link PEG chains to oligochitosan.⁹³ A first hydrogel with only one metal–ligand complex at the cross-linking sites between the polymers resulted in an unstable system at neutral pH. Increasing the number of metal complexes at the cross-linking sites rendered the network stable in a neutral pH buffer solution.

The previously mentioned systems required the synthesis of ligand-modified polymer chains. Hydrogels can also be designed by using metal ions to induce gelation of readily available small molecules. For example, inosine 5'-monophosphate, a commercially available ribonucleotide, has been reported to gel specifically in the presence of silver salt.³² Naturally abundant polyphenols were shown to gel in the presence of group IV metal ions, including Ti or Zr (**Figure 1.2c**).⁷⁴ These polyphenol hydrogels exhibited *in vivo* biocompatibility with low Ti accumulation in the tissue and enabled sustained release of dexamethasone over a time period of 10 days.⁹⁴

Metal–ligand interactions have also been combined with other interactions, as in the case of a gelatin–UPy–iron hydrogel.⁹⁵ In this system, iron coordination by carboxyl groups in the gelatin comprised the main driving force for gel formation and were responsible for the strength of the network. The hydrogen bonding units, on the other hand, improved the self-healing behavior of the material, enabling a higher recovery of the strength of the network after rupture. Coordination interactions have also been utilized to induce gel formation in peptide hydrogelators or as a way to form nanocomposite hydrogels (see **Section 1.2.2.6**).

1.2.2.4. Host–guest complexes

Host–guest interactions have emerged as an attractive supramolecular chemistry for the design of materials since their discovery in the 1980s.⁵⁰ In this supramolecular motif, binding is based on the interaction of a molecule (the guest) and a cavitand (the host) that is able to accommodate one or more guest molecules (**Figure 1.3**).⁹⁶ The interactions are often based on hydrophobic forces where the formation of a complex between the host and the guest is favorable to their individual existence in aqueous media—the binding releases ‘high energy’ water, releasing entropic constraints. Other factors such as polarity, size, or number of guests influence the interaction of the host and guest moieties. Due to the diversity of possible guest molecules, relative ease of formation, modularity, and specificity they have been widely used in the biomedical field to design supramolecular biomaterials.⁹⁷

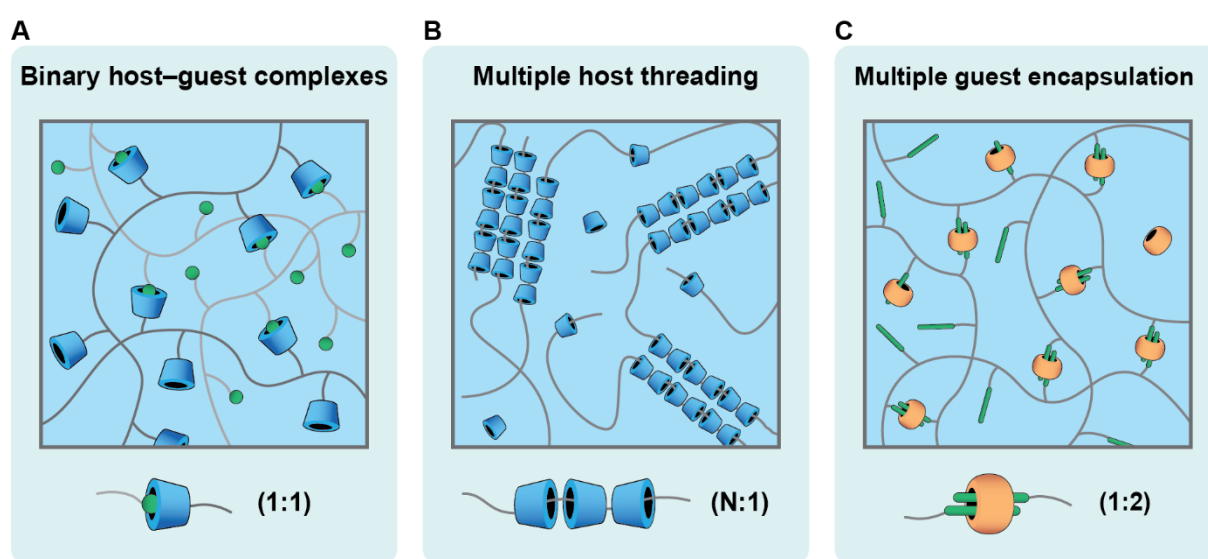


Figure 1.3. Host–guest chemistries for supramolecular hydrogel design. **A.** Schematic of different possible network formation strategies using **A.** binary host–guest complexes, i.e., CD binding to adamantane; **B.** multiple host threading, i.e., (pseudo)polyrotaxane formation between CD and PEG; and **C.** multiple guest encapsulation, i.e., CB binding multiple guests.

Usually the host (or cavitand) is a macrocyclic molecule that can be synthesized from naturally or synthetically derived monomers.⁹⁸ Commonly used cavitands include cyclodextrins, cucurbiturils, calixarenes, and pillarenes. The broad utility of this binding motif has given rise to a variety of supramolecular materials with simple or complex designs.⁹⁹ Keeping in mind that the focus here is the design of drug delivery systems, which requires facile and scalable synthesis, we highlight synthetically accessible approaches.

Cyclodextrin (CD) is commonly used as a host for the design of supramolecular hydrogels through host–guest complexation on account of its water solubility, low toxicity, and natural origin.¹⁰⁰ CD-derivatives have been employed widely in the pharmaceutical field, both in pre-clinical research and in commercial products.^{101,102} CDs are cyclic and conical oligosaccharides defined by their number of repeating glucose units. The most common CDs are α -, β - and γ -CD composed of 6, 7 or 8 repeating units, respectively.¹⁰³

Each CD has a different size of cavity making them suitable for different guests. In general, α -CD and β -CD are able to accommodate a single guest, whereas γ -CD can accommodate two guest molecules.^{104,105} The guest molecules that can be accommodated by CD can be divided in two categories: small molecules interacting with only one CD or polymers that can interact with multiple CDs via threading.¹⁰⁶ From each category different types of architecture will be created in the hydrogel resulting in different mechanical properties.

CD-based inclusion complexes have been reported with a multitude of possible guest molecules, providing tunability of the host–guest interaction and the ability to introduce stimuli-responsive behavior.^{107–110} A commonly used pair for biomedical applications is β -CD with adamantane, a bulky, hydrophobic molecule. As previously discussed with other supramolecular motifs, this interaction can be used to cross-link functionalized polymer chains. A prominent shear-thinning hydrogel was synthesized by grafting CD and adamantane on disparate hyaluronic acid populations using amine coupling or esterification, respectively.¹¹ Simple mixing of the functional polymers assembled a supramolecular hydrogel suitable for controlled drug release.^{111,112} This hydrogel system has been used for the delivery of microRNA, endothelial progenitors cells, or for the design of enzyme-degradable networks.^{112–114} By functionalizing other polymers or using larger CDs that are able to accommodate multiple guest molecules, different network architectures have been designed.^{115,116} For example, a micellar hydrogel was designed by functionalizing tetronics with adamantane for encapsulation and release of doxorubicin (DOX).¹¹⁷

Additional stimuli-responsive behavior can be introduced by incorporating a responsive guest molecule in the system. For example, azobenzene has been used as an ultraviolet light (UV)-responsive guest for binding with β -CD.¹¹⁸ Upon UV exposure the guest changes its conformation making it an unsuitable guest. As a result, hydrogel stiffness was controlled in the network by changing the amount of complex formed with external delivery of light.¹⁰⁸ The same approach enabled the formation of near-infrared light (NIR)-responsive hydrogel with the additional incorporation of upconverting nanoparticles in the hydrogel.¹¹⁹

In addition to providing a shear-thinning and self-healing supramolecular hydrogel, this cross-linking approach enabled facile incorporation of different fillers. One example is the introduction of graphene into the hydrogel by functionalizing the graphene surface with CD moieties.¹²⁰ The resulting hydrogel maintained the original mechanical properties of the base supramolecular network, while exhibiting antibacterial activity and an electrical conductivity similar to skin tissue.

In addition to using CDs as a direct cross-link between polymer chains, the capacity of CDs to thread onto polymers to form polyrotaxanes and pseudopolyrotaxanes has also been used to form supramolecular hydrogels. Harada first reported the capacity of α -CD to thread onto PEG chains forming a “molecular necklace”.¹⁰⁶ After threading, the CD can form columnar aggregates that are able to act as a cross-linking mechanism between threaded PEG chains.¹²¹ The first PEG networks made using this

cross-linking motif were too weak to be suitable materials for drug delivery due to their fast dissociation. α -CD has therefore been combined with other interactions to form stronger networks. For example, α -CD had been used to improve the mechanical properties of amphiphilic or bolaamphiphilic block copolymer systems.¹²² Most of those systems have PEG chains in the network structure, which enables CD threading and cross-linking as well as an additional hydrophobic polymer that does not interact with CD but can form hydrophobic assemblies as additional cross-links. For example, the mechanical properties of Pluronic-based gels were enhanced using this approach.⁷⁹ In another example, amphiphilic block copolymers were used to form self-assembled micelles, which formed a hydrogel upon the addition of CD.¹²³ The structure of the micellar hydrogel was modified depending on the order of formation of the different components. An inverse micelle hydrogel was formed using poly(lactic-co-glycolic acid) (PLGA) as the hydrophobic polymer and first threading α -CD on the PEG moieties and then triggering micelle formation.⁶¹ The inverted micellar hydrogel resulted in a high loading of DOX (up to 10 wt%) while providing a longer release period of the therapeutics ($t = 45$ days) compared with the equivalent micellar hydrogel ($t = 12$ hours), attributed to its increased stability in aqueous solution.

Further, the simplicity of the CD-based polyrotaxane motif, which only requires the presence of a threading polymer like PEG, has enabled the formation of hydrogels with components that are often difficult to integrate directly into the hydrogel structure. In one example, Yu et al. utilized PEG-coated gold nanoparticles and nanorods with α -CD to obtain a hydrogel with temperature dependent sol–gel transition.¹²⁴ Similarly, hydrogels were formed from arginine-functionalized dendrons by linking PEG chains to the dendron and using CD to induce gelation.¹²⁵ The hydrogel demonstrated promise as an injectable platform for gene therapy as it displayed higher transfection and lower cytotoxicity than standard poly(ethylenimine) (PEI) formulations.

Song et al. recently developed a thermoresponsive hydrogel suitable for drug delivery using CD in tandem with PEG–PNIPAm pseudo block copolymer.¹²⁶ The hydrogel exhibited a change of mechanical properties following injection. Indeed, the hydrogel was formed through the interaction of threaded α -CD on the PEG chains, making a weak hydrogel suitable for local injection. Upon injection, the PNIPAm chains present in the hydrogel aggregated due to the increase of temperature to 37 °C further increasing the hydrogel modulus. The dual-stage cross-linking enabled extended release of loaded DOX compared with pure PEG– α -CD. Additionally, during the degradation of the hydrogel, micelles formed from the PEG–PNIPAm pseudo block copolymer enabled a higher cell uptake and anticancer activity of DOX compared with free drug.

In addition to CD, cucurbituril (CB) derivatives have emerged as another useful cavitand in host–guest complexation for the formation of supramolecular hydrogels. CBs are macrocyclic molecules formed from multiple glycoluril monomers.¹²⁷ As with CD, the size of the cavity is dictated by the number of monomers in the cavitand; however, the shape of the cavity is different as CBs are cylindrical molecules that can encapsulate guests from both of their entrances resulting in a variety of binding topologies.¹²⁸

CBs have relatively strong binding constant (up to 10^{15} M^{-1}) compared with other cavitands, as their complex formation is induced both by hydrophobic and electrostatic interactions.¹²⁸

CB-based binding motifs, with viologen and naphthyl guests, were used to design hydrogels suitable for drug and protein delivery.¹²⁹ The guests were grafted to biocompatible polymers and the assembly of the network was triggered by addition of CB to a precursor solution of the functionalized polymers and drug. The resulting hydrogels were able to be formed with a high amount of water ($\sim 99.7\%$) and controlled the release of protein over the course of months. This approach did not require the chemical modification of the host molecule, which can be challenging synthetically. Reversible stiffening of similar gels was achieved by using photosensitive guests. Exploiting the ability of coumarin to dimerize upon irradiation at specific wavelength, the cross-links of the hydrogel were switched reversibly from supramolecular to covalent, resulting in controlled stiffening of the material.¹³⁰

Multiple CB-based hydrogels using binary host complexes have also been developed, demonstrating a correlation between binding strength, viscoelastic behavior, and release rate of encapsulated drug.¹³¹ The changes in strength of the cross-link directly influenced the relaxation behavior of the network; gels with the strongest binding were similar to covalent networks with a very slow relaxation time and a loss in self-healing capacity. As the relaxation of the network changed the release rate of encapsulated dextran varied accordingly, showing how the release of therapeutics can be tuned through the design of the host–guest interaction forming the network cross-links.

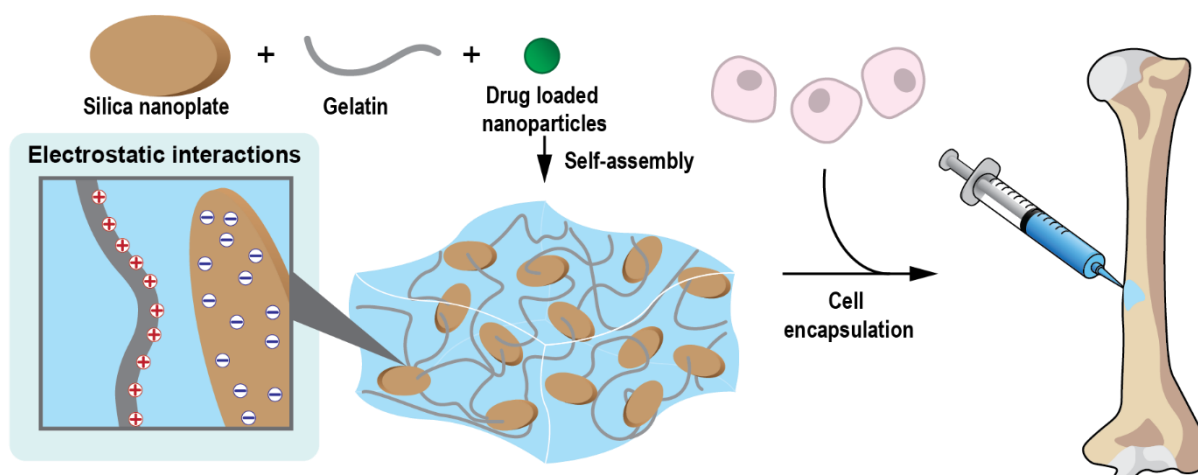
1.2.2.5. Nanocomposite hydrogels

Beyond the design of specific and directional binding motifs between polymer chains or small molecules, supramolecular interactions have also been exploited between polymer chains and nanoscale objects (**Figure 1.4**). This approach to form hydrogels through reversible interactions between appropriately paired polymers and nanoparticles enables the formation of supramolecular nanocomposite hydrogels. Nanocomposites have emerged in the biomedical field for their increased mechanical properties and functionality.¹³² Physical nanocomposite hydrogels are often formed using the nanosized object as a cross-linking motif between polymer chains.¹³³

For example multiple polymers, such as PEG and gelatin, have been shown to adsorb on the surface of biocompatible silicate nanoplates (Laponite[®]) through electrostatic interactions (**Figure 1.4a**).^{134,135} As a result shear-thinning and self-healing hydrogels were formed. The silicate nanoplates present in the gel enhanced the proliferation of human mesenchymal stem cells by providing adhesion sites and introduced hemostatic and osteogenic properties to the hydrogel due to their negatively-charged surfaces.^{136–138} Nanoclays were also used to combine proangiogenic and osteogenic properties in multicomponent peptide-based biomaterials for improved bone regeneration as compared with single component systems.¹³⁹ The viscoelastic and mechanical properties of nanocomposites based on silicate nanoplates depend on the concentration of the nanofiller. An increase of nanoplates in the material resulted in an increase in the solid-like behavior of the gel.¹⁴⁰ One consideration to take into account

while designing nanoplate-based composite hydrogels is the presence of ions and other charged molecules that can disrupt the network formation by altering the electrostatic interactions between the silicate surface and the polymers. For example, the presence of concentrated salt solutions or culture medium has been shown to induce aggregation of the nanoclays, which could be less beneficial for biomedical use.¹⁴¹

A Silicate nanoplates hydrogel



B Polymer–nanoparticles hydrogel

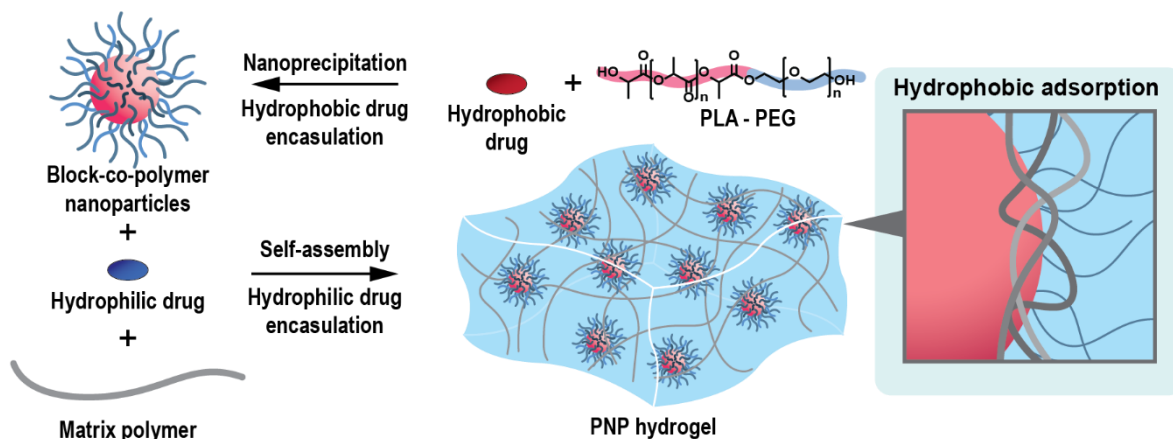


Figure 1.4: Nanocomposite hydrogel formation through supramolecular interactions. **A.** Silicate nanoplates can be combined with gelatin, which interact via electrostatics, to form osteoinductive hydrogels. In addition to their ability to load drug, encapsulate cells, and adapt to defect during injection these gels were suitable for the design of injectable bone implant materials.¹³⁶ **B.** Polymer–nanoparticle (PNP) hydrogels formed through the hydrophobic adsorption of select polymers and nanoparticle surfaces enabled the encapsulation and release of both hydrophobic and hydrophilic drugs for use as injectable drug delivery depots.¹⁸

Another class of nanocomposite hydrogel has been developed based on favorable interactions between polymers and spherical block copolymer nanoparticles (**Figure 1.4b**).¹⁸ These polymer–nanoparticle (PNP) hydrogels arise from entropic interactions between moieties on the polymer chain and the nanoparticle surface that assemble a hydrogel, likely through a combination of polymer bridging and

colloidal jamming.¹⁴² PNP hydrogels were originally developed for dual drug encapsulation and simultaneous controlled release—a hydrophobic small molecule was loaded in the nanoparticle core and a hydrophilic molecule was loaded in the aqueous phase. As with the nanoclay systems, the rheological properties of PNP hydrogels depended on the concentration of nanoparticles enabling tailored mechanical and flow behavior.¹⁴³ Additionally the viscoelastic behavior of the materials were modified by changing the hydrophobicity of the polymer, resulting in increased interaction between the polymer and the nanoparticles. The type of interaction used to form the network could also be changed by adding cationic surfactant in the nanoparticle enabling the use of anionic polymers.¹⁴⁴ Similar hydrogels, based on PEG–poly(lactic acid) (PLA) block copolymer nanoparticles, were employed for the dual delivery of vaccine components over several weeks, for the treatment of myocardial ischemia through control the delivery of pro-angiogenic protein, and for the recruitment of immune cells at the site of injection through the release of cytokine.^{16,17,145} Recently developed methods for the continuous and controlled production of the block copolymer nanoparticles forming the gel enable scale-up and further application of this class of biomaterials.^{146,147}

Other promising PNP hydrogels have been synthesized based on different interactions and types of nanoparticles. The Heilshorn group reported the design of a PNP hydrogel suitable for cell delivery based on engineered proteins.¹⁹ The hydrogel network was formed through interactions between a recombinant protein and hydroxyapatite nanoparticles. The interactions were highly specific and only resulted in gel formation in the presence of a specific amino acid sequence. The hydrogel enabled encapsulation of adipose-derived stem cells, which, with the help of osteoconductive cues provided by the hydroxyapatite nanoparticles, promoted bone regeneration without the need for ex vivo culture prior to implantation.

Another platform suited for drug delivery was designed using drug loaded magnesium silicate nanoparticles that interacted with bisphosphonate-functionalized polymer chains.¹⁴⁸ Here, network formation occurred through the coordination of the ligand on the polymers with available magnesium atoms on the surface of the nanoparticles. The drug-loaded particles were released upon degradation of the hydrogel and therapeutic delivery relied primarily on the cellular uptake and internalization of the released nanoparticles.

Injectable hydrogels have also been designed through supramolecular interactions between disparate nanoparticles. For example, nano-networks were fabricated using electrostatic interactions between positively and negatively charged polymeric nanoparticles.¹⁴⁹ A hydrogel based on PLGA enabled the release of dexamethasone encapsulated in the nanoparticles over a period of two months.¹⁵⁰ Triggered release of insulin was achieved from a nano-network designed to mimic pancreatic activity.¹⁵¹ For this purpose insulin and glucose-specific enzymes were loaded in pH-sensitive dextran nanoparticles. Through the catalytic conversion of glucose into gluconic acid by the enzymes, the pH of the environment decreased over time resulting in the degradation of the particle and the release of the

insulin. The amount of insulin release was dependent on the amount of glucose present enabling self-regulation of the therapeutic release.

1.2.2.6. Peptide-based hydrogels and hydrogelators

Another class of supramolecular hydrogels that have broad application in biomedicine leverage interactions between peptide-based molecules (**Figure 1.5**).¹⁵² Polypeptides are intrinsically biocompatible, exhibit a capacity to self-assemble into organized complex structures, and are easy to access synthetically making them attractive building blocks for the design of supramolecular materials.¹⁵³ The self-assembling behavior of peptides is mediated by multiple supramolecular interactions, including hydrogen bonding, hydrophobic interactions, and electrostatics.¹⁵⁴ Amino acids each present different characteristics that can control the assembly behavior of polypeptides. By engineering the structure of the peptides, injectable hydrogels have been obtained through various molecular design strategies. In this section, we present a few prominent designs without focusing on the specific structure of the peptide sequence itself.

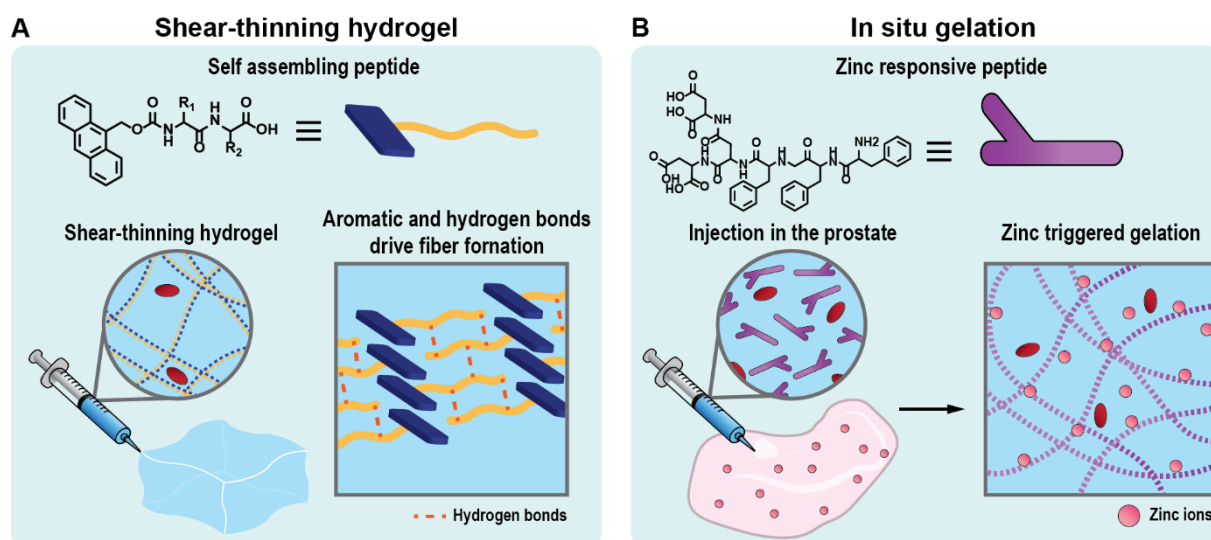


Figure 1.5. Peptide-based injectable hydrogels. **A.** Shear-thinning hydrogels were obtained via the self-assembly of small peptides exploiting supramolecular binding motifs, including hydrogen bonding and π - π interactions.¹⁵⁵ **B.** In situ gelation has been achieved via triggered peptide self-assembly in the presence of specific metal ions, enabling tissue specific gelation, for example, in the prostate.¹⁵⁶

One approach uses peptides as self-assembling building blocks for the design of shear-thinning hydrogels. These materials have been obtained via the controlled assembly of peptides in extended one-dimensional supramolecular objects (fibers) that can entangle into a network (**Figure 1.5a**).¹⁵⁵ Fibers have been formed using different aggregation mechanisms, such as the formation of anti-parallel nanotapes, coil-coil peptide motifs, or micelles formation, which were each controlled by the structure of the peptides.^{154,157} When using small peptides, elongated structures have been designed via direct amino acid interactions.¹⁵⁸ While longer polypeptide chains can first form secondary structures, such as a beta sheets or alpha helices, prior to assembly into fibers.¹⁵⁹ As the shape and assembling mechanism

of the fibers changes, the resulting hydrogels will show varied self-healing rates, making them more or less suitable for drug delivery. Additionally the shape of the fibers influenced the loading of drugs in the hydrogels.¹⁶⁰ With careful design, a shear-thinning peptide-based hydrogel having antibacterial activity was obtained.¹⁵⁵ The hydrogel showed fast recovery after injection and improved viability and proliferation of white blood cells. This platform could be applied for the delivery of therapeutics for wound healing.

The flow behavior of these peptide-based gels is challenging to predict as each network can result in different breaking and association mechanisms under shear. An insight into the flow behavior of this class of networks was provided by studying beta hairpin peptide-based hydrogels.¹⁶¹ Under shear the fiber network broke into smaller domains of randomly arranged fibers. These domains exhibited flow behavior that was similar to colloidal systems. However, the self-healing of the network can be much faster than in the case of traditional colloidal gels as, upon cessation of the shear, the fibers can rapidly reform without significant delay.

Often the interaction assembling peptide-based hydrogels is sensitive to environmental conditions and requires a precise design of the amino acid sequence to enable hydrogel formation in physiological conditions.¹⁶² Environmental sensitivity has also been leveraged to design in situ gelling materials. In situ gelation of peptides occurred upon changes in pH or temperature, and also through their interaction with metal ions.¹⁵⁷ If correctly designed, gelation can be triggered specifically at the site of application. For example, a peptide able to bind to zinc through glutamic acid residues was reported for prostate-specific gelation, due to its high zinc concentration compared with other tissues (**Figure 1.5b**).^{156,163} The hydrogel was used to encapsulate DOX and resulted in a controlled release in vitro with no initial burst of the drug over the course of several days. A similar approach could be employed for other organs with elevated zinc concentrations, such as the liver, or by using other ions that are present in elevated concentrations in other tissues.¹⁶⁴

One can also tailor the specificity of the peptide gelation by introducing cleavable amino acid sequences that hinder peptide assembly. This strategy was applied for the design of glycyrrhetic acid-modified curcumin hydrogelators for tumor targeting.¹⁶⁵ The hydrogelators were designed with a glutathione that initially prevented peptide assembly. However, upon internalization in tumors, the glutathione was reduced enabling peptide aggregation and hydrogel assembly. By conjugating curcumin to the peptide, the drug uptake in the targeted tumor was increased resulting in a higher anti-cancer activity compared with free drug.

A multitude of other strategies have also been used to form injectable hydrogels with peptides by using them in association with polymers.¹⁶⁶ Similar to the supramolecular moieties discussed in the previous sections, peptides were used to direct the cross-linking of functionalized polymer chains. Here, cross-linking can occur through different peptide motifs based on stereo-complexation, hydrogen bonding, or other supramolecular interactions. For example, PEG has been cross-linked using triple helix formation

using synthetic collagen peptides or through electrostatic interactions between a peptide and an oligosaccharide.^{167,168} An interesting dock and lock system was designed by using a peptide functionalized PEG in tandem with a polypeptide.¹⁶⁹ The polypeptide was composed of two “docking” domains that are able to form dimers, which can then be stabilized with a complementary peptide residue attached to the PEG chains. The resulting system formed shear-thinning hydrogels with rapid self-healing. The hydrogel additionally enabled the loading of dextran, and the release rate was correlated to the erosion rate of the hydrogel. In another approach, peptides were used to cross-link PNIPAm, which enabled gelation of peptide fibrils upon collapse of PNIPAm with increasing temperature.¹⁷⁰ Materials that did not require chemical reaction of the peptide to the polymer were obtained using positively charged peptide amphiphiles and negatively charged polymers.¹⁷¹ The absence of chemical modification enabled the simple formation of the material upon mixing, and the charged species provided a suitable environment for the loading of charged proteins.

Peptide-based hydrogels provide a broad range of possibilities to form injectable supramolecular hydrogels with tailored structure, tissue specific gelation, and controlled drug release. However, the rational design of such hydrogels remains challenging as the structure of the hydrogel and its properties will be highly dependent on the structure of each peptide.

1.2.3. Tailoring drug affinity through supramolecular design

Another challenge in the design of suitable platforms for drug delivery is the encapsulation of drugs within the platform and controlled release of the therapeutics from the system. In the above sections, the rheology of the materials was tailored through supramolecular design and the physical properties of the gels were used to control release via constrained diffusion. An alternative approach is to tailor the affinity of the drug to the material using supramolecular design strategies.

Drugs and therapeutics come in a variety of molecular configurations, affinity, and by extension compatibility with hydrogel matrices. Hydrophilic drugs can be loaded in a hydrogel easily as the main component is water and the loading capacity is dictated primarily by the solubility of the drugs. However, these drugs often diffuse out of the gel rapidly. Other therapeutics, including hydrophobic drugs with poor aqueous solubility, require more complex strategies as direct encapsulation can result in poor loading. Additionally, the affinity of the drug to the matrix whether hydrophilic or hydrophobic will tailor the release kinetics. That is, the affinity of the drug to the matrix itself can be used to control the release of a drug from the hydrogel.¹⁷² A high affinity will slow transport of the drug through the network whereas a low affinity will favor diffusional release of the drugs.¹⁷² By using the versatility of supramolecular interactions, strategies to incorporate and increase the loading of therapeutics have been developed with minor or no chemical modification of the drug.¹⁷³

1.2.3.1. Supramolecular binding sites to tailor drug–matrix affinity.

To increase the affinity of a drug to the hydrogel matrix, a simple approach is to design regions in the hydrogel network that are able to interact non-covalently with the drug(s) through supramolecular

interactions (**Figure 1.6a**). The loading capacity and the release kinetics will depend on the strength of the interaction and how many binding sites are present in the hydrogel.¹⁷⁴ By modifying the quantity of binding sites available for binding drugs, the release kinetics of the drug can also be tuned.¹¹¹ Note, that it is important to take the changes in release kinetics into account when engineering the interaction between the network and the drug. A strong binding can result in a loss of diffusion in the gel, shifting the release kinetics to erosion-based release.

As a vast array of drugs exist, the type of interaction required for the loading of drugs will vary. Regions that are able to interact with different classes of molecules can provide increased versatility to the platform. The introduction of hydrophobic regions in a hydrogel matrix can accommodate a broad range of water insoluble molecules due to the non-specificity of the interaction. Such systems are often based on networks formed via hydrophobic interactions, such as block copolymer, micellar, or amphiphilic peptide-based hydrogels.^{123,160} For example, a hydrogel based on PNIPAm was used to enable the loading of hydrophobic drugs.¹⁷⁵ The hydrophobic domain created by the PNIPAm was released as micelles upon degradation of the hydrogel, enhancing cellular uptake of the drug.

The previously discussed systems incorporate the binding region in the structure of the hydrogel, constraining the design of the hydrogel network. Providing binding motifs which can simply be grafted to the polymer network enable the decoupling of the drug loading and the material composition. CD has been used as a possible motif for the encapsulation of drugs through grafting or incorporation within the structure of a formed hydrogel.¹⁷⁶ A gelatin-tyramine hydrogel designed as an adhesive for wound healing demonstrated improved loading of dexamethasone and curcumin in the hydrogel.¹⁷⁷ Heparin, an anionic polysaccharide, has been employed for its capacity to bind specifically to multiple proteins, such as growth factors.^{178,179} Similarly, peptides with aromatic interactions were grafted to a polyurethane network, providing curcumin-binding domains.¹⁸⁰

For hydrogels based on the formation of supramolecular fibers, binding regions can be introduced by functionalizing some of the building blocks of the fibers with the binding motifs. Bakker et al. harnessed this approach to introduce positively-charged regions in the structure of their hydrogel.¹⁸¹ The motifs accommodated antisense oligonucleotides via electrostatic interactions.

1.2.3.2. Supramolecular integration of drug carriers

In some cases, the direct incorporation of the drug in the hydrogel can be challenging. Therefore, the design of drug carriers as components of the hydrogel that interact through supramolecular interaction has been introduced as a complementary approach. The carriers can be defined in two categories depending on their requirement to be chemically associated to the drug or not.

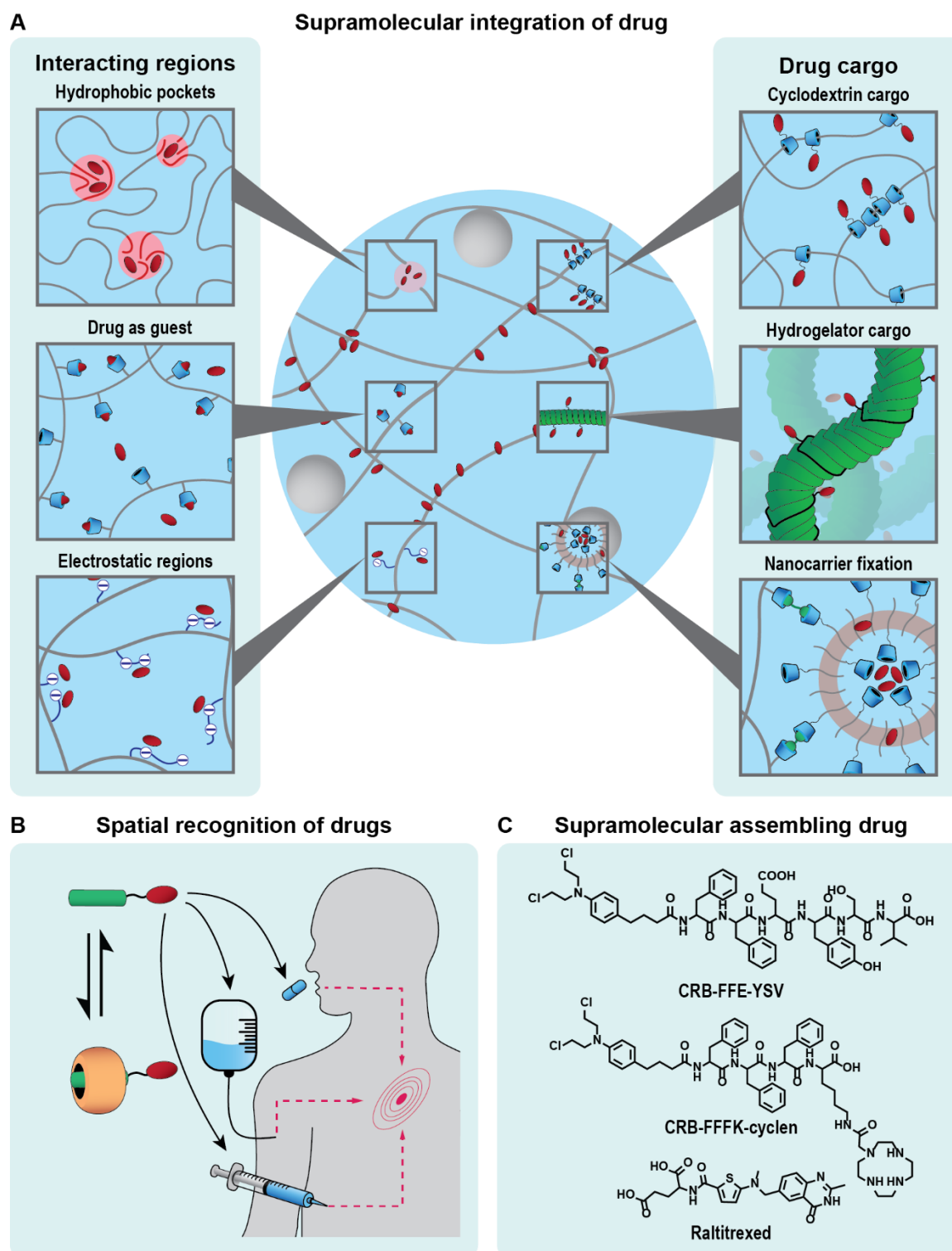


Figure 1.6: Supramolecular interactions to tailor drug–matrix affinity. **A.** Supramolecular binding motifs can be used to load drugs in the hydrogel and control the release of the drug from the hydrogel by providing specific binding sites that are able to interact non-covalently with the therapeutic or by creating drug carriers within the gel. **B.** Using host–guest chemistry, a system for spatial drug recognition was developed enabling improved accumulation of drugs at a target site in the body following systemic administration.¹⁸² **C.** Drugs themselves have also been used to self-assemble hydrogels for controlled release.^{183–185}

Drug carriers that do not require modification of the drugs are usually nanoscale objects that can encapsulate many drug molecules, such as nanoparticles or liposomes. These nanocarriers are advantageous as they can be tailored specifically to the drug of interest prior to their introduction into the hydrogel system. The incorporation of such objects in the hydrogel can be achieved by the design of supramolecular nanocomposite as previously discussed in **Section 1.2.2.5**. Block copolymer and metal nanoparticles have been employed as drug carrier in this manner.^{18,148} The introduction of the drug carrier in the hydrogel can also be achieved by designing supramolecular motifs able to bind the cargo to the hydrogel network. For example, polycaprolactone- β -CD polymerosomes were employed for the combined delivery of hydrophobic and hydrophilic drugs.¹⁸⁶ The CD present on the carrier anchored it to the hydrogel backbone. Additionally, increased retention of the drug at the target tissue site was achieved as the carrier itself exhibited adhesive properties.

Recently, supramolecular excipients have been created that avoid the need to chemically modify the drug while improving their solubility.¹⁸⁷ This method enabled increased drug loading without requiring the cargo to be part of the gel structure or to have a specific affinity to the gel matrix. CB-conjugated PEG has been used to bind reversibly to biomolecules in order to improve their solubility through supramolecular binding with hydrophilic polymer chains.¹⁸⁸ Additionally, insulin monomers were stabilized using this CB-based supramolecular excipient resulting in a tenfold increase in stability compared to commercial insulin hexamer formulations.¹⁸⁹

A second category of drug carrier relies on the conjugation of a drug to a molecule that is able to interact with the hydrogel through a supramolecular binding motif. This strategy has been particularly suitable for the incorporation of drugs in hydrogels based on supramolecular fiber formation.¹⁹⁰ For example, a peptide amphiphile functionalized with dexamethasone demonstrated controlled release of the drug over one month.¹⁹¹ In principle, this system can be designed as a platform for multicomponent therapies.

A recent strategy harnessed the capacity of CD to thread on polymer chains as a method to incorporate drug.¹⁹² CD was functionalized with DOX and thread onto Pluronic, which comprised the hydrogel network. The drug loading depended on the CD concentration and avoided the need for specific interactions between the drug (DOX) and the matrix.

Finally, drugs can be functionalized directly with guest molecules for loading into a hydrogel containing a matching CB host.¹⁸² Excitingly, this strategy uniquely enabled the spatial localization of drugs administered orally or intravenously (**Figure 1.6b**). The highly selective interaction between guest and host led to accumulation of the drug at the site where the hydrogel had been applied. This system is particularly attractive for tailored treatment with multiple drugs without requiring injection of multiple gels each loaded with a different therapeutic or for repeat dosing by exploiting the engineered homing of therapeutic molecules to the site of interest.

1.2.3.3. Drug as building block

In some cases, drug encapsulation remains a challenge even with improved drug–matrix affinity. Therefore, therapeutics have been used directly as building blocks for the formation of supramolecular hydrogels. Such materials can be used in tandem with other drugs enabling the formation of multidrug release depots. Through the use of supramolecular interactions, the therapeutics can be designed to self-assemble while avoiding extensive modification of the drugs.

This approach is common in the design of peptide-based hydrogels, as peptides themselves can act as the drug, demonstrating anti-inflammatory or anti-bacterial behavior.^{155,193} The use of peptide therapeutics enables hydrogel formation without the need for additional chemical modification of the therapeutic agent. For example, beta hairpin peptides have shown antibacterial activity and the capacity to form injectable supramolecular networks.¹⁹⁴ Some non-peptide therapeutics, such as raltitrexed or dexamethasone, can also self-assemble without requiring chemical modification, but are limited in number (Figure 6c).^{173,185}

The majority of active pharmaceutical agents require some modification of their structure to enable direct gelation. One strategy is to create an amphiphile drug hydrogelator, which is able to aggregate through the formation of hydrophobic and hydrophilic domains.¹⁸⁴ By conjugating drugs—tyroservatide, a peptide drug, and chlorambucil, an anticancer agent—with different affinities for water, an amphiphilic hydrogelator was designed (**Figure 1.6c**).¹⁸³ This system also exhibited additional stability of the drugs. A similar strategy was employed for the design of an in situ self-assembling hydrogel.¹⁹⁵ The drug amphiphile was composed of Taxol, a hydrophobic anti-cancer drug, and tyroservatide, an anti-cancer peptide, linked through an ester bond. Upon injection the ester bond was able to self-hydrolyze inducing the self-assembly of the free Taxol with the amphiphiles into a fibrous hydrogel. This approach resulted in enhanced cellular uptake of the anti-cancer drugs.

Other strategies beyond the use of drug as the hydrogelator were developed to broaden the scope of possible methods to use drugs as building blocks in material design. For example, DOX nanospheres were employed to crosslink peptide fibers to form a supramolecular hydrogel.¹⁹⁶ This was possible based on electrostatic interactions between the negatively charged fibers and the positively charged DOX nanospheres. This concept was extended to the formation of multiple hydrogels from anionic drugs, including suramin, clodronate, heparin, and trypan blue.¹⁹⁷ Similarly, a STING agonist was used to cross-link nanotubes formed from a peptide–drug conjugate, resulting in the formation of a self-assembling hydrogel containing multiple therapeutics in its structure.¹⁹⁸

Through supramolecular interactions drugs are able to be used as building blocks for the design of hydrogels, providing an additional method to introduce therapeutics into supramolecular hydrogels. However, this approach requires careful molecular design to avoid loss of drug efficacy or stability.

1.3. OUTLOOK

The use of supramolecular interactions in the design of hydrogel platforms for drug delivery has shown broad potential in the design of materials with controlled release, suitable mechanical properties, and improved therapeutic delivery. In total, supramolecular hydrogels demonstrate broad potential as next-generation drug delivery platforms to improve medical care. However, much of this work has been at the bench and few systems have entered the clinic.

Clinical approval remains a challenge, especially for complex hydrogels in part due to the use of new synthetic materials. Fortunately, a suitable path forward has been presented by other non-hydrogel-based supramolecular therapeutics that have entered clinical trials or been commercialized. For example, Suggamadex, comprised of functionalized CD for sequestration of anesthetics, has been commercialized and employed in the clinic to resolve neuromuscular blockade.¹⁹⁹ Furthermore, Ziylo Ltd is developing glucose responsive insulin by combining insulin with a supramolecular macrocycle technology that binds and detects glucose. Larger systems, including the polymeric nanoparticle based on cyclodextrin and camptothecin (CD-CPT) developed by the Davis group, have been explored clinically as possible therapeutics for targeted cancer therapy.^{200,201} Another promising technology is a supramolecular scaffold for cardiovascular regeneration being developed by Xeltis, a clinical-stage medical device company.²⁰² This material has been used for the design of pulmonary heart valves and is currently undergoing a Phase 3 clinical trial as a platform for small diameter blood vessel regeneration.

As the field continues to grow, the design of safe, smart, and biocompatible supramolecular materials will become more accessible. The field will learn from the examples that have advanced to the clinical stage and from many others that are in development. To ease clinical acceptance, research should avoid overly complex systems and consider early on in the development the feasibility of the material to be approved by regulatory agencies and its suitability for industrial production. Many of the supramolecular motifs that are available currently form a robust basis for the design of elegant and functional drug delivery platforms. Further, as the field evolves, a more detailed understanding as to how molecular details of the supramolecular motifs influence the mechanical and release properties of the gels will improve our ability to engineer this powerful class of materials to address unmet translational needs.

1.4. CONCLUSION

Supramolecular interactions have proven promising for the design of hydrogels for controlled drug delivery. The incorporation of various supramolecular binding motifs in the hydrogel matrix enables rational engineering of the rheological behavior of the materials, such as shear-thinning and self-healing behavior, suitable for injection via narrow diameter syringes or catheters. Additionally, the incorporation of therapeutics in the hydrogel and release from the materials can be improved via supramolecular design of the drug–matrix affinity. Our ability to fabricate and apply this useful class of supramolecular hydrogels to the field of drug delivery will expand with basic advances in supramolecular chemistry and a more robust understanding of structure–function relationships in associating polymer networks.

1.5. ACKNOWLEDGEMENTS

This work was supported by the Swiss National Science Foundation under project number 200021_184697 and start-up funds from ETH Zurich. The authors declare no conflict of interest.

CHAPTER 2

SUPRAMOLECULAR REINFORCEMENT OF POLYMER–NANOPARTICLE HYDROGELS FOR MODULAR MATERIALS DESIGN

SUMMARY *Moldable hydrogels are increasingly used as injectable or extrudable materials in biomedical and industrial applications owing to their ability to flow under applied stress (shear-thin) and reform a stable network (self-heal). Nanoscale components can be added to dynamic polymer networks to modify their mechanical properties and broaden the scope of applications. Viscoelastic polymer–nanoparticle (PNP) hydrogels comprise a versatile and tunable class of dynamic nanocomposite materials that form via reversible interactions between polymer chains and nanoparticles. However, PNP hydrogel formation is restricted to specific interactions between select polymers and nanoparticles, resulting in a limited range of mechanical properties and constraining their utility. Here, a facile strategy to reinforce PNP hydrogels through the simple addition of α -cyclodextrin (α CD) to the formulation is introduced. The formation of polypseudorotaxanes between α CD and the hydrogel components resulted in a drastic enhancement of the mechanical properties. Furthermore, supramolecular reinforcement of CD–PNP hydrogels enabled decoupling of the mechanical properties and material functionality. This allows for modular exchange of structural components from a library of functional polymers and nanoparticles. α CD supramolecular binding motifs are leveraged to form CD–PNP hydrogels with biopolymers for high-fidelity 3D bioprinting and drug delivery as well as with inorganic NPs to engineer magnetic or conductive materials.*

This chapter is adapted from: Giovanni Bovone, Elia A. Guzzi, Stéphane Bernhard, Tim Weber, Dalia Dranseike and Mark W. Tibbitt, *Adv. Mater.* **2021**, 34 (9), 2106941. **AUTHOR CONTRIBUTIONS:** G.B., E.A.G., and S.B. contributed equally to this work. S.B. provided primary contributions on the chemical design, materials synthesis, and mechanical characterization. G.B., E.A.G., and M.W.T. conceived of the research project. G.B., E.A.G., and S.B. equally planned and executed the experiments, interpreted the data, and co-wrote the manuscript. T.W. provided initial feasibility data on the materials design. D.D. assisted with the 3D printing. M.W.T. coordinated the research project and supported the writing of the manuscript.

2.1. INTRODUCTION

Moldable and injectable polymer networks are increasingly used for a range of biomedical and industrial applications.^{203–205} Dynamic polymer networks are commonly prepared using reversible interactions, enabling the materials to flow under applied stress—shear-thin—and to reform a stable network—self-heal—after removal of the stress.^{206,207} The rheological properties of dynamic polymer networks make them useful as minimally invasive injectable biomaterials,^{208,209} ejectable inks for additive manufacturing,^{207,210} and reconfigurable materials.^{211–213} The inclusion of nanoscale fillers in dynamic polymer materials has been leveraged to enhance their rheological properties and expand their functionality.^{132,214–216} Dendritic binders were mixed with clay nanosheets to assemble tough and moldable hydrogels.²¹⁷ Silicate nanoplates have been combined with gelatin to prepare injectable and tissue adhesive hydrogels for the treatment of hemorrhage in mice.¹³⁷

Polymer–nanoparticle (PNP) hydrogels comprise an emerging strategy to engineer dynamic nanocomposite hydrogels.^{18,133,218} PNP hydrogels are formulated by mixing a liquid suspension of nanoparticles (NPs; e.g., poly(ethylene glycol)-block-poly(lactide) [PEG-*b*-PLA] NPs) and a liquid solution of polymer (e.g., hydroxypropylmethylcellulose [HPMC]). Reversible interactions between the polymer chains and NPs enable the formation of a viscoelastic network with shear-thinning and self-healing properties.^{133,142} Owing to their facile preparation and dynamic mechanical properties, PNP hydrogels have been applied as injectable hydrogels for drug delivery,¹⁸ postoperative adhesion barriers,²¹⁹ minimally invasive biomaterials for immune cell recruitment,¹⁷ moldable materials for pipeline maintenance,²⁰³ sprayable coatings for wildfire mitigation,²²⁰ and bioinks for additive manufacturing of personalized biomaterials.^{15,143} While PNP hydrogels comprise a highly versatile and tunable platform to design moldable polymer nanocomposites, hydrogel formation has been restricted to specific interactions between select polymers and NPs. This has limited the accessible ranges of mechanical properties and dynamicity in this class of materials. Further, the specificity of the interaction to the building blocks of the hydrogel has restricted the pool of network component to limited classes of polymer and NPs.

To expand the design landscape of PNP hydrogel, we envisioned that a simple and elegant supramolecular motif could be leveraged to reinforce and generalize this class of materials to other NPs and other polymers. Cyclodextrins (CDs) are macrocyclic oligosaccharides, that are capable of forming water-soluble inclusion complexes with (macro)molecular guests with varying affinity depending of the size of their cavity.²²¹ They have emerged as a versatile and accessible class of molecules for the assembly of supramolecular hydrogels, with a specific emphasis on host–guest binding between β CD and adamantane or azobenzene.^{66,108,222–224} Of interest, some CDs can thread on polymer chains resulting in the formation of poly(pseudo)rotaxanes.^{106,225–227} This threading behavior varies with the size of the host cavity—for example, α CD threads efficiently onto PEG while β CD onto poly(propylene glycol).²²⁷ In the case of multiple α CD molecules threading on a single PEG chain, a polypseudorotaxane, or molecular necklace, is formed.¹⁰⁶ This extended arrangement often results in the formation of larger

crystalline aggregates, that can facilitate interactions between polymer chains or material building blocks.^{211,228} Polypseudorotaxanes have been exploited as supramolecular cross-links to assemble hydrogels from polymeric and nanoparticulate building blocks, including for drug delivery applications.^{124,229–233} Of note, Dreiss and co-workers demonstrated that α CD could precipitate PEGylated silica NPs into hydrogels and characterized the design space for gel formation.²³¹ Similar design principles have been applied to assemble colloidal hydrogels from block copolymer NPs, PEGylated inorganic NPs, and PEG-functionalized dendrimers or branched polymers.^{124,232–236} Motivated by these findings¹⁰⁵, we hypothesized that the formation of polypseudorotaxanes on the surface of PEGylated NPs would serve as a generalizable interaction between polymers and NPs for the formation of PNP hydrogels, enabling modular exchange of the constituent components and enhancing their mechanical properties.¹⁰⁶

In this work, we demonstrate that α CD-based supramolecular polypseudorotaxanes comprise a facile strategy to reinforce and expand the PNP hydrogel platform. The inclusion of α CD with PEGylated NPs and a support polymer formed CD-modified PNP hydrogels (CD–PNP hydrogels). The mechanical properties of CD–PNP hydrogels were enhanced by orders of magnitude as compared with non-modified PNP hydrogels while maintaining shear-thinning and self-healing properties, enabling injectability of robust hydrogels. Further, the use of this simple supramolecular motif allowed us to decouple rheological properties and material functionality. The modular nature of the CD–PNP platform enabled us to exchange structural components from a library of polymers and functional NPs. CD–PNP hydrogels were formed with biopolymers for high-fidelity 3D printing and tissue engineering as well as with inorganic NPs to engineer conductive or magnetic materials. Overall, supramolecular reinforcement provided facile assembly of a diverse set of functional and moldable nanocomposite hydrogels.

2.2. RESULT AND DISCUSSION

2.2.1. Supramolecular reinforcement of PNP hydrogel

Base PNP hydrogels were prepared by mixing HPMC (1 wt%) with colloiddally-stable block-co-polymer NPs (PEG_{6k}-b-PLA_{18k} NPs, 5 wt%; **Figure 1a**), relying on the hydrophobic interactions between the components for network formation.¹⁸ Simple mixing of the two liquid suspensions spontaneously formed a viscoelastic gel with shear-thinning and self-healing behavior. The PNP hydrogels formed with a shear storage modulus of $G' \approx 18.4$ Pa ($\omega = 10$ rad s⁻¹). This is consistent with similar formulations of PNP hydrogels in the literature ($G' \approx 10$ –1000 Pa at $\omega = 10$ rad s⁻¹).^{143,203,219} The base PNP hydrogels exhibited shear-thinning and self-healing properties, which have enabled their use as injectable and sprayable biomaterials.^{17,219,237,238} However, one constraint of this versatile platform is the limited range of mechanical properties accessible through hydrophobic polymer–nanoparticle interactions. Further, the building blocks are restricted to select pairs of polymers and NPs.²⁰³

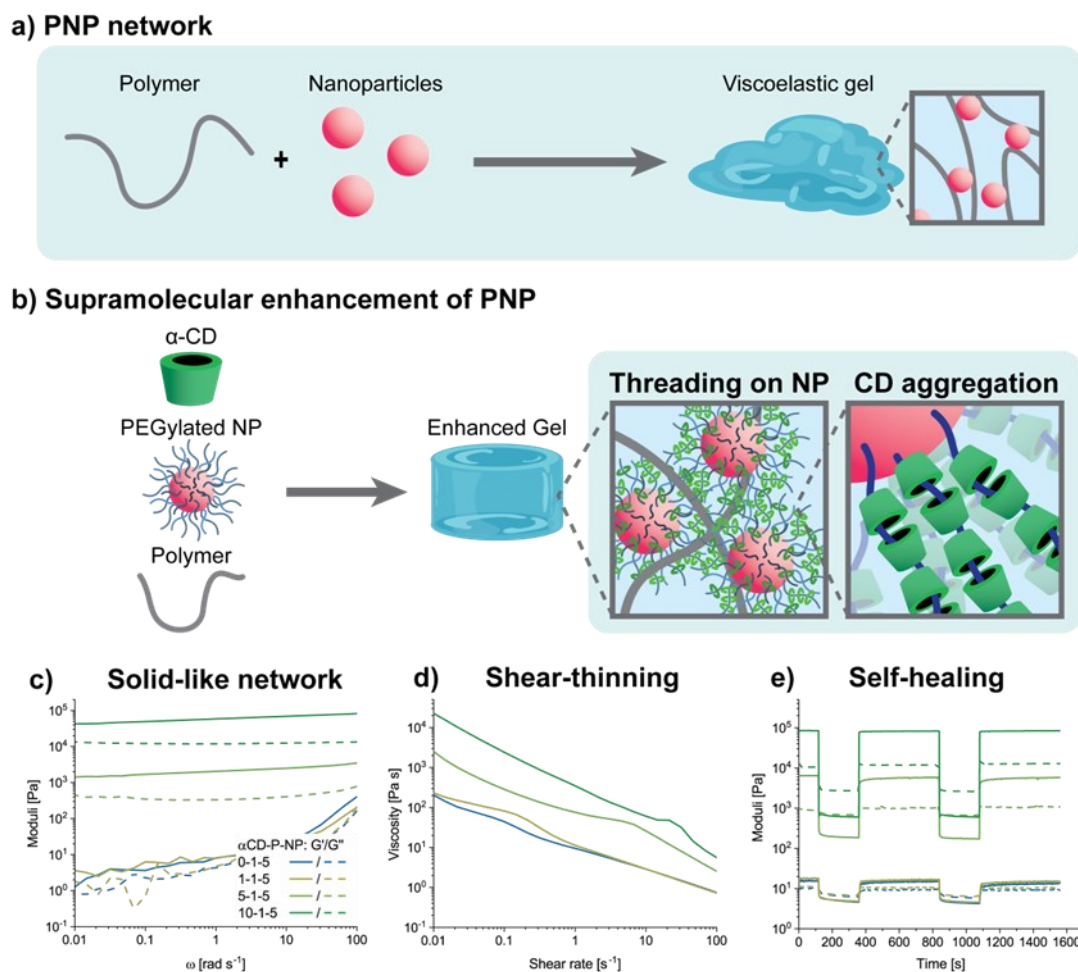


Figure 1: Supramolecular reinforcement of polymer-nanoparticle (PNP) hydrogels. *a)* PNP hydrogels form upon mixing separate liquid solutions of polymer and nanoparticles. The reversible interactions between the polymer chains and NPs result in the formation of a viscoelastic network. *b)* α CD was used here as a supramolecular motif to enhance the mechanical properties of PNP hydrogels. The addition of α CD resulted in the formation of polypseudorotaxanes on the surface of the PEGylated NPs. *c)* The addition of α CD to the formulation increased the shear storage modulus, G' , by several orders of magnitude, indicating enhanced polymer–nanoparticle and/or nanoparticle–nanoparticle interactions. Further, the storage moduli of α CD–PNP formulations exhibited attenuated frequency dependence as compared with base PNP hydrogels (PNP: $G' \sim \omega^{0.3}$; CD–PNP: $G' \sim \omega^{0.1}$). *d)* An increase in low-shear viscosity, η_0 , was measured with increasing α CD content, while the shear-thinning properties were preserved. *e)* CD–PNP hydrogels retained the ability to recover their initial viscoelastic properties rapidly (self-heal) following cycles of high strain ($\gamma > 10\%$).

In the literature, α CD has been used to precipitate solid-like hydrogels via increased NP–NP interactions.^{124,229–233} Based on these findings, we hypothesized that including α CD in the PNP formulation would induce NP–NP interaction through polypseudorotaxane formation, resulting in enhanced mechanical properties and modular design (**Figure 1b**). Addition of α CD increased the shear

storage modulus of the hydrogels by several orders of magnitude (samples containing 1, 5, and 10 wt% α CD exhibited $G' \approx 1.7 \times 10^1$, $\approx 3.0 \times 10^3$, and $\approx 6.5 \times 10^4$ Pa at $\omega = 10$ rad s⁻¹, respectively; **Figure 1c**; **Figure S1**). Further, the storage moduli of α CD-reinforced PNP hydrogels (CD–PNP) exhibited attenuated frequency dependence as compared with standard PNP hydrogels (PNP: $G' \approx \omega^{0.3}$; CD–PNP: $G' \approx \omega^{0.1}$), consistent with slower dynamics and increased particle jamming.^{142,239} The reinforcement with α CD was effective for NPs presenting PEG with a range of molecular weights (3–11 kDa; **Figure S2**). The concentration-dependent increase in mechanical properties suggested enhanced polymer–nanoparticle and/or nanoparticle–nanoparticle interactions (**Figure 1b, c**). We hypothesized that the mechanical reinforcement was the result of increased NP jamming through the formation of supramolecular polypseudorotaxane interactions following α CD threading on the PEG chains at the NP surface.¹⁰⁶ Further supporting the hypothesis, α CD induced the precipitation of the NPs in the absence of a support polymer (**Figure S3**). β CD and γ CD, which have affinity to PEG, showed limited mechanical reinforcement (**Figure S4**) and interaction with the NPs (**Figure S5**), further supporting the threading of α CD on PEG as driving force of the enhancement.

The increase in shear moduli was, however, only present for formulation with α CD content at or beyond 5 wt% (**Figure S1**). Formulations with lower α CD content (1 wt% and 2.5 wt%) did not show significant changes as compared with control PNP hydrogels without α CD. The threshold α CD concentration did not show dependence from NP content as formulations with varying NP content (1, 2, 3, and 5 wt%; **Figure 1c**, **Figure S6**) as each formulation required a minimum of 5 wt % α CD to formulate a robust, solid-like network ($G' > G''$, **Tables S1 and S2**; **Figures S6-7**). We associated this behavior to a minimum α CD concentration required to induce sufficient aggregation of the NPs, below which the polymer–NP interactions remained dominant, whereas above NP–NP interactions prevailed. The changes in dominant interaction were speculated to influence the microstructure of the material resulting in the observed changes in the emerging macroscopic properties. The possible changes in PNP microstructure in the presence of α CD were investigated further in **Chapter 4** using super-resolution optical microscopy.

The ability to flow upon applied stress and reform a stable network after cessation of the applied stress are critical design features of injectable or ejectable materials. Addition of α CD to the PNP hydrogels did not hinder injectability, with CD–PNP hydrogel exhibiting shear-thinning and self-healing behaviors (**Figure 1d, e**). The low-shear viscosity, η_0 , increased with α CD content while maintaining a high flow index ($n \approx 0.25$; **Figure 1d**). The apparent yield stress, σ_y , also increased with α CD content ($\sigma_y \approx 2.1$, 2.5, 17.5, and 165.5 Pa at $dy/dt = 0.01$ s⁻¹ for α CD = 0, 1, 5, and 10 wt%, respectively), consistent with the increased modulus. The yield strain, γ_y , decreased with increasing α CD content (**Figure S1b**), again consistent with increasing NP jamming.^{240,241} The dramatic increase in G' compensated for the lower γ_y , providing for the significant increase in σ_y . Importantly, CD–PNP hydrogels recovered their initial viscoelastic properties rapidly (self-healed) following cycles of high strain ($\gamma > 10\%$; **Figure 1e**).

Overall, these results demonstrated that the simple addition of α CD could be used as a supramolecular reinforcement to augment the viscoelastic properties of this class of materials. In this manner, we were able to modulate the viscoelastic properties of CD–PNP hydrogels by tuning the concentration of α CD in the system while maintaining shear-thinning and self-healing properties.

2.2.2. Supramolecular Bonding Enables Modular Design of CD–PNP Hydrogels

In addition to enhancing their mechanical properties, the inclusion of α CD enabled modular design of CD–PNP gels. As CD–PNP network formation leveraged the supramolecular binding motif in addition to interactions between polymer chains and NPs, the constituent polymer and/or the NP could be exchanged (Figure 2a).

a) Building block tunability

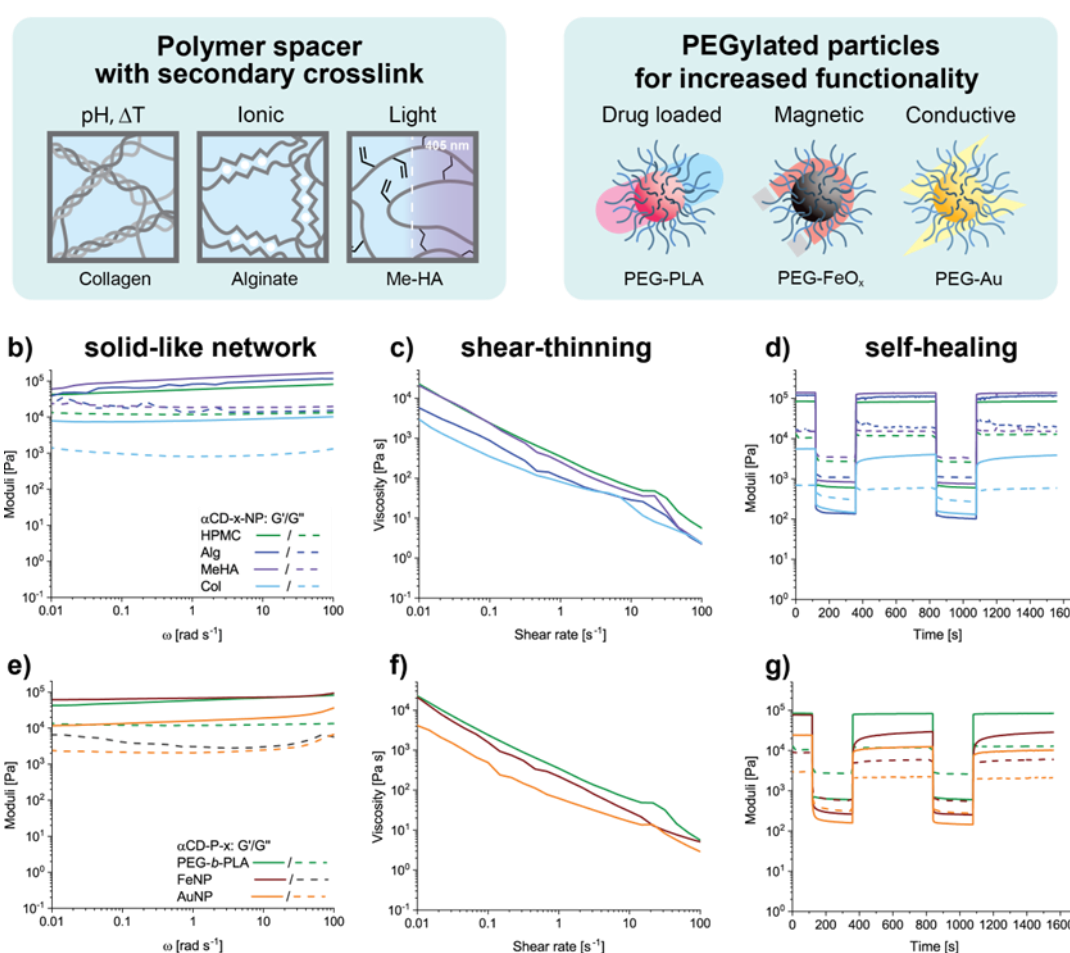


Figure 2: Supramolecular bonding enables modular design of CD–PNP hydrogels. a) The inclusion of α CD enabled us to exchange the constituent polymer and/or the NP in CD–PNP hydrogels. HPMC was exchanged for methacrylated hyaluronic acid (MeHA), alginate (Alg), and collagen type I (Col). Additionally, we prepared CD–PNP hydrogels with other PEGylated NPs, such as iron oxide NPs (FeNPs) and gold NPs (AuNPs). b) CD–PNP hydrogels formed solid-like materials ($G' \gg G''$) with attenuated frequency dependence for all polymers tested. c) Similar shear-thinning properties were observed independent of the formulation. d) The self-healing behavior was retained for CD–PNP

hydrogels formulated with different polymers. e) CD–PNP hydrogels formed solid-like materials ($G' \gg G''$) with low frequency dependence f) Similar shear-thinning properties were observed independent of the NPs used. g) The self-healing behavior was retained for all CD–PNP gels.

HPMC was substituted with other biopolymers commonly used in hydrogel fabrication, including methacrylated hyaluronic acid (MeHA 1 wt%), alginate (Alg 2 wt%), and collagen type I (Col 0.4 wt%). Each CD–PNP formulation exhibited solid-like properties ($G' \gg G''$) with low frequency dependency ($G' \approx \omega^{0.05-0.1}$, **Figure 2b**). As previously stated, we hypothesized that the formation of polypseudorotaxanes and increased NP–NP interaction controlled network formation and properties above a threshold concentration. As a result, specific polymer–NP interactions were less relevant for network formation, enabling the use of various support polymers including those with limited interactions with the NPs. The absence of noticeable interactions between α CD and the various support polymers (HPMC, MEHA, Alg, or Col) corroborated this hypothesis (**Figure S8**). Further, the presence of the support polymer was still required for network formation as without the mixture of α CD and NP precipitated, indicating that the polymer was necessary to keep the interacting particles colloidally stable. The shear-thinning and self-healing behavior was preserved for CD–PNP gels comprised of each polymer (**Figure 2c,d**). The exchange of the support polymer allowed for secondary cross-linking and stabilization of the CD–PNP hydrogels. Secondary cross-linking was achieved with light (MeHA), addition of divalent cations (Alg), or environmental control (temperature and pH; Col). For each polymer, the CD–PNP gel exhibited suitable rheology for injection or 3D printing and provided a handle for stabilization of the material after initial application.

After demonstrating that supramolecular reinforcement enabled interchange of the support polymer, we also explored the ability to exploit α CD to form CD–PNP gels with different NPs. Exploiting α CD threading onto PEG chains, we prepared CD–PNP hydrogels with other PEGylated NPs, namely iron oxide NPs (FeNPs) and gold NPs (AuNPs). In each case, the inorganic NPs were functionalized with 5 kDa PEG. In the case of AuNPs, we combined AuNPs (5 wt%) with PEG-*b*-PLA NPs (2.5 wt%), demonstrating the utility of the supramolecular motif for the formation of multicomponent nanocomposite hydrogels. Each CD–PNP formulation exhibited solid-like properties over the whole frequency spectrum (**Figure 2e, S9**). Further, modifying the NP character did not affect the shear-thinning and self-healing properties of the gels (**Figure 2f,g**).

2.2.3. Supramolecular Bonding Enables Modular Design of CD–PNP Hydrogels

In direct ink writing, or semi-solid extrusion, inks with shear-thinning and self-healing properties are needed to enable extrusion through the nozzle and ensure shape retention after printing.²⁴² Based on the rheological properties of CD–PNP hydrogels, Col- and MeHA-based formulations were prepared as biomaterial inks to fabricate complex structures with a pneumatic-driven 3D printer (BioX) and to enable secondary cross-linking after the printing for material stability. Col and MeHA can be difficult to use as single component bioinks as their viscosity is often too low for suitable shape retention.²⁴³ We

printed a miniaturized trachea using a Col-CD-PNP ink (α CD 7.5 wt%, PEG-*b*-PLA NPs 5 wt%, Col 0.4 wt%) as a representative 3D anatomical model (Figure 3a,b). The robust elasticity and apparent yield stress allowed for direct printing of high profile and free-standing 3D objects (32 layers, 0.3 mm layer height). A model heart valve was printed with a MeHA-CD-PNP ink (α CD 10 wt%, PEG-*b*-PLA NPs 5 wt%, MeHA 1 wt%; **Figure 3c**). The complex scaffold retained its shape with high fidelity prior to and after photo-cross-linking ($\lambda = 405$ nm, $I = 10$ mW cm⁻², and $t = 2$ min), which was performed at the end of the printing process.

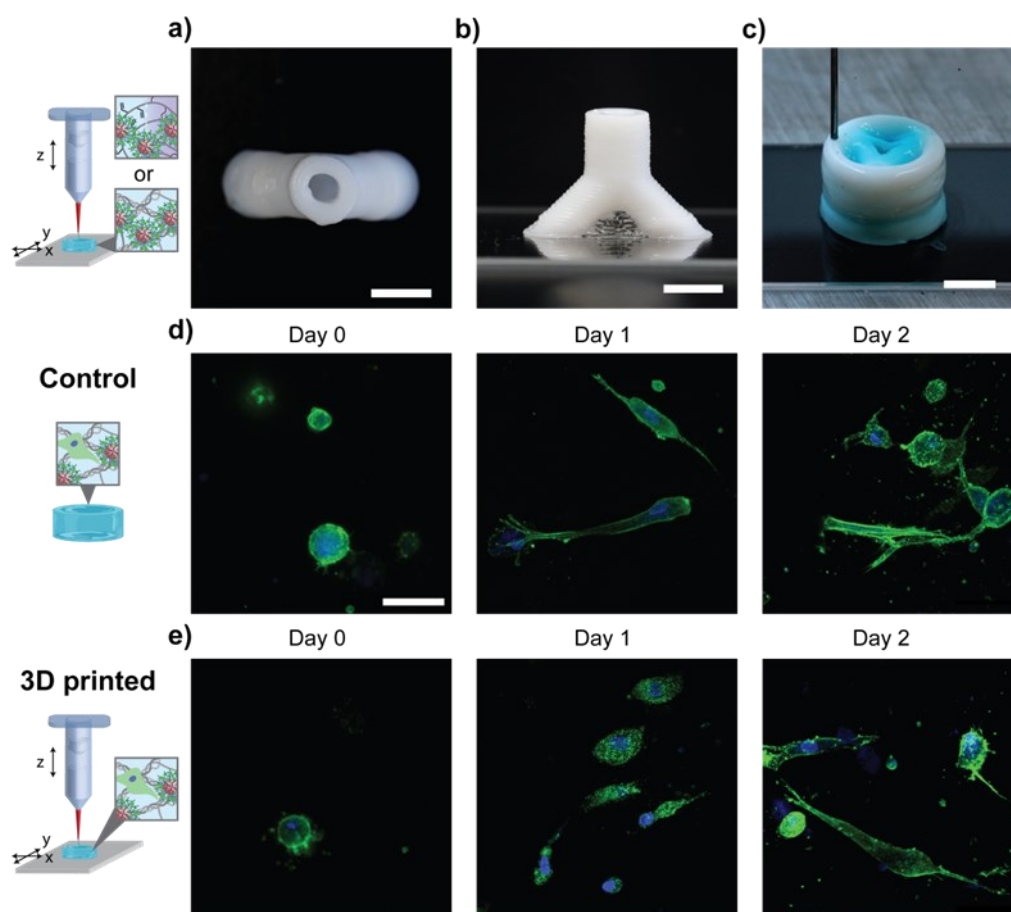


Figure 3: Direct ink writing and biofabrication with CD-PNP (bio)inks. a) A mini trachea model was printed with a Col-CD-PNP ink (α CD 7.5 wt%, 5 PEG-*b*-PLA NPs wt% and Col 0.4 wt%) at 7 °C. Top view image of the free- standing mini-trachea. b) Lateral image of the mini trachea. Scale bars, 5 mm. c) A model heart valve was printed using a MeHA-CD-PNP ink (α CD 10 wt%, PEG-*b*-PLA NPs 5 wt%, and MeHA 1 wt%). During and after extrusion, the printed scaffold retained its shape and was subsequently photo-cross-linked ($\lambda = 405$ nm, $I = 10$ mWcm⁻², and $t = 2$ min) to stabilize the printed construct. Scale bar, 5 mm. d) Primary human mesenchymal stem cells (hMSCs; 2×10^6 cells mL⁻¹) were encapsulated in a Col-CD-PNP bioink (α CD 5 wt%, PEG-*b*-PLA NP 5 wt%, and Col 0.4 wt%). The cell-laden bioink was used to prepare non-printed control gels and bioprinted constructs. The samples were imaged over the course of 2 days to monitor cell spreading. The cell nucleus was labelled DAPI (blue) and the actin cytoskeleton was labelled with Alexa Fluor 488 Phalloidin (green). Confocal

images at day 0, 1, and 2 after printing revealed similar spreading in both control and printed samples. Scale bar, 50 μm .

CD–PNP inks were also used for bioprinting. Here, primary human bone-marrow-derived stromal cells (hMSCs; 2×10^6 cells mL^{-1}) were included in the Col-CD–PNP bioink (αCD 5 wt%, PEG-*b*-PLA NP 5 wt%, and Col 0.4 wt%). A formulation containing αCD 5 wt% was used to provide sufficient mechanical properties for bioprinting while mitigating potential cytotoxicity.²⁴⁴ The presence of cells did not affect the printability and the constructs were stabilized after printing by inducing collagen fibrillogenesis (37 °C, 5% CO_2 for 90 min). The cells exhibited similar viability (>80%, **Figures S10 and S11**) in nonprinted control and bioprinted scaffolds. The high viability was attributed to the reduced shear stress experienced by the cells in the shear-thinning and self-healing bioink.^{245–248} Collagen provides a beneficial environment for cell adhesion and spreading through natural peptide motifs, such as RGD peptides. Encapsulated cells spread similarly in both nonprinted control and bioprinted samples at days 0 and 2 after encapsulation (**Figure 3d, e**). These results demonstrated the potential of the CD–PNP platform to formulate (bio)inks for direct ink writing and biofabrication. Cytocompatible biopolymers usually difficult to print were easily included in the CD–PNP hydrogels, allowing for modular (bio)ink design. The properties of the CD–PNP (bio)inks enabled high print fidelity and the fabrication of high-aspect ratio structures while supporting cell growth. Further, all components used in the CD–PNP (bio)inks are generally regarded as safe (GRAS), facilitating their future use for biomedical applications.

2.2.4. Modular Design Enables Tailored Functionality of CD–PNP Hydrogels

The supramolecular polypseudorotaxane motif enabled modular design of CD–PNP hydrogels with facile exchange of PEGylated NPs. We leveraged the functionality of each NP as a drug carrier, electroconductive component, or magnetic building block to design CD–PNP hydrogels with versatile properties.

PEG-*b*-PLA NPs were leveraged for the design of dual release of hydrophilic and hydrophobic therapeutics. On one hand, we entrapped FITC-labeled bovine serum albumin (FITC-BSA) in the hydrogel matrix as a model hydrophilic macromolecular therapeutic, while Oil Red O (OR) was loaded in the core of PEG-*b*-PLA NPs as a model hydrophobic small molecule therapeutics (**Table S3**).^{18,143} Release of the FITC-BSA, followed a diffusion-based release of the therapeutics, which did not show strong dependence from the introduction of αCD . The release of OR, followed an erosion-based release from the hydrogels which showed a slight delay with addition of αCD that correlated with the increase of mechanical properties induce by αCD . Further analyses of the release studies were performed by Giovanni Bovone and can be found in the Appendix. Overall, these results demonstrated that αCD -reinforcement had a minimal effect on the release of hydrophilic macromolecules; however, it slowed the erosion of CD–PNP scaffolds and delayed the release of OR by 2 days.

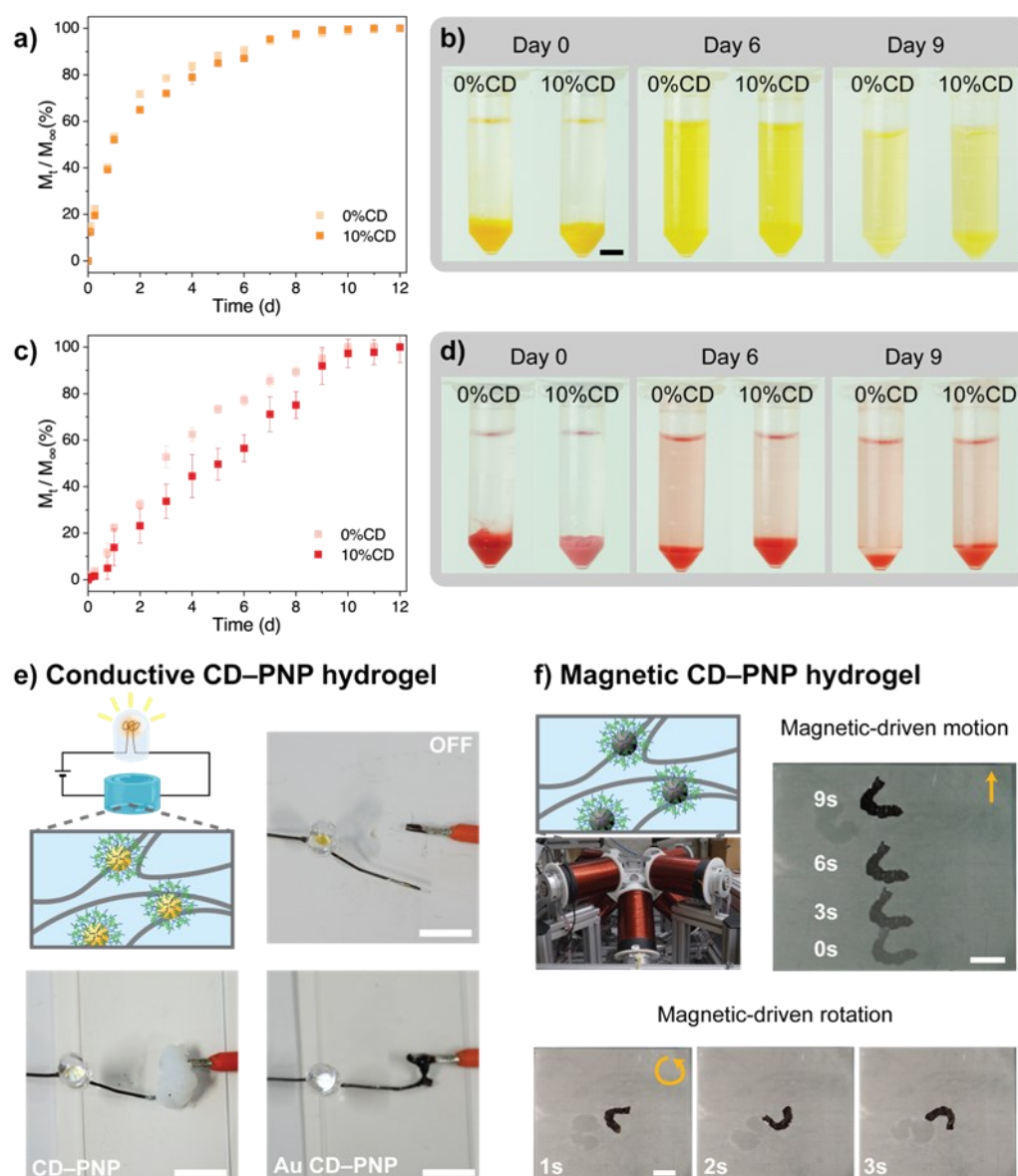


Figure 4: Modular design enables tailored functionality of CD-PNP hydrogels. *a)* Fractional release of the hydrophilic macromolecule FITC-BSA, entrapped in the bulk of the hydrogel, over 12 days. Hydrogels with (α CD 10 w/w%, PEG-*b*-PLA NPs 5 wt%, HPMC 1 wt%, and FITC-BSA 1 wt%) and without (α CD 0 wt%, PEG-*b*-PLA NPs 5 wt%, HPMC 1 wt%, and FITC-BSA 1wt%) α CD released the macromolecular cargo via diffusion at a similar rate (**Figure S12a**). *b)* Pictures of the hydrogels loaded with FITC-BSA on days 0, 6, and 9. Scale bar, 0.5 cm. *c)* Fractional release of the hydrophobic small molecule Oil Red O (OR), encapsulated in the core of PEG-*b*-PLA NPs, over 12 days (OR-loading \sim 0.2 wt%). Hydrogel samples without α CD 0 wt% released 80% of the OR cargo over 6 days, whereas CD-PNP gels with 10 wt% α CD exhibited slower release (**Figure S12b**). *d)* Pictures of the hydrogels loaded with OR at days 0, 6, and 9. *e)* CD-PNP hydrogels were formed with PEGylated AuNPs (Au-CD-PNP: α CD 10 wt%, AuNPs 5 wt%, PEG-*b*-PLA NPs 2.5 wt% and HPMC 1 wt%). The gel was connected with a LED and a battery in series. When the circuit was closed, the LED emitted light

demonstrating the ability of the Au-CD-PNP hydrogel to conduct electrical current. Scale bar, 1 cm. f) An electromagnetic manipulation setup, OctoMag, was used to guide locomotion magnetically of iron oxide NP CD-PNP hydrogels (Fe-CD-PNP: α CD 10 wt%, FeNPs 6wt%, and Alg 2 wt%). [63] A time-lapse of Fe-CD-PNP gel floating in a solution shows gel motion in the x-y plane. Similarly, the Fe-CD-PNP sample was rotated in a rotating magnetic field. Scale bar, 4 mm.

To further expand the scope of possible applications of CD-PNP hydrogels, iron oxide NPs (FeNPs) and gold NPs (AuNPs) were included as structural components. To engineer electroconductive CD-PNP hydrogels, we included PEGylated AuNPs into the CD-PNP formulation (Au-CD-PNP: α CD 10 wt%, AuNPs 5 wt%, PEG-*b*-PLA NPs 2.5 wt%, and HPMC 1 wt%) and integrated the hydrogel as part of an electric circuit. (**Figure 4e**). By closing and opening the circuit using the Au-CD-PNP hydrogel, it was possible to switch a light-emitting diode (LED) on and off, demonstrating the conductive properties of the material. A nonconductive CD-PNP hydrogel (α CD 10 wt%, PEG-*b*-PLA NPs 5 wt%, and HPMC 1 wt%) did not allow current to flow through the circuit. To design magnetic CD-PNP hydrogels, we formulated samples with PEGylated FeNPs (Fe-CD-PNP: α CD 10 wt%, FeNPs 6 wt%, and Alg 2 wt%). The hydrogels were molded into a horseshoe shape, stabilized via Ca^{2+} cross-linking, and placed in an aqueous bath (**Figure 4f**). The floating position of the scaffold was controlled by an electromagnetic manipulation setup, OctoMag.²⁴⁹ The axial and lateral movement of the hydrogel was controlled by using an external magnetic field (1 mT). Similarly, we rotated (clockwise or counter-clockwise) the Fe-CD-PNP construct by rotating the applied magnetic field (0.3 Hz, 1 mT). Overall, α CD-reinforcement enabled us to include various PEGylated NPs as hydrogel building blocks to design drug-loaded, conductive, and magnetic materials. This modular approach broadened the application spectrum of CD-PNP hydrogels without the need to re-engineer the network interactions.

2.3. CONCLUSION

We applied a simple supramolecular approach to expand the possible interactions for the formation of PNP hydrogels. Our approach was motivated by evidence that α CD can thread onto PEGylated NPs, enhancing NP-NP interactions through polypseudorotaxane formation.^{124,229–236} We leveraged this approach to engineer CD-PNP hydrogels through the inclusion of α CD in the formulation, which provided mechanical reinforcement and modular exchange of the hydrogel building blocks. As characterized via shear rheometry, α CD enhanced the viscoelastic properties of CD-PNP hydrogels by orders of magnitude while preserving the ability to shear-thin and self-heal. Further, the inclusion of α CD enabled the use of a variety of functional polymers and PEGylated nanoparticles without significant changes in the viscoelastic properties. To demonstrate the versatility of this platform, we formulated (bio)inks for direct ink writing, and fabricated complex 3D structures and bioprinted cell-laden scaffolds for tissue engineering. Biocompatible CD-PNP hydrogels were also prepared as drug delivery platforms for the release of small molecule and macromolecular compounds. Finally, electroconductive Au-CD-PNP hydrogels were formulated with PEGylated AuNPs and PEGylated FeNPs were used as building blocks to introduce magnetic responsive properties. The overall approach

to leverage supramolecular binding motifs to enhance the mechanical properties and expand the possible building blocks of polymer–nanoparticle hydrogels simplifies (bio)material design and broadens the range of applications that can be targeted with this class of materials.

2.4. MATERIALS & METHODS

2.4.1. Materials

α -Cyclodextrin (α CD, Ref C0776) hydroxypropyl- β -CD (β CD, Ref H0979), and γ -cyclodextrin (γ CD, Ref C0869) were purchased from TCI Chemicals (Tokyo, Japan). Hydroxypropylmethylcellulose (HPMC; Mn \sim 700 kDa, Ref. H3785), poly (ethylene glycol) methyl ether (PEG; Mn 5000 Da, Ref. 81323), poly(ethylene glycol) methyl ether (PEG; Mn 10 kDa, Ref. 732621), methacrylic anhydride (MA; Ref 276685), 3,6-dimethyl-1,4-dioxan-2,5-dion (lactide; Ref. 303143), tin(II)-2-ethylhexanoate (SnOct2; Ref. S3252), 4-(2-hydroxyethyl)-1-piperazine-ethanesulfonic acid (Hepes; 99%, Ref H3375), oil Red O (OR; Ref O0625), iron(II)oxide (FeCl₂, Ref 372870), iron(III)oxide (FeCl₃, Ref 157740), (3-aminopropyl)triethoxysilane (Ref A33648), triethylamine (Ref T0886), calcium chloride (CaCl₂; Ref 21074), sodium hydroxide (NaOH, Ref 71690) diethyl ether(Ref. 32203), ethyl acetate(Ref. 34858), and methanol (MeOH, Ref 34885) were purchased from Sigma-Aldrich (Buchs, Switzerland). Methoxy poly (ethylene glycol)-*b*-poly(D,L-lactide) (PEG-*b*-PLA; Mw 3000:20'000 Da; Ref. AK165) was purchased from AKiNA. Toluene (Ref 36441) and hexane (Ref 36437) were purchased from Chemie Brunschwig AG. Sodium alginate (Alg; Grade I-1G-80) was purchased from Kimica International (Tokyo, Japan). Sodium hyaluronate (HA; Mw \sim 700 kDa, Ref HA700K) was purchased from Lifecore (Chaska, MN, USA). Collagen (Col;10 mg/ml, Ref 5133) was purchased from Advanced BioMatrix (San Diego, CA, USA). Acetone (Ref 20066.296) was purchased from VWR Chemicals. Low glucose DMEM (Ref 22320-022), Pen Strep (PS, Ref 15140-122), FGF (Ref. PHG0026), and fetal bovine serum (FBS; Ref 10270106), LIVE/DEAD Viability/Cytotoxicity kit (Ref L3224), AlexaFluor 488 Phalloidin (Ref A12379) were purchased from ThermoFisher. Spherical gold NPs with a diameter of 10 nm were purchased from Nanopartz (Ref A11-10-CIT-DIH-1). For the synthesis of iron oxide NPs oleic acid (Ref AB333867) was purchased from ABCR chemicals (Karlsruhe, Germany). Inorganic NP PEGylation was performed with methoxy PEG–thiol (Mw \sim 5 kDa, Ref A3029, JenKem, USA) or methoxy PEG–succinimidyl succinamide (Mw \sim 5 kDa, Ref A3143, JenKem, USA).

2.4.2. Instrumentation and characterization

UV-visible and fluorescent spectroscopy

UV-visible and fluorescent spectroscopy were performed on a Hidex Sense plate reader.

Nuclear magnetic resonance (NMR)

¹H-NMR spectra were acquired on a Bruker Avance III 400 (Bruker BioSpin GmbH). Chemical shifts were reported relative to the respective solvent peak. (CDCl₃: δ = 7.26 ppm; D₂O: δ = 4.79 ppm) Molecular weight of methyl ether-PEGs were determined using the terminal CH₃ groups as a reference.

Fourier-transform infrared spectroscopy

Attenuated total reflection Fourier-transform infrared spectroscopy (ATR-FTIR) spectra were acquired on a Perkin-Elmer, ATR Spectrum TWO equipped with a UATR single reflection diamond. Sample powders were pressed onto the diamond crystal with a pressure arm and a spectrum was recorded between 500 and 4000 cm^{-1} averaging over 32 scans.

Dynamic light scattering and electrophoretic mobility

The hydrodynamic diameter, D_h of the formed NPs were measured by dynamic light scattering (DLS; Malvern ZetaSizer Nano ZS). The NP suspensions were placed into a semi-micro cuvette (Brand, Path length: 10 mm) and the measurements were performed at 25 °C, and with a wavelength of 633 nm and a scattering angle of 173°. The properties of each sample were measured three times, and we reported the z-average diameter and dispersity, \bar{D} .

Size exclusion chromatography

The polymer dispersity (PDI) of PEG-*b*-PLA was characterized via size exclusion chromatography (SEC; Viscotek TDAmx) (**Figure S13**). The system was equipped with a differential refractive index detector (TDA 302, Viscotek) and two columns (D3000, poly(styrene)-co-divinylbenzene). The synthesized polymers were dissolved in the mobile phase, DMF with 0.1 wt% LiBr, and filtered with 0.2 μm polytetrafluoroethylene (PTFE) syringe filters. The polymer properties were compared to a poly(methyl methacrylate) standard curve (PSS Polymer Mainz; 2500 to 89, 300 g mol^{-1}) which was determined using a mobile phase flow rate of 0.5 mL min^{-1} . The PDI was computed as the ratio of the weight average molecular weight (M_w) over the number average molecular weight (M_n) from three independent samples of the same batch.

2.4.3. Synthetic procedures

*PEG-*b*-PLA synthesis*

General procedure for the synthesis of PEG-*b*-PLA. The synthesis is described for PEG 6 kDa as limiting reagent. In a similar manner PEG 11 kDa was used as a reagent. Except if stated otherwise, PEG length used for the studies was 6 kDa. In a flame-dried flask, lactic acid (11.2 g, 77.5 mol) and polyethylene glycol ($M_n = 5000$, 3.5 g, 698.8 μmol) were dissolved in 30 mL of dry freeze pump thawed toluene under an argon atmosphere. The mixture was heated to 100°C and stirred upon complete dissolution of the starting materials. Then, SnOct_2 (317 μL , 978 μmol) was added to the reaction mixture. The temperature was subsequently raised to 140°C and the reaction was left under reflux for 6h. The mixture was then poured in cold ether. The solid residue was filtered and redissolved in DCM. The precipitation was repeated twice. The resulting colorless solid was dried in vacuo to obtain PEG-*b*-PLA. Characterization: $^1\text{H-NMR}$ (400 MHz, CDCl_3): $\delta = 5.29 - 5.05$ (m, 237H), 4.39 – 4.21 (m, 3H), 3.76 – 3.52 (m, 555H), 3.37 (s, 3H), 1.64 – 1.41 (m, 725H). Molecular weight by $^1\text{H-NMR}$: PEG 6 kDa, PLA

18 kDa. GPC (poly(styrene)-co-divinylbenzene calibration): $M_n = 34$ kDa, $M_w = 41$ kDa, PDI = 1.23. **(Figure S13-15)**

PEG-b-PLA NP formation

Polymeric core-shell NPs were formed via batch nanoprecipitation. 140 mg of PEG-*b*-PLA were dissolved in 2.5 mL acetone. The solution was added dropwise to 10 mL of H₂O under stirring. Acetone was evaporated overnight by keeping NP suspension in an open container inside the fume hood. NPs were subsequently concentrated via ultrafiltration with an Amicon Ultra centrifugation filter (MWCO: 30 kDa, 4500 RPM, 1.1h). The NPs were resuspended to a final concentration of 20 wt%. Size of the NPs was determined by DLS measurements (**Table S5**).

PEGylated gold NP synthesis

PEGylation of gold NPs was performed as described previously.²⁵⁰ Protocol is formulated for 1 mg of PEG. A 10 mg/mL stock solution of 5 kDa PEG-SH in milli-Q water was prepared. In an eppendorf 1900 μ L gold nanoparticle (0.05 mg/mL, 10 nm, stabilized with citric acid) were mixed with 100 μ L of the PEG-SH stock solution. The reaction was stirred at room temperature overnight. The excess mPEG-SH was removed through multiple cycles of centrifugation at 15 000 rpm for 2 hours. The supernatant was removed and disposed of between each cycle followed by resuspension of the NP in water. The Presence of PEG on the particle was determined by ¹H-NMR (**Figure S16, 17**).

PEGylated iron oxide NP synthesis

Oleic acid-coated iron oxide NP synthesis. The synthesis of iron oxide NPs was carried out following the work of Sun and coworkers.²⁵¹ 0.7 g FeCl₃ ($4.28 \cdot 10^{-3}$ mol) and 0.26 g FeCl₂ ($2.01 \cdot 10^{-3}$ mol) were dissolved in 20 mL water that was degassed via sonication and argon sparging. 20 mL of 1 M NaOH solution, 10 mL acetone, and 0.2 mL oleic acid were degassed and heated to 83°C. The iron-solution was added dropwise while mechanically stirring. Additional 0.8 mL of oleic acid were added dropwise, and the suspension was stirred for additional 10 min. The iron oxide NPs were washed three times with 200 mL of acetone/methanol (1:1), separated from the supernatant with the help of a neodymium magnet, and dried. Ligand exchange and particle PEGylation A method developed by Larsen et al. was used for iron oxide NPs PEGylation.^{252,253} 10 mg of oleic acid-coated iron oxide nanoparticles were dissolved in toluene at a concentration of 5 mg mL⁻¹. 125 mg of NHS-PEG 5 kDa were dissolved in the NP suspension. 3 μ L SI-NH₂, 0.5 mL of triethylamine, and 10 μ L of H₂O were added sequentially to the NP solution. The suspension was stirred for 24 h and the iron oxide NPs were precipitated in 20 mL hexane and NPs sedimented onto a neodymium magnet. The supernatant was discarded, and the residual hexane was evaporated. The dry iron oxide NPs were resuspended in 1.5 mL of acetone and recollected after centrifugation. The washing step was repeated with 1.5 mL H₂O. After centrifugation, the supernatant was discarded, and the particles were resuspended in a total of 176 μ L H₂O. The Presence of PEG on the particle was determined by FT-IR (**Figure S18**).

Methacrylate hyaluronic acid synthesis

Methacrylate hyaluronic acid (MeHA) was synthesized as described previously.¹¹ In brief, hyaluronic acid (HA, 2.5 g) was dissolved in dH₂O (150 mL) and the initial pH of the solution was adjusted to 8.5. While stirring the HA solution at 4 °C (on ice bath) methacrylic anhydride (MA, 4.64 mL) was added dropwise. Thereafter, the pH of MeHA-solution was maintained constant at pH 8.0 – 9.0 with addition of 1 M NaOH for 5 hours. The solution was kept overnight on stirring at room temperature (22 °C). Then, the solution was transferred to dialysis tubing (SnakeSkin™ dialysis tubing, 3.5 MWCO, Ref 88244, Thermo Scientific) and dialyzed against water for 7 days. The water was changed twice daily. The MeHA solution was then frozen (-20 °C) and lyophilized for 3 days. ¹H-NMR in D₂O was used to quantify the degree of functionalization of 20% from integration of the vinyl group ($\delta = 5.8$, 1H and $\delta = 6.2$, 1H) normalized to the HA backbone ($\delta = 3.12 - 4.21$, 10H) (**Figure S19**).

Lithium phenyl-2,4,6-trimethylbenzoylphosphinate (LAP) synthesis

LAP was synthesized as described previously.^{254,255} In brief, dimethyl phenylphosphonite (3g; 0.018 mol) was dissolved at room temperature in 2,4,6-trimethylbenzoyl chloride (3.2g; 0.018 mol) under argon and stirring. The reaction proceeded for 18 h at room temperature. Lithium bromide (6.1 g; 0.072 mol) was dissolved in 100 mL of 2-butanone, which was then added to the reaction mixture. To induce product precipitation the reaction was heated to 50°C for 10 min, and then cooled to room temperature for 4 h. The LAP solution was filtered to recover the precipitate, washed 3x with 2-butanone (100 mL) and dried under vacuum. LAP quality was confirmed via ¹H-NMR. ¹H-NMR (400 MHz, D₂O): $\delta = 7.74-7.70$ (m, 2H), 7.57 (m, 1H), 7.47 (m, 2H), 6.89 (s, 2H), 2.24 (s, 3H), 2.03 (s, 6H) (**Figure S20**).

PNP hydrogel formation with and without CDs

PNP and α CD–PNP hydrogels were prepared using a similar procedure. In a luer lock syringe, the polymer (e.g., hydroxypropylmethyl cellulose, HPMC, MeHA, collagen, or alginate) were dissolved at known mass in PBS (pH = 7.4) and let equilibrate overnight (T = 25 °C). In case of α CD–PNP formulations, α CD was added at known mass directly to this syringe. In a different luer lock syringe, a known mass of nanoparticles (NP) solution was prepared. The polymer-containing syringe (with and without α CD) and NP-containing syringes were connected through a female-to-female luer lock adapter (Cellink, Sweden) and gently mixed together for 5 minutes. The formulation was equilibrated overnight and stored at 4 °C until further use.

CD–PNP hydrogel formation with various PEG molecular weight

Seminal work from Harada et al. demonstrated that the threading behavior of α CD on PEG is influenced by the length of the polymer chains.²²⁵ Low threading was observed below 2 kDa and the threading behavior increased with PEG molecular weight. Therefore, PEGs of different molecular weight (3 kDa, 6 kDa and 11 kDa) were used for the formation of α CD–PNP hydrogel (HPMC 1 wt%, α CD 10 wt%, and NP 5 wt%). Each formulation resulted in the formation of a reinforced hydrogel as compared with

the base PNP formulation (**Figure S2**). Based on this, we opted to use ~5 kDa PEG for all subsequent formulations. No further investigations were performed.

Rheological characterization

Rheological measurements were performed with a strain-controlled shear rheometer (MCR 502; Anton Paar; Zofingen, Switzerland). Measurements for the formulations: PNP, α CD–PNP, MeHA CDPNP, and Alg CDPNP were performed using a plate-plate geometry of 20 mm diameter and at a plate temperature of 25 °C. In case of Col CDPNP formulation, the measurements were performed using a plate-plate geometry of 20 mm diameter and a plate temperature of 4 °C. In case of Au-based CDPNP and Fe-based CDPNP, the measurements were performed using a plate-plate geometry of 8 mm diameter and a plate temperature of 20 °C. A gap size of 0.5 mm was used for all rheological measurements. In order to reduce any loading history of the sample, after loading the sample in the geometry, an oscillatory pre-conditioning interval ($\omega = 0.1 \text{ rad s}^{-1}$, $\gamma = 0.01 \%$, $t = 30 \text{ min}$) was performed. Dynamic oscillatory strain amplitude sweep measurements were performed with constant angular frequency ($\omega = 10 \text{ rad sec}^{-1}$) to investigate the linear-viscoelastic region (LVR) of different PNP and CD–PNP formulations. Dynamic oscillatory frequency sweep measurements were conducted with a decreasing angular frequency (from 100 to 0.01 rad s^{-1}) and a constant strain amplitude. In case of PNP formulation $\gamma = 0.3 \%$, for α CD–PNP, MeHA CDPNP, and Alg CDPNP, $\gamma = 0.01 \%$; for Col CDPNP $\gamma = 0.1 \%$; and for Au-based CDPNP and Fe-based CDPNP $\gamma = 0.05 \%$. The flowability was investigated by performing rotational shear rate measurements, in which the shear rate, $\delta\gamma/\delta t$, was increased from 0.01 s^{-1} to 100 s^{-1} . In case of PNP and α CD–PNP formulations the measured dynamic viscosity, η , was used to fit a power law model (equation 1) in the linear range.

$$\eta = K_{\text{PL}}(\delta\gamma/\delta t)^{n-1} \quad (1)$$

with fitting parameters n being the shear-thinning index, and K_{PL} being consistency index. Self-healing properties were characterized with dynamic oscillatory time sweep measurements with alternating intervals of low strain (γ_{low} in the LVR and $\omega = 10 \text{ rad s}^{-1}$) and high strain (γ_{high} outside the LVR and $\omega = 10 \text{ rad s}^{-1}$). All measurements were performed at least in triplicate.

Direct Ink Writing and bioprinting

A pneumatic 3D printer (BioX, Cellink) was used for the 3D printing, direct ink writing, experiments. For all tests, 3 mL cartridges mounted with straight nozzles (22 G, $\Phi = 0.41 \text{ mm}$) were used. The 3D model of the cardiac valve was downloaded from grabCAD (<https://grabcad.com>) and modified using NX Siemens CAD software, whereas the miniaturized trachea was designed using NX Siemens CAD software. The respective G-code were generated with BioX internal software. The G-code used to print the 3D square structures (5 x 5 mm, 3 layers of 0.25 mm thickness) for bioprinting cell experiment was written manually. Plurionics F-127 (23 w/v%) was used as support material for the overhanging structures.

Cell viability

Human mesenchymal stem cells (hMSC, passage 6) were encapsulated in Col CDPNP (Col 0.4 wt%, aCD 5 wt%, and NP 5 wt%) hydrogels at 2.0×10^6 cells mL⁻¹ final concentration. Square scaffolds were bioprinted, placed in a Petri dish and stored in an incubator (37°C, 5% CO₂) for 90 min to enable the cross-linking of the scaffolds. Cell-laden but non-printed control samples were placed directly in an incubator (37°C, 5% CO₂) for 90 min to enable the cross-linking of the construct. After cross-linking, bioprinted and non-printed control cell-laden constructs were placed in cell culture medium (low glucose DMEM, 1% PS, 5 ng mL⁻¹ FGF, and 10% FBS) and incubated (37°C, 5% CO₂) until analysis. The cell culture medium was refreshed 30 min after bioprinting or encapsulation, and then once every day for the duration of culture. A Live/Dead viability/cytotoxicity kit (ThermoFisher) was used according to the manufacturer's protocol. To evaluate membrane integrity at different time points after encapsulation, images of the cell-laden scaffolds were taken using inverted fluorescence microscope (EVOS M5000) and analyzed with ImageJ (Fiji, ImageJ 1.51s). To image cell morphology within both bioprinted and non-printed scaffolds, cell cytoskeleton and cell nucleus were respectively stained with AlexaFluor 488 Phalloidin and DAPI according to manufacturer's protocol.

Drug encapsulation

Model drug encapsulation. The hydrophobic small molecule Oil red O (OR) was encapsulated in PEG-*b*-PLA NPs. The theoretical model drug loading was defined as the OR mass in the precursor solution over the total mass of the formulation.

$$\text{Theoretical Drug Loading (\%)} = \text{tDL} = \frac{m_{\text{model drug initial}}}{m_{\text{total formulation}}} \cdot 100\% \quad (2)$$

To target 1 wt% OR loading, 1.4 mg OR and 140 mg PEG-*b*-PLA were dissolved into 2.5 mL acetone. The precursor solution was added dropwise to water under stirring. The NP properties were measured via DLS and dynamic electrophoretic mobility. Acetone was evaporated overnight by leaving the NP suspension in an open container inside a fume hood. Unencapsulated OR crystals were separated from the NP suspension via syringe filtration with 0.2 μm PTFE filters. NPs were concentrated and resuspended to 20 wt% via ultracentrifugation with Amicon Ultra centrifugation filters (MWCO: 30 kDa, 4500 RCF, 1.1 h). To quantify the OR content, the NP suspension was mixed with acetonitrile in a 1:1 ratio and sonicated. The OR absorbance was measured at $\lambda \approx 520$ nm and the concentration was estimated by means of a calibration curve. The remaining dry polymer and OR mass of the polymeric NPs samples was measured after lyophilization of the NP suspension. The effective drug loading of the NPs was estimated by dividing the measured model drug concentration and the total mass present after lyophilization.

$$\text{Effective Drug Loading (\%)} = \text{eDL} = \frac{m_{\text{model drug final}}}{m_{\text{total final}}} \cdot 100\% \quad (3)$$

OR-loaded PNP gels were prepared by using a OR-encapsulating NPs to achieve a final loading of ~ 0.02 wt%. The hydrophilic macromolecule albumin was loaded into PNP gels by entrapping FITC-labeled albumin into the network. 10 mg FITC-albumin were dissolved into 250 μL of 20wt% preformed PEG-*b*-PLA NPs suspension. The suspension was subsequently used to formulate PNP hydrogels and achieve a final FITC-albumin loading of ~ 1 wt%.

Model drug release

Model drug-loaded hydrogels were prepared by forming CD–PNP gels with the OR-loaded NPs or NPs and FITC-albumin. To study the release properties of the hydrophilic model drug, 200 mg of CD–PNP gels loaded with FITC-albumin (10 wt% α CD, 1 wt% HPMC, 5 wt% of PEG-*b*-PLA NPs, and 1 wt% FITC-albumin) were placed at the bottom of an Eppendorf tube. Analogously, for the hydrophobic model drug 200 mg of OR-loaded CD–PNP gels were placed at the bottom of an Eppendorf tube (10 wt% α CD, 1 wt% HPMC, and 5 wt of OR-loaded PEG-*b*-PLA NPs). The release of model therapeutics was started by adding 1.5 mL of 1x PBS supernatant on top of the CD–PNP hydrogels and incubating all samples at 37 °C. On each timepoint, the supernatant was gently mixed three times and 700 μL of supernatant were collected and replaced with fresh PBS. The supernatant concentration of FITC-albumin was quantified by comparing calibration curves with UV-vis spectroscopy ($\lambda_{\text{abs}} \approx 495$ nm) or fluorescence spectroscopy data ($\lambda_{\text{abs}} = 485$ nm, $\lambda_{\text{ex}} \approx 535$ nm). The total released concentration of OR was quantified via UV-vis spectrophotometry. The released sample was diluted 1:1 with acetonitrile, the sample absorbance was measured at $\lambda \approx 520$ nm and compared with a calibration curve.

Modeling of drug release

The CD–PNP release properties were further analyzed by fitting experimental data to the Ritger-Peppas model.⁶⁸ The cumulative fractional release of model drug, M_t , was calculated by dividing the released mass of model therapeutic up to a specific timepoint t , M_t , by the total mass of model therapeutic loaded into the hydrogel, M_∞ . The first 60% of the fractional release was compared to the following equation:

$$\frac{M_t}{M_\infty} = k' t^n \quad (4)$$

The diffusional exponent, n , and the pre-exponential factor, k' , were fitted to the experimental data by minimizing the mean square error.

Conductive measurements

Conductivity of the CD–PNP hydrogels was assessed using an open electronic circuit containing an LED and a battery in series (**Figure S21**). The circuit was closed by connecting the open ends of the circuit to ~ 50 μL CD–PNP hydrogels. In case of AuNP CD–PNP formulations (AuNP 5 wt %, α CD 10 wt %, PEG-*b*-PLA NP 2.5 wt %, and HPMC 1 wt % dissolved in MilliQ water) the LED turned on indicating conductive properties of the hydrogel. As a reference, classic CD–PNP hydrogel formulation

(α CD 10 wt %, PEG-*b*-PLA NP 5 wt %, and HPMC 1 wt %) was used and no conductive property was observed.

Hydrogel magnetic manipulation

The iron oxide PNP hydrogel (α CD 10 wt%, alginate 2 wt%, and PEGylated iron oxide NPs 6 wt%) was molded into the shape of a horseshoe. The material was stabilized by cross-linking the hydrogel in a 0.2 M CaCl₂ bath. The cross-linked gel was placed floating on the surface of a 20 wt% glycerol solution that was saturated with NaCl. Magnetic-driven locomotion was controlled with a five degree-of-freedom (5-DOF) electromagnetic manipulation setup (Octomag).²⁴⁹ The magnetic PNP hydrogel was horizontally or vertically moved with a magnetic field of 2 mT. Hydrogel rotation was enabled by rotating the magnetic field with a frequency of 0.3 Hz.

2.5. ACKNOWLEDGEMENTS

This work was supported by ETH Zurich start-up funds and the Swiss National Science Foundation (Project Grant 200021_184697). The authors are indebted to Dr. Dietmar Appelhans (Leibniz Polymer Research Center), who after the gala dinner of the Bordeaux Polymer Conference 2018 at the Place de la Victoire in Bordeaux, France suggested to M.W.T. to investigate the properties of polymer–nanoparticle hydrogels with the addition of β CD. This insightful suggestion planted a fruitful seed for the present work. The authors thank Prof. Ivan Martin at the University Hospital Basel for providing the hMSCs, and Lisa Krattiger and Prof. Martin Ehrbar at the University Hospital Zurich for their support with cell culture. The authors thank the Particle Technology Laboratory (ETH Zurich, Prof. Sotiris E. Pratsinis) and the Multi-Scale Robotics Laboratory (ETH Zurich, Prof. Bradley J. Nelson) for access to their labs. In particular, Anastasia Terzopoulou, Samuel Charreyron, Lukas Hertle, and Dr. Erdem Siringil assisted with access to the instruments needed for magnetism-related experiments. The authors thank Nevena Paunovic and the Drug Formulation and Delivery Laboratory (ETH Zurich, Prof. Jean-Christophe Leroux) for providing access to their size exclusion chromatography instrument, and Dario Gomez and the Electrochemical Energy Systems Laboratory (ETH Zurich, Prof. Maria R. Lukatsakya) for assisting with electroconductive materials. The authors thank also Daniel Trottmann for assembling the circuit utilized for conductivity measurements.

Open access funding provided by Eidgenossische Technische Hochschule Zurich.

CHAPTER 3

MODULAR AND PHOTOREVERSIBLE POLYMER– NANOPARTICLE HYDROGELS VIA HOST–GUEST INTERACTIONS

SUMMARY *Polymer–nanoparticle (PNP) hydrogels are a class of nanocomposite materials showing potential as injectable platforms for biomedical applications. Their design is limited by an incomplete knowledge of how the binding motif impacts the viscoelastic properties of the material and is generally constrained to non-responsive supramolecular interactions. Expanding the scope of available interactions and advancing our understanding of how defined interactions influence network formation for tailored rheological properties would accelerate the design of PNP hydrogels. To address this gap in the design of PNP hydrogels, we designed and investigated a tunable platform based on beta-cyclodextrin (β CD) host–guest cross-links between functionalized polymers and nanoparticles. We synthesized a host-functionalized polymer (β CD hyaluronic acid) and guest harboring block co-polymer (PEG-*b*-PLA) NPs. The presence and accessibility for binding of the host and guest moieties was characterized via isothermal titration calorimetry. PNP hydrogels with varying concentrations of functionalized polymer and NPs revealed a limited window of concentrations for gelation. We hypothesized that the network formation was governed by the capacity of polymer chains to effectively bridge nanoparticles, which was related to the host–guest ratios present in the system. Further, we incorporate photo-responsive guests to engineer photoreversible gelation of PNP hydrogels via exposure to specific wavelengths of light.*

This chapter is adapted from: Stéphane Bernhard, Lauritz Ritter, Marco Müller, Wenqing Guo, Elia A. Guzzi, Giovanni Bovone, and Mark W. Tibbitt, *submitted*. **AUTHOR CONTRIBUTIONS:** S.B and M.W.T. conceived of the research project. S.B., L.R., M.M., W.G. planned and executed the experiments. S.B., L.R., M.M., W.G., E.A.G, G.B. and M.W.T participated in the analysis of the experiments. S.B. and M.W.T. wrote the manuscript.

3.1. INTRODUCTION

Injectable hydrogels have demonstrated broad utility as drug delivery platforms, inks for additive manufacturing, or cell-laden materials for tissue engineering applications.^{9,11,256–259} The injectability of these polymer networks is often achieved through the inclusion of reversible cross-links based on non-covalent, physical interactions.⁵⁸ The weak and reversible nature of the cross-links enables them to break and reform upon applied mechanical stress, allowing the material to flow with liquid-like behavior—shear-thinning—and to recover solid-like properties after removal of the stress—self-healing or elastic recovery.^{52,260} Various supramolecular interactions, such as hydrophobic forces,^{17,261} hydrogen bonding,^{161,262} or host–guest interactions,^{117,263} have been investigated for the formation of injectable hydrogels.²⁶⁴ As the range of binding strengths ($\sim 40\text{--}600\text{ kJ mol}^{-1}$; $K_{\text{eq}} \sim 10^5\text{--}10^{45}\text{ M}^{-1}$) and dynamics of supramolecular interactions is broad,^{80,260} their mechanical properties is similarly vast, spanning the formation of weak injectable materials to tough elastic materials.^{265–267} The engineering of hydrogels that takes into account the influence of the reversible interactions on the macroscopic mechanics is therefore critical to tailor the viscoelastic behavior and injectability for the specific applications of interest.

One prominent class of injectable hydrogels are based on reversible polymer–nanoparticle (PNP) interactions.¹⁸ These PNP hydrogels are injectable nanocomposite materials that form through physical interactions between polymers and nanoparticles. Previous work demonstrated their potential as a multifunctional drug delivery platform, sprayable fire retardant, or a modular ink for bioprinting.^{17,143,220,268} Within this class materials, most examples are based on non-specific, hydrophobic adsorption of polymer chains on nanoparticle surfaces. Other supramolecular interactions were used to fabricate PNP hydrogels, such as metal–ligand interactions or self-assembling peptide motifs.^{19,20} However, many of these systems exhibit limited tunability of the mechanical properties, due to the dependence on cross-linking interactions with a small range of binding strengths and dynamics. To overcome these limitations, PNP hydrogels have been modified through the use of additives that augment the polymer–nanoparticle or nanoparticle–nanoparticle interactions via electrostatic forces or host–guest complex formation.^{144,269} In both cases the presence of supramolecular additives increased the range of moduli available for the hydrogel by providing an additional interaction mechanisms. Overall, these findings demonstrate that engineering the interfacial interactions between the constituent polymers and nanoparticles can be used to engineer the macroscopic properties of PNP hydrogels.

To further advance the engineering design and modularity of this class of materials, there is a need to better understand the fabrication paradigms involved in their formation. To date, several studies have investigated how polymer and nanoparticle interactions result in emergent viscoelastic behavior. Early reports of PNP hydrogels suggested a correlation between interaction strength and moduli as increasing hydrophobicity of the polymer chain resulted in an increase in the mechanical properties of the formed materials.¹⁸ Further investigations of polymer adsorption on nanoparticles and rheological studies

provided additional insights into fundamental mechanisms, including entropic driving forces, involved in the formation of PNP hydrogels.^{142,270} However a clear correlation between the molecular interactions at the dynamic junctions formed between nanoparticles and polymers and their influence on macro-scale properties, such as gel formation, viscoelasticity, and flow point, is still missing.

In this project, we explore the underlying mechanisms governing the viscoelastic properties of PNP hydrogels using defined reversible interactions between the constituent polymers and nanoparticles. To do this, we introduced host–guest cross-links, based on adamantane and β -cyclodextrin complexes, between polymer and nanoparticle into PNP hydrogels by functionalizing hyaluronic acid with β -cyclodextrin (β CD-HA) and poly (ethylene glycol)-*b*-poly (lactic acid) (PEG-*b*-PLA) NPs with adamantane (Ada-NPs). The availability and binding efficiency of the host (β CD) and guest (Ada) on the hyaluronic acid and PEG-*b*-PLA NPs, respectively, was confirmed using isothermal titration calorimetry (ITC). When attached to their respective polymers, we observed higher binding affinities for both functionalized reactants compared with free β CD and Ada though the binding resulted in lower stoichiometry, indicating incomplete accessibility of the ligands. The degree of functionalization and binding efficiency enabled the formation of shear-thinning and self-healing PNP hydrogels upon mixing β CD-HA and Ada-NPs. Hydrogel formation depended strongly on the mixing conditions, suggesting strain-induced effects on network structure. In addition, only a defined window of polymer and NP concentrations resulted in hydrogel formation. We related the building block concentrations and host–guest ratios in the formulations to the viscoelastic properties of the network, highlighting critical roles of the Ada-NP concentration on gelation and of the β CD-HA concentration on the material viscosity. Given the modular nature of the host–guest interactions employed, we exchanged the guest molecule on the PEG-*b*-PLA NPs to azobenzene to fabricate photo-reversible PNP hydrogels. Photo-reversible PNP gels confirmed that gelation required host–guest complexation and enabled on–demand sol–gel transitions. Overall, this work furthers our understanding of the underlying mechanisms that govern the mechanical properties of PNP hydrogels, while providing a cross-linking scheme for tailored gel formation and stimuli-responsive viscoelastic materials.

3.2. RESULT AND DISCUSSION

3.2.1. Synthesis and Formation of Host–Guest PNP Hydrogels

We first set out to engineer supramolecular nanocomposite hydrogels to investigate how interfacial interactions between polymers and nanoparticles influence the mechanical properties of the resultant PNP hydrogels. We identified host–guest complexes based on β -cyclodextrin (β CD), a biocompatible macrocyclic oligosaccharide,¹⁰¹ as suitable cross-links for this aim, given their wide range of available guests and existing synthetic protocols for functionalizing long-chain polymers with pendant β CD.^{11,104,271} Adamantane (Ada) was chosen as an initial guest based on its relatively high binding affinity ($K \sim 10^4$), which has proven suitable for hydrogel formation in a variety of studies.^{66,111,272} We

hypothesized that a PNP hydrogel could be assembled by mixing a β CD-functionalized polymers with Ada-functionalized PEG-*b*-PLA nanoparticles (**Figure 3.1a**).

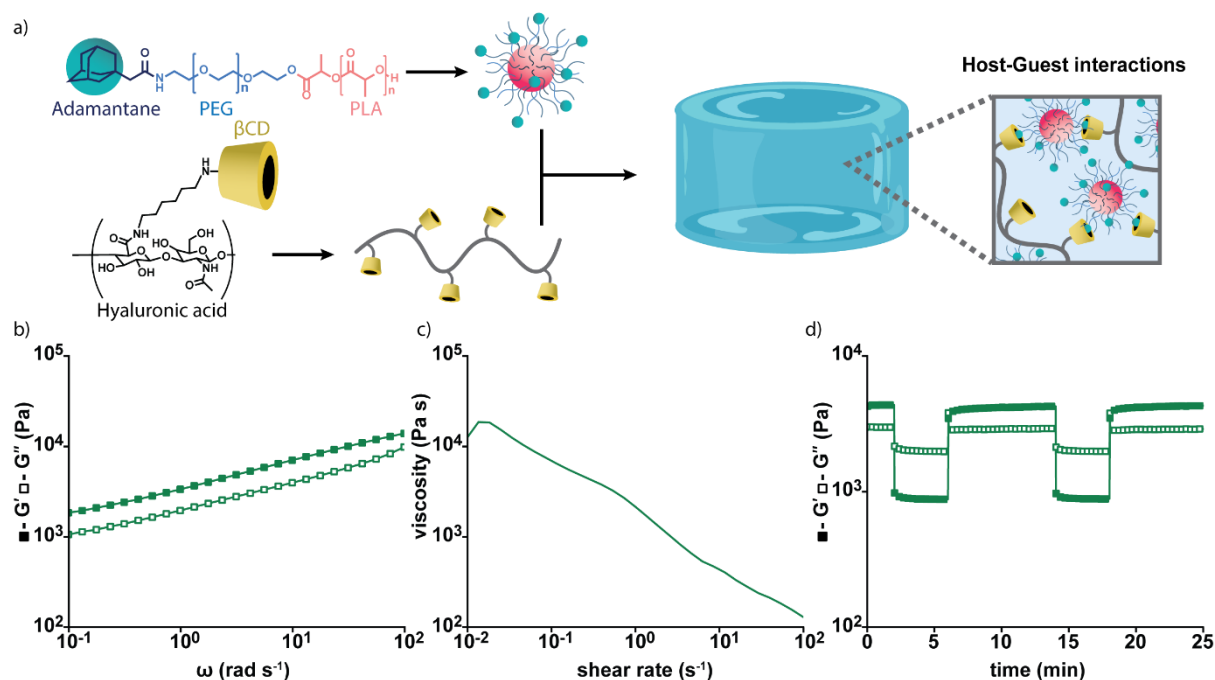


Figure 3.1. a) PNP hydrogels based on host–guest interactions were designed by combining adamantane-functionalized block-co-polymer nanoparticles with β CD-functionalized hyaluronic acid. b) Frequency sweep of 6 wt% β CD-HA with 20 wt% Ada-NP formulation. The resulting gel showed c) shear-thinning and d) self-healing properties ($\gamma_{low} = 1\%$; $\gamma_{high} = 1000\%$).

To prepare the gel precursor materials, hyaluronic acid (HA; $M_n \sim 60$ kDa) was functionalized with β CD (**Figure S22a**).²⁷³ Completion of each synthesis step was confirmed via $^1\text{H-NMR}$ spectroscopy (**Figure S22-26**). After purification, we calculated a degree of functionalization of β CD-HA of $\sim 25\%$ (**Figure S26**), corresponding to ~ 40 β CD molecules per HA chain. In parallel, guest-labeled NPs were prepared by first coupling 1-adamantane acetic acid on one end of a poly (ethylene glycol) (PEG; $M_n \sim 5$ kDa) chain, followed by the polymerization of poly (lactic acid) (PLA) from the other end of the synthesized Ada-PEG (**Figure S22b**). The presence of the guest and the PLA chain on the synthesized Ada-PEG_{5k} and Ada-PEG_{5k}-*b*-PLA_{9k} were confirmed by $^1\text{H-NMR}$ (**Figures S27-28**). Ada-functionalized PEG-*b*-PLA NPs (Ada-NPs; $\text{Ø} = 85$ nm; $D = 0.26$) were formed via nanoprecipitation of the block-co-polymer. To prepare host–guest PNP hydrogels, we combined β CD-HA (6 wt%) and Ada-NPs (20 wt%) in a single formulation (**Figure 3.1a, b**). The host–guest hydrogel exhibited viscoelastic behavior with a shear elastic modulus of $G' \approx 7000$ Pa ($\omega = 10$ rad s^{-1}). Furthermore, the hydrogel exhibited shear-thinning and self-healing properties, indicating its suitability as an injectable material (**Figure 3.1c, d**).

During host–guest PNP hydrogel formation, we observed that the properties of the resultant gel depended strongly on the mixing method used to combine the β CD-HA and Ada-NPs (**Figure 3.2a**). Three mixing regimes, labeled as “weak”, “moderate”, or “strong”, were applied to a single host–guest

PNP hydrogel formulation (6 wt% β CD-HA, 20 wt% Ada-NP). The “weak” mixing regime did not involve mechanical mixing and yielded a viscoelastic liquid over the whole range of frequencies with a shear modulus of $G' \approx 1210$ Pa ($\omega = 10$ rad s^{-1} , $\alpha = 0.8$). The “moderate” mixing regime comprised mechanical mixing with a spatula in a microcentrifuge tube and resulted in a material with frequency-dependent properties ($\alpha = 0.5$) and $G' \approx 1620$ Pa ($\omega = 10$ rad s^{-1}). Lastly, a “strong” mixing regime was performed by shearing the formulation with a spatula on a glass slide, similar to kneading bread dough. The “strong” mixing regime led to the formation of a gel over the whole range of sampled frequencies with $G' \approx 7000$ Pa ($\omega = 10$ rad s^{-1}) and an attenuated frequency dependence ($\alpha = 0.3$). This indicated that applied shear was needed to form robust host–guest PNP hydrogels with solid-like properties ($G' > G''$) and increased shear moduli. We hypothesized that this behavior was related to the disruption of cohesive interactions between HA chains. HA is known to form non-covalent interactions (e.g., electrostatics, hydrogen bonding, chain entanglements) between polymer chains^{274–276} and shearing HA chains is capable of disrupting these interactions.²⁷⁷ In the context of β CD-HA, applied shear likely disrupted the non-covalent interactions present in the HA, opening up the polymer chains and increasing the availability of the β CD for binding to the NPs and the likelihood of HA chains bridging distinct NPs, leading to the formation of robust PNP hydrogels via β CD–Ada cross-links. Reproducible mechanical properties were obtained using the “strong” mixing regime across different formulations (**Figure S29a**). Based on these results, all formulations in this work were prepared using the “strong” mixing regime. Attempts to translate the “strong” mixing regime to pre-processing on the shear rheometer were unsuccessful, likely due to insufficient strain.

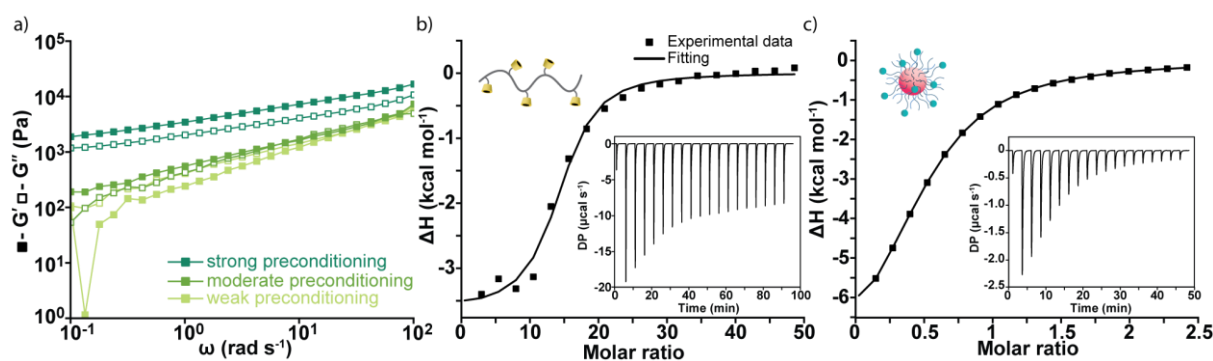


Figure 3.2. a) Influence of mixing regime on the viscoelastic properties of a single formulation of 6 wt% HA-CD with 20 wt% Ada-NP. ITC analysis of b) β CD-HA titration using Ada-PEG (molar ratio expressed as Ada: β CD) and c) Ada-NP titration using β -CD (molar ratio expressed as β CD:Ada).

PNP hydrogel formation was attributed to specific host–guest interactions between β CD-HA and Ada-NPs. Formulations with non-functionalized HA formed weak viscoelastic liquids ($G' \approx 8$ Pa, $\omega = 10$ rad s^{-1} ; **Figure S29b**). We hypothesized that the ability of β CD-HA and Ada-NPs to form a robust network was directly related to the quantity and strength of the cross-links, or host–guest complexes. In previous work, functionalization or grafting of β CD and Ada to polymers have affected their complexation affinities.^{272,278–280} To characterize the binding properties and derive the effective number of hosts or

guests available for complexation in the gel-forming building blocks, we characterized the starting materials using isothermal titration calorimetry (ITC; **Table 3.1**). Fitting of the reported heat curves was performed after subtraction of the relevant controls (**Figure S30**). Due to the poor solubility of Ada in water, Ada-PEG was used as a ligand to titrate free β CD (**Figure S31**; **Table 3.1**). β CD titration using Ada-PEG resulted in a binding stoichiometry ($N \sim 0.9$) close to the expected theoretical 1:1 ratio, implying minimal effect of the PEG chain on the capacity of Ada to bind. On the other hand, the dissociation constant was lower ($K_D \sim 10^{-5}$) than literature values for free β CD–Ada binding ($K_D \sim 10^{-4}$), indicating stronger binding for the functionalized Ada.^{271,272,281} This difference suggested a possible stabilizing effect due to coupling of the guest to a polymer. Similar effects have been reported for Ada coupled to PEG interacting with β CD on a surface.²⁸²

Table 3.1. Molar ratio(N), equilibrium dissociation constants (K_D), and binding enthalpies (ΔH) of the host–guest interactions from ITC experiments.

Cell	Syringe	N	K_D (M)	ΔH ($kcal\ mol^{-1}$)
β CD	Ada-PEG	$0.889 \pm 3.8 \times 10^{-3}$	$2.98 \times 10^{-5} \pm 9.19 \times 10^{-7}$	$-5.92 \pm 5.3 \times 10^{-2}$
β CD-HA	Ada-PEG	13.7 ± 0.34	$3.09 \times 10^{-5} \pm 8.27 \times 10^{-6}$	-3.64 ± 0.156
Ada-NP	β CD	$0.495 \pm 2.4 \times 10^{-2}$	$5.33 \times 10^{-5} \pm 9.71 \times 10^{-7}$	$-8.49 \pm 7.8 \times 10^{-2}$

We then used Ada-PEG to titrate β CD-HA (**Figure 3.2b**; **Table 3.1**). The ITC measurements indicated that ~ 14 β CD were available for complexation per polymer chain, corresponding to an effective degree of functionalization (DF_{eff}) of $\sim 9\%$. The available number of β CD groups for binding on each HA chain (DF_{eff}) was lower than the amount calculated from $^1\text{H-NMR}$ spectroscopy. This difference was attributed to possible loss of mobility or conformation effects due to functionalization on HA chains, which could hinder β CD–Ada binding.^{279,280} No significant changes in binding strength were observed compared to the β CD–Ada-PEG system, showing no additional effect of the HA chains on the binding strength compared to the PEG. Similarly, the availability of Ada on the NPs was confirmed using β CD as a ligand to titrate Ada-NPs (**Figure 3.2c**). Fitting of the titration curve showed that ~ 0.5 β CD guests were able to bind per Ada present on the NPs (**Table 3.1**). We hypothesized that the hydrophobic nature of the guest combined with possible hindrance of the NPs or of β CD itself may have reduced the availability of the guests present in the hydrophilic corona of the NPs.²⁸³ Similarly to the previous system, the observed dissociation constant was lower than the one reported for free β CD and Ada. This again indicated stronger binding for polymer-functionalized ligands, while the NP formation itself did not seem to impact significantly the binding strength.²⁸² Overall, both Ada-NPs and β CD-HA showed lower effective availability of host and guest compared with the theoretical amounts present in the system.

3.2.2. Mechanical Characterization

To understand the factors governing the formation and properties of the resulting gels, we quantified the viscoelastic properties of formulations with varying concentrations of β CD-HA (2–10 wt%) and Ada-

NPs (2.5–20 wt%) via shear rheometry. First, we investigated the influence of Ada-NP concentration on host–guest PNP hydrogel mechanics (**Figure 3.3a–c; Figure S32**). Increasing Ada-NP concentration from 2.5 to 20 wt% resulted in increased shear moduli for all formulations ($G' \approx 2\text{--}150$ Pa at 2.5 wt% Ada-NP to $G' \approx 760\text{--}7000$ Pa at 20 wt%, $\omega = 10$ rad s^{-1} ; **Figure 3.3a, b**). The loss factor decreased with increasing Ada-NP concentration ($\tan \delta \approx 1.62\text{--}11.1$ at 2.5 wt% Ada-NP to $\tan \delta \approx 0.56\text{--}1.09$ at 20 wt%, $\omega = 10$ rad s^{-1} ; **Figure 3.3c**), corroborating the formation of robust gels with increasing NP content. Only formulations containing 20 wt% or 15 wt% Ada-NPs exhibited solid-like behavior ($G' > G''$) over the whole frequency range. Similarly, the strain at the flow point (point of crossover of G' and G'') of the gels increased with increasing Ada-NP concentration (**Figure 3.3d, f; Figure S33**). Overall, these results indicated that the concentration of Ada-NP governed the gelation capacity of the PNP formulations and the strength of the formed networks.

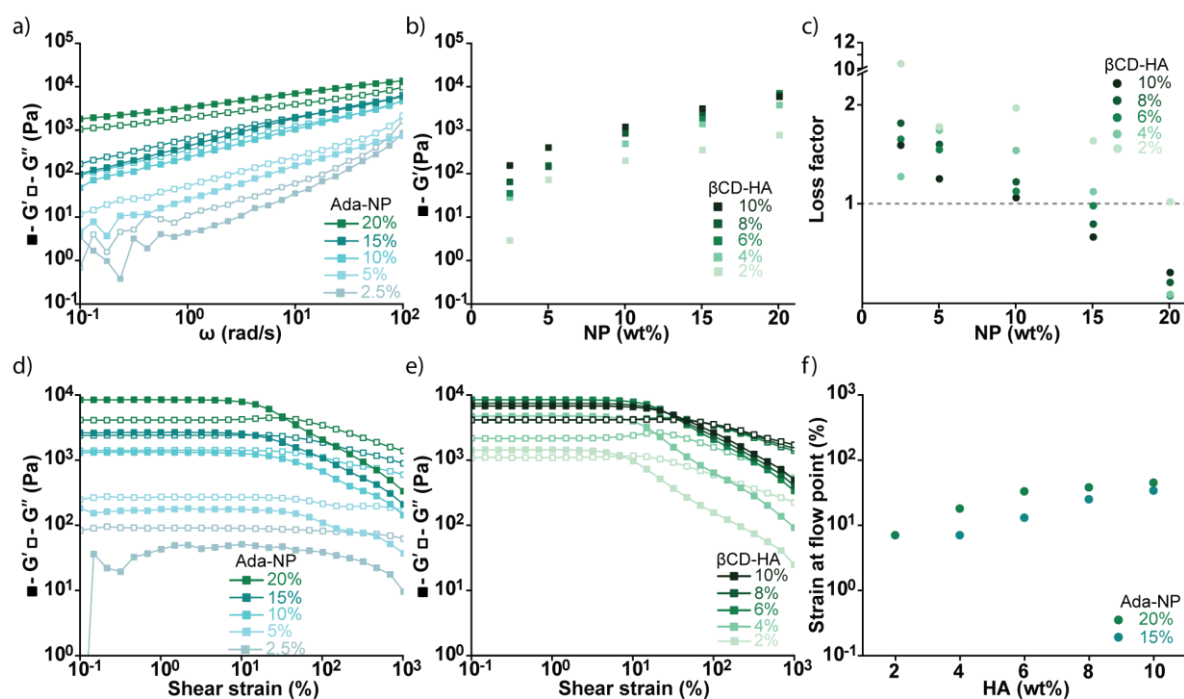


Figure 3.3. a) Frequency sweep of 6 wt% β CD-HA gels with varying concentration of Ada-NPs. b) Storage modulus at $\omega = 10$ rad s^{-1} as a function of Ada-NP concentration. c) Loss factor at $\omega = 10$ rad s^{-1} as a function of Ada-NP concentration. d) Strain sweep of 6 wt% β CD-HA gels with varying concentration of Ada-NPs. e) Strain sweep of 20 wt% Ada-NP gels with varying concentration of β CD-HA. f) Strain at flow point of 20 wt% and 15 wt% Ada-NP gels as a function of β CD-HA concentration.

Similarly, increasing β CD-HA concentration increased the overall the shear moduli for all formulations ($G' \approx 2\text{--}760$ Pa at 2 wt% β CD-HA to $G' \approx 150\text{--}6000$ Pa at 10 wt% β CD-HA, $\omega = 10$ rad s^{-1} ; **Figure 3.3b, Figure S32**). However, the impact of β CD-HA on the modulus was less prominent at higher NP concentrations; the shear moduli of formulations containing 10, 15 and 20 wt% Ada-NPs approached a plateau beyond 6 wt% β CD-HA ($G' \approx 1050\text{--}7000$ Pa at 6 wt% β CD-HA to $G' \approx 1180\text{--}5870$ Pa at 10 wt% β CD-HA, $\omega = 10$ rad s^{-1} ; **Figure 3.3b, Figure S32**). These results indicated a limited influence of

β CD-HA on the network modulus above a certain concentration for fixed Ada-NP content. Changes in loss factor further supported these findings. Overall, increases in β CD-HA promoted network formation for formulations with an Ada-NP content below 20 wt%, as shown by the decrease in loss factor ($\tan \delta \approx 1.09$ – 11.1 at 2 wt% β CD-HA to $\tan \delta \approx 0.66$ – 1.62 at 10 wt% β CD-HA, $\omega = 10 \text{ rad s}^{-1}$; **Figure 3.3c**, **Figure S32**). On the other hand, formulations containing 20 wt% Ada-NP exhibited an increase in loss factor with increasing β CD-HA concentration above 4 wt% ($\tan \delta \approx 0.56$ at 6 wt% β CD-HA to $\tan \delta \approx 0.66$ at 10 wt% β CD-HA, $\omega = 10 \text{ rad s}^{-1}$; **Figure 3.3c**). In this case, further increasing the β CD-HA concentration increased the viscous properties of the network. Further, the strain at flow point exhibited an attenuated increase with higher β CD-HA content (**Figure 3.3e, f**). Overall, these results suggest that a sufficient concentration of β CD-HA (relative to Ada-NPs) is needed to percolate a network, but that beyond this point the β CD-HA primarily contributes to the viscous phase of the material. That is, the cross-linking is primarily driven by the NPs, which require a dense polymer solution for network formation, and further increasing the polymer phase does not substantially affect the cross-linking.

To further understand the influence of the host–guest complex formation on the viscoelastic properties of the material, the rheological properties of the material were correlated to host:guest ratios (β CD:Ada) based on the DF_{eff} determined through ITC for β CD-HA and Ada-NPs (**Figure 3.4a**). As the ratios were determined based on the amount of NP or polymer present in the system, an increase in Ada-NP corresponds to a decrease in this ratio, while increasing β CD-HA concentration corresponds to an increase in this ratio.

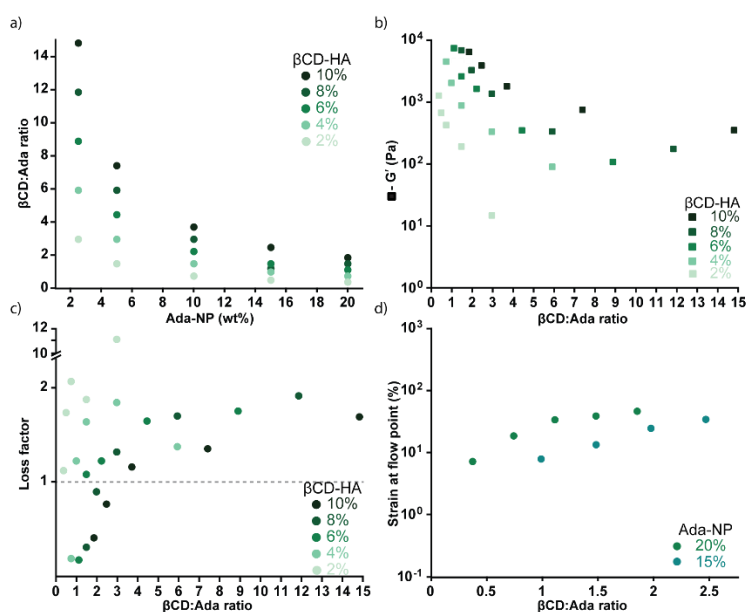


Figure 3.4. a) β CD:Ada ratios derived from ITC measurements as a function of Ada-NP content. Colors represent various β CD-HA concentrations. b) Storage modulus (G') at $\omega = 10 \text{ rad s}^{-1}$ as a function of β CD:Ada ratio. Colors represent various β CD-HA concentrations. c) Loss factor at $\omega = 10 \text{ rad s}^{-1}$ as a function of β CD:Ada ratio. Colors represent various β CD-HA concentrations. d) Strain at flow point as a function of β CD:Ada ratio. Colors represent various Ada-NP concentrations.

Across individual β CD-HA concentrations, a lower β CD:Ada ratio resulted in an increase in the strength of the network—increased storage moduli and decreased loss factor (**Figure 3.4b, c**). More precisely the amount of Ada in the system increased due to an increase in NP concentration, resulting in a relative decrease in the β CD:Ada ratio going from a stoichiometric excess to almost equimolar concentrations (ratio ≈ 2.3 – 14.8 at 2.5 wt% Ada-NP to ratio ≈ 0.4 – 1.9 at 20 wt% Ada-NP). This change in stoichiometry explains the increase of mechanical properties associated with the increase in NP concentration. As NP concentration increased, the relative amount of Ada increased to a concentration range similar to the one of the β CD, enabling the formation of a higher number of host–guest complexes, and by extension cross-links. This effect was particularly noticeable for hydrogel formulations with 20 wt% NPs, which all have similar amounts of Ada and β CD (ratio ≈ 0.4 – 1.9 ; **Figure 3.4b, c**). Indeed, the closer the β CD:Ada ratio was to 1 the more robust the network was, while a lower or higher ratio resulted in attenuated viscoelastic properties.

On the other hand, for formulations with NP contents below 20 wt%, an increased β CD:Ada ratio resulted in an increase in the strength and gel-like behavior (**Figure 3.4b, c**). The increase in stoichiometry related to an increase of β CD-HA in the formulation without increasing the quantity of possible host–guest complexes formed. We therefore hypothesized that this behavior was not directly related to the host–guest complex formation but instead to possible changes in network viscosity introduced by the additional HA chains in the polymer phase. In a similar manner, the strain at flow point increased with increasing β CD:Ada ratio, without clear correlation to the host–guest complex formation (**Figure 3.4d**). Overall, by determining host–guest quantities in the system, the impact of the NP could be correlated to an increase in cross-linking density by bringing host–guest ratio closer to a 1:1 complex formation, while the influence of β CD-HA again related primarily to changes in the viscosity of the polymer phases.

3.2.3. Photoreversible Supramolecular PNP hydrogels

Given that tailored interactions between NP surfaces and functionalized HA chains drove network formation, we can in principle exchange the host–guest complex to tailor the gel properties or introduce additional functionality to the system. Based on the previously determined conditions for robust network formation, adamantane was exchanged with azobenzene (AzB), a photoreversible molecule, that can complex with β CD in its trans conformation, to synthesize photoreversible PNP hydrogels. Uniquely, AzB can switch between the cis and trans conformations upon exposure to different wavelengths of light (**Figure 3.5a**). The trans conformation is favored upon exposure to visible light ($\lambda > 400$ nm) or heat, while the cis conformation is dominant following exposure to UV light ($\lambda < 365$ nm). The capacity of AzB to serve as a guest for β CD is dependent on its conformation. The trans conformation has favorable interactions with β CD enabling host–guest complex formation, while the physical hindrance of the cis conformation makes complex formation unfavorable. We hypothesized that we could engineer photoreversible PNP hydrogels using AzB-functionalized NPs based on the observation that specific binding between polymers and nanoparticles formed host–guest PNP hydrogels.

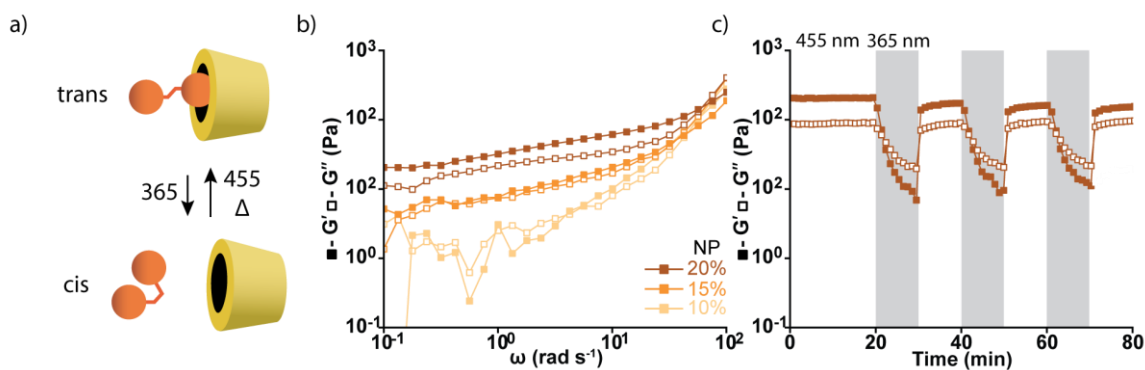


Figure 3.5. a) The reversible capacity of azobenzene to bind β CD upon exposure to various wavelengths. b) Frequency sweep of gels with increasing NP concentration. c) Time sweep showing the photo reversible behavior of the PNP system upon exposure to $\lambda = 455$ nm or 365 nm light.

The presence of AzB on the PEG-*b*-PLA polymers was confirmed using $^1\text{H-NMR}$ spectroscopy (**Figure S34-35**). The change in guest did not affect the size of the resulting nanoparticle ($\text{O} = 81$ nm; $D = 0.17$). Photoreversible PNP hydrogels were formed using similar formulations that exhibited robust viscoelastic properties for β CD-HA and Ada-NP. As for the previous system a range AzB-NPs (5–20 wt%) were mixed with β CD-HA (6 wt%). The formulation with 5 wt% AzB-NPs did not induce gelation. Formulations with 10, 15, and 20 wt% AzB-NPs resulted in gel formation over the whole frequency regime with frequency dependent behavior, the scaling parameter decreased with increasing NP concentrations ($\alpha = 1.36$ at 10 wt% Ada-NP to $\alpha = 0.3$ at 20 wt% Ada-NP; **Figure 3.5b**). The increase in NP concentration resulted in an increased modulus of the material with 20 wt% having a storage modulus of 300 Pa. Similar to the Ada-NP-based gels, AzB-NP-based gels showed concentration dependent changes in moduli. The storage moduli of AzB-NP gels were overall lower than the one of Ada-NP-based gels. These changes were associated with the decreased binding affinity of AzB to β CD as compared with Ada.²⁸⁴

The photoreversibility of the materials was probed by characterizing the viscoelastic properties of the materials at two selected wavelengths ($\lambda = 365$ and 455 nm; **Figure 3.5c**). In the absence of light exposure, the gels exhibited solid-like properties. Upon exposure to 365 nm light, the gels transformed into viscoelastic liquids with a light-dependent decrease in storage and loss moduli. The formulation with 20 wt% AzB-NP underwent a transition to a liquid state ($G' < G''$). Upon switching to a 455 nm light, the materials rapidly recovered their gel-like properties. The gels underwent multiple cycles of photo-induced gel–sol–gel transitions without noticeable loss in mechanical properties. The impact of light exposure on the mechanical properties of the formed gels, based on photoactive changes in the interactions between AzB-NPs and β CD-HA corroborates the observations that tailored host–guest interactions are required for gel formation. The photoreversible nature of this material combined with the to recover its mechanics in the dark makes it a suitable system for the design of on-demand injectable hydrogels for biological applications, wherein the injection is carried out in the low viscosity state ($\lambda = 365$ nm) that will reform a gel after injection.

3.3. CONCLUSION

In this work, we leverage β CD based host–guest complexes for the formation of modular PNP hydrogels. Hydrogel formation required extensive shearing of the precursor solution to break intramolecular interaction in the HA backbone and enabling efficient NP bridging. To properly characterize the availability of the host and guest, ITC measurement was performed showing an effective degree of functionality lower than the theoretical functionalization of the material. By combining effective host:guest ratios with rheological characterization, we could correlate the NP impact to the cross-linking density, while understanding the primary role of the polymer phase as a viscosity enhancer required for robust network formation. Given that the host–guest interactions between NP and polymer drive network formation, we leveraged AzB, a photoresponsive guest, to engineer light responsive gelation of the hydrogel system. Overall, this work broadens the current understanding of the underlying mechanisms governing network formation and the resulting viscoelastic properties of PNP hydrogels. The designed hydrogel further provided a cross-linking scheme for tailored gel formation and stimuli-responsive viscoelastic materials.

3.4. MATERIALS & METHODS

3.4.1. Materials

Acetone (Sigma-Aldrich); Acetonitrile (VWR Chemicals); 1-Adamantaneacetic acid (TCI); Benzotriazol-1-yl-oxy-tris-(dimethylamine)-phosphonium-hexafluorophosphate (BOP, Novabiochem); Benzotriazole-1-yl-oxy-tris-pyrrolidino-phosphonium hexafluorophosphate (PyBOP, Sigma-Aldrich); Chloroform-d (CDCl_3 , Fisher Scientific); β -cyclodextrin (TCI); Deuteriumoxide (D_2O , Sigma-Aldrich); Dichloromethane (DCM, Sigma-Aldrich); Dichloromethane (DCM, extra Dry over MS, Fisher Scientific); Diethyl ether (Et_2O , VWR Chemicals); *N,N*-diisopropylethylamine (DIPEA, Sigma-Aldrich); 3,6-dimethyl-1,4-dioxane-2,5-dione (lactide, Sigma-Aldrich); *N,N*-Dimethylformamide (DMF, Sigma-Aldrich); *N,N*-Dimethylformamide (DMF, extra dry, Acros Organics); Dimethylsulfoxid (DMSO, extra dry, Acros Organics); Dimethyl sulfoxide-d₆ (DMSO-d₆, Sigma-Aldrich); Dowex 50Wx8 (abcr GmbH); Hexafluorophosphate azabenzotriazole tetramethyl uronium (HATU, abcr GmbH.); Hexamethylenediamine (HDA, Sigma-Aldrich); Hydroxyl-poly(ethylene glycol)-amine (HO-PEG-NH₂, 5 kDa, JenKem); 4-(Phenylazo)benzoic acid (AzoB, 98%, Sigma-Aldrich); Sodium chloride (NaCl, Sigma-Aldrich); Sodium hydroxide (NaOH, Sigma-Aldrich); Sodium Hyaluronate (NaHA, 60 k, Lifecore); Tetrabutylammonium hydroxide solution (TBAOH, 40 wt% in H_2O , Sigma-Aldrich); Tin(II) 2-ethylhexanoate (SnOct_2 , Sigma-Aldrich); Toluene (extra dry, Acros Organics); p-Toluolsulfonyl chlorid (TCI).

3.4.2. Instrumentation and methods

Nuclear magnetic resonance

¹H-NMR spectra were acquired on a Bruker Avance III 400 (Bruker BioSpin GmbH). Chemical shifts were reported relative to the respective residual solvent peak. (CDCl_3 : $\delta = 7.26$ ppm; DMSO-d_6 : $\delta = 2.50$; D_2O : $\delta = 4.79$ ppm)

Dynamic light scattering

The hydrodynamic diameters of the formed NPs were measured by dynamic light scattering (DLS) on a Malvern ZetaSizer Nano ZS. The NP suspensions were placed into a semi-micro cuvette (Brand, Path length: 10 mm). The measurements were performed at 25 °C with a wavelength of 633 nm and a scattering angle of 17°C. The properties of each sample were measured three times reported as z-average diameter and dispersity.

Polymeric NP formation

Polymeric core-shell NPs were formed via batch nanoprecipitation. 70 mg of functionalized PEG-*b*-PLA were dissolved in 1 mL acetone. The solution was added dropwise to 10 mL of milli-q water under stirring. Acetone was evaporated overnight by keeping NP suspension in an open container on a shaking plate. NPs were subsequently concentrated via ultrafiltration with an Amicon Ultra centrifugation filter (MWCO: 30 kDa, 4500 rcf, 1.2h). The NPs were resuspended to a final concentration of 30 wt%.

Polymer-nanoparticle (PNP) hydrogel formation

All gels were formed using similar procedure. A representative procedure for a 200 mg gel with 4 wt% polymer (HA-CD) and 15 wt% NP (Ad-PEG-*b*-PLA) is described. In an Eppendorf 8 mg of HA-CD was dissolved in 92 μ L of milli-q water. After full dissolution, 100 μ L of a 30 wt% NP solution were added using a viscous pipette. Mixing of the hydrogel was done by shearing the hydrogel on a glass slide using a spatula (**Supplementary video 3.1**). The gels were then let to equilibrate overnight in the fridge ($T = 4$ °C).

Rheological characterization

Rheological measurements were performed with a strain-controlled shear rheometer (MCR 502; Anton Paar; Zofingen, Switzerland). Measurements for the formulations were performed using a plate-plate geometry of 8 mm diameter and at a plate temperature of 25 °C. A gap size of between 0.2 – 0.5 mm was used for all rheological measurements. In order to reduce any loading history of the sample, after loading the sample in the geometry, an oscillatory pre-conditioning interval ($\omega = 0.1$ rad s^{-1} , $\gamma = 0.01$ %, $t = 30$ min) was performed. Dynamic oscillatory strain amplitude sweep measurements were performed with constant angular frequency ($\omega = 10$ rad s^{-1}) to investigate the linear-viscoelastic region (LVR) of formulations. Dynamic oscillatory frequency sweep measurements were conducted with a decreasing angular frequency (from 100 to 0.1 rad s^{-1}) and a constant strain amplitude ($\gamma = 1$ %). The flowability was investigated by performing rotational shear rate measurements, in which the shear rate, $\delta\gamma/\delta t$, was increased from 0.01 s^{-1} to 100 s^{-1} . Self-healing properties were characterized with dynamic oscillatory time sweep measurements with alternating intervals of low strain ($\gamma_{low} = 1$ % in the LVR and $\omega = 10$ rad s^{-1}) and high strain ($\gamma_{high} = 1000$ % outside the LVR and $\omega = 10$ rad s^{-1}). The photo-sensitive behavior of AzoB-PNP samples were investigated using dynamic oscillatory time sweep measurements ($\gamma = 1$ %, $\omega = 10$ rad s^{-1}) with alternating $\lambda = 455$ nm ($I = 0.92$ mW cm^{-2}) and $\lambda = 365$ nm ($I = 39.3$ mW cm^{-2}) light.

Isothermal titration calorimetry characterization

ITC measurements were performed on a Malvern MicroCal PEAQ-ITC. Experiments were conducted at 25 °C with a stirring speed of 750 rpm, and injections of 4 μ L with a spacing of 120 – 150 s. Control titrations of ligand into solvent were subtracted for each experiment. The data were fitted to a single binding site model and analyzed using the provided MicroCal PEAQ-ITC Analysis Software from Malvern.

3.4.3. Synthetic procedures*6-o-monotosyl-6-deoxy- β -cyclodextrin (β CD-Tos)*

β CD-Tos was synthesized as previously reported.¹¹ β CD (10 g, 8.8 mmol, 1 eq.) was suspended in 60 ml milli-Q water and cooled in an ice bath. In parallel, p-toluensulfonyl (2.02 g, 10.6 mmol, 1.2eq.) was dissolved in 5 mL acetonitrile, and then added dropwise to the cooled solution of β CD. The solution was stirred on ice for 2 h. After removal of the ice bath, sodium hydroxide (1.06 g, 26.4 mmol, 3 eq.) dissolved in 4 ml of water was added dropwise to the reaction mixture. The solution was stirred for 30 min at room temperature. Flocculation of the β CD-Tos was then induced by adjusting the pH to 8.5 – 9 using Ammonium chloride. The solid was then centrifuged (4500 rcf., 15 min, 4 °C) and the supernatant was discarded. The solid was further washed by resuspension of the solid in water and repeat of the centrifugation cycle. The washing step was repeated once more with water, thrice with ice-cold acetone and twice with ice-cold Et₂O. Finally, the product was dried in vacuo to yield a white powder (2.77 g, 24 % yield). Characterization: ¹H-NMR (400 MHz, DMSO-d₆) δ 7.75 (d, 2H), 7.43 (d, 2H), 5.70 (s, 13H), 4.84 (s, 5H), 4.77 (s, 2H), 4.49 – 4.11 (m, 2H), 3.83 – 3.46 (m, 31H), 2.43 (s, 3H).

6-(6-aminohexyl)amino-6-deoxy- β -cyclodextrin (β CD-HDA)

β CD-HDA was synthesized as previously reported.¹¹ β CD-Tos (1 g, 0.8 mmol, 1 eq.) was dissolved under argon in 5 mL dry DMF. In parallel, 1,6-hexanediamine was melted at 60°C. Upon melting, HDA (4 g, 34.4 mmol, 43 eq.) were added to the dissolved β CD-Tos. The reaction was stirred at 80 °C under argon for 18 h. Precipitation of the product was then induced by the addition of 45 mL ice-cold acetone. The solid was then centrifuged (4500 rcf., 15 min, 4 °C) and the supernatant was discarded. The resulting solid was redissolved in 5 mL DMF. The precipitation was repeated three times. The product was then washed once with ice-cold acetone and twice with ice-cold Et₂O. Finally, the product was dried in vacuo to yield a white powder (807 mg, 84 % yield). Characterization: ¹H-NMR (400 MHz, DMSO-d₆) δ 5.90 – 5.46 (m, 14H), 4.98 – 4.73 (m, 7H), 4.42 (t, 5H), 3.76 – 3.48 (m, 29H), 1.56 – 1.21 (m, 5H).

Tetrabutylammonium salts of HA (HA-TBA)

HA-TBA was synthesized as previously reported.¹¹ NaHA (M_n ~60 kDa, 1g, 17 μ mol, 1eq.) was dissolved in 50 ml of deionized water, followed by the addition of 3 g of Dowex 50W \times 8. The solution was stirred for 30 min at room temperature. The resin was then filtered off and the pH was increased in steps using tetrabutylammonium hydroxide (TBA-OH) solutions in water of various concentrations

(40 % v/v, 20 % v/v, 8 % v/v and 2 % v/v). First the pH was adjusted to 4 using 40 % v/v TBA-OH. Sequentially the pH was then adjusted to 5 using 20 % v/v, 6 using 8 % v/v, and finally 7.02 – 7.05 using 2% v/v TBA-OH solution. The resulting solution was lyophilized to yield a light orange solid (1.2 g, 73 % yield). Characterization: $^1\text{H-NMR}$ (400 MHz, D_2O) δ 4.64 – 4.47 (m, 2H), 4.09 – 3.36 (m, 12H), 3.31 – 3.16 (m, 13H), 2.03 (s, 3H), 1.79 – 1.56 (m, 13H), 1.38 (h, 13H), 0.96 (t, 20H).

β CD modified HA (β CD-HA)

HA-TBA (200 mg, 2.03 μmol , 1eq.) and CD-HDA (237 m g, 192 μmol , 95 eq) were dissolved under argon in 10 mL of dry DMSO. In parallel, BOP (85 mg, 192 μmol , 95 eq.) was dissolved under argon in 1.6 mL of dry DMSO. Upon dissolution of all components, the BOP solution was transferred via cannulation to the reaction mixture. The reaction was left to react for 3h at room temperature, followed by the addition of 0.8 mL of deionized water. The reaction mixture was then dialyzed (M_w cutoff of 1 kDa) against a sodium chloride solution (1.5 g per liter of water) for 5 days. The precipitated solid was then filtered off, followed by additional dialysis against distilled water for 5 days. The dialyzed solution was then lyophilized to yield a light yellow solid (205 mg, 40 % yield). Characterization: $^1\text{H-NMR}$ (400 MHz, D_2O) δ 5.20 – 5.06 (m, 1H), 4.61 – 4.45 (m, 2H), 4.03 – 3.05 (m, 18H), 2.04 (s, 3H), 1.82 – 1.32 (m, 2H).

Functional PEG-b-PLA

Both adamantane-PEG-b-PLA and Azobenzene-PEG-b-PLA were synthesized in a two-step synthesis following the same procedures. They only differ in the use of either 1-adamantane acetic acid for Ada-PEG-b-PLA or 4-(phenylazo)benzoic acid for AzB-PEG-b-PLA.

The procedure for Ada-PEG-b-PLA is described below.

Ada-PEG

HO-PEG-NH₂ ($M_n \sim 5$ kDa, 1g, 198 μmol , 1eq.) was dissolved under argon in 10 mL of dry DCM. Upon dissolution, 1-adamantane acetic acid (77 mg, 397 μmol , 2 eq.), PyBOP (309 mg, 595 μmol , 3 eq.) and a drop of DIPEA (51 mg, 397 μmol , 3 eq.) were added sequentially to the reaction mixture. The reaction was left to stirred overnight at room temperature. Afterwards, the solution was poured in cold Et₂O, to induce precipitation of the polymer. The solid was recovered through filtration, dissolved in water, and dialyzed (M_w cutoff of 100-500 Da) against distilled water for 2 days. The solution was then lyophilized yielding a white powder (943 mg, 91 % yield).

Ada-PEG Characterization: $^1\text{H-NMR}$ (400 MHz, CDCl_3) δ 5.93 (s, 1H), 3.64 (s, 450H), 1.96 (s, 3H), 1.92 (s, 2H), 1.74 – 1.51 (m, 12H).

AzB-PEG Characterization: $^1\text{H-NMR}$ (400 MHz, CDCl_3) δ 8.12 – 7.83 (m, 5H), 7.68 – 7.46 (m, 5H), 7.17 (s, 1H), 3.64 (s, 450H).

Guest -PEG-b-PLA

Ada-PEG (1 g, 193 μmol , 1 eq.) and lactic acid (4.32 g, 30 mmol, 155 eq.) were dissolved in 30 mL of dry freeze pump thawed dry toluene under an argon atmosphere. The mixture was heated to 100°C and stirred upon complete dissolution of the starting materials. Then, SnOct₂ (88 μL , 271 μmol , 1.4 eq.) was added and the temperature was raised to 140°C. The reaction was stirred under reflux for 6h. The solution was then poured into cold Et₂O to induce precipitation of the polymer. The resulting solid was dried in vacuo and yielded a white powder (1.3 g, 47 % yield).

Ada-PEG-b-PLA Characterization: ¹H-NMR (400 MHz, CDCl₃) δ 6.02 (s, 1H), 5.37 – 4.92 (m, 126H), 4.46 – 4.19 (m, 4H), 3.63 (s, 450H), 1.97 – 1.90 (m, 5H), 1.64 – 1.34 (m, 423H). Molecular weight using the PEG_{5k} peak as a reference: PLA 9 kDa.

AzB-PEG-b-PLA Characterization: ¹H-NMR (400 MHz, CDCl₃) δ 8.16 – 7.82 (m, 5H), 7.64 – 7.45 (m, 3H), 7.16 (s, 1H), 5.36 – 4.77 (m, 250H), 3.64 (s, 450H), 1.74 – 1.36 (m, 780H). Molecular weight using the PEG_{5k} peak as a reference: PLA 18 kDa.

3.5. ACKNOWLEDGEMENT

This work was supported by ETH Zurich start-up funds and the Swiss National Science Foundation (Project Grant 200021_184697).

CHAPTER 4

RESOLVING INTERNAL STRUCTURE OF POLYMER-NANOPARTICLE HYDROGELS THROUGH SUPER RESOLUTION IMAGING

SUMMARY *Characterization and understanding the structure of hydrogel networks is usually accomplished through testing of mechanical properties and relating them to theoretical models of the expected network structure. However, several classes of hydrogels are comprised of more complex network architectures, such as non-covalent molecular cross-links and secondary macromolecular interactions, which deviate from ideal polymer networks. In the case of polymer–nanoparticle (PNP) hydrogels, the hydrogel network is formed through polymer–nanoparticle interactions or nanoparticle–nanoparticle interactions, which imbues them with the observed bulk viscoelasticity. While these materials are often used as injectable hydrogels for the delivery of therapeutics and 3D printing, the origin of their dynamic mechanical properties is poorly understood, which can be addressed through the development of characterization techniques that are able to resolve the microstructure of the networks. In this chapter, we used total internal reflection fluorescence (TIRF) microscopy and direct stochastic optical reconstruction microscopy (dSTORM) to investigate the nanoparticle distribution within the hydrogel and relate it to the macroscopic properties of PNP hydrogels as a model system. We formulated PNP hydrogels with various α -cyclodextrin (α CD) concentrations and employed dye-labelled nanoparticles for the imaging. At low concentrations of α CD, we observed a porous network-like distribution of the nanoparticles with minimal aggregation, while at higher concentrations aggregates of increased size formed within the network indicative of increase NP–NP interactions. This work lays the foundation for existing microscopy techniques to be employed to fill the gap between understanding of the molecular behavior, changes in topology, and macroscopic properties in hydrogel characterization.*

AUTHOR CONTRIBUTIONS: SB and MWT conceived the idea and wrote the manuscript. SB designed and executed the experiments.

4.1. INTRODUCTION

Hydrogels are cross-linked, water-swollen polymer networks, widely used in the biomedical field for their biocompatibility, high water content, and similarity to the extracellular matrix.⁷ Use of hydrogels in various biomedical applications has been driven by rational engineering of the polymer networks to obtain distinct mechanical properties, which requires understanding of their underlying structure–function relationships.^{264,285} For ideal networks where the interactions are direct cross-links of the network strands, the origin of the observed mechanical response (e.g., modulus, stiffness, yield strain, and swelling) classically relates to molecular parameters or the network (e.g., polymer length, cross-link number, or cross-link dynamics).^{54,65,286} However, many recent advances involve the design of hydrogels with complex network architectures, which do not conform to the structure–function relationships developed for ideal polymer networks. For example, peptide-based hydrogels comprise various molecular interactions (hydrogen bonding as well as electrostatic and hydrophobic interactions) for the formation of nano- and microscale secondary structures (β -sheets, α -helices) that can further assemble into fibrillar structures, resulting in complex entangled networks.^{155,168,287–289} Similarly, polymer–nanoparticle (PNP) hydrogels are a class of injectable nanocomposite biomaterials, based on reversible interactions between polymer chains and nanoparticles.¹⁸ Network formation in PNP hydrogels is driven either by polymer chain bridging or by nanoparticle jamming, each resulting in unique features in the macroscopic properties of the material.²⁶⁹ While changes in mechanical response have been demonstrated by changing relative proportions of the network components, their impact on the microstructure of the hydrogel has yet to be understood. Therefore, a strategy to resolve the microstructure of hydrogel could provide the critical missing link between the molecular and macroscale properties of hierarchically structured hydrogels, providing further understanding of complex hydrogel networks and their design parameters.

Microscopy techniques, such as atomic force microscopy (AFM), scanning electron microscopy (SEM), or transmission electron microscopy (TEM), have been leveraged for the investigation of material microstructures.^{290,291} Such techniques were used to visualize fibres or pores within hydrogels, reaching a resolution up to 0.2 nm.²⁹² Despite their high resolution, these microscopy techniques pose limitations related to extensive sample preparation that is often not suited for high water content hydrogel samples, resulting in possible deterioration or changes in the microscopic architecture during freezing or evaporation processes.^{293,294} Furthermore, many of these techniques are limited to the characterization of surfaces and provided limited insight into the internal architecture of the hydrogels. On the other hand, optical microscopy techniques face the opposite challenges. While optical microscopy techniques allow for in-situ imaging and rely on relatively simple sample preparation, they are limited in resolution due to the diffraction limit of visible light (~ 200 nm).^{295,296} To extend the resolution of optical microscopy, super-resolution microscopy (SRM) techniques have been developed.^{295,297}

Direct stochastic optical reconstruction microscopy (dSTORM) is a SRM technique based on single-molecule localization, that allows resolutions of up to ~ 20 nm.^{298–300} dSTORM leverages the capacity of

a fluorophore to switch between an “ON” and “OFF” state when exposed to a laser, resulting in the activation of a certain proportion of the total fluorophores at any given time. These individual signals can be recorded and fit to enable the localization of the individual fluorophores. The localized fluorescence signals are finally assembled in a single image with a resolution correlating to the quality of localization of the fluorophore. Although the use of dSTORM in biological applications is becoming more prevalent^{301,302}, few studies have been reported where dSTORM is used for materials characterization.^{303–306} We hypothesized that leveraging fluorescence and super-resolution microscopy would enable the in-situ investigation of PNP hydrogel nano- and microstructure in a contactless manner.

In this work, we use fluorescence microscopy and dSTORM to visualize the microstructure of PNP hydrogels. PNP hydrogels were assembled using fluorescently labelled poly (ethylene glycol)-*b*-poly (lactic acid) (PEG-*b*-PLA) nanoparticles in combination with hydroxypropylmethylcellulose (HPMC). The nanoparticle distribution in the hydrogels was resolved by recording micrographs using total internal reflection fluorescence (TIRF) microscopy and performing dSTORM analysis. The resulting images revealed the formation of a porous network-like distribution of the nanoparticles in the hydrogel. Further, the microscopy technique was combined with rheological measurements to investigate the structural origins of the mechanical properties of PNP hydrogels upon addition of a α -cyclodextrin (α CD) to the hydrogel matrix. At low concentrations of α CD, the PNP hydrogels exhibited similar storage modulus and microstructure as the formulation without α CD. Above a threshold α CD concentration, the mechanical properties of the PNP hydrogels increased dramatically. This increase was associated with a change in the underlying microstructure of the hydrogel, namely the formation of nanoparticle clusters corroborating previous reports on the ability of α CD to induce nanoparticle aggregation.²⁶⁹ Overall, this work showcases the use of TIRF and dSTORM imaging to resolve PNP hydrogel microstructure, providing a potential platform for broadening our current understanding on structure–property relationships for the engineering of hierarchical hydrogels.

4.1. RESULT AND DISCUSSION

4.1.1. Resolving PNP hydrogel microstructure

In a first step toward the resolution of hydrogel microstructure through SRM, we set ourselves to investigate the microstructure of native PNP hydrogels. PNP hydrogels are primarily based on reversible interactions between polymer chains and nanoparticles. As established in **Chapter 3**, the nanoparticles are the main driving force for the network formation acting as a cross-link between the polymer chains.³⁰⁷ In this model, a sufficient polymer concentration is required to percolate the network and beyond this point additional polymer content contributes primarily to the viscosity of the system. We hypothesized that due to the influence of the nanoparticles in determining the macroscopic properties of the hydrogel, resolving their distribution in the hydrogel matrix could provide a handle to understand how microstructure leads to macroscale mechanics in PNP hydrogels.

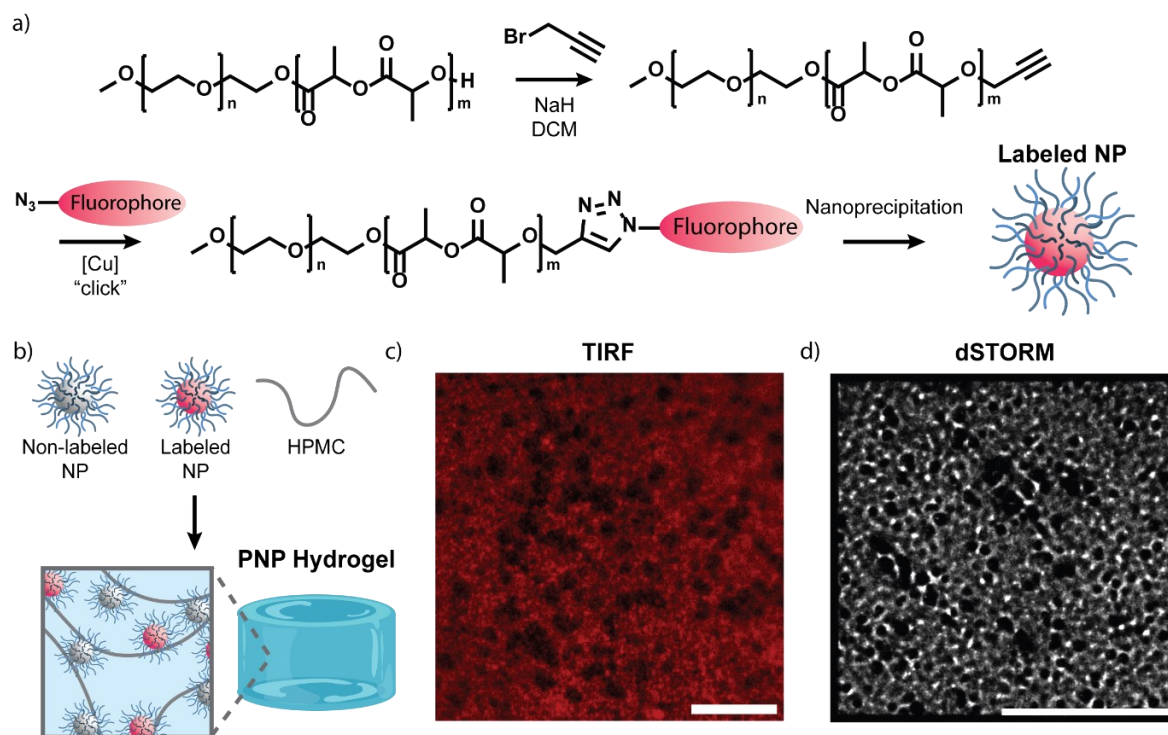


Figure 4.1: a) Synthetic strategy for the formation of labeled PEG-*b*-PLA nanoparticles. b) PNP hydrogel for imaging were assembled by mixing labeled and non-labeled nanoparticles (1:3 labeled to non-labeled) with HPMC. c) TIRF image showing the distribution of ATTO 647-labeled nanoparticles in PNP hydrogel (1 wt% HPMC, 5 wt% NPs). Scale bar, 10 μm . d) dSTORM image of the hydrogel formulation revealed a porous network-like distribution of the nanoparticles. Scale bar, 10 μm .

For this purpose, we introduced a fluorescent label in the nanoparticle design. We developed a covalent coupling strategy to avoid leakage of the fluorophore from the nanoparticle (**Figure 4.1a**). First, PEG_{10k}-*b*-PLA_{14k} block co-polymers were functionalized on the PLA end with an alkyne moiety. The alkyne moiety was in a second step coupled to azide functionalized fluorophores (ATTO 647) using copper-assisted click chemistry. Completion of the reactions was confirmed via ¹H-NMR spectroscopy (**Figure S36-38**). PEG-*b*-PLA NPs (NPs; $\text{\O} = 70 \text{ nm}$; $\text{\D} = 0.30$) were formed via nanoprecipitation of block copolymers. PNP hydrogel formation was then achieved by mixing HPMC (1 wt%) with NPs (5 wt%; **Figure 4.1b**). To enable stochastic photoswitching between the “on” and “off” state of the fluorophore, a photoswitching buffer was incorporated in the hydrogel formulation. The buffer serves as a reducing agent stabilizing the “off” state of the fluorophore.

In contrast to traditional systems imaged with dSTORM, in the PNP hydrogels the labeled feature, the NPs, are present in the entirety of the hydrogel network. As such, the fluorophores are present in high density, which can result in decreased localization accuracy due to excessive overlapping signals. To decrease fluorophore density, the NPs were formed using functionalized and non-functionalized block co-polymers (1:99 ratio of functionalized to non-functionalized). Similarly, hydrogels were formulated with a mixture of labeled and non-labeled NPs (1:3 labeled to non-labeled; **Figure 4.1b**). Further, to

reduce background fluorescent a TIRF objective was used for the image acquisition, limiting the excitation to a thin layer within the sample with a typical penetration depth of less than 300 nm.³⁰⁸ dSTORM experiments were then performed on a wide-field fluorescence microscope in TIRF mode. TIRF images were first captured followed by the recording of wide-field images (5'000-30'000 scan) under continuous laser excitation at $\lambda = 647$ nm. dSTORM images were reconstructed from determined positions the fluorophores with uncertainty below 50 nm (**Figure 4.1d**).

Both TIRF and dSTORM enabled the visualization of the nanoparticle distribution in the sample (**Figure 4.1c, d; Figure S39**). The micrographs showed a non-homogenous distribution of the nanoparticles within the hydrogel, resembling a porous network-like architecture. In the literature, PNP hydrogels formed between HPMC and PEG-*b*-PLA NPs have been proposed to form through the adsorption of the HPMC on the NPs.¹⁴² The adsorption of the nanoparticles on the HPMC polymer chains could serve as possible cross-link between polymer chains resulting in polymer bridging and the subsequent percolation of a network. Additional experiments, such as multicolor dSTORM with dye-labeled HPMC are needed to confirm the co-localization of the NPs and HPMC to corroborate this model. Further, sample microstructure imaging shortly after formation of the hydrogel (<1 day) showed fiber-like alignment of the nanoparticle over extended distances (**Figure S39**). This possible feature could be associated to alignment of the network during initial processing. The absorption of NPs on the HPMC could result in their alignment along polymer chains and subsequent alignment into higher order structures upon network formation and processing. Current understanding of the origin of the observed microstructure remains uncertain due to possible processing effect and changes of the conformation over time.

The current dSTORM setup does not differentiate fluorophores present at different depths in the sample, participating in the increased background signal. Future experiments may leverage 3D dSTORM to enhance the contrast between specific features in the sample and the background. Overall, TIRF and dSTORM imaging enable the visualization of nanoparticle distribution within PNP hydrogel, which can provide insight on changes in mechanical properties associated to changes in nanoparticle distribution.

4.1.1. Imaging of the hydrogel at various using α CD content

As shown in **Chapter 2**, the addition of α CD has a substantial impact on the mechanical properties, showing a concentration-dependent increase in shear modulus. This change in mechanical properties was hypothesized to be related to increased NP–NP interactions following the formation of polypseudorotaxanes and nanoparticle clustering. Indeed, α CD has the ability to thread on PEG to form polypseudorotaxane or so called “molecular necklaces”.¹⁰⁶ These structures can then further aggregate to form larger semi-crystalline aggregates.³⁰⁹ In the presence of PEGylated NPs, we hypothesized that the formation of polypseudorotaxanes induced the aggregation of the nanoparticles.²⁶⁹ To investigate the possible changes in PNP microstructure associated with the addition of α CD, we combined rheological

characterization with TIRF and dSTORM imaging of PNP hydrogels with different α CD concentrations (**Figure 4.2**).

In **Chapter 2**, the effect of α CD significantly enhanced the mechanical properties for concentrations above 5 wt% as compared with PNP formulations without α CD. Therefore, PNP hydrogels with 2.5 and 5 wt% α CD were compared with formulations without α CD. Rheological measurement in **Chapter 2** of formulations with 0 and 2.5 wt% α CD showed similar mechanical properties with a respective shear moduli of a $G' \approx 18.4$ Pa and $G' \approx 19.2$ Pa ($\omega = 10$ rad s⁻¹; **Figure 4.2b**).²⁶⁹ The addition of 5 wt% of α CD resulted in an increase in shear modulus of two orders of magnitude ($G' \approx 3.0 \times 10^3$ at $\omega = 10$ rad s⁻¹).

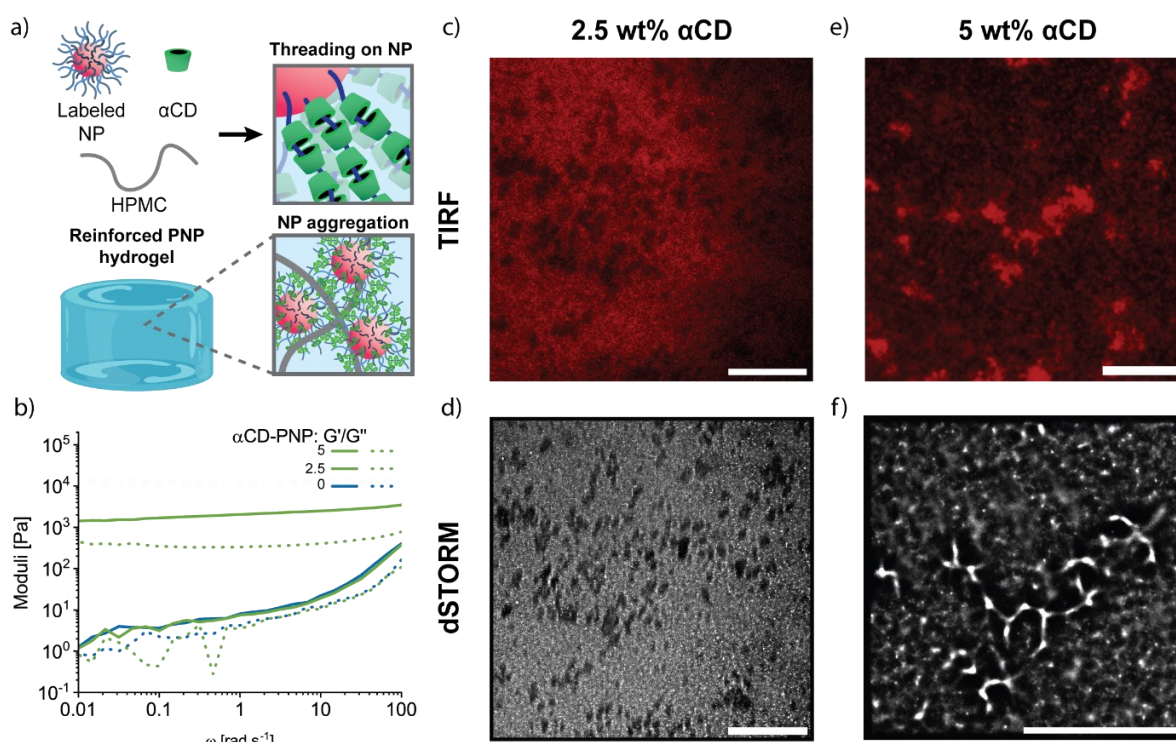


Figure 4.2: a) Proposed mechanism of reinforcement of PNP hydrogels through formation of polypseudorotaxane on PEGylate nanoparticle surfaces, leading to the aggregation of the nanoparticle. b) Frequency sweep of PNP hydrogel with 0, 2.5 and 5 wt% α CD from **Chapter 2**. Formulation with 2.5 wt% of α CD image through c) TIRF and d) dSTORM microscopy showed similar microstructure to PNP hydrogel in the absence of α CD. Formulation with 5 wt% of α CD were image through d) TRIF and e) dSTORM microscopy and showed the formation of nanoparticle aggregates. Scale bar, 10 μ m.

In accordance with the rheological measurements, formulations containing 2.5 wt% α CD showed similar nanoparticle distribution as for those without α CD (**Figure 4.2c, d**). The nanoparticle again exhibited a distribution similar to a porous network that we associated with preferential interactions with the HPMC polymer chains. On the other hand, formulations with 5 wt% α CD exhibited a dramatically different nanoparticle distribution in the sample (**Figure 4.2e, f**). In this case, the NPs arranged themselves in

dense clusters (**Figure 4.2c**). The formation of nanoparticle clusters was associated with an increased presence of NP–NP interactions.

These observations supported the proposed mechanism of reinforcement of PNP hydrogel in the presence of α CD. Upon the addition of a threshold concentration of α CD, α CD induces aggregation of the nanoparticle resulting in nanoparticle clustering. The change in the microstructure of the hydrogel resulted in the increase in shear moduli of the system. Further, the loss of the initial network structure of the nanoparticle with the increase of α CD suggested a decrease in the absorption of the nanoparticles on the HPMC polymer chains and an increase in the NP–NP interactions and clustering. The decrease of absorption could decrease polymer–nanoparticle interactions, which was proposed in **Chapter 2**. Overall, the changes in mechanical properties observed with the addition of α CD were correlated to changes in the microstructure of the hydrogel supporting the proposed mechanism of reinforcement through nanoparticle aggregation.

4.2. CONCLUSION

In this work we leveraged TIRF and dSTORM imaging to visualize the microstructure of PNP hydrogel. For this purpose, we synthesized fluorescently labelled block co-polymers for the formation of fluorescent polymeric nanoparticles. The nanoparticles were then assembled into hydrogels by mixing with HPMC. The density of the label was tuned to promote single molecule activation. The nanoparticle distribution of the resulting hydrogels was visualized via TIRF and dSTORM imaging revealing a porous-network-like distribution of the nanoparticles in the absence of α CD. The feature was associated to the adsorption of the nanoparticles on the HPMC chains. Furthermore, we were able to visualize the changes in nanoparticle aggregation induced in the presence of α CD at 5 wt%. The changes in microstructure were correlated to the resulting mechanical properties of the hydrogel to confirm previously proposed relationship between macroscopic properties and microstructure in PNP hydrogel. This work provides an application of super-resolution optical microscopy techniques to hydrogel structure elucidation.

4.3. MATERIALS & METHODS

4.3.1. Materials

α -Cyclodextrin (α CD, TCI) Acetone (Sigma-Aldrich); Chloroform-d (CDCl_3 , Fisher Scientific); Hydroxypropylmethylcellulose (HPMC, $M_n \sim 700$ kDa, Sigma-Aldrich) photoswitching buffer (100–160 mM β -mercaptoethylamine hydrochloride [MEA]; Everspark 1.0,) Dichloromethane (DCM, Sigma-Aldrich); Dichloromethane (DCM, extra Dry over MS, Fisher Scientific); propargyl bromide (80 % in toluene, Sigma-Aldrich); poly(ethylene glycol) methyl ether (PEG; M_n 5000 Da, Sigma-Aldrich) sodium hydride (NaH, Sigma-Aldrich) Diethyl ether (Et_2O , VWR Chemicals); ATTON 657- N_3 (Sigma-Aldrich); 3,6-dimethyl-1,4-dioxane-2,5-dione (lactide, Sigma-Aldrich); Tin(II) 2-ethylhexanoate (SnOct_2 , Sigma-Aldrich); Toluene (extra dry, Acros Organics);

4.3.2. Instrumentation and methods

Nuclear magnetic resonance

¹H-NMR spectra were acquired on a Bruker Avance III 400 (Bruker BioSpin GmbH). Chemical shifts were reported relative to the respective residual solvent peak. (CDCl₃: $\delta = 7.26$ ppm) Molecular weight of methyl ether-PEGs were determined using the terminal CH₃ groups as a reference.

Dynamic light scattering

The hydrodynamic diameters of the formed NPs were measured by dynamic light scattering (DLS) on a Malvern ZetaSizer Nano ZS. The nanoparticle suspensions were placed into a semi-micro cuvette (Brand, Path length: 10 mm). The measurements were performed at 25 °C with a wavelength of 633 nm and a scattering angle of 17°C. The properties of each sample were measured three times reported as z-average diameter and dispersity.

Polymeric nanoparticle formation

Polymeric nanoparticles were formed via batch nanoprecipitation. 70 mg of PEG-b-PLA (1:3 labeled to non-labeled polymer) were dissolved in 1 mL acetone. The solution was added dropwise to 10 mL of milli-q water under stirring. Acetone was evaporated overnight by keeping nanoparticle suspension in an open container on a shaking plate. NPs were subsequently concentrated via ultrafiltration with an Amicon Ultra centrifugation filter (MWCO: 30 kDa, 4500 ref, 1.2h). The NPs were resuspended to a final concentration of 30 wt%.

PNP hydrogel formation

All gels were formed using similar procedure. A representative procedure for a 500 mg gel with 1 wt% HPMC, 5 wt% nanoparticle and 5 wt% α CD is described. In a luer-lock syringe, 5 mg of HPMC and 25 mg α CD were dissolved in 187 μ L milli-q water and let to equilibrate overnight at room temperature. In a different luer-lock syringe, 83.3 mg of a 30 wt% solution of nanoparticles (1:3 labeled to non-labeled nanoparticle) was prepared. In case of sample for imaging, 200 μ L of photoswitching buffer (Everspark 1.0, 100–160 mM MEA) were added, otherwise milli-q water was used. The polymer-containing syringe and nanoparticle containing syringes were connected through a female-to-female luer lock adapter (Cellink, Sweden) and gently mixed for 30 seconds.

Mounting of PNP gel for imaging

PNP hydrogel containing photoswitching buffer were used for imaging. The preparation and mounting of the hydrogel were performed under 1 minute to avoid possible deactivation of the buffer due to exposure to oxygen. Upon formation of the PNP hydrogel, the gels were mounted in cavity slides ($\text{\O} = 15\text{--}18\text{mm}$, depth 0.6–0.8 mm) by extrusion through syringes. A cover slide was then used to cover the cavity, followed by the hermetic sealing of the sample using two-component sealant from Everspark.

Rheological characterization

Rheological data were taken from **Chapter 2**. Rheological measurements were performed with a strain-controlled shear rheometer (MCR 502; Anton Paar; Zofingen, Switzerland). Measurements for the formulations were performed using a plate-plate geometry of 20 mm diameter at a plate temperature of 25 °C. A gap size of between 0.5 – 0.8 mm was used for all rheological measurements. To reduce any loading history of the sample, after loading the sample in the geometry, an oscillatory pre-conditioning interval ($\omega = 0.1 \text{ rad s}^{-1}$, $\gamma = 0.01 \%$, $t = 30 \text{ min}$) was performed. Dynamic oscillatory frequency sweep measurements were conducted with a decreasing angular frequency (from 100 to 0.1 rad s^{-1}) and a constant strain amplitude ($\gamma = 1 \%$).

TIRF and dSTORM imaging

Images were acquired using a Nikon N-STORM microscope (Nikon UK Ltd) with an SR Apochromat TIRF 100 \times 1.49 NA oil immersion objective lens. The sample were excited using a laser at $\lambda = 647 \text{ nm}$ and emission passed through a QUAD filter set for TIRF applications (Nikon C-N STORM QUAD 405/488/561/647). Fluorescence signal was recorded with either an ANDOR EMCCD camera or an sCMOS Hamamatsu Orca Flash 4 v3. All dSTORM images were acquired with 5,000–30,000 camera frames with exposure from 10–30 ms.

d-STROM analysis

Analysis were performed using the open source FIJI plugin ThunderSTORM.³¹⁰ Localizations were fitted to an integrated Gaussian point spread function. Further, the images were processed using drift-correction and filters for localization precision ($<50 \text{ nm}$) as well as filter for full width at half maximum ($\sigma < 700 \text{ nm}$).

4.3.3. Synthetic procedures

PEG-b-PLA

PEG-b-PLA was synthesized as reported in **Chapter 2**.²⁶⁹ Characterization: $^1\text{H-NMR}$ (400 MHz, CDCl_3) δ 5.32 – 4.98 (m, 189H), 4.60 – 4.16 (m, 4H), 3.71 – 3.56 (m, 933H), 3.37 (s, 3H), 1.66 – 1.49 (m, 566H). (**Figure S36**)

PEG-b-PLA-Alkyne

PEG-b-PLA (1 g, 41.6 μmol , 1 eq.) was dissolved in DCM (8 mL) and cooled to 0 °C using an ice bath. Propargyl bromide (80 % in toluene, 4.27 μL , 49.9 μmol , 1.2 eq.), followed by the addition of sodium hydride (60 % in oil, 2 mg, 49.9 μmol , 1.2 eq.). The reaction mixture was stirred overnight at room temperature. The mixture was then poured in cold Et_2O to precipitate the polymer. The product was dried in vacuo resulting in a white powder. Characterization: $^1\text{H-NMR}$ (400 MHz, CDCl_3) δ 5.27 – 5.06 (m, 128H), 4.76 – 4.69 (m, 1H), 4.40 – 4.16 (m, 3H), 3.69 – 3.55 (m, 845H), 3.37 (s, 3H), 2.49 (t, 1H), 1.53 – 1.48 (m, 386H). (**Figure S37**)

PEG-b-PLA-Dye

PEG-b-PLA-alkyne (30 mg, 1.24 μmol , 10 eq.) was dissolved in 3 mL of THF. Subsequently, ATTON 647-N₃ (0.1mg, 0.12 μmol , 1 eq.), CuSO₄ (1 mg, 6.27 μmol , 52 eq.) and ascorbic acid (1 mg, 5.68 μmol , 47 eq.) were added to the solution and let to stir overnight. The solvent was then evaporated in vacuo resulting in a blue solid. (**Figure S38**)

4.4. ACKNOWLEDGEMENTS

This work was supported by ETH Zurich start-up funds and the Swiss National Science Foundation (Project Grant 200021_184697). The authors would like to thank the Scientific Center for Optical and Electron Microscopy (ScopeM), especially Dr. Pinotsi Dorothea for assisting in imaging.

CHAPTER 5

REDOX RESPONSIVE NANOGEL FOR INTRACELLULAR DRUG DELIVERY

SUMMARY *Nanogels are a class of drug nanocarriers that combine the favorable properties of hydrogels, such as high-water content and biocompatibility, with facilitated cellular uptake for intracellular therapeutic delivery. However, specific and tailored release of the therapeutic from nanogels often remains a challenge. If the therapeutic is simply encapsulated, diffusion-based release occurs resulting in offsite release before internalization of the carrier. Covalent attachment of the therapeutic can ensure targeting to the site of interest but presents challenges for release and maintained bioactivity. Therefore, we designed nanogels to enable covalent attachment of therapeutics with triggered and traceless disruption of the linker upon internalization, reducing offsite effects. Specifically, a responsive nanogel drug delivery system was engineered using a glutathione-cleavable and self-immolative disulfide linker to couple therapeutics to the nanogel backbone. The linker design enabled coupling to model protein therapeutics in mild phosphate buffer conditions within an hour and selective cleavage in glutathione concentrations similar to those observed inside of cells. Overall, this work focused on an easy to couple responsive nanogel drug delivery carrier for intracellular release of therapeutics free of chemical modification.*

This chapter is reproduced from: Stéphane Bernhard, Carolina Söll, Lorena Rodriguez Curiel, Gabriela Da Silva André, Leslie Cunningham, Rea Frischknecht, Giovanni Bovone, Emanuele Mauri, and Mark W. Tibbitt *in preparation*. **AUTHOR CONTRIBUTIONS:** SB, GB, EM, and MWT conceived the ideas, designed the experiments, and wrote the manuscript. SB, CS, LRC, GDSA, LC, and RF executed the experiments and analyzed the data. SB, CS, and MWT wrote the manuscript.

5.1. INTRODUCTION

Conventional drug delivery systems rely on systemic administration of therapeutics, exposing the active molecule to extended blood circulation times and the need to cross multiple physiological barriers prior to reaching the site of interest.^{311,312} As a result, much of the therapeutic load can be lost prematurely before uptake by the cell, reducing efficacy and possibly inducing unwanted side effects. Diverse nanocarriers have been developed to protect therapeutics during transit as a strategy to address the challenges associated with conventional drug delivery systems.^{313,314} In many cases, nanocarriers have been able to increase uptake efficiency, reduce risk of early clearance by the immune system, and reduce off-target effects, overall increasing therapeutic efficacy.³¹⁵

Nanogels are a class of nanocarriers comprised of cross-linked polymer networks with nanometer dimensions.³¹⁶ They combine the favorable properties of hydrogel biomaterials, such as high water content, biocompatibility, and swellability,⁵⁴ with properties of nanoscale objects, such as facilitated cellular uptake and longer blood circulation time.^{317–319} Common strategies to release the therapeutic from the nanogels rely on changes in the swelling of the nanogel due to environmental stimuli, such as pH, temperature, or salt concentration. Upon exposure to the environmental stimuli the nanogels swell, inducing a change in mesh size of the polymer network, increasing diffusion, and ultimately accelerating the release of the cargo.^{320,321} Diffusion-based processes, however, show limited tunability and control over the release profile due to their dependency on the network structure.^{54,322} Engineering specific and responsive drug–nanogel interactions, provides an alternative release mechanism with increase control over therapeutic release.

Covalent attachment of molecular therapeutics to the nanogel through a responsive linker has improved control over the release kinetics by delaying the release.³²³ In these approaches, therapeutic release required degradation of the linker through external stimuli, such as pH-sensitive hydrazone linkers, redox responsive disulfide bonds, or enzyme-sensitive peptides.^{324–326} However, the covalent attachment of molecular therapeutics often requires chemical modification, which upon release from the linker might retain some traces of the degraded linker, resulting in loss of efficacy and possible side effects.^{327,328} Therefore, strategies are needed that allow coupling of therapeutics to nanogels for protection and stability while ensuring complete release without traces of chemical modification.

Additionally, by carefully designing the chemical structure bridging the linker and the therapeutic, cleavage of the linker can induce an intramolecular rearrangement of the linker—self-immolation—inducing the formation of nontoxic by-product and traceless release of the therapeutic without chemical modification.³²⁹ Recently, linkers based on self-immolative disulfide chemistries were introduced to label and release therapeutics without traces of chemical modification upon internalization by cells.³³⁰ Disulfide bonds are highly responsive to their environment and can be reduced readily into their unlinked thiol counterpart, making them suitable triggers for therapeutic release.^{331,332} Of particular interest is the responsivity of the disulfide bonds to glutathione (GSH), an antioxidant involve in

mammalian cells metabolism.³³³ GSH is able to reduce disulfide bonds under ambient conditions and within biological settings to their thiol counterpart. In this manner, specific degradation of disulfide bonds can be induced upon cell internalization due to the difference of GSH concentration of a few orders of magnitude between extracellular fluid, such as the blood ($<20\ \mu\text{M}$)³³³ and the cytosol (1–2 mM),³³³ with the highest concentration in cancer or liver cells (10 mM).³³⁴

In this work, we designed a redox-responsive nanogel drug delivery system for intracellular drug delivery of biologics. For this purpose, functional nanogels were synthesized through emulsion-evaporation of azide-functionalized poly (ethylene glycol) (PEG) and polyethyleneimine (PEI). In parallel, a responsive linker was designed to combine a GSH-responsive disulfide bond, self-immolative cleavage, and easy coupling to biologics under mild reaction conditions. Linker cleavage occurred for GSH concentrations above a threshold concentration (1 mM), sufficiently higher than extracellular GSH levels (2–20 μM).³³³ We monitored the self-immolative and traceless removal of the linker through the loss of absorbance on an added rhodamine B (RhB) cargo and NMR spectroscopy. By incorporation of nitrophenyl in the linker design, protein coupling was achieved in mild pH 8 phosphate buffer within 1 h. Preliminary cell experiments demonstrated nanogel uptake by liver cells without appreciable cytotoxicity.

RESULT AND DISCUSSION

5.1.1. Building block synthesis

To engineer our redox-responsive nanogels, we set out to design biocompatible nanogels that enabled linking of amine-containing therapeutics to the nanogel backbone via a GSH-responsive, self-immolative linker (**Figure 5.1a**). In this manner, the therapeutic would remain bound to the nanogel in circulation and the extracellular space (low GSH concentration) and be released intracellularly (high GSH concentration). We also designed a multifunctional linker to enable protein labelling through the inclusion of a nitrophenyl moiety, GSH-responsive release through the inclusion of a disulfide, and coupling to the alkyne-containing nanogels through the inclusion of an azide (**Figure 5.1b**). To prepare the nanogels, we first focused on the synthesis of the azide-functionalized polymer precursors for network formation and enable coupling in later stages to a linker attached to a therapeutic (**Figure 5.1c**). Azide–alkyne click chemistry was identified as a suitable coupling reaction due to its biorthogonality, enabling the specific reaction of the linker to the nanogels, without risk of side reaction with the therapeutic. First, azide-functionalized nanogels were prepared from linear poly(ethylene glycol) (PEG; $M_n \sim 8\ \text{kDa}$) and linear poly (ethylene imine) (PEI; $M_w \sim 2.5\ \text{kDa}$) following literature procedure (**Figure 5.1c**).³³⁵ PEG was first functionalized with epoxy end groups, to allow the following addition of azide functional groups, while conserving hydroxyl functionalities. The terminal hydroxy groups were then activated through carbonyldiimidazole chemistry for later coupling with PEI. Azide-functionalized nanogels were finally prepared by cross-linking the activated PEG with the secondary amines in PEI via an emulsion evaporation process resulting in an aqueous suspension of nanogels (\emptyset

= 185 nm; \bar{D} = 0.3). Completion of each synthesis step and presence of the azide groups were confirmed via $^1\text{H-NMR}$ and FTIR spectroscopy (Figure S40-45).

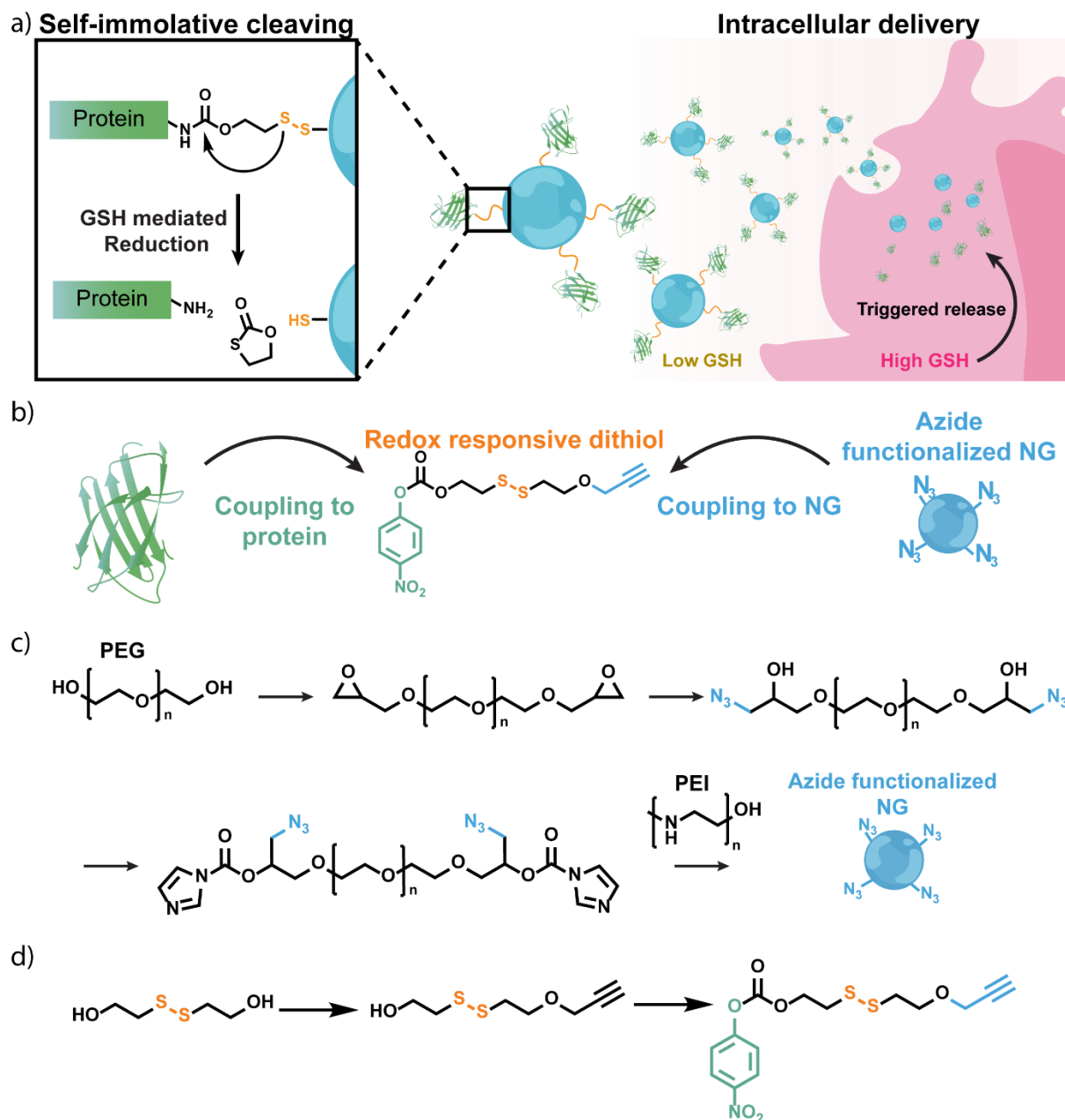


Figure 5.1. a) Nanogels were designed for self-immolative cleavage in the presence of GSH, enabling responsive intracellular delivery of therapeutics. b) A self-immolative disulfide linker was designed to enable easy coupling to proteins and functionalization via click chemistry to the nanogels. Synthesis scheme of c) azide-functionalized nanogel and of d) a disulfide linker for easy coupling of proteins to the nanogels.

In parallel, a self-immolative disulfide linker was designed. To enable self-immolation of the linker and traceless release, a carbamate linkage was used to anchor to amine containing therapeutics (Figure 5.1b, d).³³⁶ Upon reduction of the disulfide bond, the formed thiols can undergo an intramolecular rearrangement by attacking the carbamate bond and releasing the cargo with the intact free amine.

However, the formation of a carbamate between the linker and amine in the therapeutic can result in loss of bioactivity or degradation of the therapeutic in case of harsh coupling conditions, such as organic solvents and high or low pH.^{337–339} To avoid loss of the therapeutic during the carbamate formation, mild coupling conditions between the linker and therapeutic were required. Therefore, we leveraged the increased reactivity of amines with nitrophenyl carbonates to form the carbamate in mild aqueous conditions.³⁴⁰ The linker was synthesized in a two-step process (**Figure 5.1d**). First, 2-hydroxyethyl disulfide was coupled to propargyl bromide, to introduce the alkyl moiety required for click chemistry with the nanogels. In a second step, the remaining hydroxyl group was converted into a nitrophenyl carbonate, to enable facile carbamate formation with amine-containing therapeutics and for the self-immolative cleaving of the dithiol bond. Completion of each synthesis step and presence of the functional groups was confirmed via ¹H-NMR spectroscopy (**Figure S46, 47**).

5.1.2. Self-immolative cleavage

To investigate the cleavage behavior of the linker and to verify that it was self-immolative, we coupled the linker to a responsive that loses its absorbance upon cleavage from the linker and reformation of the NH₂ (**Figure 5.2; Figure S48, 49**). Indeed, RhB and RhB derivatives are known to exist in two main conformations: a “closed” conformation with low absorbance and an “open” conformation with high absorbance (**Figure 5.2a**).^{341,342}

In contrast to RhB, RhB-NH₂ does not exhibit an observable absorbance peak at 570 nm (**Figure 5.2b**). This behavior was associated with a “closed” conformation due to the formation of a spirolactam ring with the neighboring nitrogen.³⁴³ As spirolactam rings can be broken by protonation of the nitrogen, the presence of the ring was confirmed by titration of RhB-NH₂ using HCl. With the increase in HCl, the absorbance increased, supporting the hypothesis that there was an opening of the spirolactam ring under acidic conditions (**Figure 5.2c**). Upon coupling of the RhB-NH₂ to the linker (RhB-linker), the molecule showed an increase in absorbance (**Figure 5.2b**). We associated the increase in absorbance to a predominant “open” conformation for the RhB-linker; however, the overall absorbance of the reacted RhB was still lower than that of unfunctionalized RhB. Thanks to this difference in the absorbance between the RhB-linker and RhB-NH₂, the cleavage reaction and the self-immolative behavior of the linker could be investigated through loss of absorbance of the RhB cargo (**Figure 5.2d**).

Cleaving of the RhB-linker was investigated by monitoring UV-vis absorbance at 570 nm in the presence of varying GSH concentration from 0.01 mM,³³³ similar to blood levels, to 10 mM, which is observed in the liver (**Figure 5.2e**).³³⁴ Over the course of 30 h, the absorbance decreased for all conditions including a control without GSH. The general decrease of absorbance was associated to two overlapping effects: the loss of absorbance of RhB due to bleaching of the fluorophore.³⁴⁴ and the loss of absorbance due to the release of the RhB-NH₂. When compared with the control, the RhB-linker did not show significant changes in absorbance when exposed to 0.01 and 0.1 mM of GSH. A dose-dependent and accelerated decrease in absorbance was observed for 1 and 10 mM GSH. These results indicate a

concentration dependent reduction of the dithiol bond beyond a threshold GSH concentration of >0.1 mM.

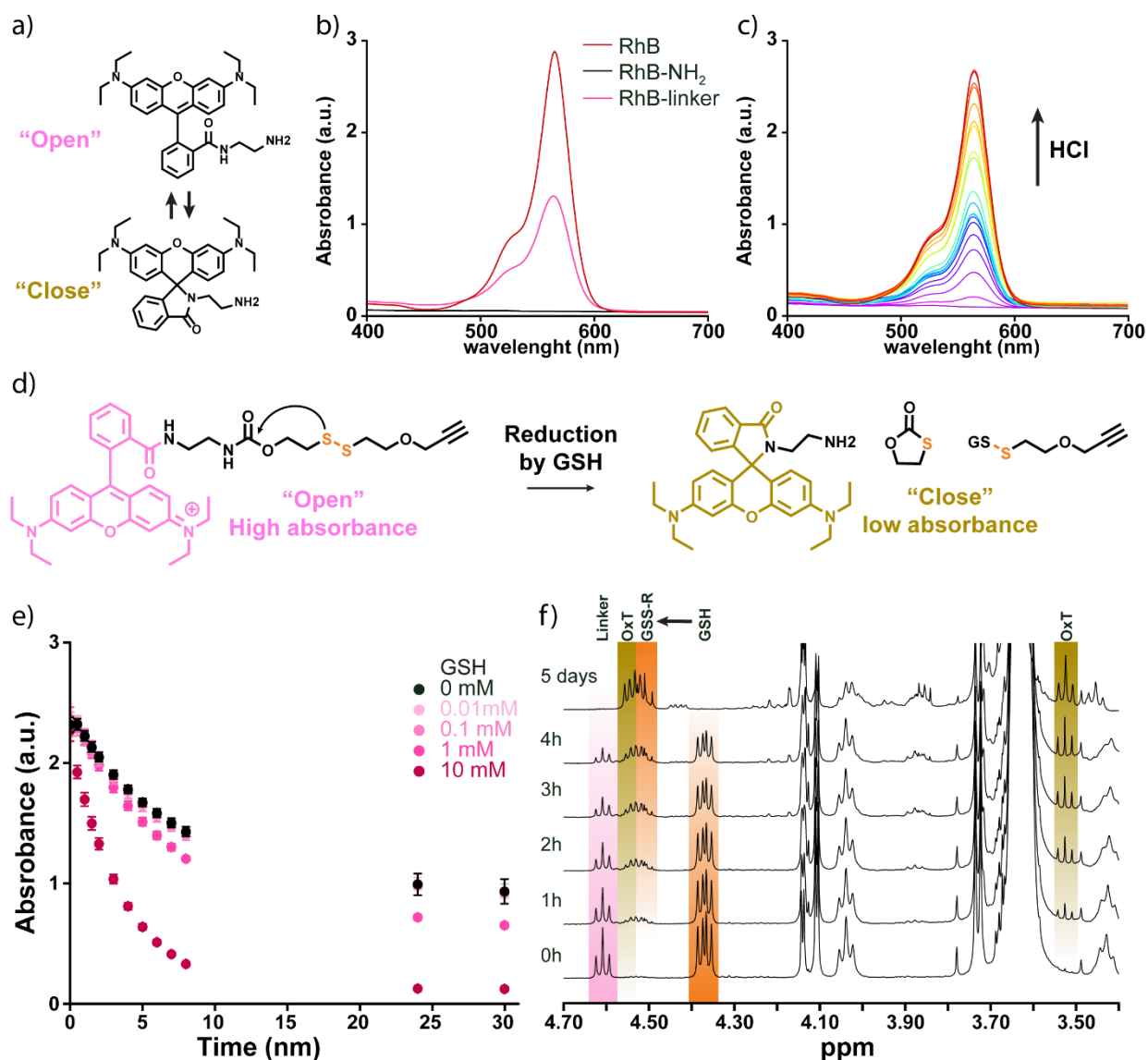


Figure 5.2. a) RhB-amine "open" and "closed" conformation. b) Absorbance spectra in DMSO of RhB (128 μ M), RhB-NH₂ (10 mM), and RhB-linker (10 mM). c) Absorbance spectra of 10 mM RhB-NH₂ in DMSO with increasing HCl concentration. d) Self-immolative mechanism of a RhB amine labeled linker in the presence of GSH. Cleaving of the disulfide linker results in the release of RhB rhodamine amine, which changes in conformation and loses its absorption. b) Change in UV-vis absorbance at 570 nm of RhB linker in the presence of various GSH concentration. c) ¹H-NMR spectra of RhB amine linker in the presence of 10 mM GSH recorded over time in DMSO-d₆.

To further ensure the selective cleaving and self-immolative mechanism, ¹H-NMR spectra of RhB-linker in the presence of GSH (0.01, 0.1, 1, 5, and 10 mM) were recorded overtime (Figure 5.2f; Figures S50-54). Similarly, to the UV-vis absorbance result, no changes in the spectra were observed for 0.01 and 0.1 mM of GSH. In addition, the spectra for 1 mM GSH did not show substantial changes

during the course of the experiment. In contrast, the $^1\text{H-NMR}$ spectra for solutions containing 5 mM and 10 mM indicated cleavage and self-immolative rearrangement. More specifically, the peak corresponding to the CH_2 neighboring the carbamate in the linker and the CH of the cysteine residue of the GSH, at 4.61 and 4.37 ppm respectively, decreased while new a peak at 4.53 ppm appeared associated with the oxidized GSH. Furthermore, with the reduction of the GSH, a peak at 3.52 ppm appeared. The new signal was assigned to the CH_2 neighboring the sulfur of the 1, 3-oxathiolan-2-one (OxT) by-product. The signal of the remaining CH_2 of the OxT overlapped with the 4.53 ppm signal of the oxidized GSH. The formation of the OxT confirmed the self-immolative reshuffling of the linker.

Overall, the linker cleaved in a concentration range similar to those for GSH in the cytosol while lower concentration, seen in blood or the extracellular space, were insufficient. Furthermore, the cleaving through a self-immolative mechanism was supported by the appearance of the 1, 3-oxathiolan-2-one product in the NMR.

5.1.3. Protein coupling

One of the main challenges in therapeutic delivery using covalent linkers is the coupling to biological therapeutics without impacting bioactivity. Indeed, biological therapeutics, such as antibodies, proteins, or growth factors, have limited stability outside physiological conditions (aqueous, pH 7, 37 °C).³⁴⁵ Many chemical reaction on the other hand rely on organic solvents and/or strong bases or acids. Finding suitable reaction enabling coupling of the linker to biologics in mild aqueous environment is of high interest to avoid loss of therapeutic efficiency. For this purpose, a nitrophenyl carbonate was incorporated in the linker design due to its increased reactivity with amines in relatively mild reaction condition (pH 8.5 phosphate buffer; **Figure 5.3a**).³⁴⁰ Furthermore, upon reaction to a primary amine to form a carbamate group, the nitrophenyl side product is release in the reaction media. The release of the nitrophenyl result in an increase in absorbance at 413 nm.³⁴⁰ In this manner, the completion of the reaction could be monitored using the change of absorbance from the release of the nitrophenyl using UV-vis spectroscopy.

To test the coupling efficiency of the linker to a biologic, we used bovine serum albumin (BSA) as a model protein. The coupling reaction was performed through the simple addition of the linker pre-dissolved in DMSO to BSA in a slightly basic (pH 8.5) phosphate buffer (**Figure 5.3a**). As expected, upon addition of the linker the solution quickly turned yellow and the change in absorbance ($\lambda = 413$ nm) was monitored for the reaction mixture using UV-vis spectroscopy (**Figure 5.3b**). The absorbance increased rapidly with the first minute after mixing the solutions and reached a plateau after ~ 1 h, indicating reaction completion. To ensure that the change in absorbance was not due to degradation of the linker due to the aqueous environment or pH effect, absorbance of the linker in the absence of BSA in the phosphate buffer (pH ~ 8.5) and in water were also recorded (**Figure 5.3b**). After 90 min, only a slight increase of absorbance appeared in the UV-vis spectra of the control conditions, indicating no release of nitrophenyl and by extension reaction. Furthermore, no change in absorbance was apparent

when performing the coupling between BSA and the linker in PBS (pH ~7). We concluded that the linker was stable in aqueous media and required slightly basic conditions to react.

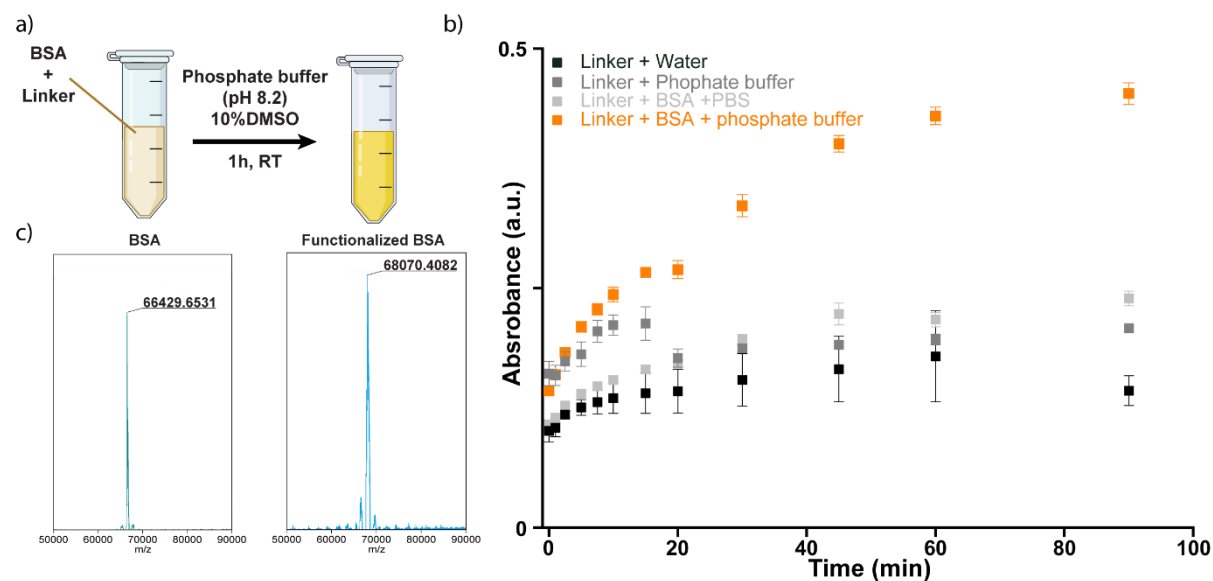


Figure 5.3. a) Protein coupling was enabled by simple mixing in mild aqueous phosphate buffer. b) Absorbance over time at $\lambda = 413$ nm. c) Mass spectra of unfunctionalized and functionalized BSA.

To further confirm the coupling of the linker to BSA, liquid chromatography–mass spectrometry (LC–MS) was performed on BSA before and after functionalization (**Figure 4c**). Before coupling a mass of $m/z = 66\,429.65$ g mol⁻¹ was detected and associated to the unfunctionalized BSA ($M_w = 66\,430.3$ g mol⁻¹). After coupling, we observed a mass of $m/z = 68\,070.44$ g mol⁻¹. Taking into account the formation of acetonitrile (ACN) as an adduct, the mass corresponded to a BSA molecule with 7 linkers ($68\,070.4133$ g mol⁻¹ [BSA + 2 ACN + Na]).³⁴⁶ The mass spectroscopy result further confirmed the coupling of the linker to the BSA.

Overall, we were able to couple the linker to a model protein in an aqueous phosphate buffer under mild conditions.

5.1.4. Coupling to nanogel and uptake efficiency

Finally, to complete the redox-responsive nanogel system, the linker was coupled through click chemistry to the azide-functionalized nanogels. Quantification of the coupling will be confirmed in the next steps through fluorescent imaging using albumin–fluorescein isothiocyanate conjugate (FITC–BSA).

Preliminary uptake study of the nanogels were performed on epidermoid carcinoma cancer cells, using RhB-labelled nanogels (**Figure 5.4**). Colocalization of the fluorescent signal of the hydrogel and brightfield images of the cells suggested efficient uptake of the nanogels by the cancerous cells. Further cell studies with proper viability assays will have to be performed to fully assess the uptake and cytotoxicity of the design system.

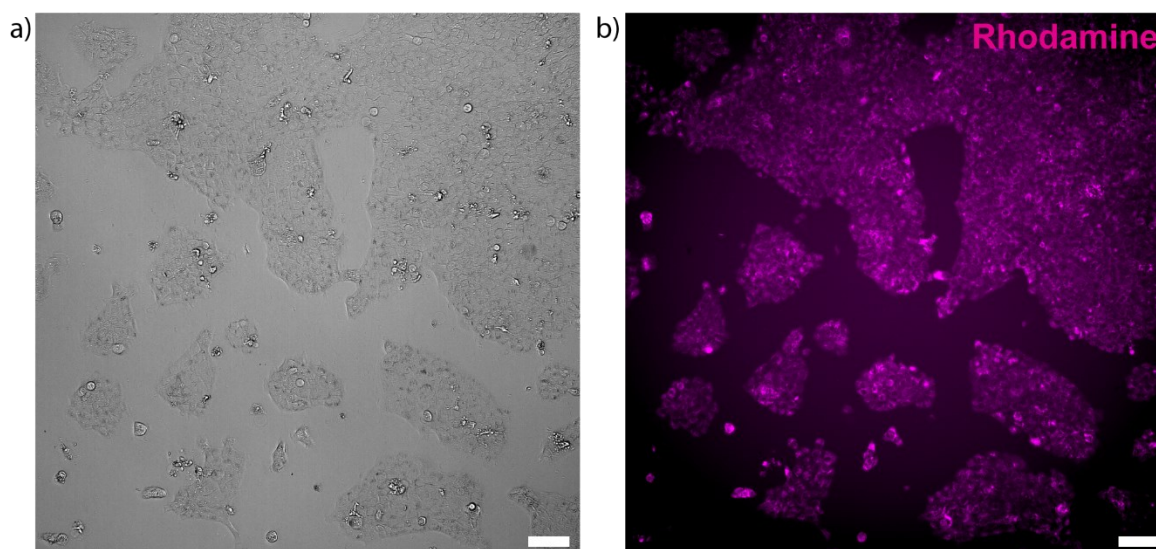


Figure 5.4. a) Bright field and b) fluorescent signal of Rhodamine labeled NGs in epidermoid carcinoma cancer cells (A431 cell line). Scale bar 100 μm .

5.2. CONCLUSION

In this work, we focused on the design of a redox responsive nanogel system via careful engineering of a glutathione-responsive disulfide linker. Using self-immolative disulfide bonds, cleavage of the linker was selective to GSH concentrations of the cytosol. We confirmed the self-immolative nature of the linker using a responsive RhB cargo. Furthermore, the integration of a nitrophenyl carbonate in the linker design enabled coupling of the linker to the amines of a model protein in mild phosphate buffer conditions within 1 h. The protein-linker cargo was further coupled to the nanogels using azide–alkyne click chemistry. Overall, we designed a responsive drug nanocarrier system able to be easily coupled to biologics. The current system shows high potential for intracellular delivery but still requires additional release studies *ex-vivo* and cell studies to confirm proper release and activity of the therapeutics *in vitro*.

5.3. MATERIALS & METHODS

5.3.1. Materials

Poly(ethylene glycol) (PEG, $M_n = 8000$ Da; Sigma-Aldrich), polyethyleneimine (PEI, $M_w = 2500$ Da; Polysciences), (\pm)-epichlorohydrin (Sigma-Aldrich), sodium hydroxide (NaOH; Sigma-Aldrich), sodium azide (NaN_3 ; Sigma-Aldrich), sodium hydride (NaH; Sigma-Aldrich), sodium sulfate (Na_2SO_4 ; Sigma-Aldrich), copper sulfate (CuSO_4 ; Sigma-Aldrich), sodium phosphate monobasic (NaH_2PO_4 ; Sigma-Aldrich), sodium phosphate dibasic (Na_2HPO_4 ; Sigma-Aldrich), 4-nitrophenyl chloroformate (Sigma-Aldrich), rhodamine B base (RhB; Sigma-Aldrich), 1,1'-carbonyldiimidazole (CDI; Sigma-Aldrich), 2-hydroxyethyl disulfide (Sigma-Aldrich), propargyl bromide (solution 80 % in toluene; Sigma-Aldrich), ethylene diamine (Sigma-Aldrich), L-glutathione reduced (GSH; Sigma-Aldrich), (+)-sodium L-ascorbate (Sigma-Aldrich), ethylenediaminetetraacetic acid (EDTA; Sigma-Aldrich), methanol (MeOH; Sigma-Aldrich), dichloromethane (DCM; Sigma-Aldrich), acetonitrile (ACN; Sigma-Aldrich), diethyl ether (Et_2O ; Sigma-Aldrich), tetrahydrofuran (THF; Sigma-Aldrich), N,N-

dimethylformamide (DMF; Sigma-Aldrich), dimethyl sulfoxide (DMSO; Sigma-Aldrich), deuterated chloroform (CDCl_3 ; Sigma-Aldrich). Ethyl acetate (EtOAc; Fisher Chemicals), Ethanol (EtOH; Alcosuisse AG), Ammonium chloride (NH_4Cl ; VWR Chemicals), petroleum ether 40-60 °C (PE; VWR Chemicals), sodium chloride (NaCl ; VWR Chemicals), hydrochloric acid (HCl ; VWR Chemicals) Deuterated DMSO (DMSO-d_6 ; Eurisotop) and deuterated water (D_2O ; Eurisotop). Bovium serum albumin (BSA, protease-free; Roche) Dulbecco's Modified Eagle Medium (DMEM, 1x, with 4.5 g/L D-glucose and without L-glutamine and pyruvate; Gibco), phosphate buffered saline (PBS, pH 7.4, 1x; Gibco), fetal bovine serum (FBS; Gibco), sodium pyruvate (100x; Gibco), L-glutamine 200 mM (100x; Gibco), trypsin-EDTA (Gibco), Normocin (Invivogen) RhB-nanogel provided by Prof. Emanuele Mauri. All materials were used as purchased without further purification.

5.3.2. Instrumentation and characterization

Nuclear magnetic resonance (NMR)

^1H -NMR and ^{13}C -NMR spectra were acquired on a Bruker Avance III 400 (Bruker BioSpin GmbH). Chemical shifts were reported relative to the respective solvent peak. (^1H -NMR: CDCl_3 : $\delta = 7.26$ ppm; DMSO-d_6 : $\delta = 2.50$ ppm, D_2O : $\delta = 4.79$ ppm). The peak of the PEG ($M_w \sim 8$ kDa) repeating unit was set to 720 Hz for all ^1H NMR as a reference peak.

Fourier-transform infrared spectroscopy

Attenuated total reflection Fourier-transform infrared spectroscopy (ATR-FTIR) spectra were acquired on a Perkin Elmer ATR Spectrum TWO equipped with a UATR single reflection diamond. Sample powders were pressed onto the diamond crystal with a pressure arm. The spectra were recorded between 500 and 4000 cm^{-1} averaging over 32 scans.

Dynamic light scattering

The hydrodynamic diameter, D_h , of the formed nanogels were measured by dynamic light scattering (DLS; Malvern ZetaSizer Nano ZS). The nanogel suspensions were placed into a semi-micro cuvette (Path length: 10 mm) and the measurements were performed at 25 °C with a wavelength of 633 nm and a scattering angle of 173°. The properties of each sample were measured three times. The z-average size and the polydispersity index (PDI) were reported.

UV-vis spectroscopy

Plate reader: Absorbance was recorded from a Hidex Sense Microplate Reader (Hidex; Turku, Finland) using clear 96-well tissue culture plates (flat bottom; TPP).

Nanodrop One: Absorbance was recorded from a Nanodrop One Microvolume Spectrophotometer (ThermoFisher, Switzerland).

High-resolution mass spectrometry (HRMS)

HRMS were acquired using a Bruker Daltonics SOLARIX equipped with a MALDI/ESI source and a Q-TOF ion analyzer.

Liquid chromatography- mass spectrometry

LC/MS analyses were performed using a Bruker Solarix XR 1 system equipped with a MALDI/ESI source and a Q-TOF ion analyzer coupled to an Agilent Eclipse Plus, C18 column. For the mobile phase, solvent mixtures A, H₂O (+ HCOOH), and B, ACN (+ HCOOH). The eluent was run at a gradient of 95:5 → 5:95 (water/acetonitrile) over the course of 10 min. Measurements were carried out at a flow rate of 1 mL/min at 25 °C.

Fluorescence Microscopy

Fluorescence images were acquired on a THUNDER Live Cell microscope. The samples were imaged using an HC PL Fluorotar 10x/0.32 PH1 objective. Images were post-processed using ImageJ (Fiji, ImageJ 1.51s).

5.3.3. Synthetic procedures

Nanogel synthesis

Synthesis of the functional nanogels were adapted from the procedure published by Mauri et al.³⁴⁷

Diepoxy-PEG

PEG_{8k} (5 g, 0.63 mmol, 1 eq.) and epichlorohydrin (1.5 mL, 18.80 mmol, 30 eq.) were dissolved in toluene (30 mL). The mixture was heated to 50 °C. NaOH (750 mg, 18.77 mmol, 30 eq.) was added as a powder to the stirred solution. The reaction was stirred for 8 h at 50 °C. After completion of the reaction, the formed precipitate was filtered out, followed by cooling of the mixture to room temperature. Afterwards, the solution was extracted twice with distilled water (20 mL), followed by neutralization of the aqueous phase with NaCl. Further extractions with DCM (4 × 20 mL) were then performed to move the product in the organic phase. The combined organic phases were dried with anhydrous sodium sulfate and concentrated in vacuo. The concentrated mixture was then poured in cold Et₂O, resulting in the precipitation of the polymer. The formed solid was collected by vacuum filtration and redissolved in DCM. The precipitation and recovery of the product was repeated a second time to yield a white powder (4g, 0.49 mmol, 79 %). Characterization: ¹H-NMR (400 MHz, CDCl₃) δ 3.64 (s, 720H), 3.16 (ddt, J = 5.9, 4.2, 2.9 Hz, 2H), 2.79 (dd, J = 5.0, 4.2 Hz, 2H), 2.61 (dd, J = 5.0, 2.7 Hz, 2H). (**Figure S40**)

PEG-OH-N₃

Diepoxy-PEG (3.5 g, 0.43 mmol, 1 eq.) was dissolved in 80 mL DMF and heated to 60 °C, flowed by the addition of sodium azide (565 mg, 8.70 mmol, 20 eq.) and ammonium chloride (925 mg, 17.50 mmol, 40 eq.) The reaction mixture was stirred for 64 h at 60 °C. Afterwards, the solution was filtered, and solvent was removed in vacuo. The residue was redissolved in distilled water and dialyzed (M_w,

cutoff of 100-500 Da) against distilled water for 3 days. After lyophilization the purified polymer was obtained as white powder (2.57 g, 0.31 mmol, 73 %). Characterization: $^1\text{H-NMR}$ (400 MHz, CDCl_3) δ 3.62 (s, 720H), 3.37 – 3.27 (m, 4H). (**Figure S41**)

PEG-N₃-CDI

In a flame dried 25 mL round bottom flask, PEG-OH-N₃ (1 g, 0.12 mmol, 1 eq.) was dissolved in 10 mL dry ACN. After addition of CDI (396 mg, 2.50 mmol, 20 eq), the slightly yellow solution was stirred at 40 °C under inert atmosphere for 4 days. The solution was then concentrated in vacuo and poured into cold Et₂O to induce precipitation of the polymer. The resulting slurry was centrifuged (10 min at 4500 rpm) and the supernatant was discarded. The remaining solid was redissolved in DCM. The precipitation and recovery of the product were repeated twice. The product was dried in vacuo resulting in a white powder (790 mg, 94 μmol , 77 %). Characterization: $^1\text{H-NMR}$ (400 MHz, CDCl_3) δ 8.45 (dd, $J = 3.9, 2.1$ Hz, 2H), 7.55 – 7.53 (m, 2H), 7.22 – 7.20 (m, 2H), 3.64 (s, 720H), 3.51 – 3.40 (m, 4H). (**Figure S42**)

Nanogel formation

Nanogels were formed via a modified emulsification-evaporation method. PEG-N₃-CDI (25mg, 3 μmol , 1.5eq.) was dissolved in 1 mL DCM. In parallel PEI (4.2mg, 2 μmol , 1.0 eq.) was dissolved in 2 mL of a water:MeOH solution (2:3). Under vigorous stirring, the organic phase was added drop wise to the aqueous phase. The resulting solution was then sonicated for 30 min. The resulting solution was kept under stirring overnight with open cap to lead to evaporate the DCM. The obtention of nanogel was confirmed through DLS, FT-IR and $^1\text{H-NMR}$ measurements (**Figure S44, 45**)

Linker synthesis

2-propynoxyethyl disulphanylethanol

The synthesis was adapted from a published protocol.³⁴⁷ 2-Hydroxyethyl disulfide (10.0 g, 64.8 mmol, 1.0 eq.) was dissolved in THF (100 mL) and the mixture was cooled to 0 °C in an ice bath. Propargyl bromide (80 % in toluene, 4.8 g, 32.4 mmol, 0.5 eq.) was added dropwise to the chilled solution, followed by the addition of sodium hydride (60 % in oil, 1.6 g, 39.0 mmol, 0.6 eq.). The reaction mixture was stirred for 9 h at room temperature. Afterwards, 20 drops of distilled water were added to stop the reaction. The mixture was then stirred overnight at room temperature. The resulting orange solution was filtered, and the solvent was removed in vacuo. The product was further purified by column chromatography (3:1 petroleum ether: ethyl acetate) to yield an orange oil (2.9 g, 15.1 mmol, 23% yield). Characterization: $^1\text{H-NMR}$ (400 MHz, CDCl_3) δ 4.18 (dd, $J = 2.4, 1.6$ Hz, 2H), 3.89 (q, $J = 5.8$ Hz, 2H), 3.79 (td, $J = 6.4, 3.7$ Hz, 2H), 2.96 – 2.83 (m, 4H), 2.46 (q, $J = 2.4$ Hz, 1H), 2.15 (t, $J = 1.3$ Hz, 1H). $^{13}\text{C-NMR}$ (400 MHz, CDCl_3) δ 79.5, 75, 68.3, 60.4, 58.9, 41.6, 38.5. (**Figure S46**)

Para-nitrophenylcarbonate-linker

The synthesis was adapted from a published protocol.³⁴⁰ 2-propynoxyethylsulphanylethanol (104 mg, 0.5 mmol, 1.00 eq.) was dissolved in DCM (2 mL) and 4-nitrophenyl chloroformate (122 mg, 0.6 mmol, 1.15 eq.) was added to the solution. The reaction mixture was cooled in an ice bath for 20 min followed by the dropwise addition of pyridine (49 μ L, 0.6 mmol, 1.15 eq.) under vigorous stirring. The solution was stirred for 24 h at room temperature, followed by the evaporation of the solvent in vacuo. The crude product was purified by column chromatography (100% DCM). The product was obtained as colorless oil (40 mg, 0.11 mmol, 21 % yield). Characterization: ¹H-NMR (400 MHz, CDCl₃) δ 8.37 – 8.23 (m, 2H), 7.47 – 7.31 (m, 2H), 4.56 (t, J = 6.6 Hz, 2H), 4.20 (d, J = 2.4 Hz, 2H), 3.81 (t, J = 6.3 Hz, 2H), 3.05 (t, J = 6.6 Hz, 2H), 2.96 (t, J = 6.4 Hz, 2H), 2.46 (t, J = 2.4 Hz, 1H). (**Figure S47**)

Ethylenediamine modified rhodamine B (RhB-NH₂)

The synthesis was adapted from a published protocol.³⁴⁷ Rhodamine B base (1 g, 2.1 mmol, 1.0 eq.) was dissolved in 25 mL ethanol. Ethylenediamine (1 mL, 15 mmol, 7.5 eq.) was added dropwise. The violet solution was stirred under reflux overnight to give an orange solution. Residual solvent was evaporated under reduced pressure, and the residue was dissolved in distilled water. The formed precipitate was collected by vacuum filtration and dried *in vacuo*. The product was obtained as pink powder (732 mg, 1.5 mmol, 72 % yield). Characterization: ¹H-NMR (400 MHz, CDCl₃) δ 7.92 – 7.87 (m, 1H), 7.48 – 7.40 (m, 2H), 7.11 – 7.06 (m, 1H), 6.43 (d, J = 8.9 Hz, 2H), 6.37 (d, J = 2.6 Hz, 2H), 6.27 (dd, J = 8.9, 2.6 Hz, 2H), 3.33 (q, J = 7.2 Hz, 8H), 3.20 (t, J = 6.4 Hz, 2H), 2.47 (t, J = 6.4 Hz, 2H), 1.16 (t, J = 7.0 Hz, 12H). HRMS (ESI) m/z calc. for C₃₀H₃₈N₄O₂: 485.290; found 485.2903. (**Figure S48**)

Rhodamine B amine coupled to linker (RhB-linker)

The synthesis was adapted from a published protocol.³⁴⁷ 2-propynoxyethylsulphanylethanol (60.0 mg, 0.31 mmol, 1.0 eq.) was dissolved in 2 mL of DCM. The solution was then added dropwise to a solution of 1,1'-carbonyldiimidazole (CDI, 50.6 mg, 0.31 mmol, 1.0 eq.) 2 mL of DCM at 0 °C. The reaction mixture was stirred for 4 h at room temperature. Afterwards, RhB-NH₂ (150 mg, 0.31 mmol, 1.0 eq.) was added to the reaction mixture. The purple solution was stirred for 18 h at room temperature. After the reaction, the solution was extracted three times using 1 M HCl solution and dried using sodium sulfate. The remaining solvent was evaporated under reduced pressure to yield a purple oil. (9.5 mg, 0.13 mmol, 42 % yield). Characterization: ¹H-NMR (400 MHz, CDCl₃) δ 7.99 – 7.93 (m, 1H), 7.57 – 7.48 (m, 2H), 7.08 – 7.03 (m, 1H), 4.70 (t, J = 6.5 Hz, 1H), 4.22 (d, J = 6.6 Hz, 1H), 4.20 (dd, J = 2.4, 1.3 Hz, 2H), 4.18 (d, J = 2.4 Hz, 2H), 3.80 (dd, J = 6.4, 2.1 Hz, 2H), 3.79 – 3.75 (m, 2H), 3.51 – 3.36 (m, 6H), 3.35 – 3.26 (m, 2H), 3.08 (t, J = 6.5 Hz, 1H), 2.98 – 2.94 (m, 2H), 2.94 – 2.89 (m, 3H), 2.89 – 2.83 (m, 4H), 2.46 (dt, J = 3.8, 2.4 Hz, 2H), 1.26 (t, J = 6.9 Hz, 12H). HRMS (ESI) m/z calc. for C₃₈H₄₇N₄O₅S₂: 703.2982; found 703.297. (**Figure S49**)

5.3.4. Experimental procedures

RhB amine pH response

2 mg RhB amine were dissolved in 2 mL DMSO to produce a 2.05 mM stock solution. 100 μ L of the stock solution were filled in 20 wells of a 96 well plate. In each well a specific amount (0–100 μ L) of a 10 mM HCl solution were added 5 μ L increment. Absorbance spectra were recorded after 30 minutes of incubation.

UV-vis RhB-linker release study

11.31 mg of RhB-linker were dissolved in 1607 μ L DMSO to get a 10 mM stock solution. In parallel, stock solutions of 100 mM, 10 mM, 1 mM, and 0.1 mM GSH were prepared.

In a 96 well plate triplicates of RhB-linker in 10 mM, 1 mM, 0.1 mM and 0.01 mM GSH environment were prepared. For this 10 μ L of the corresponding GSH stock solutions were added to 90 μ L of RhB-linker stock solutions. As a control, pure RhB-linker solution was added to the well plate. Finally, absorbance at 570 nm was measured overtime.

NMR RhB-linker release study

11.56 mg of RhB-linker were dissolved in 2.5 mL DMSO- d_6 . A 100 mM GSH stock solution was prepared by dissolving 7.25 mg GSH in 236 μ L D₂O. This solution was diluted with D₂O to obtain stock solutions with the concentrations of 50 mM, 10 mM, 1 mM, and 0.1 mM.

NMR tubes were prepared with 0.4 mL of RhB SS-OH linker stock solution. GSH concentrations of 10, 5, 1, 0.1 and 0.01 mM were obtained by adding 44 μ L of the respective stock solutions. The ¹H-NMR of the resulting solutions were then recorded.

Coupling of BSA to para-nitrophenylcarbonate-linker

The procedure was adapted from a published protocol.³⁴⁰ First, a phosphate buffer (0.1 M) was prepared. 4.07 g of potassium phosphate dibasic and 221.9 mg of potassium phosphate monobasic were dissolved in distilled water to reach a final total volume of 250 mL. Afterwards, pH of the solution was adjusted by addition of 1 M NaOH to reach a pH of 8.5.

2.3 mg BSA (0.035 μ mol, 1 eq.) were dissolved in 1 mL of phosphate buffer (pH 8.5). In parallel, para-nitrophenylcarbonate-linker (0.28 mg, 0.78 μ mol, 22 eq.) were dissolved in 230 μ L THF. 100 μ L the linker stock solution was added to the BSA solution. The reaction was stirred at room temperature overnight. After reaction the solution was dialyzed (MWCO 3.5 kDa) against distilled water overnight. After lyophilization the purified polymer was obtained as white powder. Functionalization was confirmed through LC-MS. HRMS (ESI) m/z calc. for 68070.4133 [BSA + 7linker (C₈O₃S₂H₁₁) + 2 ACN + Na] found 68070.4082.

Coupling of BSA-linker to NG

A BSA-linker solution in water (2.39 mg ml⁻¹ of BSA) was added to a solution a suspension of N₃-nanogels (35 mg ml⁻¹). Sequentially, CuSO₄ (1.6 mg, 10 μmol) and ascorbic acid (2 mg, 10 μmol) were added to the reaction mixture. The solution was stirred overnight at room temperature. After reaction, the resulting solution was dialyzed (MWCO 3.5 kDa) against distilled water for 2 days.

Cancer Cell Culture

A431 cells (ATCC), a human epidermoid carcinoma cell line, were cultured in DMEM, high glucose, no phenol red supplemented with 10% (v/v) Fetal Bovine Serum (FBS), 1 % pyruvate, 1 % L-glutamine (Gibco, Thermo Fisher Scientific) and 0.2% normocin (Invivogen) at 5% CO₂ and 37°C. To passage and perform experiments, cells were washed with PBS (Gibco, Thermo Fisher Scientific) before a 6 min incubation with 0.05% Trypsin-EDTA (Gibco, Thermo Fisher Scientific) for cell detachment. Two days prior to the nanogel experiment cells were seeded with a density of 15'000 cells/ cm² on a 48-well plate, allowing cells to attach and form clusters at 5% CO₂ and 37°C, ahead of nanogel addition.

5.4. ACKNOWLEDGEMENTS

The mass measurements were conducted by the Molecular and Biomolecular Analysis Service (MoBiAS) of ETH Zürich. This work was supported by the Swiss National Science Foundation (200021_184697).

CONCLUSION AND OUTLOOK

RESULTS OVERVIEW

In this thesis, we aimed to leverage supramolecular and stimuli-responsive interactions to design nanoparticle-based hydrogels for drug delivery applications. We combined a variety of characterization techniques to broaden current understanding of supramolecular interactions and their impact on macroscopic properties and applied them to design modular and responsive materials with additional responsivity.

First, in **Chapter 1** we review the current uses of supramolecular interactions as tools for designing hydrogels for drug delivery applications. We first focused on the use of supramolecular interactions as structural components in the design of self-assembling, injectable or responsive hydrogels. In the second part we described potential methods to leverage supramolecular interactions to tune drug–matrix interaction resulting in enhanced uptake, kinetics, or targeting.

In **Chapter 2**, we first utilized a simple and elegant supramolecular motif based on the threading behavior of α -cyclodextrin (α CD) on poly (ethylene glycol)—formation of polypseudotaxane—to reinforce polymer–nanoparticle (PNP) hydrogels. The addition of the macrocycle enabled concentration-dependent reinforcement of the mechanical properties of the hydrogel, while retaining its injectability. The changes in mechanical properties were associated with the formation of NP–NP interactions upon addition α CD, which decreased the dependency of the system on interactions between polymer and nanoparticle. As a result, building blocks could be chosen from a broad pool of polymers and PEGylated nanoparticles, enabling the formation of 3D bioinks, conductive materials, and magnetically responsive hydrogels.

In **Chapter 3**, we used β CD inclusion complexes to investigate the underlying mechanism governing the emergence of the mechanical properties in PNP hydrogels. Specifically, we leveraged β CD–adamantane complexation as cross-linking interactions for the formation of PNP hydrogels. Combining molecular and rheological characterization of the system, we were able to relate effective amount of host and guest in the system, building block content, and viscoelastic behavior of the hydrogels. We uncovered the role of the nanoparticles as main cross-links of the network, while the polymer mostly contributed to the required polymer content and viscosity for gelation. Further, we observed that the gelation of the system was optimal for a host–guest ratio close to 1, with excess or deficit of nanoparticles resulting in decreased mechanical properties. Overall, we shed light on the correlation between the molecular and macroscopic scale in the rational design of PNP hydrogel.

In **Chapter 4**, we leveraged fluorescent and super-resolution optical microscopy to investigate the microstructure of PNP hydrogels. Through the addition of a fluorophore to nanoparticles and the control of label density in the system, we were able to visualize the nanoparticle distribution within

the hydrogel matrix. In control PNP hydrogels, we observed a porous network-like distribution of the nanoparticles possibly due to interactions with polymers or extrusion effects during sample preparation. Further, we correlated the increase of mechanical properties observed with the addition of α CD to formation of nanoparticle clusters in the microstructure of the hydrogels.

In **Chapter 5**, we designed a redox responsive nanogel drug delivery carrier for the intracellular delivery of therapeutics free of chemical modifications. For this purpose, we designed a self-immolative glutathione (GSH) responsive linker based on disulfide bonds to covalently bridge the nanogels and the therapeutics. The degradation of the linker through self-immolative reshuffling was achieved for GSH concentrations similar to intracellular levels. Further, protein coupling to the linker was performed in mild phosphate buffer condition. Finally, preliminary release studies and cell experiments demonstrated the release of a model protein and uptake of the nanogel by cells.

OUTLOOK

In this work, we focused on the development of nanoparticulate hydrogels using supramolecular and stimuli-responsive interactions. We demonstrated various strategies to leverage those interactions as structural components for the design of modular and responsive materials, use them as a handle to correlate molecular and macroscopic properties, and for the responsive release of therapeutics. Nonetheless, the PNP system, microscopic investigation, and nanogel drug delivery carrier still require further investigation.

PNP hydrogels have shown promising results in their current applications for vaccine delivery, immune cell recruitment, and as printing platforms. The main challenge associated with this system remains to be the limited range of interactions available for their design and a lack of understanding in structure–property relationships. While we provided new PNP hydrogel designs based on host–guest interactions, a wide range of supramolecular interactions remain unexplored. As such, in collaboration with Nika Petelinšek, we are currently investigating the possibility to utilize metal–ligand interactions, specifically histidine–metal complexes, to increase nanoparticle interactions within PNP hydrogels. Before the integration of these interactions in a PNP system, we are first exploring the efficiency of binding and bridging of histidine and histidine-labeled nanoparticles. Upon obtaining a NP system able to enhance inter-nanoparticle interactions, we aim to use the resulting PNP system to investigate the impact of the interactions of the emerging macroscopic properties, similarly to **Chapters 2** and **3**.

We aim to further investigate the PNP system in combination with the microscopy tool investigated in **Chapter 4**. While the initial results provided insight into the microstructure of the PNP hydrogels, the current visualizations only depict nanoparticle distribution and do not represent the entire system. Visualization of the organization of the support polymer would provide the missing component. Furthermore, the current setup only allows for 2D imaging of the sample. Expanding the

investigation to a 3D STORM setup would enable better understanding of the spatial changes in the microarchitecture of the hydrogel.

Despite the above-mentioned limitation, optical microscopy still enabled the investigation of the changes in mechanical properties observed in **Chapter 2**. However, further investigations are needed to fully understand the origins of the changes in microstructures. Temporal factors, with changes in microstructure due to extrusion of the sample through syringes or extended formation kinetics could possibly result in the observed structure. As such, we will further investigate the system and possibly complement the investigation with additional characterization techniques, such as extensional rheology, which could provide insight on fiber alignment, or SAXS, which could provide length scale of the formed aggregates. Currently, this work only focused on the PNP hydrogels, but has the potential to be a generalized tool for investigating material microarchitectures. Those microscopy techniques can be used to investigate further hydrogel systems developed in our laboratory, such as peptides, proteins, or jammed microgels, to gain extensive insight into the structure–property relationships of the respective hydrogels.

Finally, designing biomaterials would not be complete without their application in biological system. In **Chapter 5**, we showed the potential of a responsive nanogel system as a platform for intracellular release of therapeutics. In collaboration with Leslie Cunningham and Florian Huwyler, we are currently investigating the platform for liver regeneration. Indeed, due to the limited availability of transplantable organs, researchers are trying to harness the intrinsic regeneration capacity of the liver, to regrow the organ *ex vivo* from partial tissues. As such, enhancing the regenerative capacity of the liver through administration of therapeutics is of high interest. We have identified β -catenin as a potential cargo for improving regeneration of liver tissues and are currently conducting preliminary uptake and release studies of the nanogel on 2D liver cell cultures. The overall goal is to translate the nanocarrier system to precision cut liver slices to investigate their uptake in the highly structure liver microenvironment and, ultimately, administer them to *ex vivo* perfused livers.

APPENDIX

APPENDIX FOR CHAPTER 2

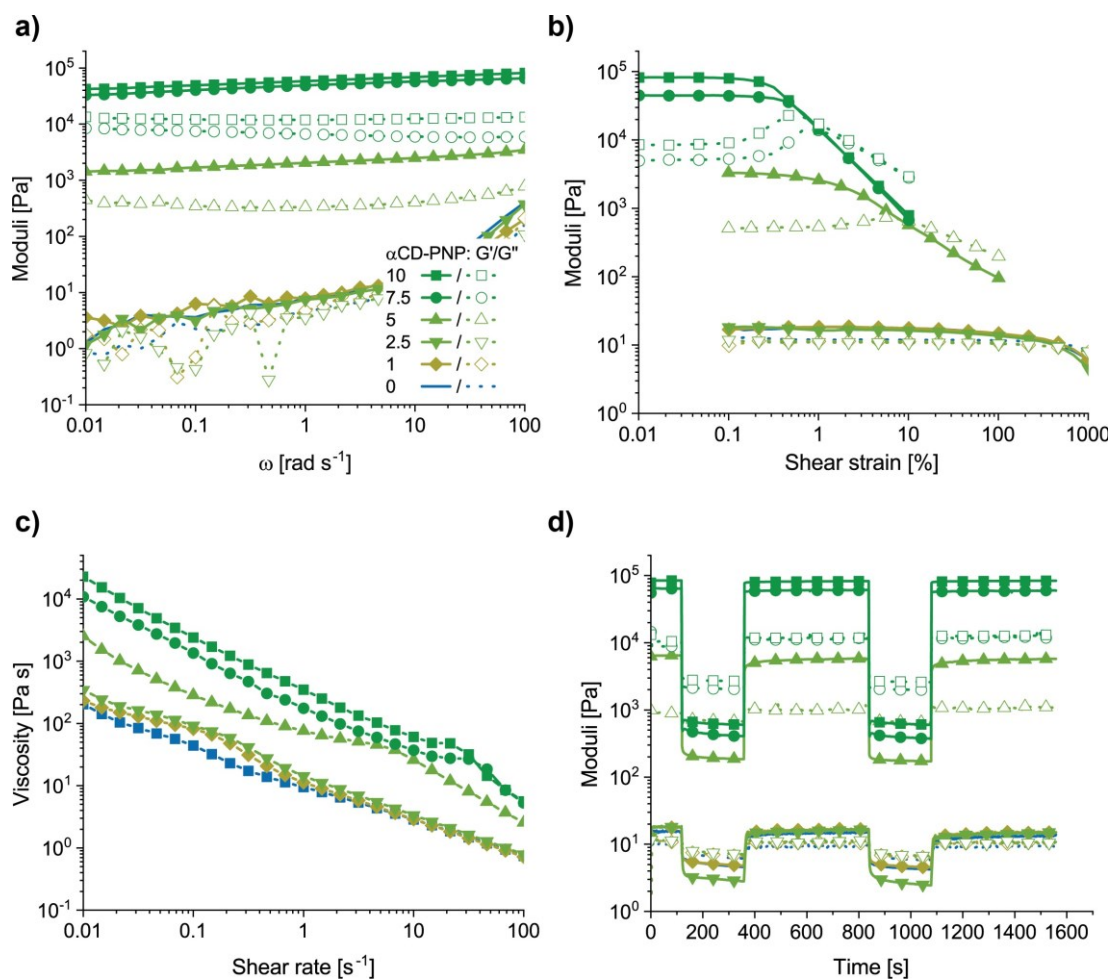


Figure S1. Rheological properties of PNP hydrogel (HPMC 1 wt % and PEG-*b*-PLA 5 wt %) reinforced with different concentration of α CD (0, 1, 2.5, 5, 7.5, and 10 wt %). a) Frequency sweep measurements. b) Shear strain measurements demonstrated a decrease in yield strain, γ_y , with increasing α CD content. c) Shear rate ramp measurements of all formulation showed pronounced shear-thinning properties ($n \sim 0.2-0.3$). The low-shear viscosity drastically increased with increasing content of α CD. d) CD-PNP hydrogels retained the ability to recover rapidly their initial viscoelastic properties (self-heal) following cycle of high strain (>10 %).

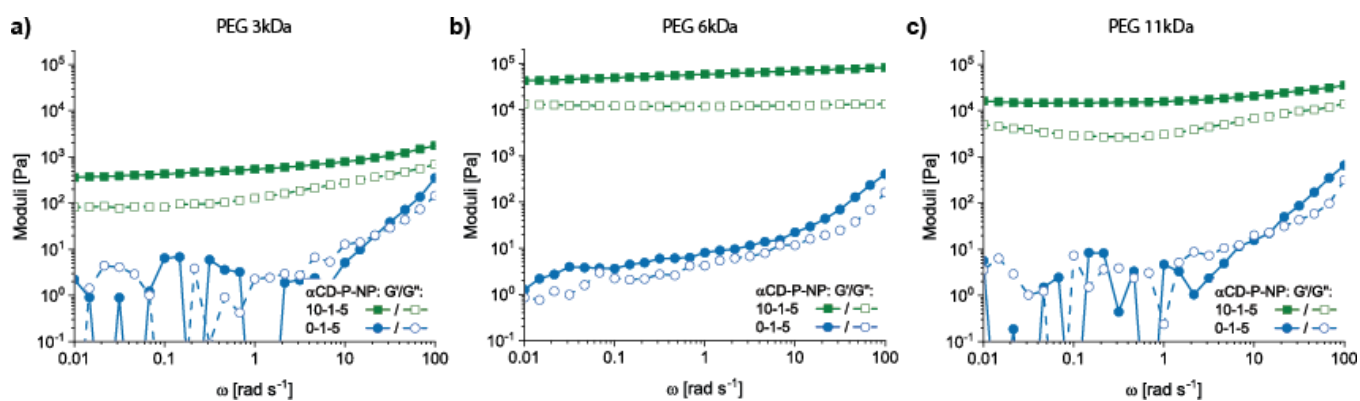


Figure S2. Rheological properties of CD–PNP hydrogel (HPMC 1 wt%, PEG-b-PLA NPs 5 wt% and α CD 10 wt%) with NPs presenting PEG with various molecular weights. a) PEG 3 kDa, b) PEG 6 kDa and c) PEG 11 kDa. Overall, the frequency sweeps indicated that α CD reinforced the materials for each length of PEG tested.

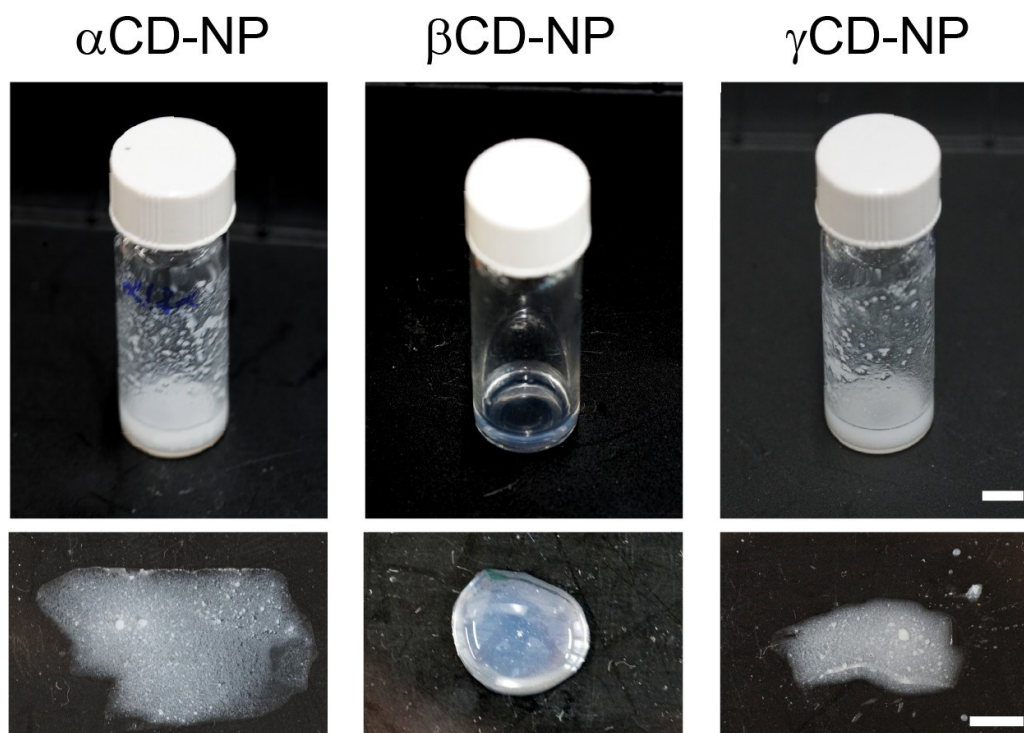


Figure S3. Formulations containing CDs and NP without support polymer result in precipitation (in case of α CD and γ CD) or form a cloudy solution (in case of β CD). Scale bar, 5 mm.

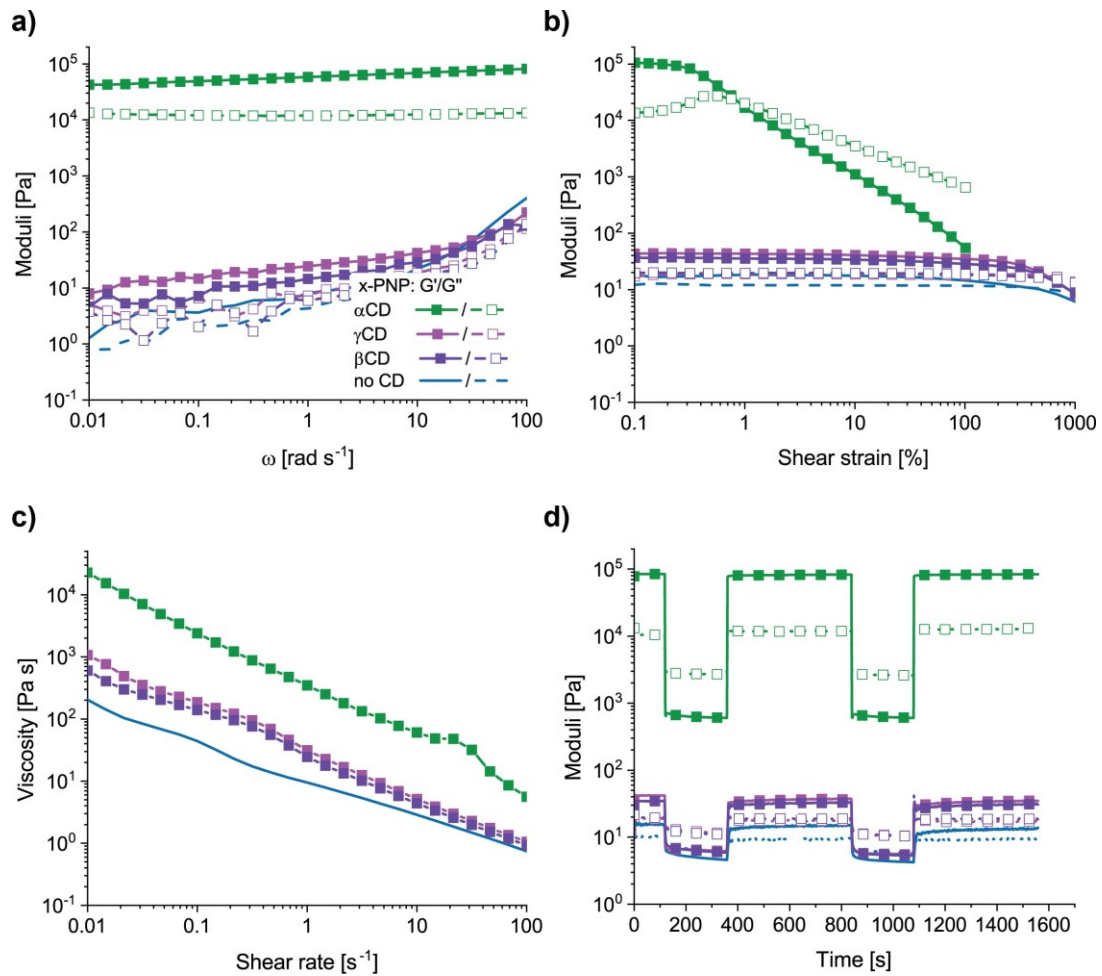


Figure S4. Rheological properties of PNP hydrogel (HPMC 1 wt % and PEG-b-PLA 5 wt %) reinforced with different cyclodextrins (10 wt %): αCD, βCD, and γCD. a) Frequency sweep measurements of αCD–PNP hydrogels showed a drastic increase in viscoelastic properties compared to unmodified hydrogels and to βCD–PNP and γCD–PNP. b) Shear strain measurements demonstrated a drastic decrease in yield strain, γ_y , in case of αCD–PNP formulation. In case of βCD–PNP and γCD–PNP no drastic change was observed. c) Shear rate ramp measurements of all formulation showed pronounced shear-thinning properties ($n \sim 0.2-0.3$). The low-shear viscosity, η_0 , drastically increased for formulation containing αCD whereas minimal increase was observed in case of βCD–PNP and γCD–PNP. d) CD–PNP hydrogels retained the ability to recover rapidly their initial viscoelastic properties (self-heal) following cycle of high strain ($>10\%$).

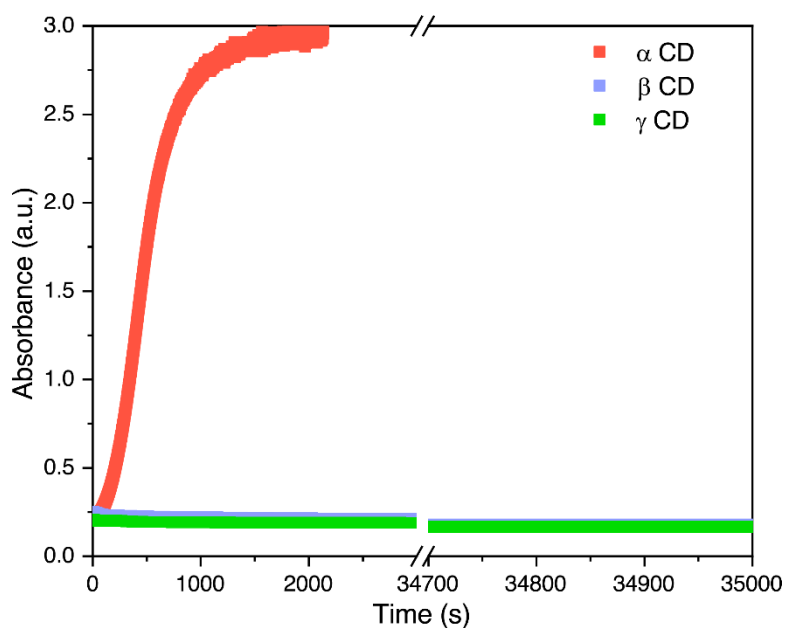


Figure S5. Poly pseudorotaxane formation of PEG-b-PLA NPs and CD. a) Sample turbidity of 10 wt% α CD, hydroxypropyl- β CD, or γ CD and 5 wt% PEG-b-PLA NPs over time. Turbidity increase of α CD showed interaction between NPs and CD, whereas no macroscopic interaction was detected with hydroxypropyl- β CD or γ CD. b) α CD–NP poly pseudorotaxane formation was macroscopically visible with the naked eye. At the end of the measurement, the liquid-like sample became solid-like.

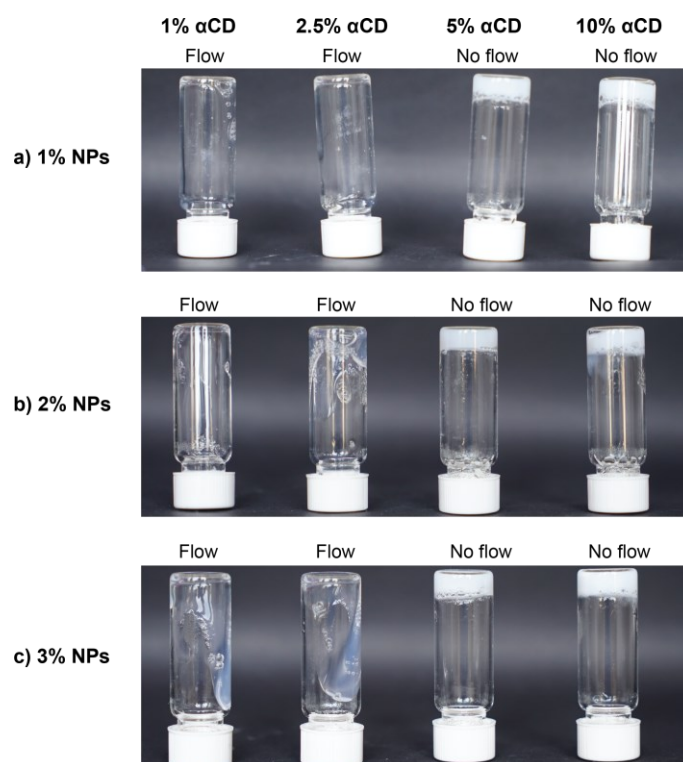


Figure S6. Qualitative assessment of the viscoelastic properties of different CD–PNP formulations to determine conditions that demonstrated no flow upon inverting the vials—interpreted here as solid-like viscoelastic properties and indicative of gel formation.

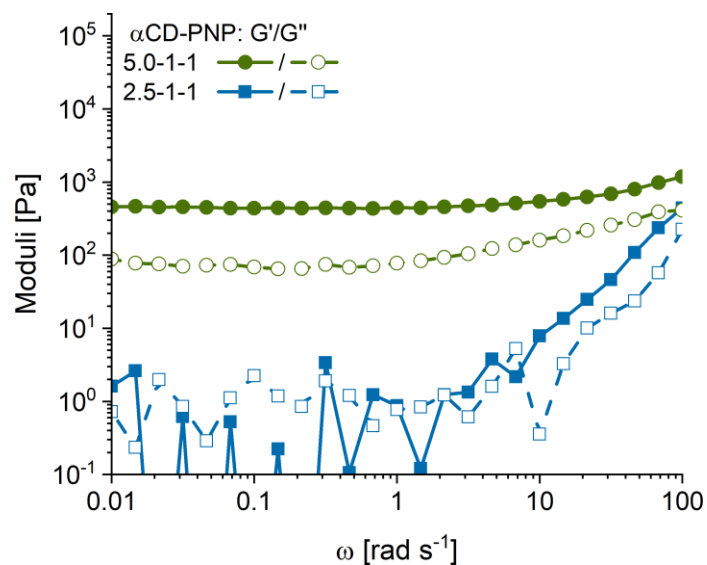


Figure S6. Rheological properties of CD–PNP hydrogels (HPMC 1 wt% and PEG-b-PLA 1 wt%) reinforced with α CD (2.5 wt% and 5 wt%). The frequency sweeps indicate that the minimum amount of α CD required to reinforce PNP hydrogels and form a solid-like network was \sim 5wt%.

Table S1. In all α CD-PNP hydrogels α CD was present in overstoichiometric quantities. Component molecular weights: α CD \approx 0.973kDa, HPMC \approx 700 kDa, PEG \approx 6 kDa.

α CD	HPMC	NP	α CD / PEG molar ratio
0	1	5	0
1	1	5	5
2.5	1	5	13
5	1	5	25
7.5	1	5	38
10	1	5	50

Table S2. Screening of the minimal concentration of α CD, HPMC, and PEG-b-PLA NPs which form a gel. Component molecular weights: α CD \approx 0.973kDa, HPMC \approx 700 kDa, PEG \approx 6 kDa.

α CD	HPMC	NP	α CD / PEG molar ratio
1	1	1	25
2.5	1	1	63
5	1	1	126
10	1	1	252
1	1	2	13
2.5	1	2	32
5	1	2	63
10	1	2	126
1	1	3	8
2.5	1	3	21
5	1	3	42
10	1	3	84

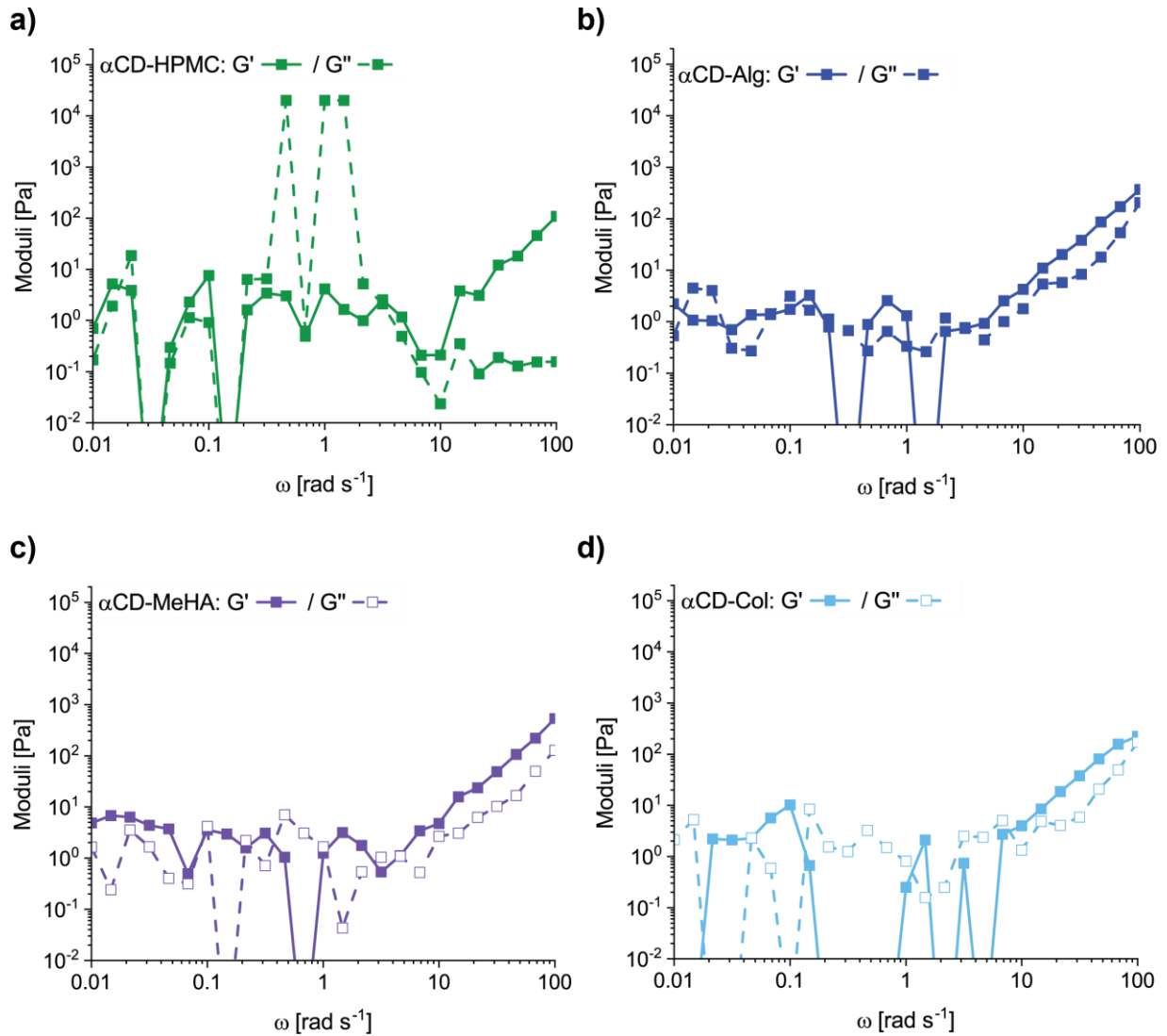


Figure S8. Rheological properties of formulations containing α CD and support polymers prepared in the absence of PEGylated NPs. a) α CD 10 wt% and HPMC 1 wt%, b) α CD 10 wt% and Alg 1 wt%, c) α CD 10 wt% and MeHA 1 wt%, and α CD 10 wt% and Col 0.4 wt%. Overall, the frequency sweeps indicated that all conditions resulted in liquid-like formulations, indicative of the absence of gel formation.

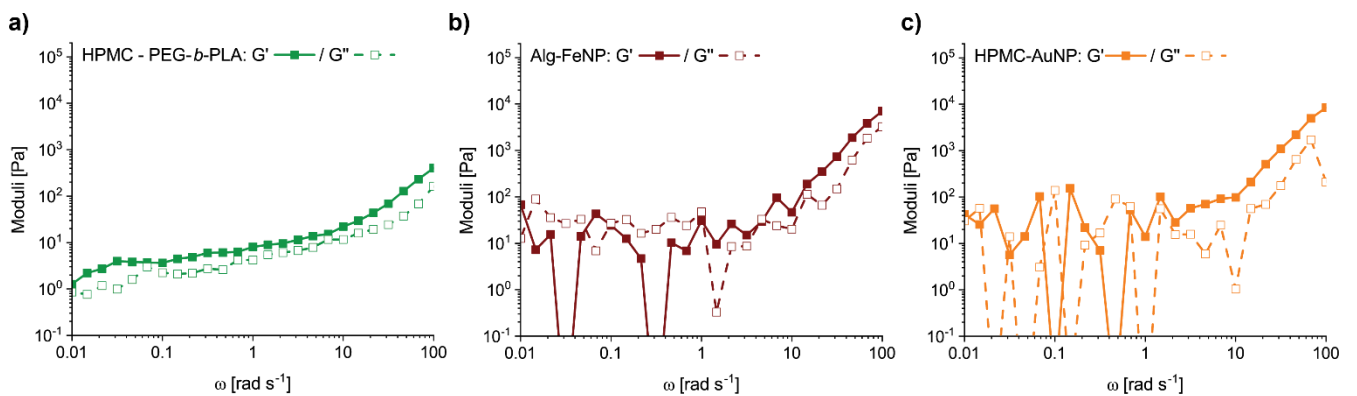


Figure S9. Rheological properties of polymer–nanoparticle hydrogels formulated without α CD. a) HPMC 1 wt% and PEG-b-PLA NPs 5 wt%, b) Alg 1 wt% and FeNP 6 wt%, and c) HPMC 1 wt% and

AuNP 5 wt%. Overall, the frequency sweeps measurements indicated that only the standard formulation of HPMC and PEG-b-PLA NPs formed a solid-like network, whereas Alg and FeNPs and HPMC and AuNPs formed formulations, indicative of the absence of gel formation.

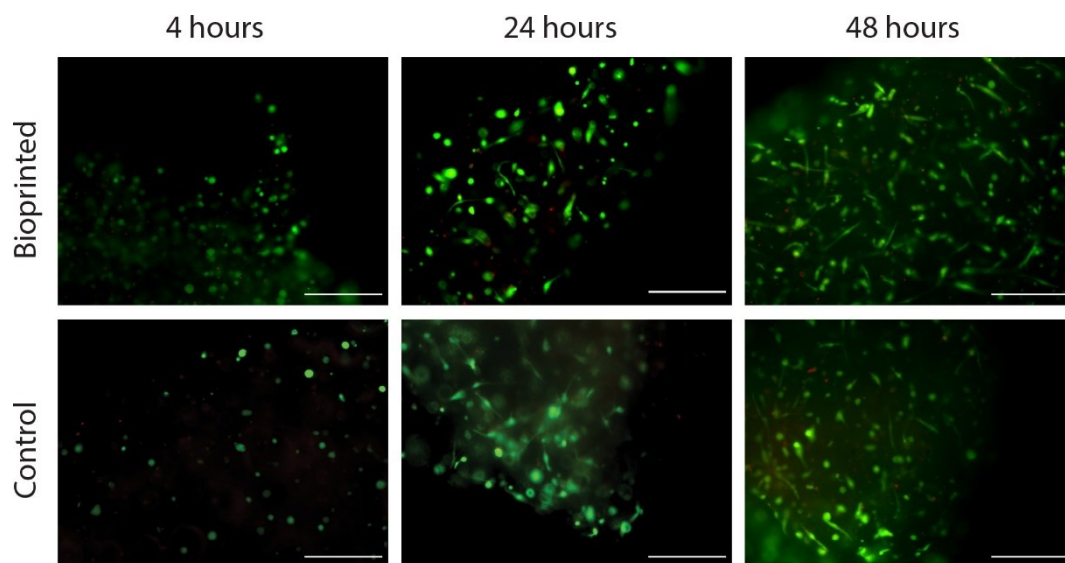


Figure S10. Cell viability of bioprinted and non-printed control scaffolds was determined by assessing the membrane integrity with calcein AM (green, considered as living cells) and ethidium homodimer (red, considered as dead cells). Scale bars, 300 μm .

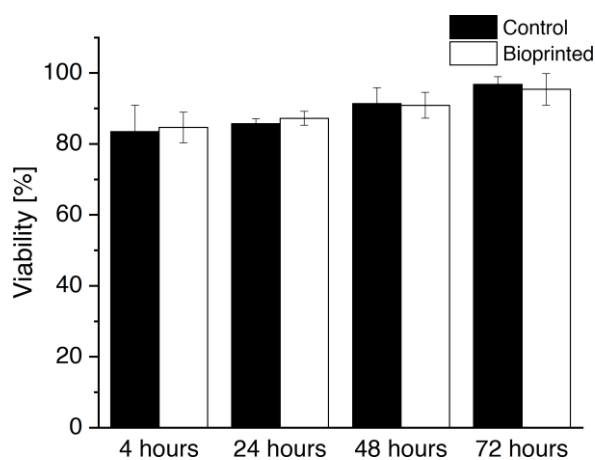


Figure S11. Similar viability was observed between both bioprinted and non-printed control group at all time points.

Table S3. OR encapsulation in the core of PEG-b-PLA NPs (n = 3).

Theoretical loading parameters	
$m_{\text{model drug initial}}$	1.4 mg
$m_{\text{total formulation}}$	141.4 mg
<hr/>	
tDL	1 wt%
<hr/>	
Effective loading parameters	
$m_{\text{model drug final}}$	0.7 mg
$m_{\text{total final}}$	103 mg
<hr/>	
eDL	0.7 wt%

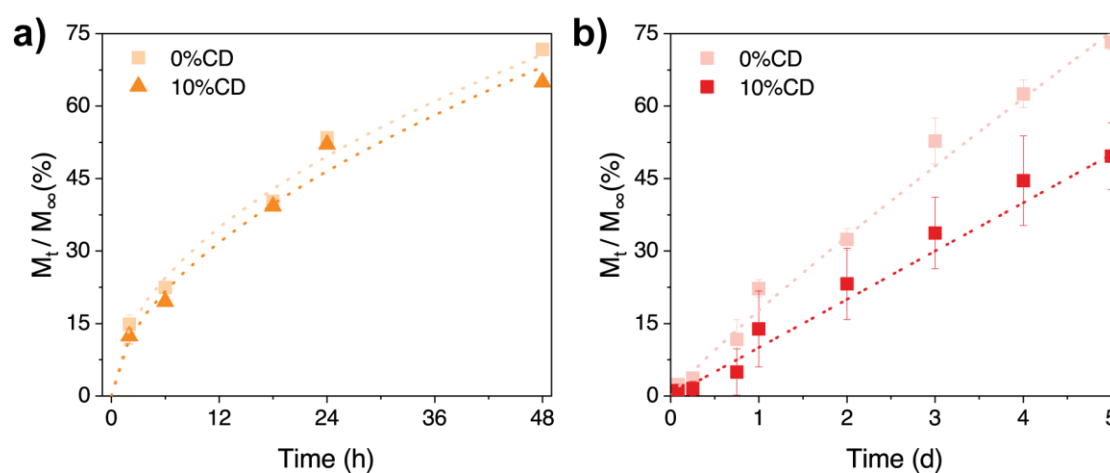


Figure S12. First 60 % of the model drug fractional release is fitted to Ritger-Peppas equation. a) Fractional release of the hydrophilic macromolecule FITC-BSA over time (PNP: α CD 10 wt%, PEG-b-PLA NPs 5 wt%, HPMC 1 wt%, and FITC-BSA 1 wt%; CD–PNP: α CD 0 wt%, PEG-b-PLA NPs 5 wt%, HPMC 1 wt%, and FITC-BSA 1 wt%).

Fitting parameters are shown in Table S4 b) Fractional release of the hydrophobic small molecule Oil Red O (OR), encapsulated in the core of PEG-b-PLA NPs (OR-loading \sim 0.2 wt%; PNP: α CD 10 wt%, PEG-b-PLA NPs 5 wt%, and HPMC 1 wt%; CD–PNP: α CD 0 wt%, PEG-b-PLA NPs 5 wt%, and HPMC 1 wt%). Fitting parameters are shown in **Table S4**

Table S4. Fitting results of the experimental data to the Ritger Peppas equation (Eq. 4).

Regression parameters		n	k'	R ²
FITC-albumin release	0 wt% α CD	0.5	9.8	0.987
	10 wt% α CD	0.6	8.1	0.985
OR release	0 wt% α CD	0.90	17.7	0.980
	10 wt% α CD	1.04	10.0	0.961

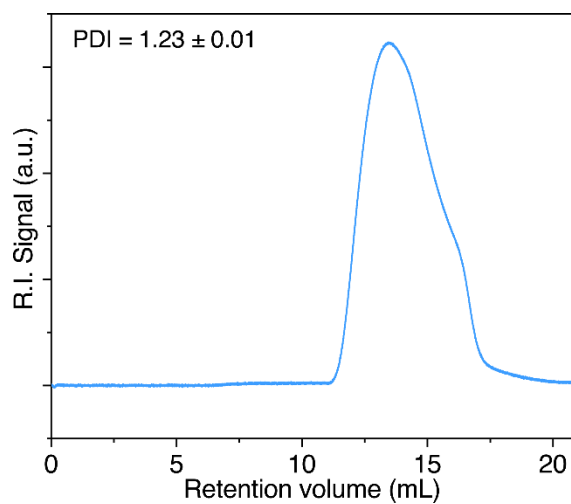


Figure S15. Refractive index signal of a PEG-b-PLA chromatogram. The figure insert reports the measured mean PDI \pm s.d..

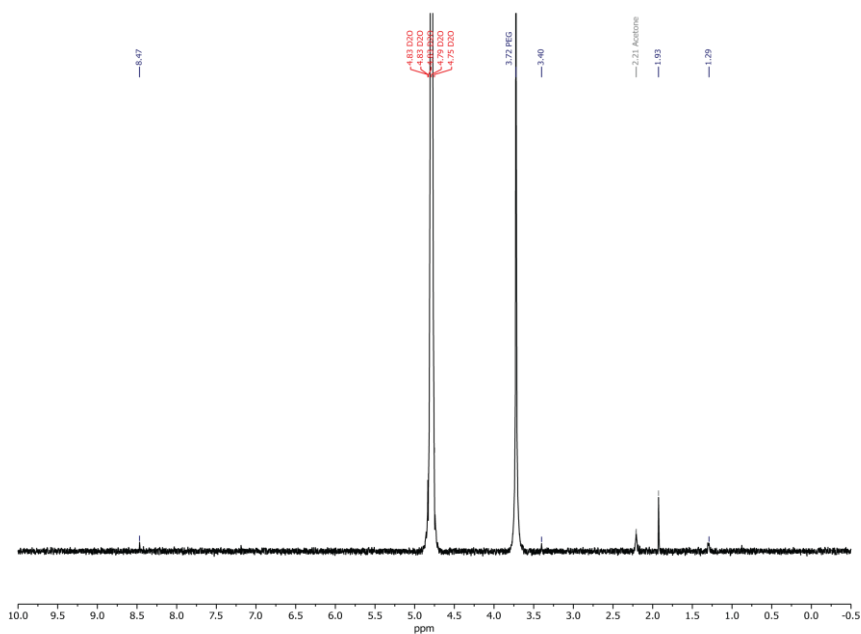


Figure S16. $^1\text{H-NMR}$ spectrum of Pegylated Gold NPs in D_2O .

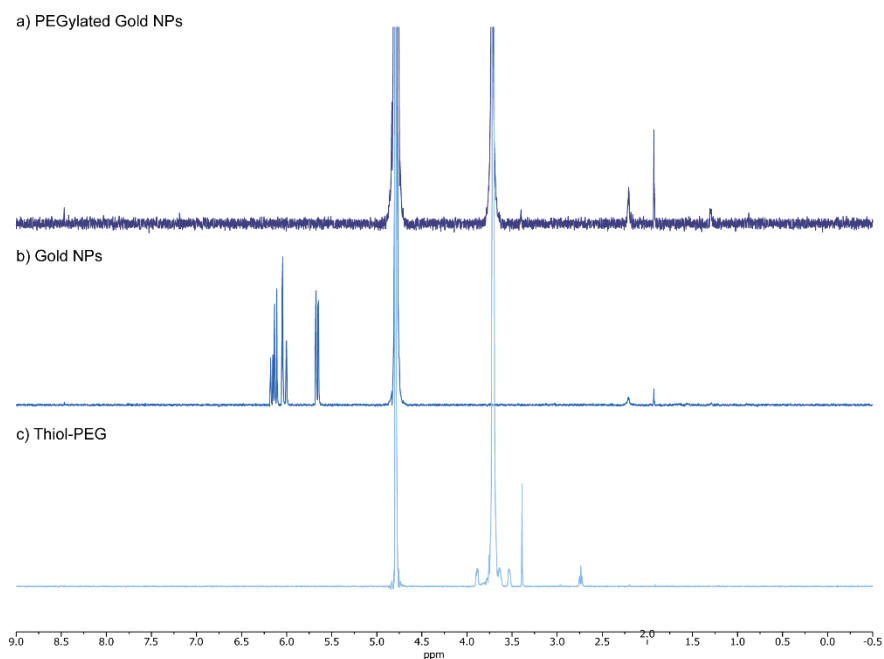


Figure S17. $^1\text{H-NMR}$ spectrum in D_2O of a) Pegylated Gold NPs, b) purchased Gold NPs and c) purchase PEG-thiol.

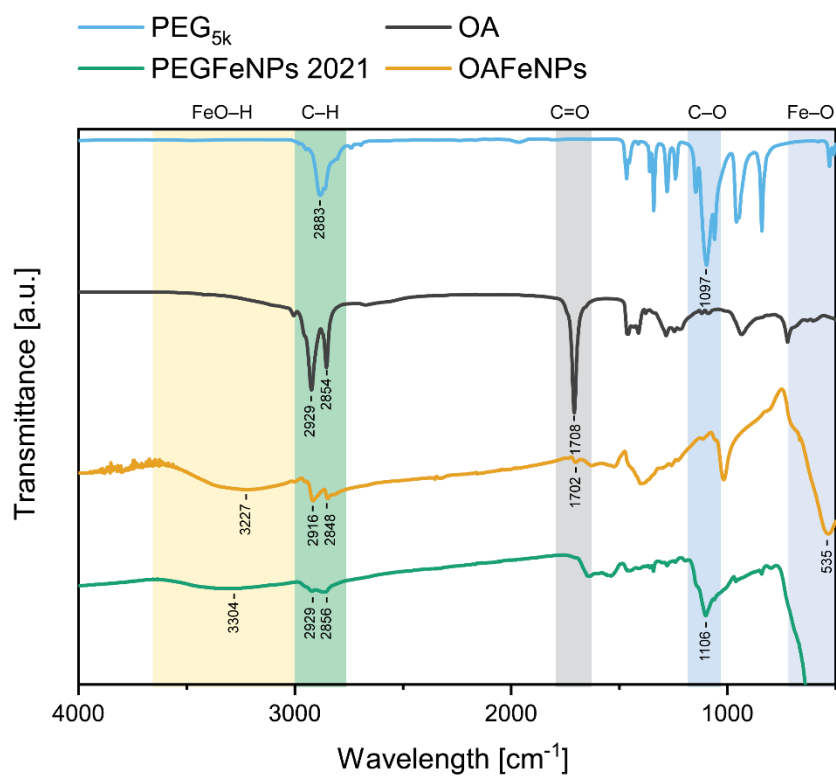


Figure S18. FT-IR spectrum of PEG (blue), oleic acid (black), Oleic acid coated Fe NPs (yellow) and PEGylated Fe NPs (green).

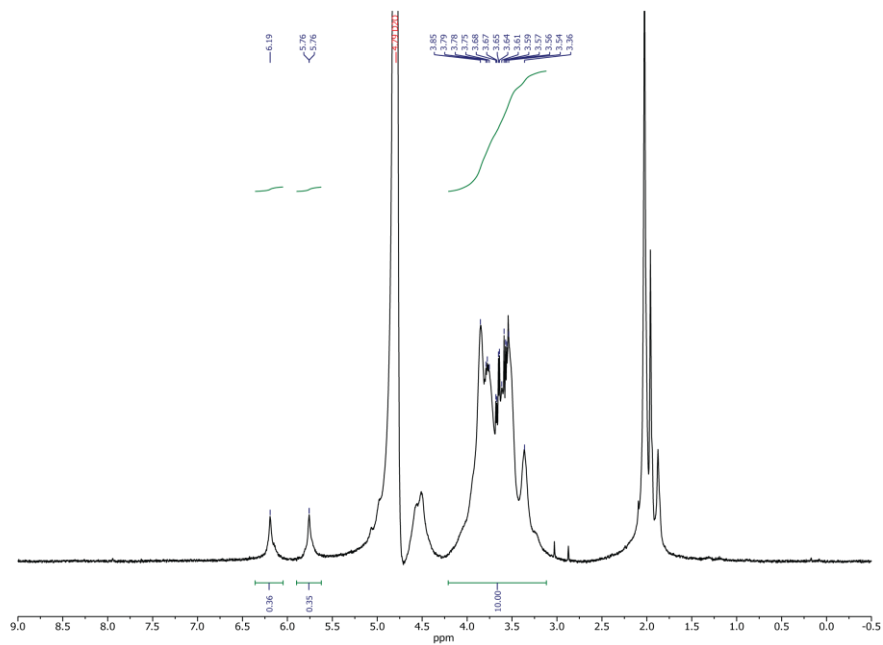


Figure S19. $^1\text{H-NMR}$ spectrum in D_2O of MeHA.

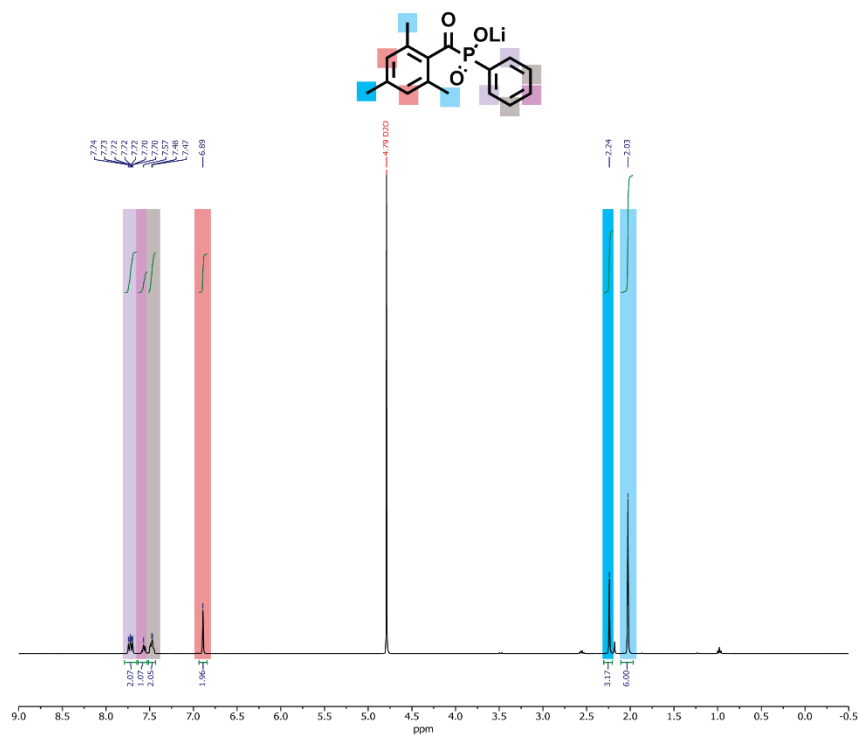


Figure S20. $^1\text{H-NMR}$ spectrum of LAP in D_2O .



Figure S21. Electric circuit composed of a battery and LED.

Table S5. Particle hydrodynamic diameter and dispersity.

	D_h	Đ
PEG6k-b-PLA18k NPs	$52 \pm 1 \text{ nm}$	0.14 ± 0.01
PEG3k-b-PLA20k NPs	$110 \pm 1 \text{ nm}$	0.15 ± 0.01
PEG10k-b-PLA15k NPs	$98 \pm 1 \text{ nm}$	0.17 ± 0.02
OR-encapsulating PEG-b-PLA NPs	$48 \pm 1 \text{ nm}$	0.09 ± 0.02
Gold NPs	$43 \pm 1 \text{ nm}$	0.12 ± 0.04
Iron NPs	$298 \pm 51 \text{ nm}$	0.39 ± 0.04

APPENDIX FOR CHAPTER 3

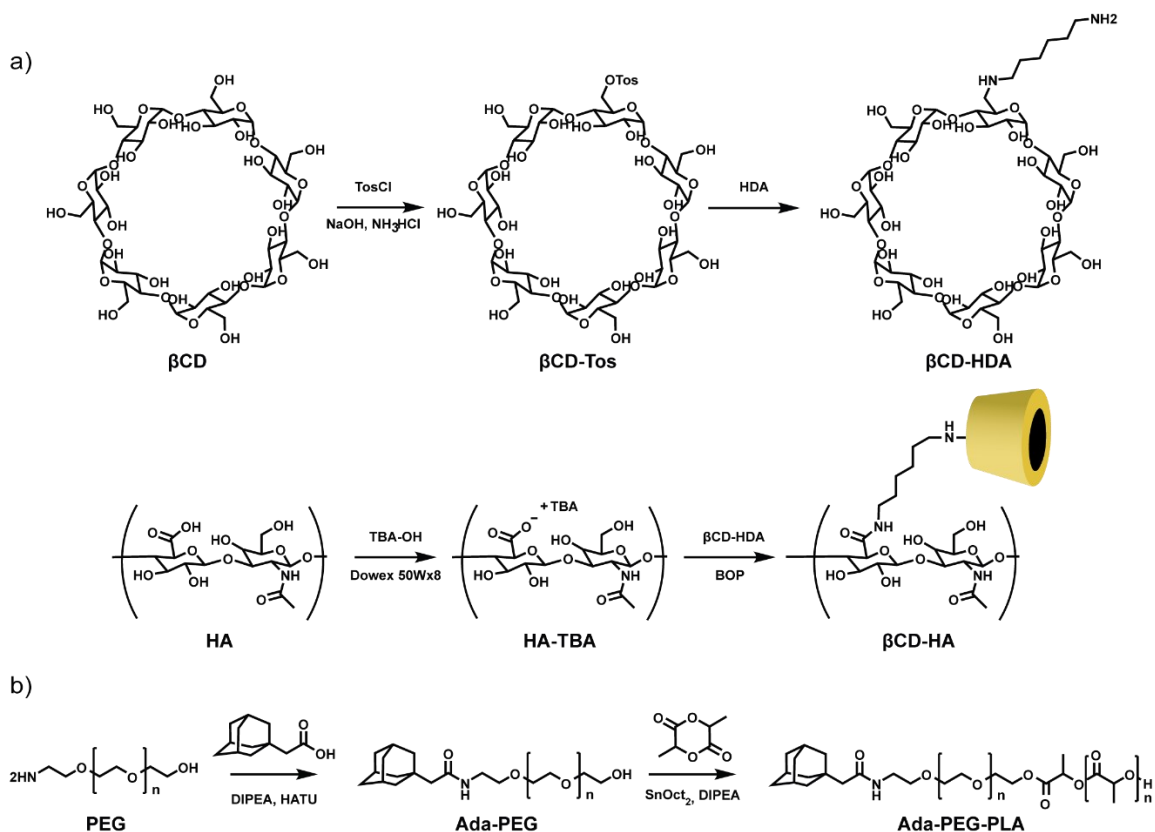


Figure S22. Synthesis strategies to a) functionalization hyaluronic acid with βCD ,¹¹ and b) synthesize Adamantane-PEG-b-PLA.

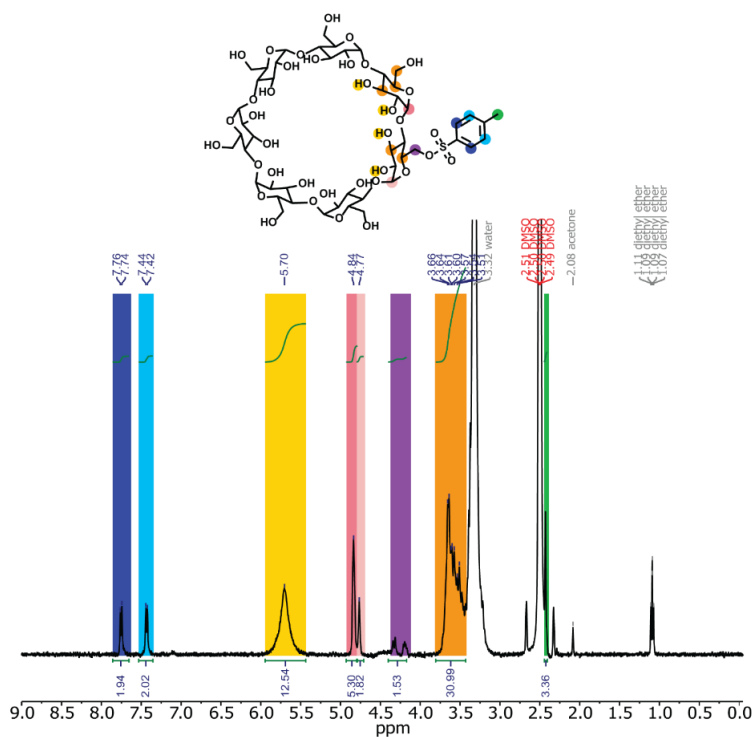


Figure S23. $^1\text{H-NMR}$ spectrum of $\beta\text{CD-Tos}$ in DMSO-d_6 .

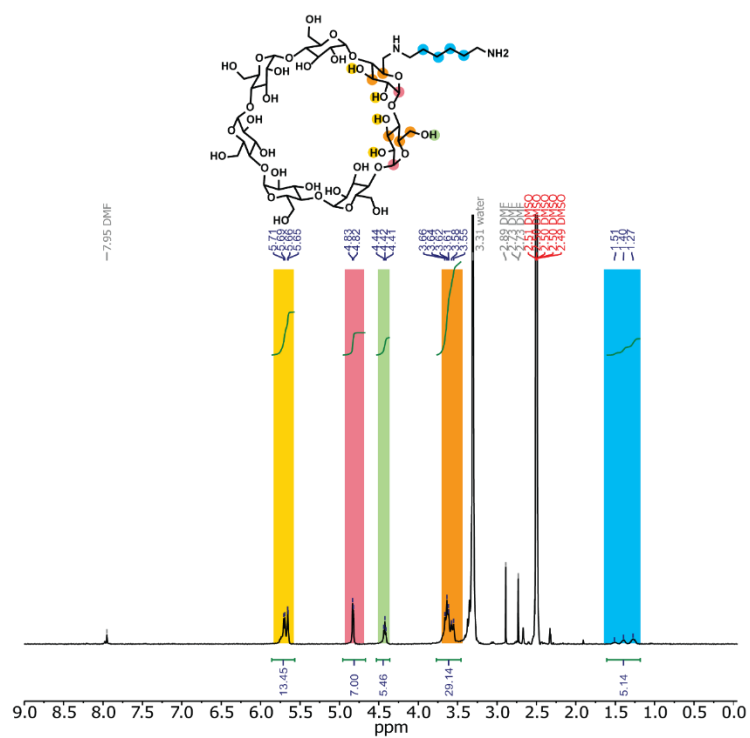


Figure S24. $^1\text{H-NMR}$ spectrum of β CD-HDA in DMSO-d_6 .

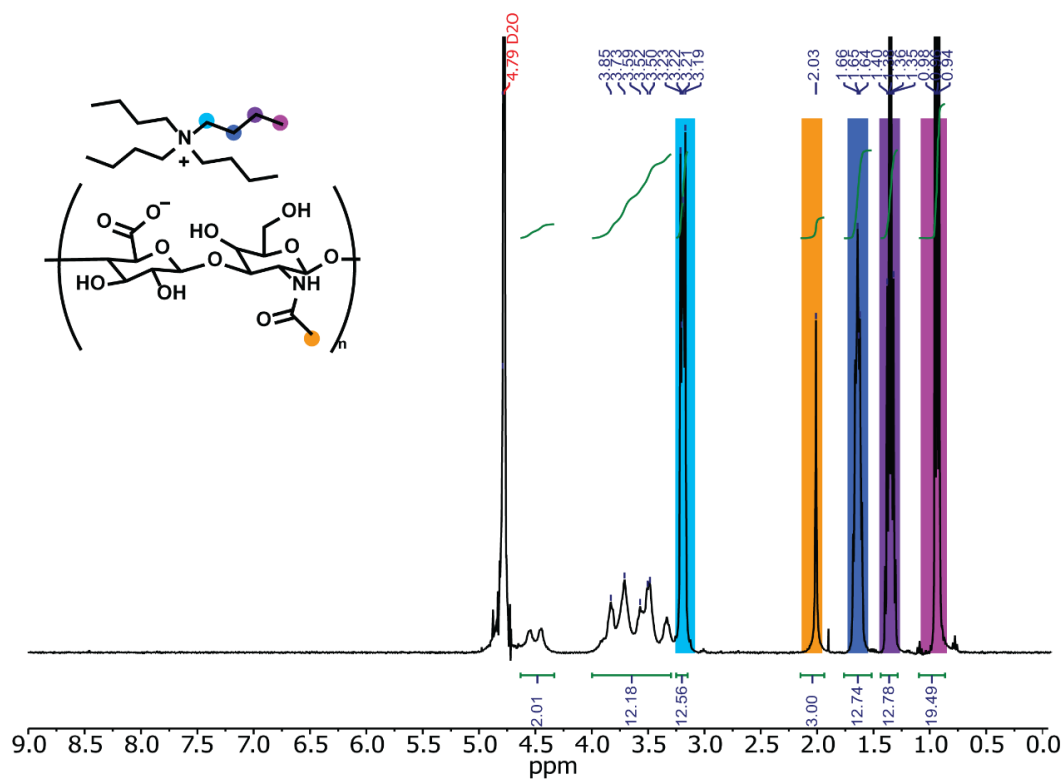


Figure S25. $^1\text{H-NMR}$ spectrum of HA-TBA in D_2O .

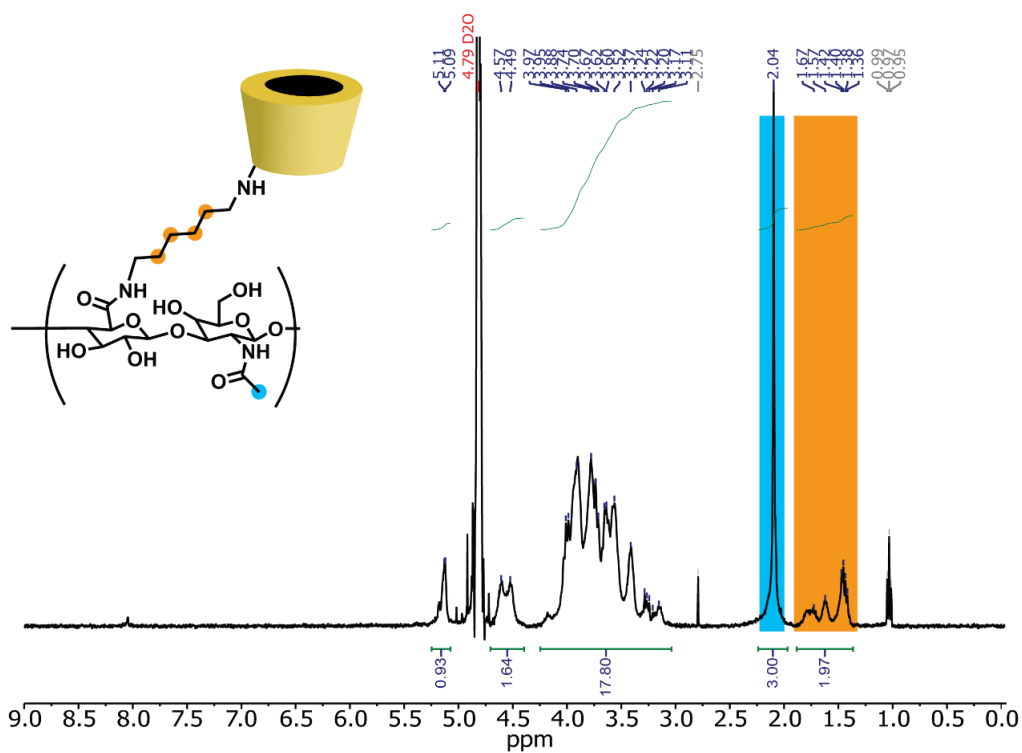


Figure S26. $^1\text{H-NMR}$ spectrum of β CD-HA in D_2O .

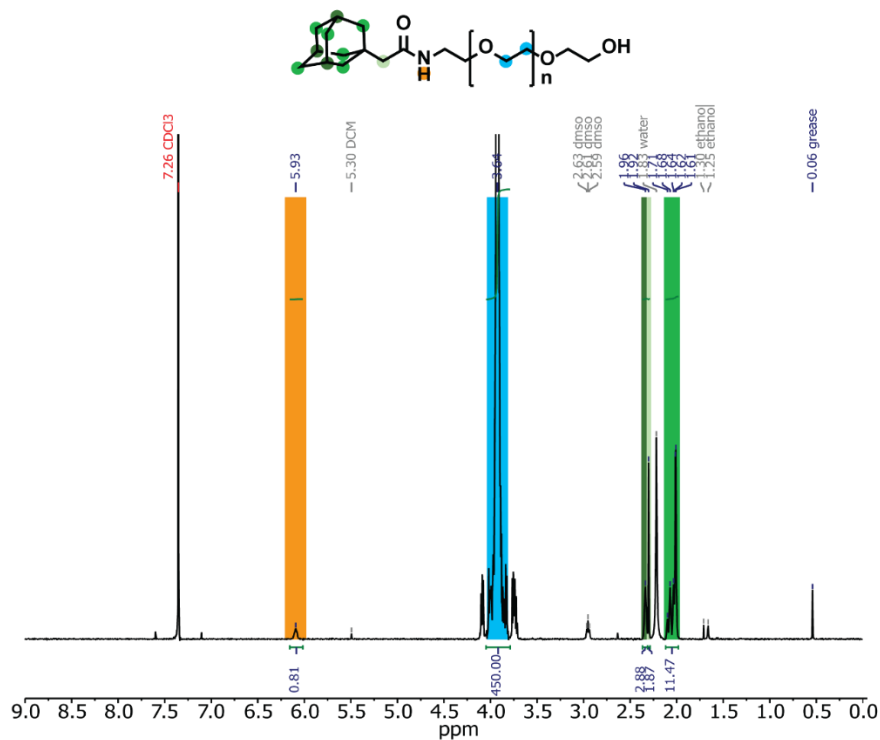


Figure S27. $^1\text{H-NMR}$ spectrum of Ada-PEG_{5k} in CDCl_3 .

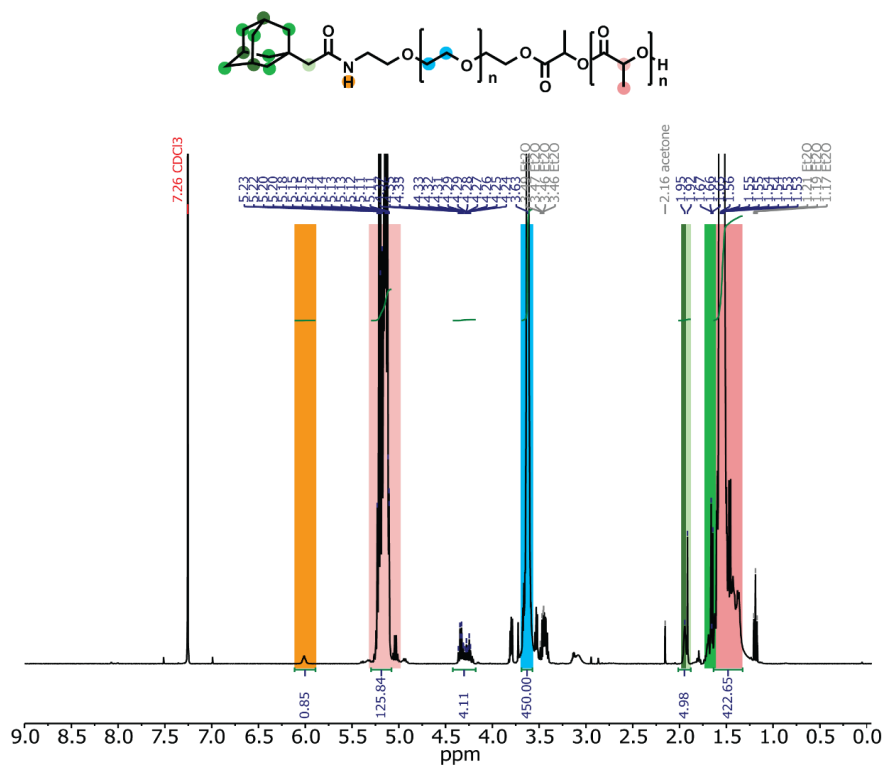


Figure S28. $^1\text{H-NMR}$ spectrum of Ada-PEG_{5k}-PLA_{9k} in CDCl_3 .

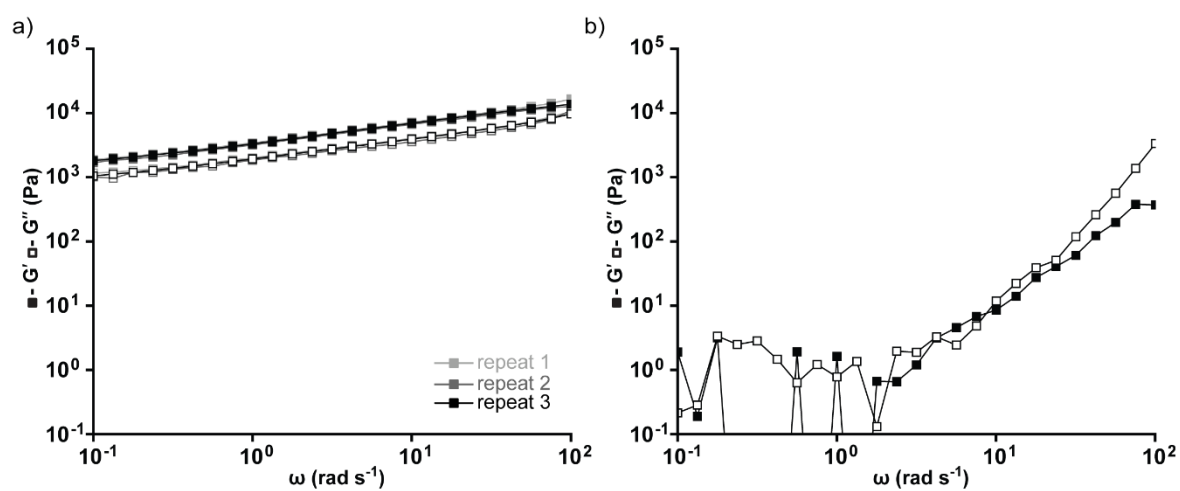


Figure S29. Frequency sweep of a) three repeats of 6 wt% HA-CD with 20 wt% Ada-NPs formulation exposed to a “strong” preconditioning, b) formulation with 6 wt% unfunctionalized HA with 20 wt% Ada-NPs.

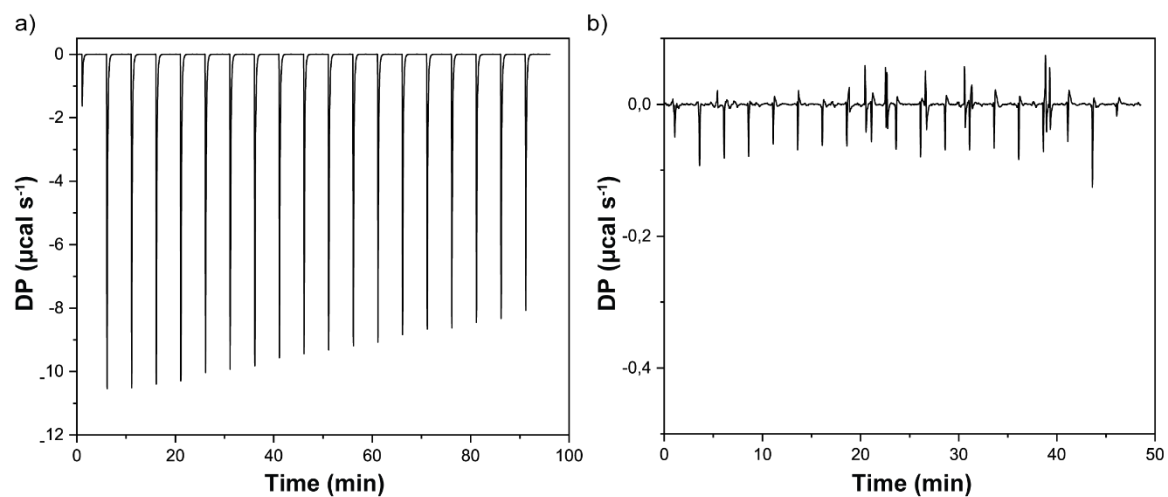


Figure S30. Thermogram of the titration of a) Ada-PEG_{5k} in water and b) β CD in water.

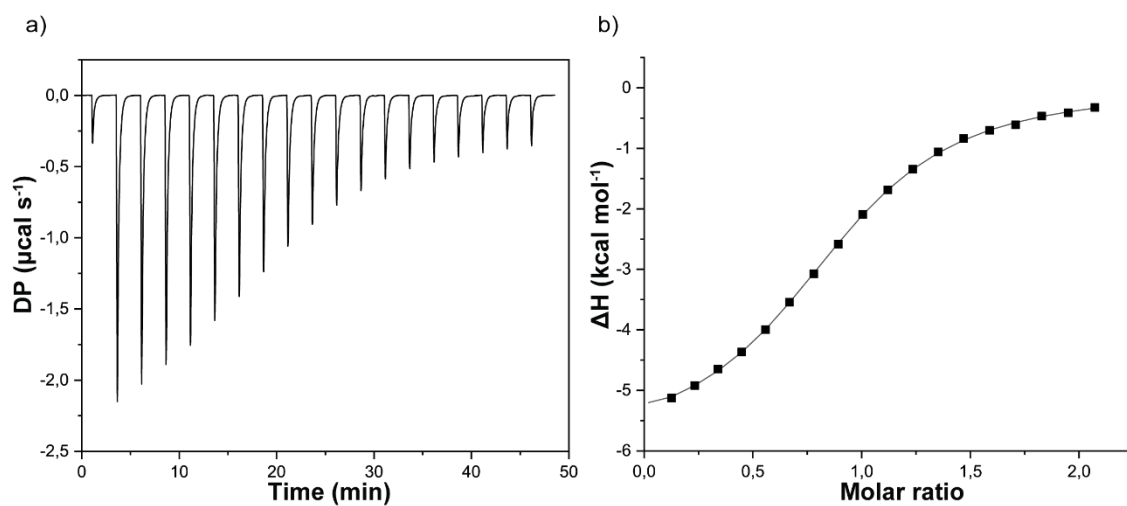


Figure S31. ITC analysis of β CD titration using Ada-PEG_{5k}. a) Thermogram of the titration. b) Integrated heat pulse as a function of molar ratio (Ad-PEG_{5k}: β CD) with fitting to a single site binding model.

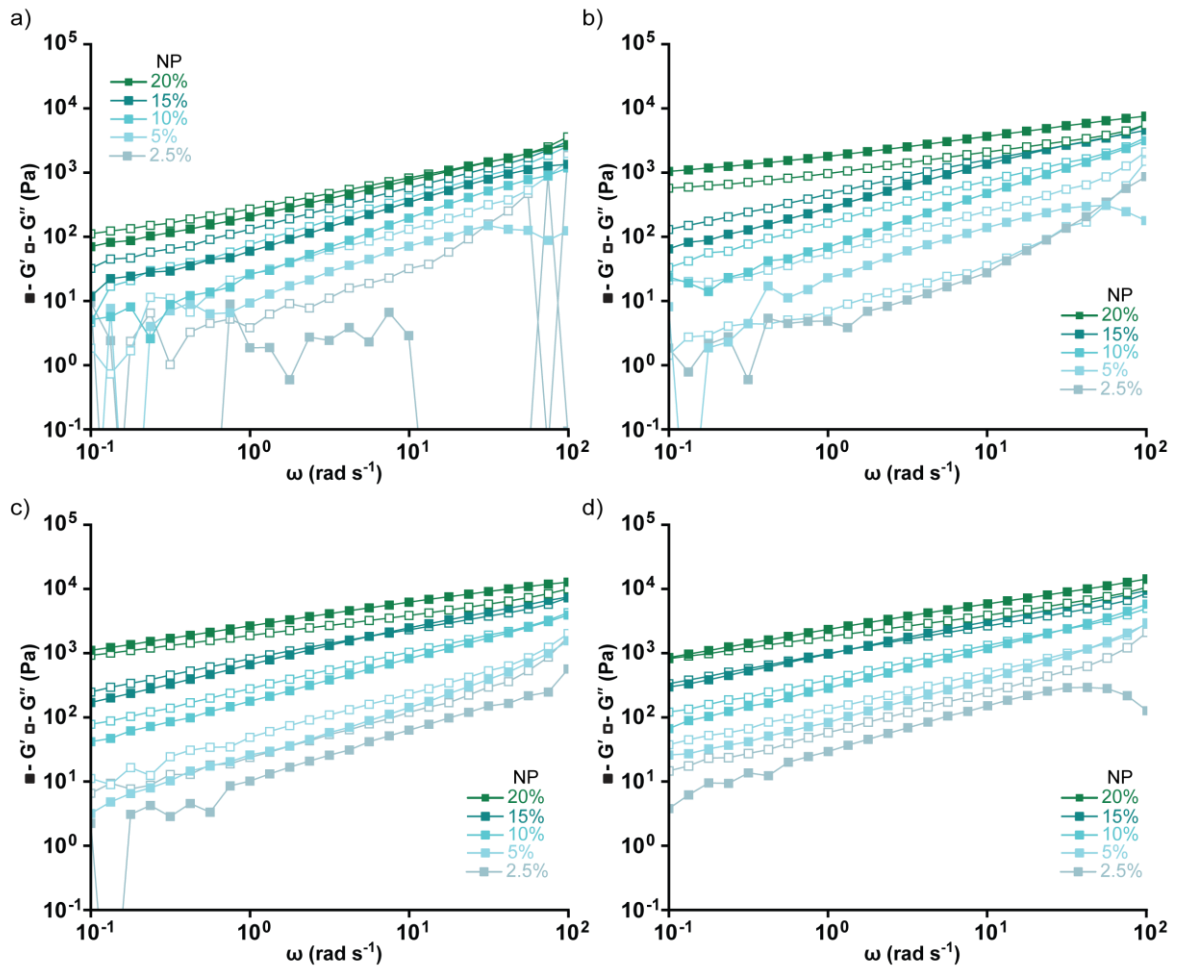


Figure S32. Frequency and strain sweep with varying Ad-NP concentrations of a) 2 wt% β CD-HA, b) 4 wt% β CD-HA, c) 8 wt% β CD-HA and d) 10 wt% β CD-HA.

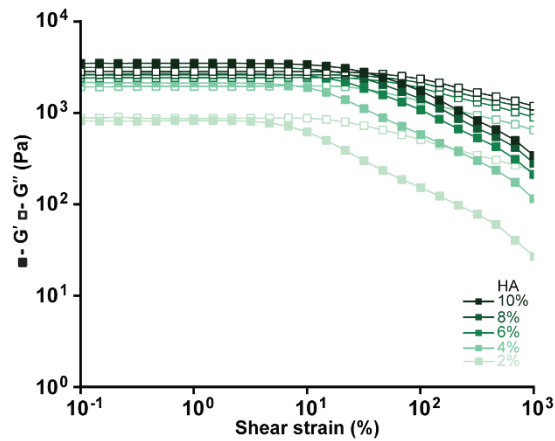


Figure S33. Strain sweep of 15 wt% Ada-NP gels with varying concentration of HA-CD.

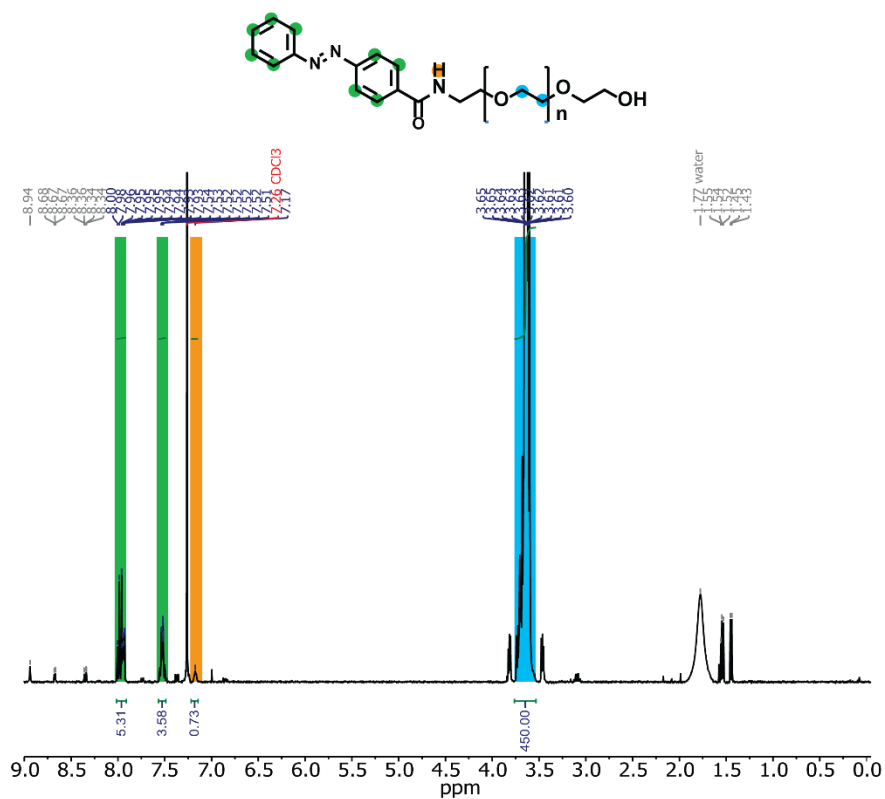


Figure S34. ¹H-NMR spectrum of AzB-PEG_{5k} in CDCl₃.

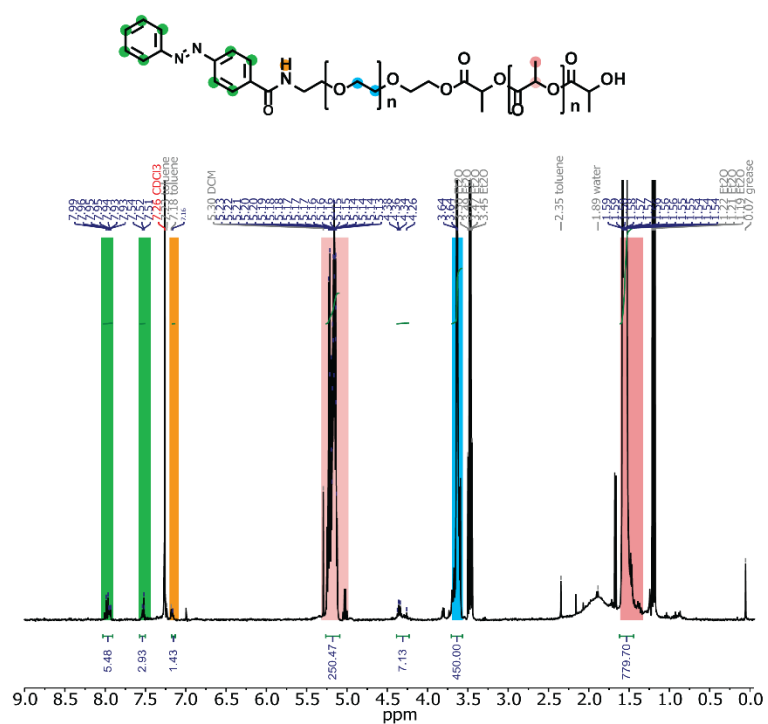
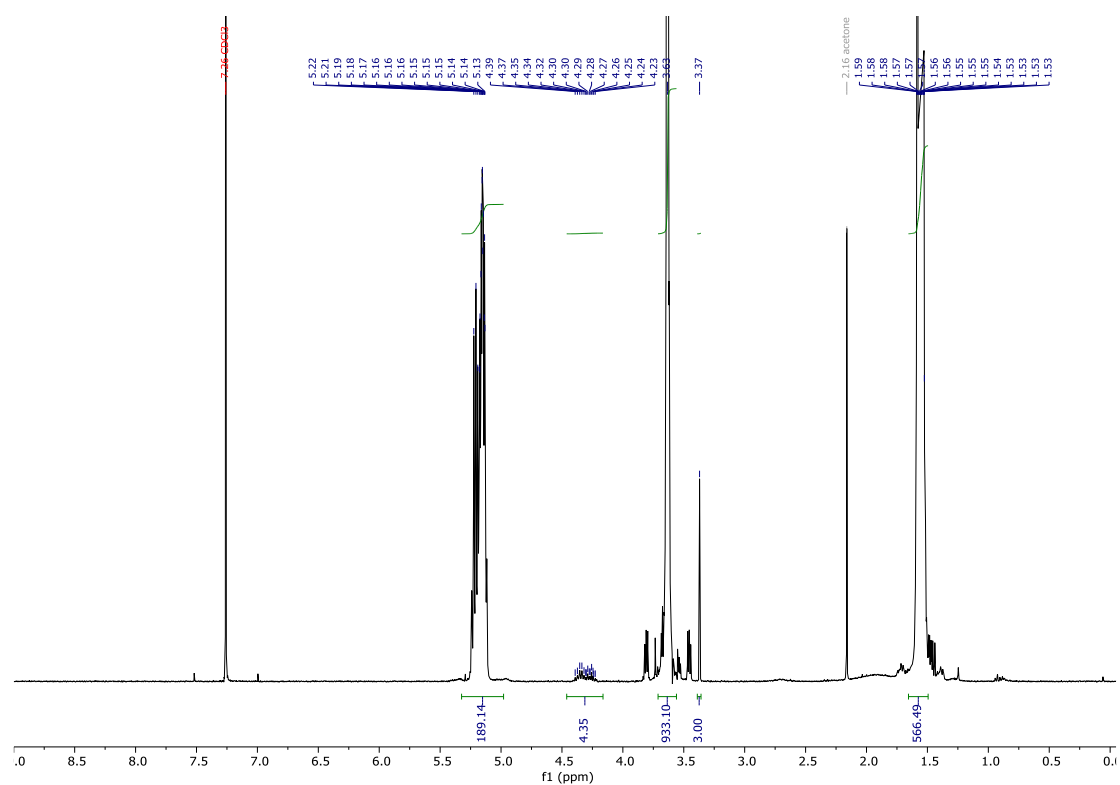
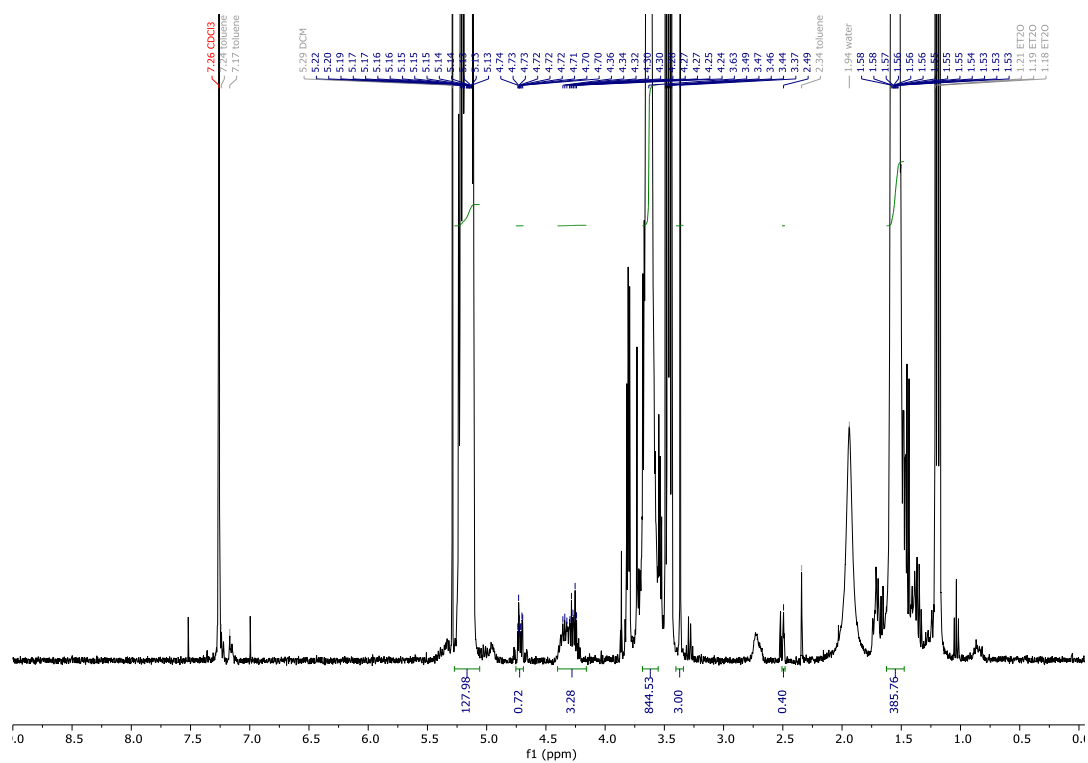


Figure S35. ¹H-NMR spectrum of AzB-PEG_{5k}-PLA_{18k} in CDCl₃.

APPENDIX FOR CHAPTER 4

Figure S36. $^1\text{H-NMR}$ spectrum of PEG_{10k}-PLA_{14k} in CDCl_3 .Figure S37. $^1\text{H-NMR}$ spectrum of PEG_{10k}-PLA_{14k}-alkyne in CDCl_3 .

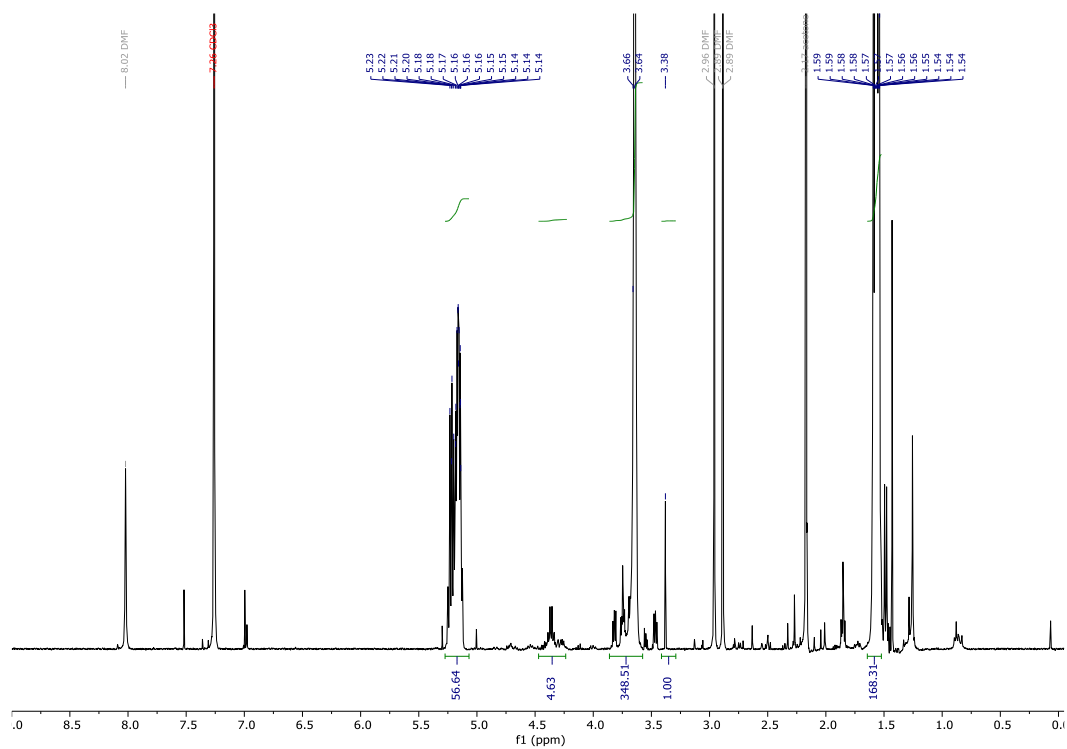


Figure S38. $^1\text{H-NMR}$ spectrum of PEG_{10k}-PLA_{14k}-alkyne in CDCl_3 .

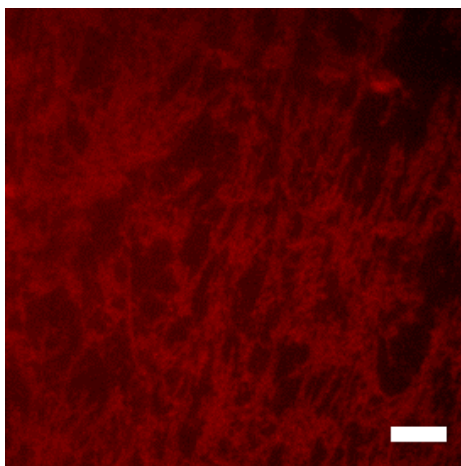
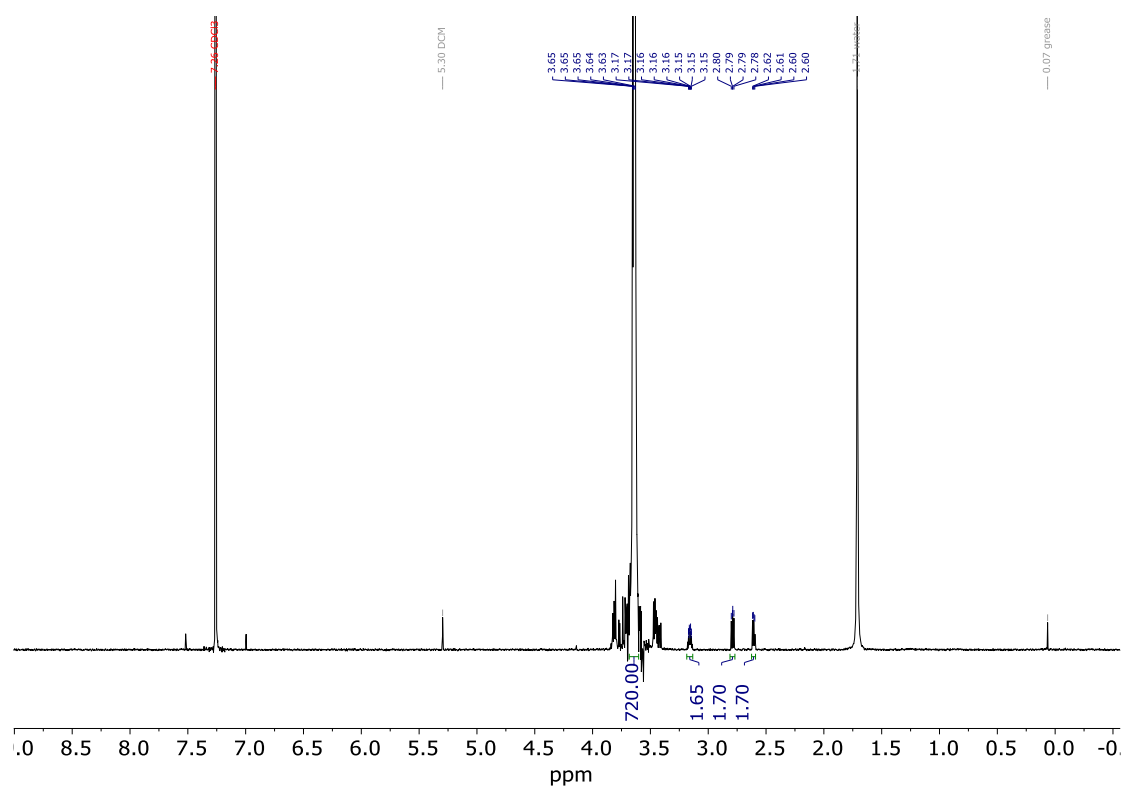
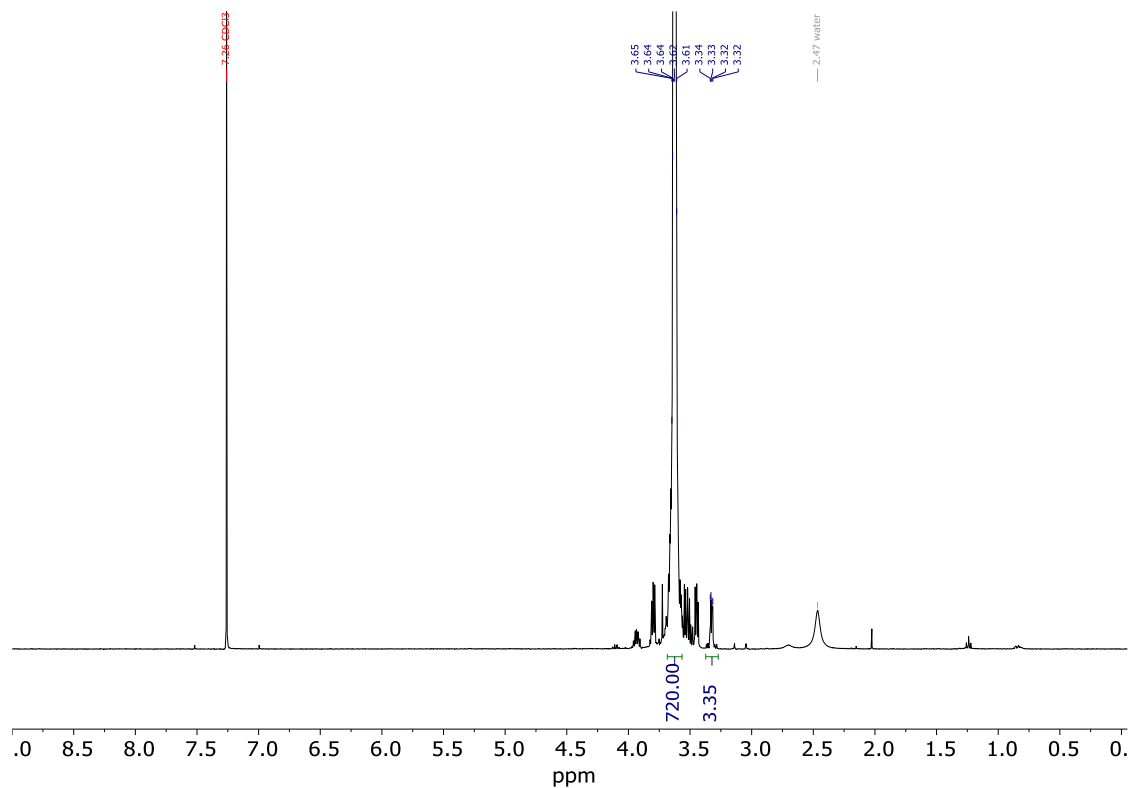


Figure S39. TIRF image showing the distribution of labeled nanoparticles in PNP hydrogel (1 wt% HPMC, 5 wt% NPs). Scale bar, 10 μm .

APPENDIX FOR CHAPTER5

Figure S40. $^1\text{H-NMR}$ spectrum of Diepoxy-PEG in CDCl_3 .

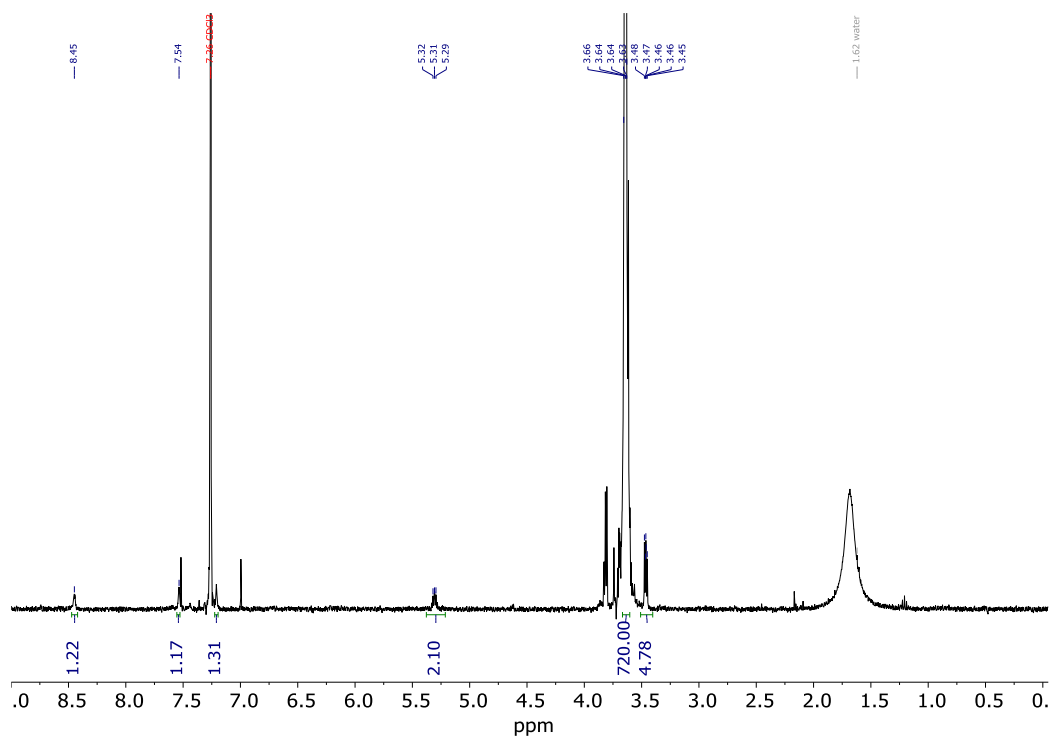


Figure S42. $^1\text{H-NMR}$ spectrum of PEG- N_3 -CDI in CDCl_3 .

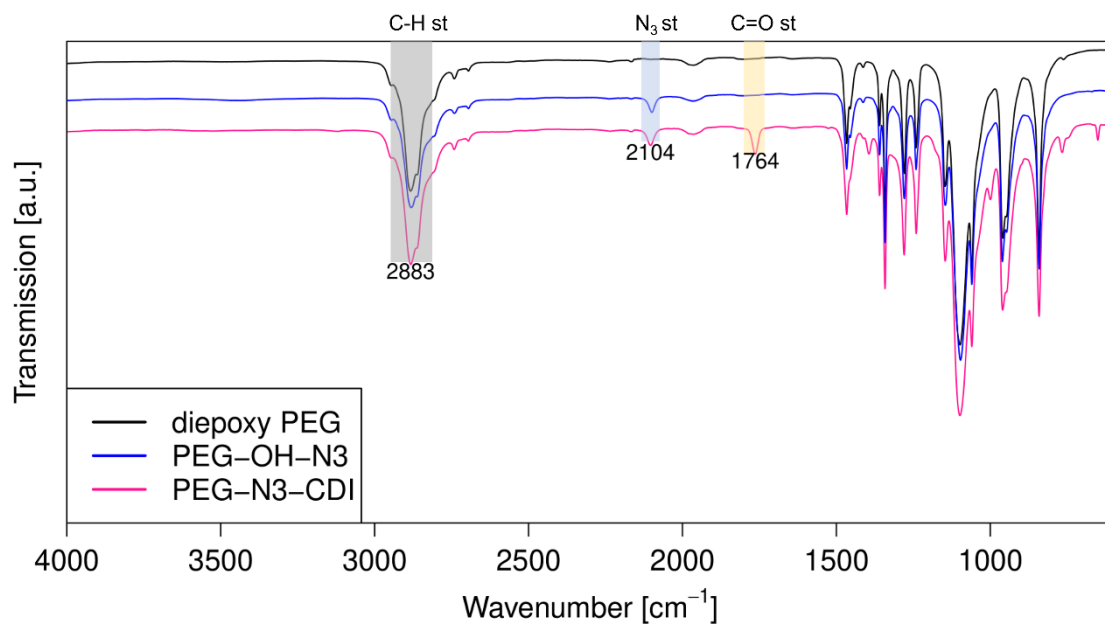


Figure S43. FT-IR spectrum of Diepoxy-PEG (black), PEG-OH- N_3 (blue) and PEG- N_3 -CDI (pink).

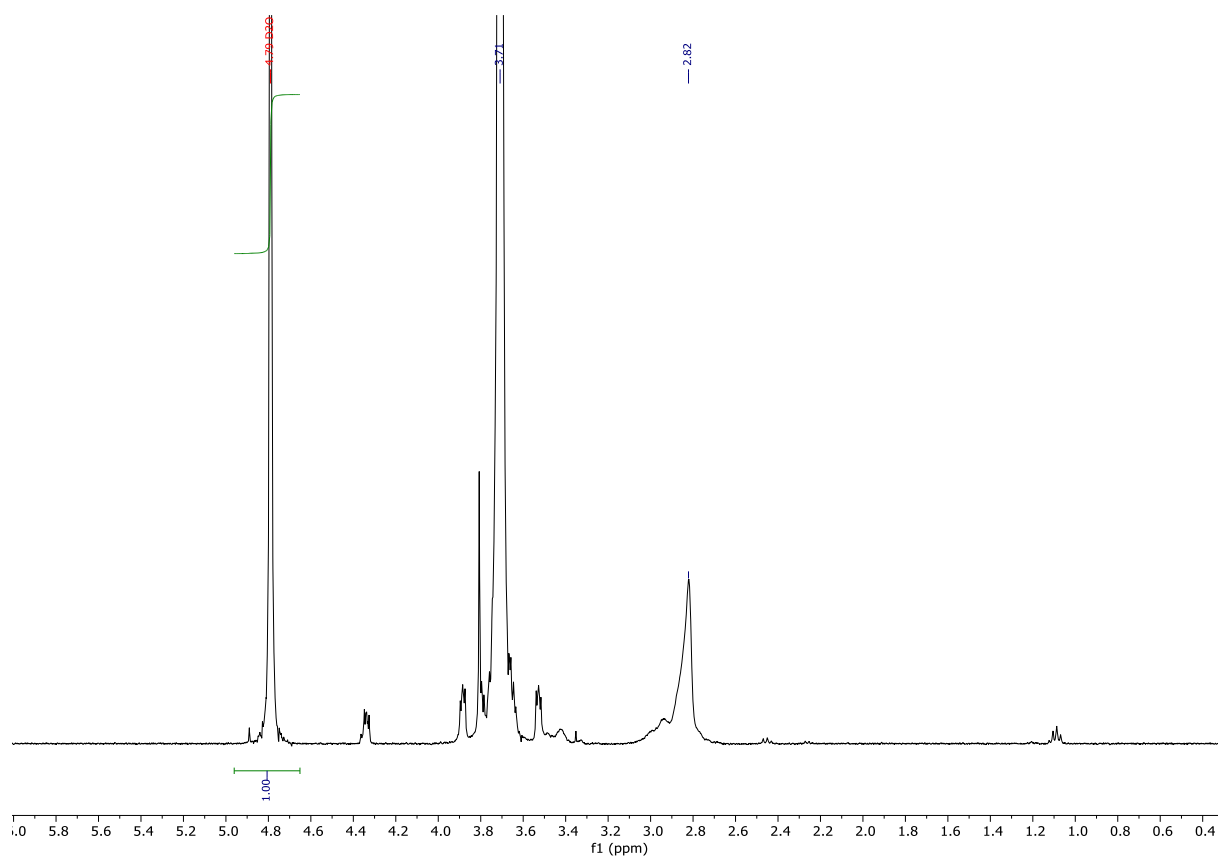


Figure S44. $^1\text{H-NMR}$ spectrum of nanogel- N_3 in D_2O .

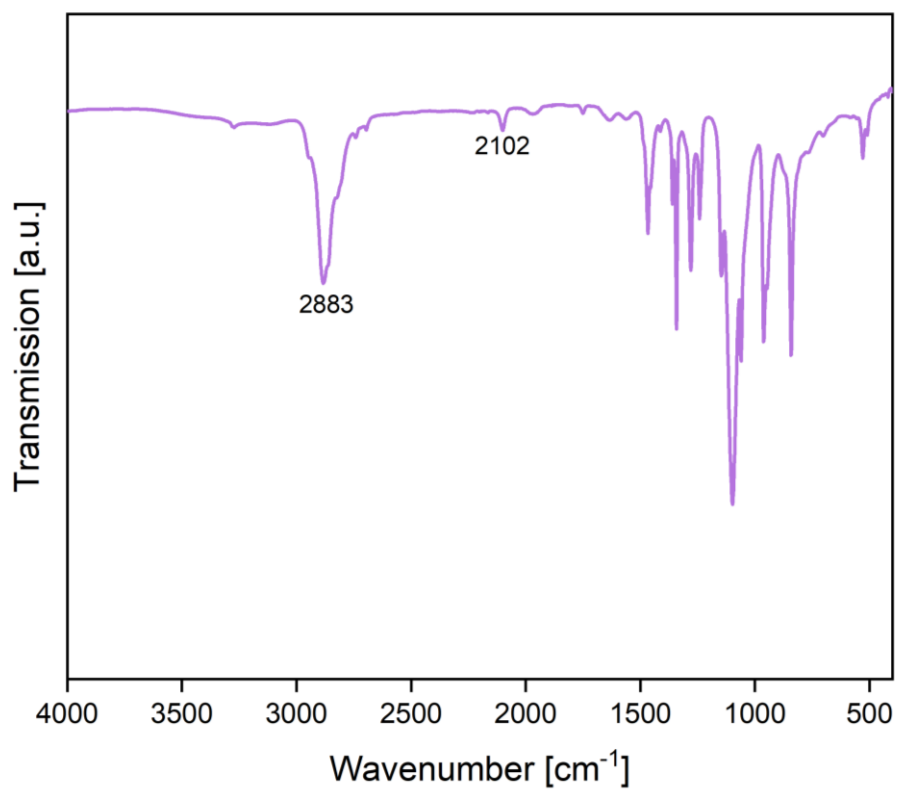


Figure S45. FT-IR spectrum of NG- N_3 .

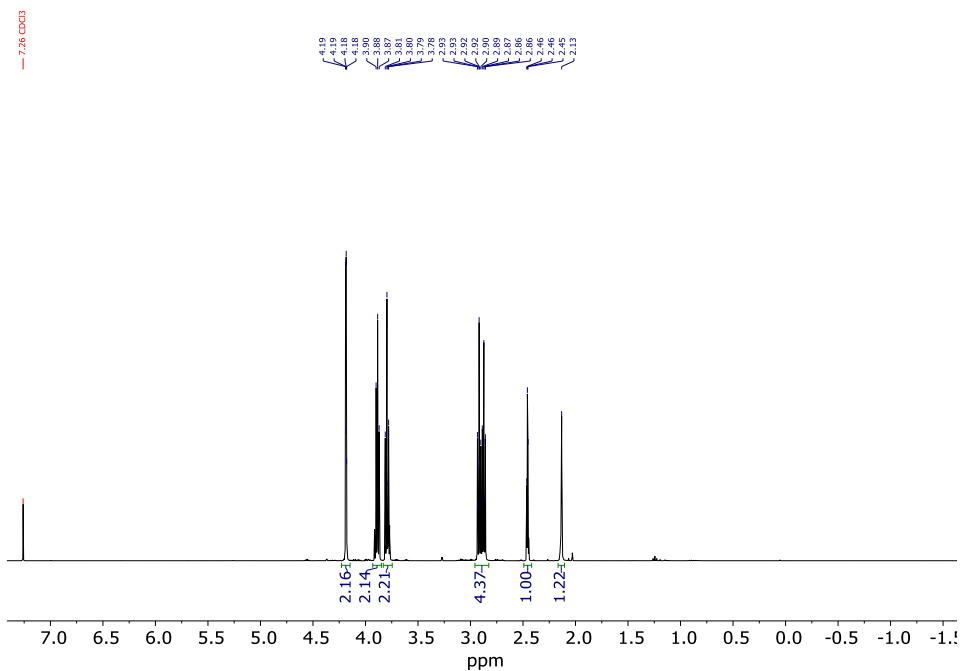


Figure S46. ¹H-NMR spectrum of 2-propynyloxyethyl disulphanylethanol in CDCl₃

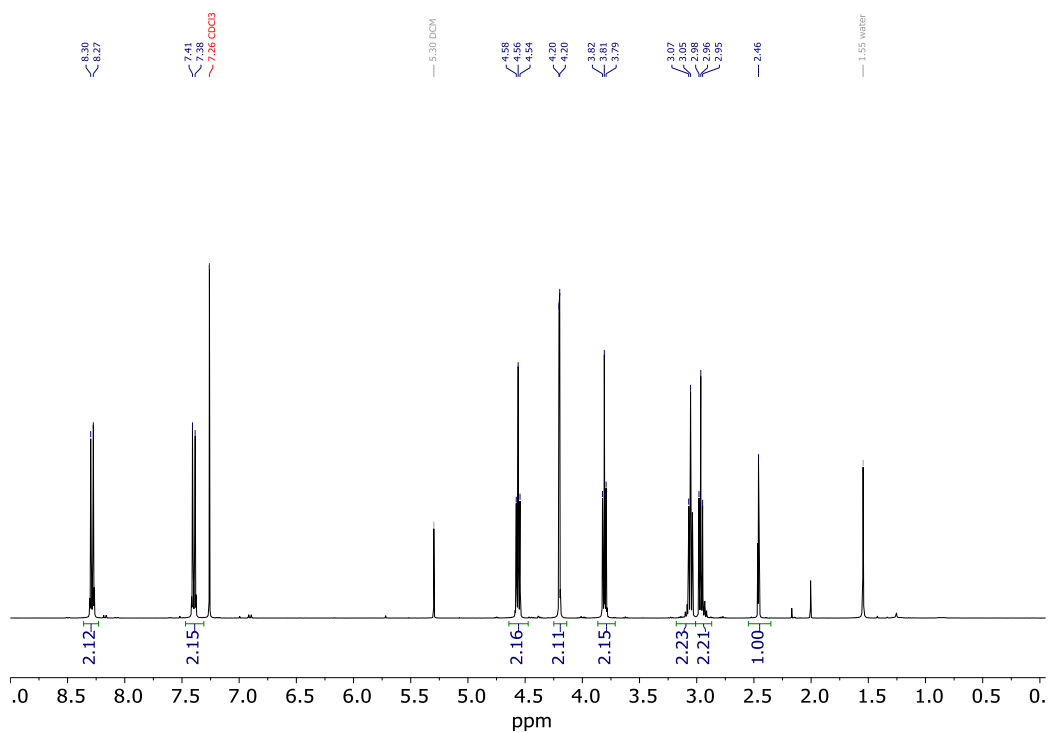
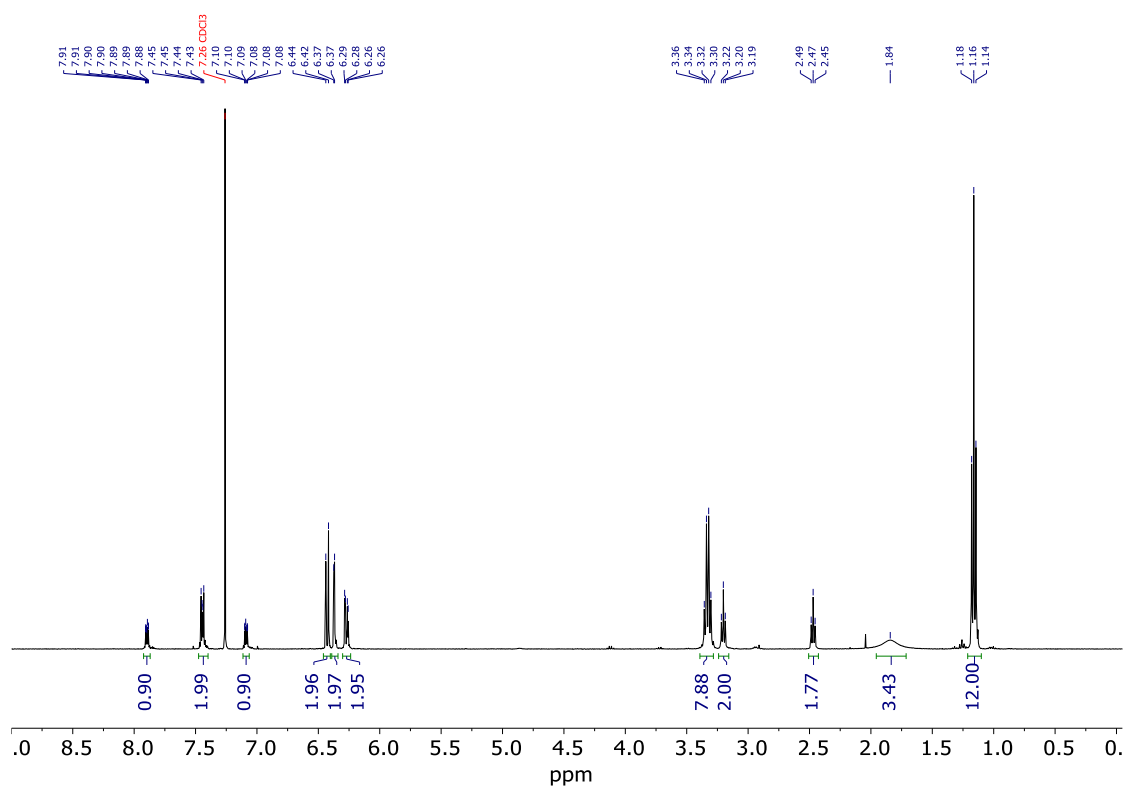
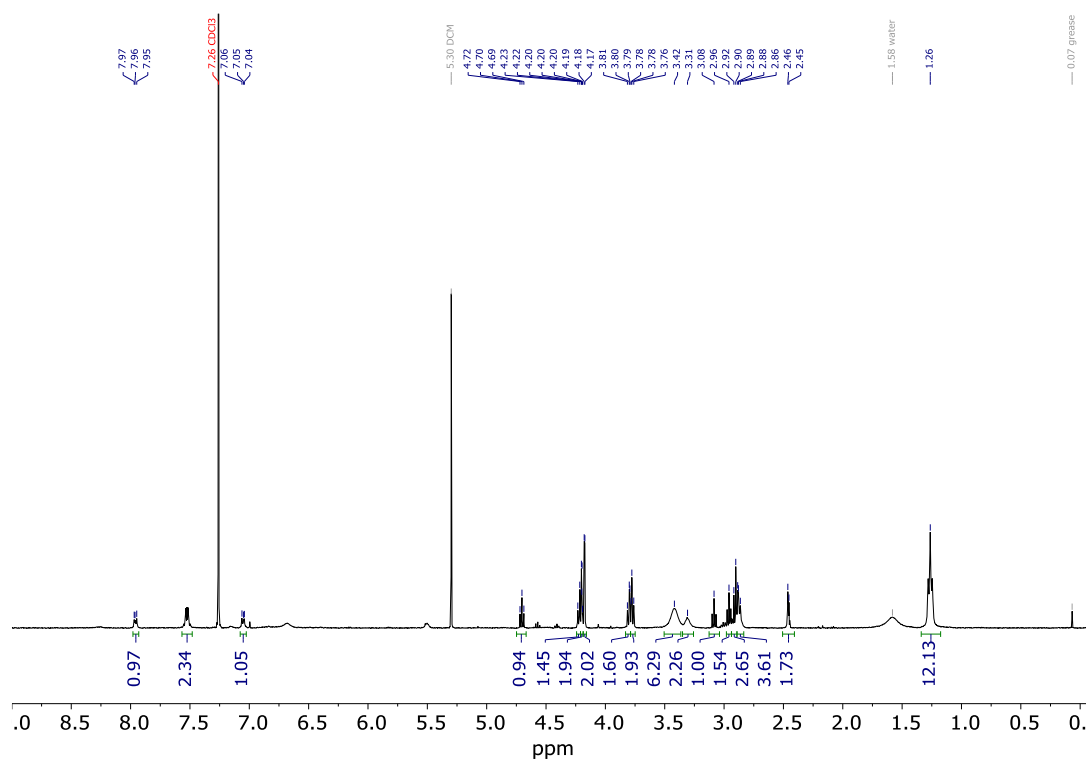


Figure S47. ¹H-NMR spectrum of para-nitrophenylcarbonate-linker in CDCl₃

Figure S48. $^1\text{H-NMR}$ spectrum of RhB-NH₂ in CDCl₃Figure S49. $^1\text{H-NMR}$ spectrum of RhB-linker in CDCl₃

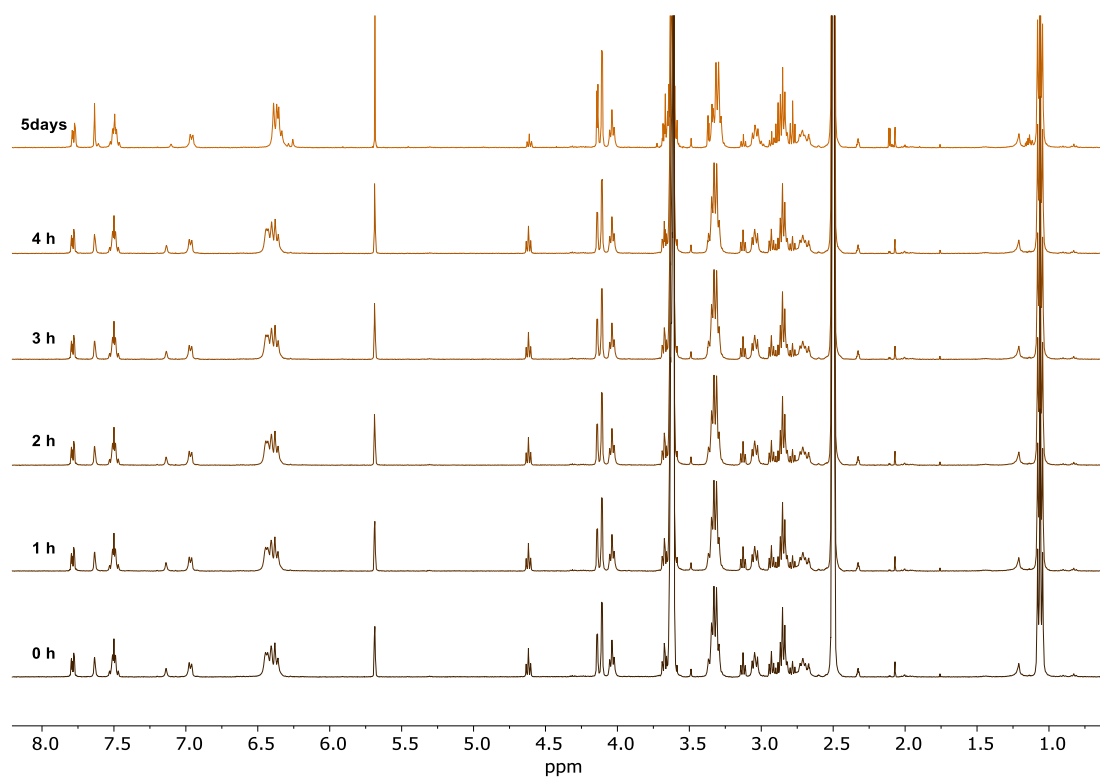


Figure S50. ¹H-NMR spectra of RhB amine linker in the presence of 0.01 mM GSH recorded over time in DMSO-d₆

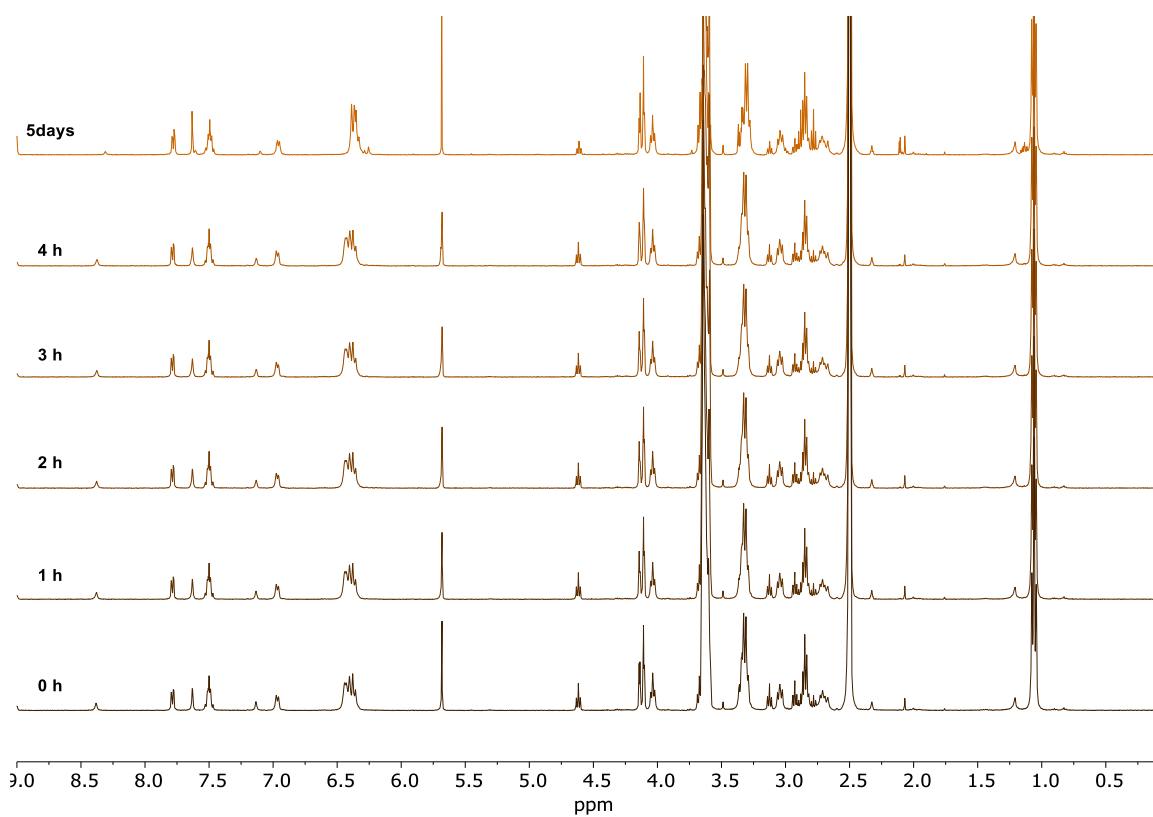


Figure S51. ¹H-NMR spectra of RhB amine linker in the presence of 0.1 mM GSH recorded over time in DMSO-d₆

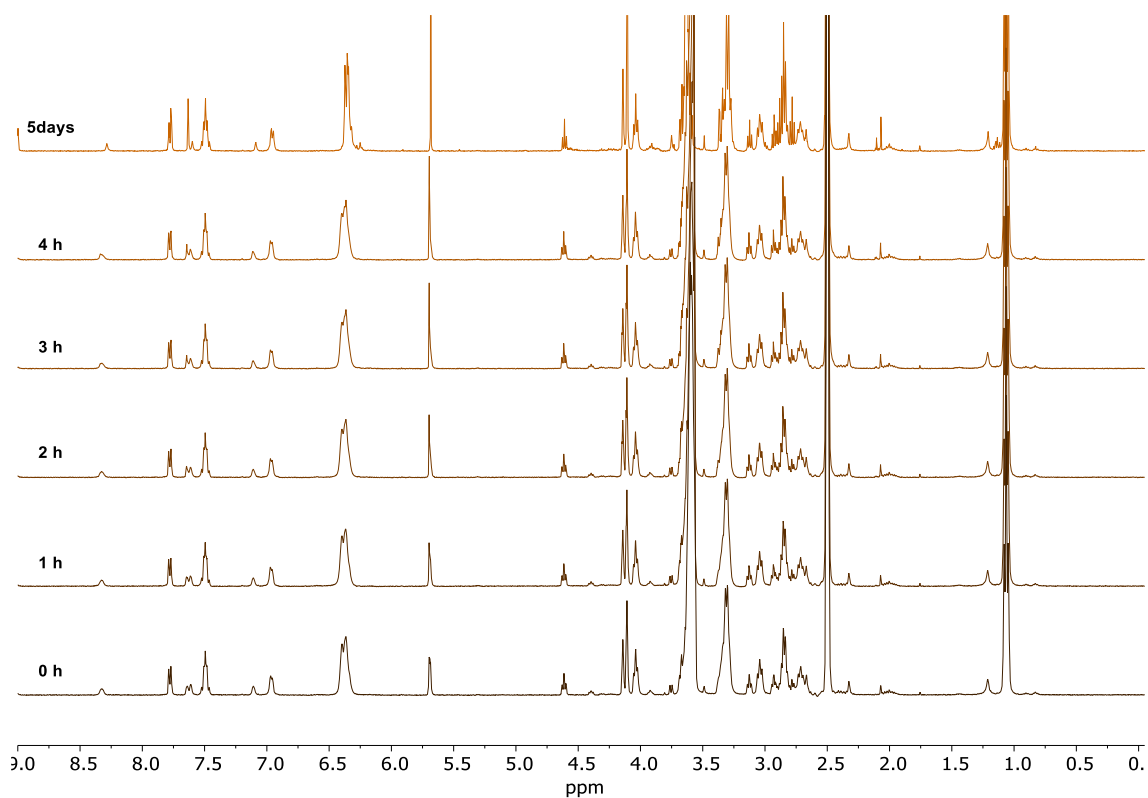


Figure S52. $^1\text{H-NMR}$ spectra of RhB amine linker in the presence of 1 mM GSH recorded over time in DMSO-d_6

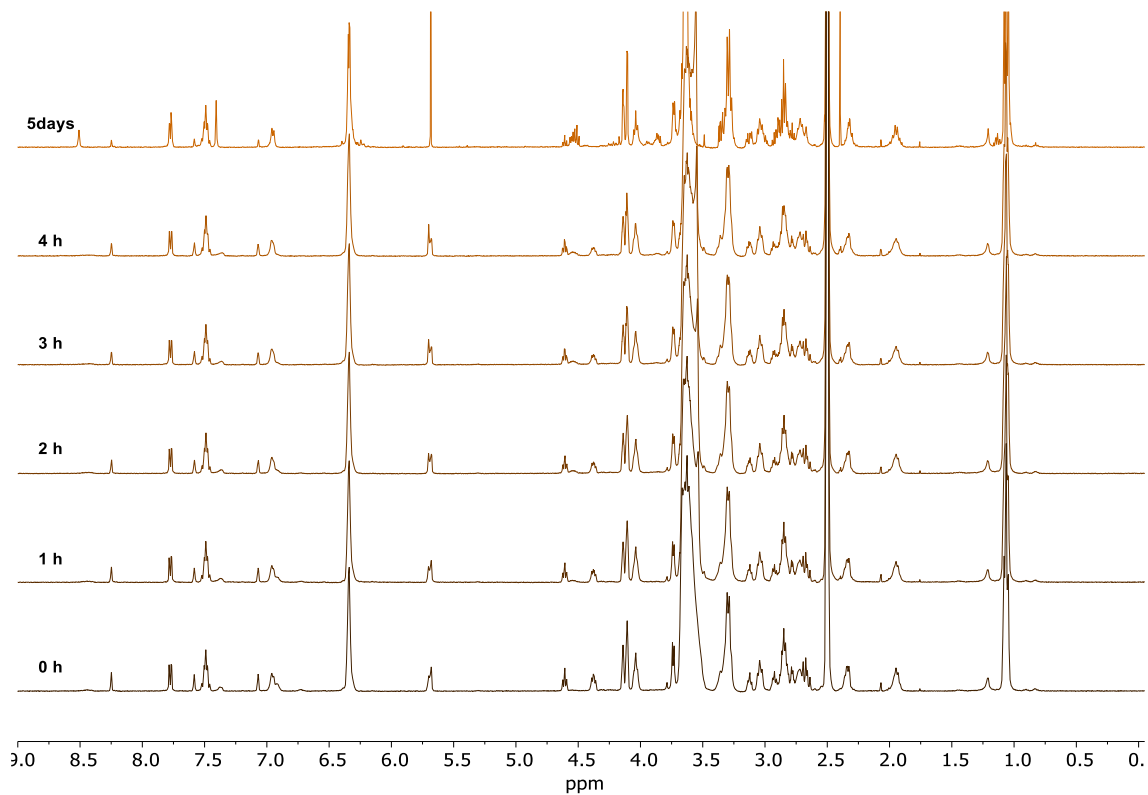


Figure S53. $^1\text{H-NMR}$ spectra of RhB amine linker in the presence of 5 mM GSH recorded over time in DMSO-d_6

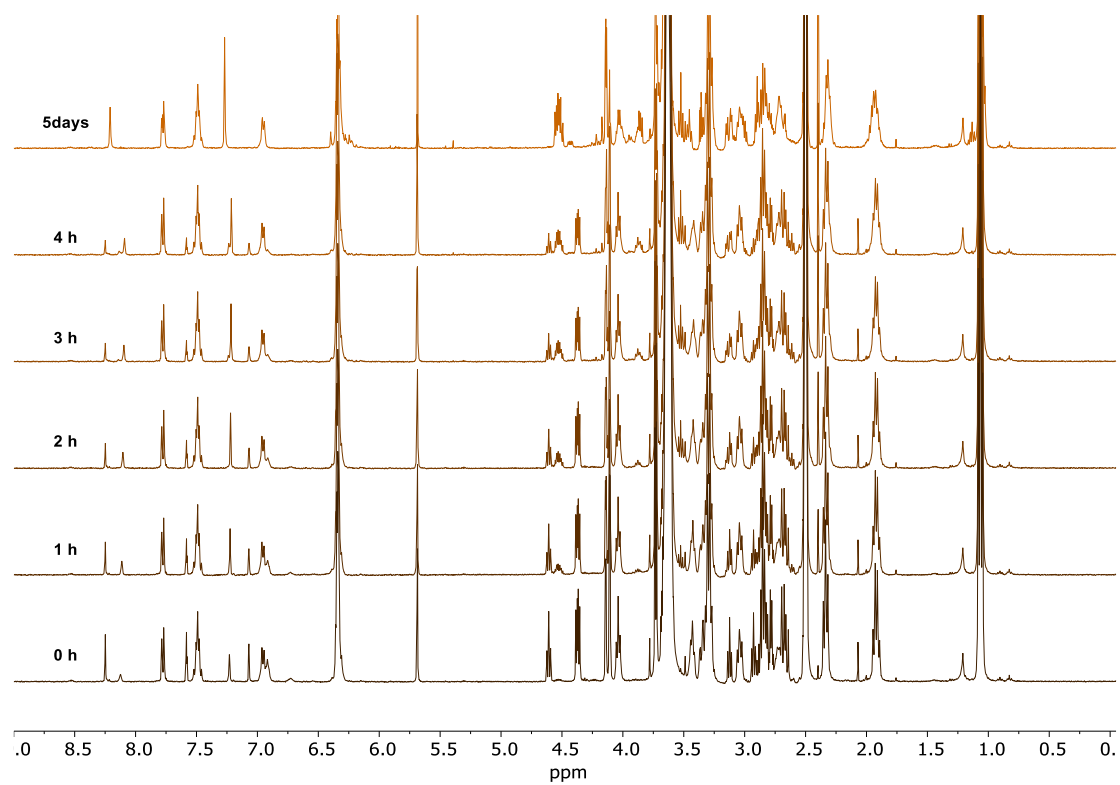


Figure S54. ¹H-NMR spectra of RhB amine linker in the presence of 10 mM GSH recorded over time in DMSO-d₆

BIBLIOGRAPHY

- (1) Wong, C. H.; Siah, K. W.; Lo, A. W. Estimation of Clinical Trial Success Rates and Related Parameters. *Biostatistics* **2019**, *20* (2), 273–286. DOI: 10.1093/biostatistics/kxx069.
- (2) Jain, K. K. An Overview of Drug Delivery Systems. *Methods Mol. Biol.* **2020**, *2059*, 1–54. DOI: 10.1007/978-1-4939-9798-5_1.
- (3) Homayun, B.; Lin, X.; Choi, H.-J. Challenges and Recent Progress in Oral Drug Delivery Systems for Biopharmaceuticals. *Pharmaceutics* **2019**, *11* (3). DOI: 10.3390/pharmaceutics11030129.
- (4) Ruiz, M. E.; Scioli Montoto, S. Routes of Drug Administration. In *ADME processes in pharmaceutical sciences: dosage, design, and pharmacotherapy success*; Talevi, A., Quiroga, P. A. M., Eds.; Springer International Publishing: Cham, 2018; pp 97–133. DOI: 10.1007/978-3-319-99593-9_6.
- (5) Tibbitt, M. W.; Dahlman, J. E.; Langer, R. Emerging Frontiers in Drug Delivery. *J. Am. Chem. Soc.* **2016**, *138* (3), 704–717. DOI: 10.1021/jacs.5b09974.
- (6) Buwalda, S. J.; Boere, K. W. M.; Dijkstra, P. J.; Feijen, J.; Vermonden, T.; Hennink, W. E. Hydrogels in a Historical Perspective: From Simple Networks to Smart Materials. *J. Control. Release* **2014**, *190*, 254–273. DOI: 10.1016/j.jconrel.2014.03.052.
- (7) Peppas, N. A.; Khare, A. R. Preparation, Structure and Diffusional Behavior of Hydrogels in Controlled Release. *Adv. Drug Deliv. Rev.* **1993**, *11* (1–2), 1–35. DOI: 10.1016/0169-409X(93)90025-Y.
- (8) Fu, Y.; Kao, W. J. Drug Release Kinetics and Transport Mechanisms of Non-Degradable and Degradable Polymeric Delivery Systems. *Expert Opin. Drug Deliv.* **2010**, *7* (4), 429–444. DOI: 10.1517/17425241003602259.
- (9) Uman, S.; Dhand, A.; Burdick, J. A. Recent Advances in Shear-thinning and Self-healing Hydrogels for Biomedical Applications. *J. Appl. Polym. Sci.* **2020**, *137* (25), 48668. DOI: 10.1002/app.48668.
- (10) Sahoo, J. K.; VandenBerg, M. A.; Webber, M. J. Injectable Network Biomaterials via Molecular or Colloidal Self-Assembly. *Adv. Drug Deliv. Rev.* **2018**, *127*, 185–207. DOI: 10.1016/j.addr.2017.11.005.
- (11) Loebel, C.; Rodell, C. B.; Chen, M. H.; Burdick, J. A. Shear-Thinning and Self-Healing Hydrogels as Injectable Therapeutics and for 3D-Printing. *Nat. Protoc.* **2017**, *12* (8), 1521–1541. DOI: 10.1038/nprot.2017.053.

- (12) Criado-Gonzalez, M.; Wagner, D.; Rodon Fores, J.; Blanck, C.; Schmutz, M.; Chaumont, A.; Rabineau, M.; Schlenoff, J. B.; Fleith, G.; Combet, J.; Schaaf, P.; Jierry, L.; Boulmedais, F. Supramolecular Hydrogel Induced by Electrostatic Interactions between Polycation and Phosphorylated-Fmoc-Tripeptide. *Chem. Mater.* **2020**, *32* (5), 1946–1956. DOI: 10.1021/acs.chemmater.9b04823.
- (13) Xing, R.; Li, S.; Zhang, N.; Shen, G.; Möhwald, H.; Yan, X. Self-Assembled Injectable Peptide Hydrogels Capable of Triggering Antitumor Immune Response. *Biomacromolecules* **2017**, *18* (11), 3514–3523. DOI: 10.1021/acs.biomac.7b00787.
- (14) Chen, J.; Peng, Q.; Thundat, T.; Zeng, H. Stretchable, Injectable, and Self-Healing Conductive Hydrogel Enabled by Multiple Hydrogen Bonding toward Wearable Electronics. *Chem. Mater.* **2019**, *31* (12), 4553–4563. DOI: 10.1021/acs.chemmater.9b01239.
- (15) Guzzi, E. A.; Bischof, R.; Dranseikiene, D.; Deshmukh, D. V.; Wahlsten, A.; Bovone, G.; Bernhard, S.; Tibbitt, M. W. Hierarchical Biomaterials via Photopatterning-Enhanced Direct Ink Writing. *Biofabrication* **2021**, *13* (4). DOI: 10.1088/1758-5090/ac212f.
- (16) Roth, G. A.; Gale, E. C.; Alcántara-Hernández, M.; Luo, W.; Axpe, E.; Verma, R.; Yin, Q.; Yu, A. C.; Hernandez, H. L.; Maikawa, C. L.; Smith, A. A. A.; Davis, M. M.; Pulendran, B.; Idoyaga, J.; Appel, E. A. Injectable Hydrogels for Sustained Co-Delivery of Subunit Vaccines Enhance Humoral Immunity. *BioRxiv* **2020**. DOI: 10.1101/2020.05.26.117465.
- (17) Fenton, O. S.; Tibbitt, M. W.; Appel, E. A.; Jhunjhunwala, S.; Webber, M. J.; Langer, R. Injectable Polymer-Nanoparticle Hydrogels for Local Immune Cell Recruitment. *Biomacromolecules* **2019**, *20* (12), 4430–4436. DOI: 10.1021/acs.biomac.9b01129.
- (18) Appel, E. A.; Tibbitt, M. W.; Webber, M. J.; Mattix, B. A.; Veiseh, O.; Langer, R. Self-Assembled Hydrogels Utilizing Polymer-Nanoparticle Interactions. *Nat. Commun.* **2015**, *6*, 6295. DOI: 10.1038/ncomms7295.
- (19) Parisi-Amon, A.; Lo, D. D.; Montoro, D. T.; Dewi, R. E.; Longaker, M. T.; Heilshorn, S. C. Protein-Nanoparticle Hydrogels That Self-Assemble in Response to Peptide-Based Molecular Recognition. *ACS Biomater. Sci. Eng.* **2017**, *3* (5), 750–756. DOI: 10.1021/acsbiomaterials.6b00286.
- (20) Nejadnik, M. R.; Yang, X.; Bongio, M.; Alghamdi, H. S.; van den Beucken, J. J. J. P.; Huysmans, M. C.; Jansen, J. A.; Hilborn, J.; Ossipov, D.; Leeuwenburgh, S. C. G. Self-Healing Hybrid Nanocomposites Consisting of Bisphosphonated Hyaluronan and Calcium Phosphate Nanoparticles. *Biomaterials* **2014**, *35* (25), 6918–6929. DOI: 10.1016/j.biomaterials.2014.05.003.
- (21) Dugger, S. A.; Platt, A.; Goldstein, D. B. Drug Development in the Era of Precision Medicine. *Nat. Rev. Drug Discov.* **2018**, *17* (3), 183–196. DOI: 10.1038/nrd.2017.226.

- (22) Langer, R. Drug Delivery and Targeting. *Nature* **1998**, *392* (6679 Suppl), 5–10.
- (23) Traverso, G.; Langer, R. Perspective: Special Delivery for the Gut. *Nature* **2015**, *519* (7544), S19. DOI: 10.1038/519S19a.
- (24) Liu, Y.-L.; Chen, D.; Shang, P.; Yin, D.-C. A Review of Magnet Systems for Targeted Drug Delivery. *J. Control. Release* **2019**, *302*, 90–104. DOI: 10.1016/j.jconrel.2019.03.031.
- (25) Liu, Q.; Das, M.; Liu, Y.; Huang, L. Targeted Drug Delivery to Melanoma. *Adv. Drug Deliv. Rev.* **2018**, *127*, 208–221. DOI: 10.1016/j.addr.2017.09.016.
- (26) Kumari, P.; Ghosh, B.; Biswas, S. Nanocarriers for Cancer-Targeted Drug Delivery. *J. Drug Target.* **2016**, *24* (3), 179–191. DOI: 10.3109/1061186X.2015.1051049.
- (27) Autio, K. A.; Dreicer, R.; Anderson, J.; Garcia, J. A.; Alva, A.; Hart, L. L.; Milowsky, M. I.; Posadas, E. M.; Ryan, C. J.; Graf, R. P.; Dittamore, R.; Schreiber, N. A.; Summa, J. M.; Youssoufian, H.; Morris, M. J.; Scher, H. I. Safety and Efficacy of BIND-014, a Docetaxel Nanoparticle Targeting Prostate-Specific Membrane Antigen for Patients With Metastatic Castration-Resistant Prostate Cancer: A Phase 2 Clinical Trial. *JAMA Oncol.* **2018**, *4* (10), 1344–1351. DOI: 10.1001/jamaoncol.2018.2168.
- (28) Müller, L. K.; Simon, J.; Schöttler, S.; Landfester, K.; Mailänder, V.; Mohr, K. Pre-Coating with Protein Fractions Inhibits Nano-Carrier Aggregation in Human Blood Plasma. *RSC Adv.* **2016**, *6* (99), 96495–96509. DOI: 10.1039/C6RA17028E.
- (29) Wilhelm, S.; Tavares, A. J.; Dai, Q.; Ohta, S.; Audet, J.; Dvorak, H. F.; Chan, W. C. W. Analysis of Nanoparticle Delivery to Tumours. *Nat. Rev. Mater.* **2016**, *1* (5), 16014. DOI: 10.1038/natrevmats.2016.14.
- (30) Petros, R. A.; DeSimone, J. M. Strategies in the Design of Nanoparticles for Therapeutic Applications. *Nat. Rev. Drug Discov.* **2010**, *9* (8), 615–627. DOI: 10.1038/nrd2591.
- (31) Ilium, L.; Davis, S. S.; Wilson, C. G.; Thomas, N. W.; Frier, M.; Hardy, J. G. Blood Clearance and Organ Deposition of Intravenously Administered Colloidal Particles. The Effects of Particle Size, Nature and Shape. *Int. J. Pharm.* **1982**, *12* (2–3), 135–146. DOI: 10.1016/0378-5173(82)90113-2.
- (32) Thakur, N.; Sharma, B.; Bishnoi, S.; Mishra, S. K.; Nayak, D.; Kumar, A.; Sarma, T. K. Multifunctional Inosine Monophosphate Coordinated Metal–Organic Hydrogel: Multistimuli Responsiveness, Self-Healing Properties, and Separation of Water from Organic Solvents. *ACS Sustain. Chem. Eng.* **2018**, *6* (7), 8659–8671. DOI: 10.1021/acssuschemeng.8b00963.
- (33) Kretlow, J. D.; Klouda, L.; Mikos, A. G. Injectable Matrices and Scaffolds for Drug Delivery in Tissue Engineering. *Adv. Drug Deliv. Rev.* **2007**, *59* (4–5), 263–273. DOI: 10.1016/j.addr.2007.03.013.

- (34) Chen, Q.; Wang, C.; Zhang, X.; Chen, G.; Hu, Q.; Li, H.; Wang, J.; Wen, D.; Zhang, Y.; Lu, Y.; Yang, G.; Jiang, C.; Wang, J.; Dotti, G.; Gu, Z. In Situ Sprayed Bioresponsive Immunotherapeutic Gel for Post-Surgical Cancer Treatment. *Nat. Nanotechnol.* **2019**, *14* (1), 89–97. DOI: 10.1038/s41565-018-0319-4.
- (35) Dimatteo, R.; Darling, N. J.; Segura, T. In Situ Forming Injectable Hydrogels for Drug Delivery and Wound Repair. *Adv. Drug Deliv. Rev.* **2018**, *127*, 167–184. DOI: 10.1016/j.addr.2018.03.007.
- (36) Wichterle, O.; Lím, D. Hydrophilic Gels for Biological Use. *Nature* **1960**, *185* (4706), 117–118. DOI: 10.1038/185117a0.
- (37) Ford, J. L.; Rubinstein, M. H.; Hogan, J. E. Propranolol Hydrochloride and Aminophylline Release from Matrix Tablets Containing Hydroxypropylmethylcellulose. *Int. J. Pharm.* **1985**, *24* (2–3), 339–350. DOI: 10.1016/0378-5173(85)90032-8.
- (38) Korsmeyer, R. W.; Peppas, N. A. Effect of the Morphology of Hydrophilic Polymeric Matrices on the Diffusion and Release of Water Soluble Drugs. *J. Memb. Sci.* **1981**, *9* (3), 211–227. DOI: 10.1016/S0376-7388(00)80265-3.
- (39) Graham, N. B.; Zulfiqar, M.; MacDonald, B. B.; McNeill, M. E. Caffeine Release from Fully Swollen Poly(Ethylene Oxide) Hydrogels. *J. Control. Release* **1987**, *5* (3), 243–252. DOI: 10.1016/0168-3659(88)90023-5.
- (40) Drury, J. L.; Mooney, D. J. Hydrogels for Tissue Engineering: Scaffold Design Variables and Applications. *Biomaterials* **2003**, *24* (24), 4337–4351. DOI: 10.1016/s0142-9612(03)00340-5.
- (41) Mathur, A. M.; Moorjani, S. K.; Scranton, A. B. Methods for Synthesis of Hydrogel Networks: A Review. *Journal of Macromolecular Science, Part C: Polymer Reviews* **1996**, *36* (2), 405–430. DOI: 10.1080/15321799608015226.
- (42) Koshy, S. T.; Ferrante, T. C.; Lewin, S. A.; Mooney, D. J. Injectable, Porous, and Cell-Responsive Gelatin Cryogels. *Biomaterials* **2014**, *35* (8), 2477–2487. DOI: 10.1016/j.biomaterials.2013.11.044.
- (43) Oh, J. K.; Drumright, R.; Siegwart, D. J.; Matyjaszewski, K. The Development of Microgels/Nanogels for Drug Delivery Applications. *Prog. Polym. Sci.* **2008**, *33* (4), 448–477. DOI: 10.1016/j.progpolymsci.2008.01.002.
- (44) Paul, A.; Hasan, A.; Kindi, H. A.; Gaharwar, A. K.; Rao, V. T. S.; Nikkhah, M.; Shin, S. R.; Krafft, D.; Dokmeci, M. R.; Shum-Tim, D.; Khademhosseini, A. Injectable Graphene Oxide/Hydrogel-Based Angiogenic Gene Delivery System for Vasculogenesis and Cardiac Repair. *ACS Nano* **2014**, *8* (8), 8050–8062. DOI: 10.1021/nn5020787.

- (45) Koutsopoulos, S.; Unsworth, L. D.; Nagai, Y.; Zhang, S. Controlled Release of Functional Proteins through Designer Self-Assembling Peptide Nanofiber Hydrogel Scaffold. *Proc Natl Acad Sci USA* **2009**, *106* (12), 4623–4628. DOI: 10.1073/pnas.0807506106.
- (46) Wang, C.; Wang, J.; Zhang, X.; Yu, S.; Wen, D.; Hu, Q.; Ye, Y.; Bomba, H.; Hu, X.; Liu, Z.; Dotti, G.; Gu, Z. In Situ Formed Reactive Oxygen Species-Responsive Scaffold with Gemcitabine and Checkpoint Inhibitor for Combination Therapy. *Sci. Transl. Med.* **2018**, *10* (429). DOI: 10.1126/scitranslmed.aan3682.
- (47) Liu, M.; Zeng, X.; Ma, C.; Yi, H.; Ali, Z.; Mou, X.; Li, S.; Deng, Y.; He, N. Injectable Hydrogels for Cartilage and Bone Tissue Engineering. *Bone Res.* **2017**, *5*, 17014. DOI: 10.1038/boneres.2017.14.
- (48) Johnson, T. D.; Christman, K. L. Injectable Hydrogel Therapies and Their Delivery Strategies for Treating Myocardial Infarction. *Expert Opin. Drug Deliv.* **2013**, *10* (1), 59–72. DOI: 10.1517/17425247.2013.739156.
- (49) Lehn, J.-M. Supramolecular Chemistry—Scope and Perspectives Molecules, Supermolecules, and Molecular Devices(Nobel Lecture). *Angew. Chem. Int. Ed. Engl.* **1988**, *27* (1), 89–112. DOI: 10.1002/anie.198800891.
- (50) Pedersen, C. J. The Discovery of Crown Ethers (Noble Lecture). *Angew. Chem. Int. Ed* **1988**, *27* (8), 1021–1027. DOI: 10.1002/anie.198810211.
- (51) Cram, D. J. The Design of Molecular Hosts, Guests, and Their Complexes (Nobel Lecture). *Angew. Chem. Int. Ed* **1988**, *27* (8), 1009–1020. DOI: 10.1002/anie.198810093.
- (52) Webber, M. J.; Appel, E. A.; Meijer, E. W.; Langer, R. Supramolecular Biomaterials. *Nat. Mater.* **2016**, *15* (1), 13–26. DOI: 10.1038/nmat4474.
- (53) Mura, S.; Nicolas, J.; Couvreur, P. Stimuli-Responsive Nanocarriers for Drug Delivery. *Nat. Mater.* **2013**, *12* (11), 991–1003. DOI: 10.1038/nmat3776.
- (54) Li, J.; Mooney, D. J. Designing Hydrogels for Controlled Drug Delivery. *Nat. Rev. Mater.* **2016**, *1* (12). DOI: 10.1038/natrevmats.2016.71.
- (55) Anderson, J. M.; Rodriguez, A.; Chang, D. T. Foreign Body Reaction to Biomaterials. *Semin. Immunol.* **2008**, *20* (2), 86–100. DOI: 10.1016/j.smim.2007.11.004.
- (56) Stella, V. J.; Rao, V. M.; Zannou, E. A.; Zia, V. Mechanisms of Drug Release from Cyclodextrin Complexes. *Adv. Drug Deliv. Rev.* **1999**, *36* (1), 3–16. DOI: 10.1016/s0169-409x(98)00052-0.
- (57) Li, J.; Ji, C.; Yu, X.; Yin, M.; Kuckling, D. Dually Cross-Linked Supramolecular Hydrogel as Surface Plasmon Resonance Sensor for Small Molecule Detection. *Macromol. Rapid Commun.* **2019**, *40* (14), e1900189. DOI: 10.1002/marc.201900189.

- (58) Guvendiren, M.; Lu, H. D.; Burdick, J. A. Shear-Thinning Hydrogels for Biomedical Applications. *Soft Matter* **2012**, *8* (2), 260–272. DOI: 10.1039/C1SM06513K.
- (59) Hou, S.; Wang, X.; Park, S.; Jin, X.; Ma, P. X. Rapid Self-Integrating, Injectable Hydrogel for Tissue Complex Regeneration. *Adv. Healthc. Mater.* **2015**, *4* (10), 1491–1495, 1423. DOI: 10.1002/adhm.201500093.
- (60) van Dijk-Wolthuis, W. N. E.; Hoogeboom, J. A. M.; van Steenbergen, M. J.; Tsang, S. K. Y.; Hennink, W. E. Degradation and Release Behavior of Dextran-Based Hydrogels. *Macromolecules* **1997**, *30* (16), 4639–4645. DOI: 10.1021/ma9704018.
- (61) Chen, Y.; Pang, X.-H.; Dong, C.-M. Dual Stimuli-Responsive Supramolecular Polypeptide-Based Hydrogel and Reverse Micellar Hydrogel Mediated by Host-Guest Chemistry. *Adv. Funct. Mater.* **2010**, *20* (4), 579–586. DOI: 10.1002/adfm.200901400.
- (62) Xu, D.; Hawk, J. L.; Loveless, D. M.; Jeon, S. L.; Craig, S. L. Mechanism of Shear Thickening in Reversibly Cross-Linked Supramolecular Polymer Networks. *Macromolecules* **2010**, *43* (7), 3556–3565. DOI: 10.1021/ma100093b.
- (63) Xu, D.; Liu, C.-Y.; Craig, S. L. Divergent Shear Thinning and Shear Thickening Behavior of Supramolecular Polymer Networks in Semidilute Entangled Polymer Solutions. *Macromolecules* **2011**, *44* (7), 2343–2353. DOI: 10.1021/ma2000916.
- (64) Seiffert, S.; Sprakel, J. Physical Chemistry of Supramolecular Polymer Networks. *Chem. Soc. Rev.* **2012**, *41* (2), 909–930. DOI: 10.1039/c1cs15191f.
- (65) Marco-Dufort, B.; Iten, R.; Tibbitt, M. W. Linking Molecular Behavior to Macroscopic Properties in Ideal Dynamic Covalent Networks. *J. Am. Chem. Soc.* **2020**, *142* (36), 15371–15385. DOI: 10.1021/jacs.0c06192.
- (66) Rodell, C. B.; Kaminski, A. L.; Burdick, J. A. Rational Design of Network Properties in Guest-Host Assembled and Shear-Thinning Hyaluronic Acid Hydrogels. *Biomacromolecules* **2013**, *14* (11), 4125–4134. DOI: 10.1021/bm401280z.
- (67) Qin, L.; Duan, P.; Xie, F.; Zhang, L.; Liu, M. A Metal Ion Triggered Shrinkable Supramolecular Hydrogel and Controlled Release by an Amphiphilic Peptide Dendron. *Chem. Commun.* **2013**, *49* (92), 10823–10825. DOI: 10.1039/c3cc47004k.
- (68) Ritger, P. L.; Peppas, N. A. A Simple Equation for Description of Solute Release I. Fickian and Non-Fickian Release from Non-Swellable Devices in the Form of Slabs, Spheres, Cylinders or Discs. *J. Control. Release* **1987**, *5* (1), 23–36. DOI: 10.1016/0168-3659(87)90034-4.
- (69) Amsden, B. Solute Diffusion within Hydrogels. Mechanisms and Models. *Macromolecules* **1998**, *31* (23), 8382–8395. DOI: 10.1021/ma980765f.

- (70) Axpe, E.; Chan, D.; Offeddu, G. S.; Chang, Y.; Merida, D.; Hernandez, H. L.; Appel, E. A. A Multiscale Model for Solute Diffusion in Hydrogels. *Macromolecules* **2019**, *52* (18), 6889–6897. DOI: 10.1021/acs.macromol.9b00753.
- (71) Marco-Dufort, B.; Willi, J.; Vielba-Gomez, F.; Gatti, F.; Tibbitt, M. W. Environment Controls Biomolecule Release from Dynamic Covalent Hydrogels. *Biomacromolecules* **2021**, *22* (1), 146–157. DOI: 10.1021/acs.biomac.0c00895.
- (72) Appel, E. A.; Forster, R. A.; Rowland, M. J.; Scherman, O. A. The Control of Cargo Release from Physically Crosslinked Hydrogels by Crosslink Dynamics. *Biomaterials* **2014**, *35* (37), 9897–9903. DOI: 10.1016/j.biomaterials.2014.08.001.
- (73) Dankers, P. Y. W.; Hermans, T. M.; Baughman, T. W.; Kamikawa, Y.; Kieltyka, R. E.; Bastings, M. M. C.; Janssen, H. M.; Sommerdijk, N. A. J. M.; Larsen, A.; van Luyn, M. J. A.; Bosman, A. W.; Popa, E. R.; Fytas, G.; Meijer, E. W. Hierarchical Formation of Supramolecular Transient Networks in Water: A Modular Injectable Delivery System. *Adv. Mater.* **2012**, *24* (20), 2703–2709. DOI: 10.1002/adma.201104072.
- (74) Rahim, M. A.; Björnmalm, M.; Suma, T.; Faria, M.; Ju, Y.; Kempe, K.; Müllner, M.; Ejima, H.; Stickland, A. D.; Caruso, F. Metal-Phenolic Supramolecular Gelation. *Angew. Chem. Int. Ed* **2016**, *55* (44), 13803–13807. DOI: 10.1002/anie.201608413.
- (75) Nalbandian, R. M.; Henry, R. L.; Wilks, H. S. Artificial Skin. II. Pluronic F-127 Silver Nitrate or Silver Lactate Gel in the Treatment of Thermal Burns. *J. Biomed. Mater. Res.* **1972**, *6* (6), 583–590. DOI: 10.1002/jbm.820060610.
- (76) Zhang, L.; Wang, L.; Guo, B.; Ma, P. X. Cytocompatible Injectable Carboxymethyl Chitosan/N-Isopropylacrylamide Hydrogels for Localized Drug Delivery. *Carbohydr. Polym.* **2014**, *103*, 110–118. DOI: 10.1016/j.carbpol.2013.12.017.
- (77) Jung, Y.-S.; Park, W.; Park, H.; Lee, D.-K.; Na, K. Thermo-Sensitive Injectable Hydrogel Based on the Physical Mixing of Hyaluronic Acid and Pluronic F-127 for Sustained NSAID Delivery. *Carbohydr. Polym.* **2017**, *156*, 403–408. DOI: 10.1016/j.carbpol.2016.08.068.
- (78) Zhang, G.; Chen, Y.; Deng, Y.; Ngai, T.; Wang, C. Dynamic Supramolecular Hydrogels: Regulating Hydrogel Properties through Self-Complementary Quadruple Hydrogen Bonds and Thermo-Switch. *ACS Macro Lett.* **2017**, *6* (7), 641–646. DOI: 10.1021/acsmacrolett.7b00275.
- (79) Li, J.; Li, X.; Ni, X.; Wang, X.; Li, H.; Leong, K. W. Self-Assembled Supramolecular Hydrogels Formed by Biodegradable PEO-PHB-PEO Triblock Copolymers and Alpha-Cyclodextrin for Controlled Drug Delivery. *Biomaterials* **2006**, *27* (22), 4132–4140. DOI: 10.1016/j.biomaterials.2006.03.025.

- (80) Dong, H.; Hua, W.; Li, S. Estimation on the Individual Hydrogen-Bond Strength in Molecules with Multiple Hydrogen Bonds. *J. Phys. Chem. A* **2007**, *111* (15), 2941–2945. DOI: 10.1021/jp0709860.
- (81) Yang, S. K.; Zimmerman, S. C. Hydrogen Bonding Modules for Use in Supramolecular Polymers. *Isr. J. Chem.* **2013**, *53* (8), 511–520. DOI: 10.1002/ijch.201300045.
- (82) Brunsveld, L.; Folmer, B. J.; Meijer, E. W.; Sijbesma, R. P. Supramolecular Polymers. *Chem. Rev.* **2001**, *101* (12), 4071–4098. DOI: 10.1021/cr990125q.
- (83) Folmer, B. J. B.; Sijbesma, R. P.; Versteegen, R. M.; van der Rijt, J. A. J.; Meijer, E. W. Supramolecular Polymer Materials: Chain Extension of Telechelic Polymers Using a Reactive Hydrogen-Bonding Synthone. *Adv. Mater.* **2000**, *12* (12), 874–878. DOI: 10.1002/1521-4095(200006)12:12<874::AID-ADMA874>3.0.CO;2-C.
- (84) Hirschberg, J. H.; Brunsveld, L.; Ramzi, A.; Vekemans, J. A.; Sijbesma, R. P.; Meijer, E. W. Helical Self-Assembled Polymers from Cooperative Stacking of Hydrogen-Bonded Pairs. *Nature* **2000**, *407* (6801), 167–170. DOI: 10.1038/35025027.
- (85) Guo, M.; Pitet, L. M.; Wyss, H. M.; Vos, M.; Dankers, P. Y. W.; Meijer, E. W. Tough Stimuli-Responsive Supramolecular Hydrogels with Hydrogen-Bonding Network Junctions. *J. Am. Chem. Soc.* **2014**, *136* (19), 6969–6977. DOI: 10.1021/ja500205v.
- (86) Mo, F.; Jiang, K.; Zhao, D.; Wang, Y.; Song, J.; Tan, W. DNA Hydrogel-Based Gene Editing and Drug Delivery Systems. *Adv. Drug Deliv. Rev.* **2021**, *168*, 79–98. DOI: 10.1016/j.addr.2020.07.018.
- (87) Grindy, S. C.; Learsch, R.; Mozhdghi, D.; Cheng, J.; Barrett, D. G.; Guan, Z.; Messersmith, P. B.; Holten-Andersen, N. Control of Hierarchical Polymer Mechanics with Bioinspired Metal-Coordination Dynamics. *Nat. Mater.* **2015**, *14* (12), 1210–1216. DOI: 10.1038/nmat4401.
- (88) Holten-Andersen, N.; Harrington, M. J.; Birkedal, H.; Lee, B. P.; Messersmith, P. B.; Lee, K. Y. C.; Waite, J. H. PH-Induced Metal-Ligand Cross-Links Inspired by Mussel Yield Self-Healing Polymer Networks with near-Covalent Elastic Moduli. *Proc Natl Acad Sci USA* **2011**, *108* (7), 2651–2655. DOI: 10.1073/pnas.1015862108.
- (89) Xu, X.; Jerca, V. V.; Hoogenboom, R. Self-Healing Metallo-Supramolecular Hydrogel Based on Specific Ni²⁺ Coordination Interactions of Poly(Ethylene Glycol) with Bistriazole Pyridine Ligands in the Main Chain. *Macromol. Rapid Commun.* **2020**, *41* (4), e1900457. DOI: 10.1002/marc.201900457.
- (90) Shi, L.; Carstensen, H.; Hölzl, K.; Lunzer, M.; Li, H.; Hilborn, J.; Ovsianikov, A.; Ossipov, D. A. Dynamic Coordination Chemistry Enables Free Directional Printing of Biopolymer Hydrogel. *Chem. Mater.* **2017**, *29* (14), 5816–5823. DOI: 10.1021/acs.chemmater.7b00128.
- (91) Lopez-Perez, P. M.; da Silva, R. M. P.; Strehin, I.; Kouwer, P. H. J.; Leeuwenburgh, S. C. G.; Messersmith, P. B. Self-Healing Hydrogels Formed by Complexation between Calcium Ions and

Bisphosphonate-Functionalized Star-Shaped Polymers. *Macromolecules* **2017**, *50* (21), 8698–8706. DOI: 10.1021/acs.macromol.7b01417.

(92) Tang, Q.; Zhao, D.; Zhou, Q.; Yang, H.; Peng, K.; Zhang, X. Polyhistidine-Based Metal Coordination Hydrogels with Physiologically Relevant PH Responsiveness and Enhanced Stability through a Novel Synthesis. *Macromol. Rapid Commun.* **2018**, *39* (11), e1800109. DOI: 10.1002/marc.201800109.

(93) Tang, Q.; Zhao, D.; Yang, H.; Wang, L.; Zhang, X. A PH-Responsive Self-Healing Hydrogel Based on Multivalent Coordination of Ni²⁺ with Polyhistidine-Terminated PEG and IDA-Modified Oligochitosan. *J. Mater. Chem. B Mater. Biol. Med.* **2019**, *7* (1), 30–42. DOI: 10.1039/c8tb02360c.

(94) Björnmalm, M.; Wong, L. M.; Wojciechowski, J. P.; Penders, J.; Horgan, C. C.; Booth, M. A.; Martin, N. G.; Sattler, S.; Stevens, M. M. In Vivo Biocompatibility and Immunogenicity of Metal-Phenolic Gelation. *Chem. Sci.* **2019**, *10* (43), 10179–10194. DOI: 10.1039/C9SC03325D.

(95) Zhang, G.; Lv, L.; Deng, Y.; Wang, C. Self-Healing Gelatin Hydrogels Cross-Linked by Combining Multiple Hydrogen Bonding and Ionic Coordination. *Macromol. Rapid Commun.* **2017**, *38* (12). DOI: 10.1002/marc.201700018.

(96) Biros, S. M.; Rebek, J. Structure and Binding Properties of Water-Soluble Cavitands and Capsules. *Chem. Soc. Rev.* **2007**, *36* (1), 93–104. DOI: 10.1039/b508530f.

(97) Rodell, C. B.; Mealy, J. E.; Burdick, J. A. Supramolecular Guest-Host Interactions for the Preparation of Biomedical Materials. *Bioconjug. Chem.* **2015**, *26* (12), 2279–2289. DOI: 10.1021/acs.bioconjchem.5b00483.

(98) Lagona, J.; Mukhopadhyay, P.; Chakrabarti, S.; Isaacs, L. The Cucurbit[n]Uril Family. *Angew. Chem. Int. Ed* **2005**, *44* (31), 4844–4870. DOI: 10.1002/anie.200460675.

(99) Appel, E. A.; del Barrio, J.; Loh, X. J.; Scherman, O. A. Supramolecular Polymeric Hydrogels. *Chem. Soc. Rev.* **2012**, *41* (18), 6195–6214. DOI: 10.1039/c2cs35264h.

(100) Eastburn, S. D.; Tao, B. Y. Applications of Modified Cyclodextrins. *Biotechnol. Adv.* **1994**, *12* (2), 325–339. DOI: 10.1016/0734-9750(94)90015-9.

(101) Loftsson, T.; Duchêne, D. Cyclodextrins and Their Pharmaceutical Applications. *Int. J. Pharm.* **2007**, *329* (1–2), 1–11. DOI: 10.1016/j.ijpharm.2006.10.044.

(102) Villiers, A. Sur La Fermentation de La Féculé Par l'action Du Ferment Butyrique. *Compt. Rend. Acad. Sci* **1891**, *112*, 536–538.

(103) Del Valle, E. M. M. Cyclodextrins and Their Uses: A Review. *Process Biochemistry* **2004**, *39* (9), 1033–1046. DOI: 10.1016/S0032-9592(03)00258-9.

- (104) Rekharsky, M. V.; Inoue, Y. Complexation Thermodynamics of Cyclodextrins. *Chem. Rev.* **1998**, *98* (5), 1875–1918. DOI: 10.1021/cr970015o.
- (105) Harada, A.; Li, J.; Kamachi, M. Double-Stranded Inclusion Complexes of Cyclodextrin Threaded on Poly(Ethylene Glycol). *Nature* **1994**, *370* (6485), 126–128. DOI: 10.1038/370126a0.
- (106) Harada, A.; Li, J.; Kamachi, M. The Molecular Necklace: A Rotaxane Containing Many Threaded α -Cyclodextrins. *Nature* **1992**, *356* (6367), 325–327. DOI: 10.1038/356325a0.
- (107) Nakahata, M.; Takashima, Y.; Yamaguchi, H.; Harada, A. Redox-Responsive Self-Healing Materials Formed from Host-Guest Polymers. *Nat. Commun.* **2011**, *2*, 511. DOI: 10.1038/ncomms1521.
- (108) Rosales, A. M.; Rodell, C. B.; Chen, M. H.; Morrow, M. G.; Anseth, K. S.; Burdick, J. A. Reversible Control of Network Properties in Azobenzene-Containing Hyaluronic Acid-Based Hydrogels. *Bioconjug. Chem.* **2018**, *29* (4), 905–913. DOI: 10.1021/acs.bioconjchem.7b00802.
- (109) Wang, M.; Zhang, X.; Li, L.; Wang, J.; Wang, J.; Ma, J.; Yuan, Z.; Lincoln, S. F.; Guo, X. Photo-Reversible Supramolecular Hydrogels Assembled by α -Cyclodextrin and Azobenzene Substituted Poly(Acrylic Acid)s: Effect of Substitution Degree, Concentration, and Tethered Chain Length. *Macromol. Mater. Eng.* **2016**, *301* (2), 191–198. DOI: 10.1002/mame.201500295.
- (110) Jia, Y.-G.; Zhu, X. X. Self-Healing Supramolecular Hydrogel Made of Polymers Bearing Cholic Acid and β -Cyclodextrin Pendants. *Chem. Mater.* **2015**, *27* (1), 387–393. DOI: 10.1021/cm5041584.
- (111) Mealy, J. E.; Rodell, C. B.; Burdick, J. A. Sustained Small Molecule Delivery from Injectable Hyaluronic Acid Hydrogels through Host-Guest Mediated Retention. *J. Mater. Chem. B Mater. Biol. Med.* **2015**, *3* (40), 8010–8019. DOI: 10.1039/C5TB00981B.
- (112) Rodell, C. B.; Wade, R. J.; Purcell, B. P.; Dusaj, N. N.; Burdick, J. A. Selective Proteolytic Degradation of Guest-Host Assembled, Injectable Hyaluronic Acid Hydrogels. *ACS Biomater. Sci. Eng.* **2015**, *1* (4), 277–286. DOI: 10.1021/ab5001673.
- (113) Wang, L. L.; Liu, Y.; Chung, J. J.; Wang, T.; Gaffey, A. C.; Lu, M.; Cavanaugh, C. A.; Zhou, S.; Kanade, R.; Atluri, P.; Morrissey, E. E.; Burdick, J. A. Local and Sustained miRNA Delivery from an Injectable Hydrogel Promotes Cardiomyocyte Proliferation and Functional Regeneration after Ischemic Injury. *Nat. Biomed. Eng.* **2017**, *1*, 983–992. DOI: 10.1038/s41551-017-0157-y.
- (114) Gaffey, A. C.; Chen, M. H.; Venkataraman, C. M.; Trubelja, A.; Rodell, C. B.; Dinh, P. V.; Hung, G.; MacArthur, J. W.; Soopan, R. V.; Burdick, J. A.; Atluri, P. Injectable Shear-Thinning Hydrogels Used to Deliver Endothelial Progenitor Cells, Enhance Cell Engraftment, and Improve Ischemic Myocardium. *J. Thorac. Cardiovasc. Surg.* **2015**, *150* (5), 1268–1276. DOI: 10.1016/j.jtcvs.2015.07.035.

- (115) Wang, L. L.; Sloand, J. N.; Gaffey, A. C.; Venkataraman, C. M.; Wang, Z.; Trubelja, A.; Hammer, D. A.; Atluri, P.; Burdick, J. A. Injectable, Guest-Host Assembled Polyethylenimine Hydrogel for siRNA Delivery. *Biomacromolecules* **2017**, *18* (1), 77–86. DOI: 10.1021/acs.biomac.6b01378.
- (116) Aramoto, H.; Osaki, M.; Konishi, S.; Ueda, C.; Kobayashi, Y.; Takashima, Y.; Harada, A.; Yamaguchi, H. Redox-Responsive Supramolecular Polymeric Networks Having Double-Threaded Inclusion Complexes. *Chem. Sci.* **2020**, *11* (17), 4322–4331. DOI: 10.1039/c9sc05589d.
- (117) Lee, H. J.; Le, P. T.; Kwon, H. J.; Park, K. D. Supramolecular Assembly of Tetrionic–Adamantane and Poly(β -Cyclodextrin) as Injectable Shear-Thinning Hydrogels. *J. Mater. Chem. B* **2019**, *7* (21), 3374–3382. DOI: 10.1039/C9TB00072K.
- (118) Zhao, W.; Li, Y.; Zhang, X.; Zhang, R.; Hu, Y.; Boyer, C.; Xu, F.-J. Photo-Responsive Supramolecular Hyaluronic Acid Hydrogels for Accelerated Wound Healing. *J. Control. Release* **2020**, *323*, 24–35. DOI: 10.1016/j.jconrel.2020.04.014.
- (119) Mandl, G. A.; Rojas-Gutierrez, P. A.; Capobianco, J. A. A NIR-Responsive Azobenzene-Based Supramolecular Hydrogel Using Upconverting Nanoparticles. *Chem. Commun.* **2018**, *54* (46), 5847–5850. DOI: 10.1039/c8cc03101k.
- (120) Zhang, B.; He, J.; Shi, M.; Liang, Y.; Guo, B. Injectable Self-Healing Supramolecular Hydrogels with Conductivity and Photo-Thermal Antibacterial Activity to Enhance Complete Skin Regeneration. *Chemical Engineering Journal* **2020**, *400*, 125994. DOI: 10.1016/j.cej.2020.125994.
- (121) Li, J.; Harada, A.; Kamachi, M. Sol–Gel Transition during Inclusion Complex Formation between α -Cyclodextrin and High Molecular Weight Poly(Ethylene Glycol)s in Aqueous Solution. *Polym. J.* **1994**, *26* (9), 1019–1026. DOI: 10.1295/polymj.26.1019.
- (122) Liu, Z.; Yao, P. Versatile Injectable Supramolecular Hydrogels Containing Drug Loaded Micelles for Delivery of Various Drugs. *Polym. Chem.* **2014**, *5* (3), 1072–1081. DOI: 10.1039/C3PY01083J.
- (123) Zhang, Z.; He, Z.; Liang, R.; Ma, Y.; Huang, W.; Jiang, R.; Shi, S.; Chen, H.; Li, X. Fabrication of a Micellar Supramolecular Hydrogel for Ocular Drug Delivery. *Biomacromolecules* **2016**, *17* (3), 798–807. DOI: 10.1021/acs.biomac.5b01526.
- (124) Yu, J.; Ha, W.; Sun, J.; Shi, Y. Supramolecular Hybrid Hydrogel Based on Host-Guest Interaction and Its Application in Drug Delivery. *ACS Appl. Mater. Interfaces* **2014**, *6* (22), 19544–19551. DOI: 10.1021/am505649q.
- (125) Lin, Q.; Yang, Y.; Hu, Q.; Guo, Z.; Liu, T.; Xu, J.; Wu, J.; Kirk, T. B.; Ma, D.; Xue, W. Injectable Supramolecular Hydrogel Formed from α -Cyclodextrin and PEGylated Arginine-Functionalized Poly(l-

Lysine) Dendron for Sustained MMP-9 ShRNA Plasmid Delivery. *Acta Biomater.* **2017**, *49*, 456–471. DOI: 10.1016/j.actbio.2016.11.062.

(126) Song, X.; Zhang, Z.; Zhu, J.; Wen, Y.; Zhao, F.; Lei, L.; Phan-Thien, N.; Khoo, B. C.; Li, J. Thermoresponsive Hydrogel Induced by Dual Supramolecular Assemblies and Its Controlled Release Property for Enhanced Anticancer Drug Delivery. *Biomacromolecules* **2020**, *21* (4), 1516–1527. DOI: 10.1021/acs.biomac.0c00077.

(127) Freeman, W. A.; Mock, W. L.; Shih, N. Y. Cucurbituril. *J. Am. Chem. Soc.* **1981**, *103* (24), 7367–7368. DOI: 10.1021/ja00414a070.

(128) Assaf, K. I.; Nau, W. M. Cucurbiturils: From Synthesis to High-Affinity Binding and Catalysis. *Chem. Soc. Rev.* **2015**, *44* (2), 394–418. DOI: 10.1039/c4cs00273c.

(129) Appel, E. A.; Loh, X. J.; Jones, S. T.; Dreiss, C. A.; Scherman, O. A. Sustained Release of Proteins from High Water Content Supramolecular Polymer Hydrogels. *Biomaterials* **2012**, *33* (18), 4646–4652. DOI: 10.1016/j.biomaterials.2012.02.030.

(130) Tabet, A.; Forster, R. A.; Parkins, C. C.; Wu, G.; Scherman, O. A. Modulating Stiffness with Photo-Switchable Supramolecular Hydrogels. *Polym. Chem.* **2019**, *10* (4), 467–472. DOI: 10.1039/C8PY01554F.

(131) Zou, L.; Braegelman, A. S.; Webber, M. J. Dynamic Supramolecular Hydrogels Spanning an Unprecedented Range of Host-Guest Affinity. *ACS Appl. Mater. Interfaces* **2019**, *11* (6), 5695–5700. DOI: 10.1021/acsami.8b22151.

(132) Gaharwar, A. K.; Peppas, N. A.; Khademhosseini, A. Nanocomposite Hydrogels for Biomedical Applications. *Biotechnol. Bioeng.* **2014**, *111* (3), 441–453. DOI: 10.1002/bit.25160.

(133) Bernhard, S.; Bovone, G.; Guzzi, E. A.; Tibbitt, M. W. Polymer-Nanoparticle Hydrogels. *Chimia (Aarau)* **2019**, *73* (12), 1034. DOI: 10.2533/chimia.2019.1034.

(134) Nelson, A.; Cosgrove, T. Dynamic Light Scattering Studies of Poly(Ethylene Oxide) Adsorbed on Laponite: Layer Conformation and Its Effect on Particle Stability. *Langmuir* **2004**, *20* (24), 10382–10388. DOI: 10.1021/la049323p.

(135) Li, C.; Mu, C.; Lin, W.; Ngai, T. Gelatin Effects on the Physicochemical and Hemocompatible Properties of Gelatin/Paam/Laponite Nanocomposite Hydrogels. *ACS Appl. Mater. Interfaces* **2015**, *7* (33), 18732–18741. DOI: 10.1021/acsami.5b05287.

(136) Alarçin, E.; Lee, T. Y.; Karuthedom, S.; Mohammadi, M.; Brennan, M. A.; Lee, D. H.; Marrella, A.; Zhang, J.; Syla, D.; Zhang, Y. S.; Khademhosseini, A.; Jang, H. L. Injectable Shear-Thinning Hydrogels for Delivering Osteogenic and Angiogenic Cells and Growth Factors. *Biomater. Sci.* **2018**, *6* (6), 1604–1615. DOI: 10.1039/c8bm00293b.

- (137) Gaharwar, A. K.; Avery, R. K.; Assmann, A.; Paul, A.; McKinley, G. H.; Khademhosseini, A.; Olsen, B. D. Shear-Thinning Nanocomposite Hydrogels for the Treatment of Hemorrhage. *ACS Nano* **2014**, *8* (10), 9833–9842. DOI: 10.1021/nn503719n.
- (138) Gaharwar, A. K.; Mihaila, S. M.; Swami, A.; Patel, A.; Sant, S.; Reis, R. L.; Marques, A. P.; Gomes, M. E.; Khademhosseini, A. Bioactive Silicate Nanoplatelets for Osteogenic Differentiation of Human Mesenchymal Stem Cells. *Adv. Mater.* **2013**, *25* (24), 3329–3336. DOI: 10.1002/adma.201300584.
- (139) Okesola, B. O.; Ni, S.; Derkus, B.; Galeano, C. C.; Hasan, A.; Wu, Y.; Ramis, J.; Buttery, L.; Dawson, J. I.; D’Este, M.; Oreffo, R. O. C.; Eglin, D.; Sun, H.; Mata, A. Growth-factor Free Multicomponent Nanocomposite Hydrogels That Stimulate Bone Formation. *Adv. Funct. Mater.* **2020**, *30* (14), 1906205. DOI: 10.1002/adfm.201906205.
- (140) Gaharwar, A. K.; Kishore, V.; Rivera, C.; Bullock, W.; Wu, C.-J.; Akkus, O.; Schmidt, G. Physically Crosslinked Nanocomposites from Silicate-Crosslinked PEO: Mechanical Properties and Osteogenic Differentiation of Human Mesenchymal Stem Cells. *Macromol. Biosci.* **2012**, *12* (6), 779–793. DOI: 10.1002/mabi.201100508.
- (141) Sheikhi, A.; Afewerki, S.; Oklu, R.; Gaharwar, A. K.; Khademhosseini, A. Effect of Ionic Strength on Shear-Thinning Nanoclay-Polymer Composite Hydrogels. *Biomater. Sci.* **2018**, *6* (8), 2073–2083. DOI: 10.1039/c8bm00469b.
- (142) Yu, A. C.; Smith, A. A. A.; Appel, E. A. Structural Considerations for Physical Hydrogels Based on Polymer–Nanoparticle Interactions. *Mol. Syst. Des. Eng.* **2020**, *5* (1), 401–407. DOI: 10.1039/C9ME00120D.
- (143) Guzzi, E. A.; Bovone, G.; Tibbitt, M. W. Universal Nanocarrier Ink Platform for Biomaterials Additive Manufacturing. *Small* **2019**, *15* (51), e1905421. DOI: 10.1002/smll.201905421.
- (144) Appel, E. A.; Tibbitt, M. W.; Greer, J. M.; Fenton, O. S.; Kreuels, K.; Anderson, D. G.; Langer, R. Exploiting Electrostatic Interactions in Polymer–Nanoparticle Hydrogels. *ACS Macro Lett.* **2015**, *4* (8), 848–852. DOI: 10.1021/acsmacrolett.5b00416.
- (145) Steele, A. N.; Paulsen, M. J.; Wang, H.; Stapleton, L. M.; Lucian, H. J.; Eskandari, A.; Hironaka, C. E.; Farry, J. M.; Baker, S. W.; Thakore, A. D.; Jaatinen, K. J.; Tada, Y.; Hollander, M. J.; Williams, K. M.; Seymour, A. J.; Tothorow, K. P.; Yu, A. C.; Cochran, J. R.; Appel, E. A.; Woo, Y. J. Multi-Phase Catheter-Injectable Hydrogel Enables Dual-Stage Protein-Engineered Cytokine Release to Mitigate Adverse Left Ventricular Remodeling Following Myocardial Infarction in a Small Animal Model and a Large Animal Model. *Cytokine* **2020**, *127*, 154974. DOI: 10.1016/j.cyto.2019.154974.
- (146) Bovone, G.; Guzzi, E. A.; Tibbitt, M. W. Flow-based Reactor Design for the Continuous Production of Polymeric Nanoparticles. *AIChE J.* **2019**. DOI: 10.1002/aic.16840.

- (147) Bovone, G.; Steiner, F.; Guzzi, E. A.; Tibbitt, M. W. Automated and Continuous Production of Polymeric Nanoparticles. *Front. Bioeng. Biotechnol.* **2019**, *7*, 423. DOI: 10.3389/fbioe.2019.00423.
- (148) Shi, L.; Han, Y.; Hilborn, J.; Ossipov, D. “Smart” Drug Loaded Nanoparticle Delivery from a Self-Healing Hydrogel Enabled by Dynamic Magnesium-Biopolymer Chemistry. *Chem. Commun.* **2016**, *52* (74), 11151–11154. DOI: 10.1039/c6cc05565f.
- (149) Wang, Q.; Wang, L.; Detamore, M. S.; Berklund, C. Biodegradable Colloidal Gels as Moldable Tissue Engineering Scaffolds. *Adv. Mater.* **2008**, *20* (2), 236–239. DOI: 10.1002/adma.200702099.
- (150) Wang, Q.; Wang, J.; Lu, Q.; Detamore, M. S.; Berklund, C. Injectable PLGA Based Colloidal Gels for Zero-Order Dexamethasone Release in Cranial Defects. *Biomaterials* **2010**, *31* (18), 4980–4986. DOI: 10.1016/j.biomaterials.2010.02.052.
- (151) Gu, Z.; Aimetti, A. A.; Wang, Q.; Dang, T. T.; Zhang, Y.; Veisoh, O.; Cheng, H.; Langer, R. S.; Anderson, D. G. Injectable Nano-Network for Glucose-Mediated Insulin Delivery. *ACS Nano* **2013**, *7* (5), 4194–4201. DOI: 10.1021/nn400630x.
- (152) Habibi, N.; Kamaly, N.; Memic, A.; Shafiee, H. Self-Assembled Peptide-Based Nanostructures: Smart Nanomaterials toward Targeted Drug Delivery. *Nano Today* **2016**, *11* (1), 41–60. DOI: 10.1016/j.nantod.2016.02.004.
- (153) Abbas, M.; Xing, R.; Zhang, N.; Zou, Q.; Yan, X. Antitumor Photodynamic Therapy Based on Dipeptide Fibrous Hydrogels with Incorporation of Photosensitive Drugs. *ACS Biomater. Sci. Eng.* **2018**, *4* (6), 2046–2052. DOI: 10.1021/acsbomaterials.7b00624.
- (154) Loo, Y.; Zhang, S.; Hauser, C. A. E. From Short Peptides to Nanofibers to Macromolecular Assemblies in Biomedicine. *Biotechnol. Adv.* **2012**, *30* (3), 593–603. DOI: 10.1016/j.biotechadv.2011.10.004.
- (155) Gavel, P. K.; Dev, D.; Parmar, H. S.; Bhasin, S.; Das, A. K. Investigations of Peptide-Based Biocompatible Injectable Shape-Memory Hydrogels: Differential Biological Effects on Bacterial and Human Blood Cells. *ACS Appl. Mater. Interfaces* **2018**, *10* (13), 10729–10740. DOI: 10.1021/acsmi.8b00501.
- (156) Tao, M.; Liu, J.; He, S.; Xu, K.; Zhong, W. In Situ Hydrogelation of Forky Peptides in Prostate Tissue for Drug Delivery. *Soft Matter* **2019**, *15* (20), 4200–4207. DOI: 10.1039/c9sm00196d.
- (157) Lin, B. F.; Megley, K. A.; Viswanathan, N.; Krogstad, D. V.; Drews, L. B.; Kade, M. J.; Qian, Y.; Tirrell, M. V. PH-Responsive Branched Peptide Amphiphile Hydrogel Designed for Applications in Regenerative Medicine with Potential as Injectable Tissue Scaffolds. *J. Mater. Chem* **2012**, *22* (37), 19447. DOI: 10.1039/c2jm31745a.

- (158) Mahler, A.; Reches, M.; Rechter, M.; Cohen, S.; Gazit, E. Rigid, Self-Assembled Hydrogel Composed of a Modified Aromatic Dipeptide. *Adv. Mater.* **2006**, *18* (11), 1365–1370. DOI: 10.1002/adma.200501765.
- (159) Aggeli, A.; Nyrkova, I. A.; Bell, M.; Harding, R.; Carrick, L.; McLeish, T. C.; Semenov, A. N.; Boden, N. Hierarchical Self-Assembly of Chiral Rod-like Molecules as a Model for Peptide Beta -Sheet Tapes, Ribbons, Fibrils, and Fibers. *Proc Natl Acad Sci USA* **2001**, *98* (21), 11857–11862. DOI: 10.1073/pnas.191250198.
- (160) Hu, C.; Liu, X.; Ran, W.; Meng, J.; Zhai, Y.; Zhang, P.; Yin, Q.; Yu, H.; Zhang, Z.; Li, Y. Regulating Cancer Associated Fibroblasts with Losartan-Loaded Injectable Peptide Hydrogel to Potentiate Chemotherapy in Inhibiting Growth and Lung Metastasis of Triple Negative Breast Cancer. *Biomaterials* **2017**, *144*, 60–72. DOI: 10.1016/j.biomaterials.2017.08.009.
- (161) Yan, C.; Altunbas, A.; Yucel, T.; Nagarkar, R. P.; Schneider, J. P.; Pochan, D. J. Injectable Solid Hydrogel: Mechanism of Shear-Thinning and Immediate Recovery of Injectable β -Hairpin Peptide Hydrogels. *Soft Matter* **2010**, *6* (20), 5143–5156. DOI: 10.1039/C0SM00642D.
- (162) Caplan, M. R.; Schwartzfarb, E. M.; Zhang, S.; Kamm, R. D.; Lauffenburger, D. A. Control of Self-Assembling Oligopeptide Matrix Formation through Systematic Variation of Amino Acid Sequence. *Biomaterials* **2002**, *23* (1), 219–227. DOI: 10.1016/s0142-9612(01)00099-0.
- (163) Tao, M.; Xu, K.; He, S.; Li, H.; Zhang, L.; Luo, X.; Zhong, W. Zinc-Ion-Mediated Self-Assembly of Forky Peptides for Prostate Cancer-Specific Drug Delivery. *Chem. Commun.* **2018**, *54* (37), 4673–4676. DOI: 10.1039/c8cc00604k.
- (164) Zaksas, N. P.; Soboleva, S. E.; Nevinsky, G. A. Twenty Element Concentrations in Human Organs Determined by Two-Jet Plasma Atomic Emission Spectrometry. *ScientificWorldJournal* **2019**, *2019*, 9782635. DOI: 10.1155/2019/9782635.
- (165) Chen, G.; Li, J.; Cai, Y.; Zhan, J.; Gao, J.; Song, M.; Shi, Y.; Yang, Z. A Glycyrrhetic Acid-Modified Curcumin Supramolecular Hydrogel for Liver Tumor Targeting Therapy. *Sci. Rep.* **2017**, *7*, 44210. DOI: 10.1038/srep44210.
- (166) Radvar, E.; Azevedo, H. S. Supramolecular Peptide/Polymer Hybrid Hydrogels for Biomedical Applications. *Macromol. Biosci.* **2019**, *19* (1), e1800221. DOI: 10.1002/mabi.201800221.
- (167) Pérez, C. M. R.; Panitch, A.; Chmielewski, J. A Collagen Peptide-Based Physical Hydrogel for Cell Encapsulation. *Macromol. Biosci.* **2011**, *11* (10), 1426–1431. DOI: 10.1002/mabi.201100230.
- (168) Tondera, C.; Wieduwild, R.; Röder, E.; Werner, C.; Zhang, Y.; Pietzsch, J. In Vivo Examination of an Injectable Hydrogel System Crosslinked by Peptide-Oligosaccharide Interaction in

Immunocompetent Nude Mice. *Adv. Funct. Mater.* **2017**, *27* (15), 1605189. DOI: 10.1002/adfm.201605189.

(169) Lu, H. D.; Charati, M. B.; Kim, I. L.; Burdick, J. A. Injectable Shear-Thinning Hydrogels Engineered with a Self-Assembling Dock-and-Lock Mechanism. *Biomaterials* **2012**, *33* (7), 2145–2153. DOI: 10.1016/j.biomaterials.2011.11.076.

(170) Cao, M.; Wang, Y.; Hu, X.; Gong, H.; Li, R.; Cox, H.; Zhang, J.; Waigh, T. A.; Xu, H.; Lu, J. R. Reversible Thermoresponsive Peptide-PNIPAM Hydrogels for Controlled Drug Delivery. *Biomacromolecules* **2019**, *20* (9), 3601–3610. DOI: 10.1021/acs.biomac.9b01009.

(171) Radvar, E.; Azevedo, H. S. Supramolecular Nanofibrous Peptide/Polymer Hydrogels for the Multiplexing of Bioactive Signals. *ACS Biomater. Sci. Eng.* **2019**, *5* (9), 4646–4656. DOI: 10.1021/acsbiomaterials.9b00941.

(172) Branco, M. C.; Pochan, D. J.; Wagner, N. J.; Schneider, J. P. The Effect of Protein Structure on Their Controlled Release from an Injectable Peptide Hydrogel. *Biomaterials* **2010**, *31* (36), 9527–9534. DOI: 10.1016/j.biomaterials.2010.08.047.

(173) Wu, W.; Zhang, Z.; Xiong, T.; Zhao, W.; Jiang, R.; Chen, H.; Li, X. Calcium Ion Coordinated Dexamethasone Supramolecular Hydrogel as Therapeutic Alternative for Control of Non-Infectious Uveitis. *Acta Biomater.* **2017**, *61*, 157–168. DOI: 10.1016/j.actbio.2017.05.024.

(174) Singh, B.; Dhiman, A.; Rajneesh; Kumar, A. Slow Release of Ciprofloxacin from β -Cyclodextrin Containing Drug Delivery System through Network Formation and Supramolecular Interactions. *Int. J. Biol. Macromol.* **2016**, *92*, 390–400. DOI: 10.1016/j.ijbiomac.2016.07.060.

(175) Liu, M.; Song, X.; Wen, Y.; Zhu, J.-L.; Li, J. Injectable Thermoresponsive Hydrogel Formed by Alginate-g-Poly(N-Isopropylacrylamide) That Releases Doxorubicin-Encapsulated Micelles as a Smart Drug Delivery System. *ACS Appl. Mater. Interfaces* **2017**, *9* (41), 35673–35682. DOI: 10.1021/acsami.7b12849.

(176) Zhang, M.; Wang, J.; Jin, Z. Supramolecular Hydrogel Formation between Chitosan and Hydroxypropyl β -Cyclodextrin via Diels-Alder Reaction and Its Drug Delivery. *Int. J. Biol. Macromol.* **2018**, *114*, 381–391. DOI: 10.1016/j.ijbiomac.2018.03.106.

(177) Hoang Thi, T. T.; Lee, Y.; Ryu, S. B.; Sung, H.-J.; Park, K. D. Oxidized Cyclodextrin-Functionalized Injectable Gelatin Hydrogels as a New Platform for Tissue-Adhesive Hydrophobic Drug Delivery. *RSC Adv.* **2017**, *7* (54), 34053–34062. DOI: 10.1039/C7RA04137C.

(178) Tae, G.; Scatena, M.; Stayton, P. S.; Hoffman, A. S. PEG-Cross-Linked Heparin Is an Affinity Hydrogel for Sustained Release of Vascular Endothelial Growth Factor. *J. Biomater. Sci. Polym. Ed.* **2006**, *17* (1–2), 187–197. DOI: 10.1163/156856206774879090.

- (179) Ma, D.; Zhang, H.-B.; Tu, K.; Zhang, L.-M. Novel Supramolecular Hydrogel/Micelle Composite for Co-Delivery of Anticancer Drug and Growth Factor. *Soft Matter* **2012**, *8* (13), 3665. DOI: 10.1039/c2sm25060h.
- (180) Zhang, F.; Hu, C.; Kong, Q.; Luo, R.; Wang, Y. Peptide-/Drug-Directed Self-Assembly of Hybrid Polyurethane Hydrogels for Wound Healing. *ACS Appl. Mater. Interfaces* **2019**, *11* (40), 37147–37155. DOI: 10.1021/acsami.9b13708.
- (181) Bakker, M. H.; van Rooij, E.; Dankers, P. Y. W. Controlled Release of Rnai Molecules by Tunable Supramolecular Hydrogel Carriers. *Chem. Asian J.* **2018**, *13* (22), 3501–3508. DOI: 10.1002/asia.201800582.
- (182) Zou, L.; Braegelman, A. S.; Webber, M. J. Spatially Defined Drug Targeting by in Situ Host–Guest Chemistry in a Living Animal. *ACS Cent. Sci.* **2019**. DOI: 10.1021/acscentsci.9b00195.
- (183) Yang, L.; Zhang, C.; Ren, C.; Liu, J.; Zhang, Y.; Wang, J.; Huang, F.; Zhang, L.; Liu, J. Supramolecular Hydrogel Based on Chlorambucil and Peptide Drug for Cancer Combination Therapy. *ACS Appl. Mater. Interfaces* **2019**, *11* (1), 331–339. DOI: 10.1021/acsami.8b18425.
- (184) Guo, Q.; Liu, Y.; Mu, G.; Yang, L.; Wang, W.; Liu, J.; Liu, J. A Peptide-Drug Hydrogel to Enhance the Anti-Cancer Activity of Chlorambucil. *Biomater. Sci.* **2020**, *8* (20), 5638–5646. DOI: 10.1039/d0bm01001d.
- (185) Qian, Q.; Wang, D.; Shi, L.; Zhang, Z.; Qian, J.; Shen, J.; Yu, C.; Zhu, X. A Pure Molecular Drug Hydrogel for Post-Surgical Cancer Treatment. *Biomaterials* **2021**, *265*, 120403. DOI: 10.1016/j.biomaterials.2020.120403.
- (186) Zhu, M.; Wei, K.; Lin, S.; Chen, X.; Wu, C.-C.; Li, G.; Bian, L. Bioadhesive Polymersome for Localized and Sustained Drug Delivery at Pathological Sites with Harsh Enzymatic and Fluidic Environment via Supramolecular Host-Guest Complexation. *Small* **2018**, *14* (7). DOI: 10.1002/smll.201702288.
- (187) Webber, M. J.; Appel, E. A.; Vinciguerra, B.; Cortinas, A. B.; Thapa, L. S.; Jhunjunwala, S.; Isaacs, L.; Langer, R.; Anderson, D. G. Supramolecular PEGylation of Biopharmaceuticals. *Proc Natl Acad Sci USA* **2016**, *113* (50), 14189–14194. DOI: 10.1073/pnas.1616639113.
- (188) Maikawa, C. L.; Smith, A. A. A.; Zou, L.; Meis, C. M.; Mann, J. L.; Webber, M. J.; Appel, E. A. Stable Monomeric Insulin Formulations Enabled by Supramolecular Pegylation of Insulin Analogues. *Adv. Therap.* **2020**, *3* (1). DOI: 10.1002/adtp.201900094.
- (189) Maikawa, C. L.; Smith, A. A. A.; Zou, L.; Roth, G. A.; Gale, E. C.; Stapleton, L. M.; Baker, S. W.; Mann, J. L.; Yu, A. C.; Correa, S.; Grosskopf, A. K.; Liang, C. S.; Meis, C. M.; Chan, D.; Troxell, M.; Maahs, D. M.; Buckingham, B. A.; Webber, M. J.; Appel, E. A. A Co-Formulation of

Supramolecularly Stabilized Insulin and Pramlintide Enhances Mealtime Glucagon Suppression in Diabetic Pigs. *Nat. Biomed. Eng.* **2020**, *4* (5), 507–517. DOI: 10.1038/s41551-020-0555-4.

(190) Li, X.; Li, J.; Gao, Y.; Kuang, Y.; Shi, J.; Xu, B. Molecular Nanofibers of Olsalazine Form Supramolecular Hydrogels for Reductive Release of an Anti-Inflammatory Agent. *J. Am. Chem. Soc.* **2010**, *132* (50), 17707–17709. DOI: 10.1021/ja109269v.

(191) Webber, M. J.; Matson, J. B.; Tamboli, V. K.; Stupp, S. I. Controlled Release of Dexamethasone from Peptide Nanofiber Gels to Modulate Inflammatory Response. *Biomaterials* **2012**, *33* (28), 6823–6832. DOI: 10.1016/j.biomaterials.2012.06.003.

(192) Li, C.; Li, H.; Guo, J.; Li, L.; Xi, X.; Yu, Y. Biocompatible Supramolecular Pseudorotaxane Hydrogels for Controllable Release of Doxorubicin in Ovarian Cancer SKOV-3 Cells. *RSC Adv.* **2020**, *10* (2), 689–697. DOI: 10.1039/c9ra08986a.

(193) Nandi, N.; Gayen, K.; Ghosh, S.; Bhunia, D.; Kirkham, S.; Sen, S. K.; Ghosh, S.; Hamley, I. W.; Banerjee, A. Amphiphilic Peptide-Based Supramolecular, Noncytotoxic, Stimuli-Responsive Hydrogels with Antibacterial Activity. *Biomacromolecules* **2017**, *18* (11), 3621–3629. DOI: 10.1021/acs.biomac.7b01006.

(194) Salick, D. A.; Pochan, D. J.; Schneider, J. P. Design of an Injectable β -Hairpin Peptide Hydrogel That Kills Methicillin-Resistant *Staphylococcus Aureus*. *Adv. Mater.* **2009**, *21* (41), 4120–4123. DOI: 10.1002/adma.200900189.

(195) Ren, C.; Gao, Y.; Guan, Y.; Wang, Z.; Yang, L.; Gao, J.; Fan, H.; Liu, J. Carrier-Free Supramolecular Hydrogel Composed of Dual Drugs for Conquering Drug Resistance. *ACS Appl. Mater. Interfaces* **2019**, *11* (37), 33706–33715. DOI: 10.1021/acsami.9b12530.

(196) Xue, Q.; Ren, H.; Xu, C.; Wang, G.; Ren, C.; Hao, J.; Ding, D. Nanospheres of Doxorubicin as Cross-Linkers for a Supramolecular Hydrogelation. *Sci. Rep.* **2015**, *5*, 8764. DOI: 10.1038/srep08764.

(197) Kumar, V. A.; Shi, S.; Wang, B. K.; Li, I.-C.; Jalan, A. A.; Sarkar, B.; Wickremasinghe, N. C.; Hartgerink, J. D. Drug-Triggered and Cross-Linked Self-Assembling Nanofibrous Hydrogels. *J. Am. Chem. Soc.* **2015**, *137* (14), 4823–4830. DOI: 10.1021/jacs.5b01549.

(198) Wang, F.; Su, H.; Xu, D.; Dai, W.; Zhang, W.; Wang, Z.; Anderson, C. F.; Zheng, M.; Oh, R.; Wan, F.; Cui, H. Tumour Sensitization via the Extended Intratumoural Release of a STING Agonist and Camptothecin from a Self-Assembled Hydrogel. *Nat. Biomed. Eng.* **2020**, *4* (11), 1090–1101. DOI: 10.1038/s41551-020-0597-7.

(199) Naguib, M. Sugammadex: Another Milestone in Clinical Neuromuscular Pharmacology. *Anesth. Analg.* **2007**, *104* (3), 575–581. DOI: 10.1213/01.ane.0000244594.63318.fc.

- (200) Davis, M. E. The First Targeted Delivery of siRNA in Humans via a Self-Assembling, Cyclodextrin Polymer-Based Nanoparticle: From Concept to Clinic. *Mol. Pharm.* **2009**, *6* (3), 659–668. DOI: 10.1021/mp900015y.
- (201) Gaur, S.; Chen, L.; Yen, T.; Wang, Y.; Zhou, B.; Davis, M.; Yen, Y. Preclinical Study of the Cyclodextrin-Polymer Conjugate of Camptothecin CRLX101 for the Treatment of Gastric Cancer. *Nanomedicine* **2012**, *8* (5), 721–730. DOI: 10.1016/j.nano.2011.09.007.
- (202) Bockeria, L. A.; Svanidze, O.; Kim, A.; Shatalov, K.; Makarenko, V.; Cox, M.; Carrel, T. Total Cavopulmonary Connection with a New Bioabsorbable Vascular Graft: First Clinical Experience. *J. Thorac. Cardiovasc. Surg.* **2017**, *153* (6), 1542–1550. DOI: 10.1016/j.jtcvs.2016.11.071.
- (203) Yu, A. C.; Chen, H.; Chan, D.; Agmon, G.; Stapleton, L. M.; Sevit, A. M.; Tibbitt, M. W.; Acosta, J. D.; Zhang, T.; Franzia, P. W.; Langer, R.; Appel, E. A. Scalable Manufacturing of Biomimetic Moldable Hydrogels for Industrial Applications. *Proc Natl Acad Sci USA* **2016**, *113* (50), 14255–14260. DOI: 10.1073/pnas.1618156113.
- (204) Rizzo, F.; Kehr, N. S. Recent Advances in Injectable Hydrogels for Controlled and Local Drug Delivery. *Adv. Healthc. Mater.* **2021**, *10* (1), e2001341. DOI: 10.1002/adhm.202001341.
- (205) Liao, X.; Yang, X.; Deng, H.; Hao, Y.; Mao, L.; Zhang, R.; Liao, W.; Yuan, M. Injectable Hydrogel-Based Nanocomposites for Cardiovascular Diseases. *Front. Bioeng. Biotechnol.* **2020**, *8*, 251. DOI: 10.3389/fbioe.2020.00251.
- (206) Rodell, C. B.; MacArthur, J. W.; Dorsey, S. M.; Wade, R. J.; Wang, L. L.; Woo, Y. J.; Burdick, J. A. Shear-Thinning Supramolecular Hydrogels with Secondary Autonomous Covalent Crosslinking to Modulate Viscoelastic Properties In Vivo. *Adv. Funct. Mater.* **2015**, *25* (4), 636–644. DOI: 10.1002/adfm.201403550.
- (207) Highley, C. B.; Rodell, C. B.; Burdick, J. A. Direct 3D Printing of Shear-Thinning Hydrogels into Self-Healing Hydrogels. *Adv. Mater.* **2015**, *27* (34), 5075–5079. DOI: 10.1002/adma.201501234.
- (208) Yesilyurt, V.; Webber, M. J.; Appel, E. A.; Godwin, C.; Langer, R.; Anderson, D. G. Injectable Self-Healing Glucose-Responsive Hydrogels with PH-Regulated Mechanical Properties. *Adv. Mater.* **2016**, *28* (1), 86–91. DOI: 10.1002/adma.201502902.
- (209) Zhao, F.; Wu, D.; Yao, D.; Guo, R.; Wang, W.; Dong, A.; Kong, D.; Zhang, J. An Injectable Particle-Hydrogel Hybrid System for Glucose-Regulatory Insulin Delivery. *Acta Biomater.* **2017**, *64*, 334–345. DOI: 10.1016/j.actbio.2017.09.044.
- (210) Wang, L. L.; Highley, C. B.; Yeh, Y.-C.; Galarraga, J. H.; Uman, S.; Burdick, J. A. Three-Dimensional Extrusion Bioprinting of Single- and Double-Network Hydrogels Containing Dynamic Covalent Crosslinks. *J. Biomed. Mater. Res. A* **2018**, *106* (4), 865–875. DOI: 10.1002/jbm.a.36323.

- (211) Harada, A.; Kobayashi, R.; Takashima, Y.; Hashidzume, A.; Yamaguchi, H. Macroscopic Self-Assembly through Molecular Recognition. *Nat. Chem.* **2011**, *3* (1), 34–37. DOI: 10.1038/nchem.893.
- (212) Smithmyer, M. E.; Deng, C. C.; Cassel, S. E.; LeValley, P. J.; Sumerlin, B. S.; Kloxin, A. M. Self-Healing Boronic Acid-Based Hydrogels for 3D Co-Cultures. *ACS Macro Lett.* **2018**, *7* (9), 1105–1110. DOI: 10.1021/acsmacrolett.8b00462.
- (213) Daly, A. C.; Davidson, M. D.; Burdick, J. A. 3D Bioprinting of High Cell-Density Heterogeneous Tissue Models through Spheroid Fusion within Self-Healing Hydrogels. *Nat. Commun.* **2021**, *12* (1), 753. DOI: 10.1038/s41467-021-21029-2.
- (214) Skardal, A.; Zhang, J.; McCoard, L.; Oottamasathien, S.; Prestwich, G. D. Dynamically Crosslinked Gold Nanoparticle - Hyaluronan Hydrogels. *Adv. Mater.* **2010**, *22* (42), 4736–4740. DOI: 10.1002/adma.201001436.
- (215) Wang, X.; Jiang, M.; Zhou, Z.; Gou, J.; Hui, D. 3D Printing of Polymer Matrix Composites: A Review and Prospective. *Composites Part B: Engineering* **2017**, *110*, 442–458. DOI: 10.1016/j.compositesb.2016.11.034.
- (216) Barrile, R.; van der Meer, A. D.; Park, H.; Fraser, J. P.; Simic, D.; Teng, F.; Conegliano, D.; Nguyen, J.; Jain, A.; Zhou, M.; Karalis, K.; Ingber, D. E.; Hamilton, G. A.; Otieno, M. A. Organ-on-Chip Recapitulates Thrombosis Induced by an Anti-CD154 Monoclonal Antibody: Translational Potential of Advanced Microengineered Systems. *Clin. Pharmacol. Ther.* **2018**, *104* (6), 1240–1248. DOI: 10.1002/cpt.1054.
- (217) Wang, Q.; Mynar, J. L.; Yoshida, M.; Lee, E.; Lee, M.; Okuro, K.; Kinbara, K.; Aida, T. High-Water-Content Mouldable Hydrogels by Mixing Clay and a Dendritic Molecular Binder. *Nature* **2010**, *463* (7279), 339–343. DOI: 10.1038/nature08693.
- (218) Meis, C. M.; Salzman, E. E.; Maikawa, C. L.; Smith, A. A. A.; Mann, J. L.; Grosskopf, A. K.; Appel, E. A. Self-Assembled, Dilution-Responsive Hydrogels for Enhanced Thermal Stability of Insulin Biopharmaceuticals. *ACS Biomater. Sci. Eng.* **2021**, *7* (9), 4221–4229. DOI: 10.1021/acsbomaterials.0c01306.
- (219) Stapleton, L. M.; Steele, A. N.; Wang, H.; Lopez Hernandez, H.; Yu, A. C.; Paulsen, M. J.; Smith, A. A. A.; Roth, G. A.; Thakore, A. D.; Lucian, H. J.; Tothorow, K. P.; Baker, S. W.; Tada, Y.; Farry, J. M.; Eskandari, A.; Hironaka, C. E.; Jaatinen, K. J.; Williams, K. M.; Bergamasco, H.; Marschel, C.; Chadwick, B.; Grady, F.; Ma, M.; Appel, E. A.; Woo, Y. J. Use of a Supramolecular Polymeric Hydrogel as an Effective Post-Operative Pericardial Adhesion Barrier. *Nat. Biomed. Eng.* **2019**, *3* (8), 611–620. DOI: 10.1038/s41551-019-0442-z.
- (220) Yu, A. C.; Lopez Hernandez, H.; Kim, A. H.; Stapleton, L. M.; Brand, R. J.; Mellor, E. T.; Bauer, C. P.; McCurdy, G. D.; Wolff, A. J.; Chan, D.; Criddle, C. S.; Acosta, J. D.; Appel, E. A. Wildfire

Prevention through Prophylactic Treatment of High-Risk Landscapes Using Viscoelastic Retardant Fluids. *Proc Natl Acad Sci USA* **2019**, *116* (42), 20820–20827. DOI: 10.1073/pnas.1907855116.

(221) Davis, M. E.; Brewster, M. E. Cyclodextrin-Based Pharmaceuticals: Past, Present and Future. *Nat. Rev. Drug Discov.* **2004**, *3* (12), 1023–1035. DOI: 10.1038/nrd1576.

(222) Wang, C.; Fadeev, M.; Zhang, J.; Vázquez-González, M.; Davidson-Rozenfeld, G.; Tian, H.; Willner, I. Shape-Memory and Self-Healing Functions of DNA-Based Carboxymethyl Cellulose Hydrogels Driven by Chemical or Light Triggers. *Chem. Sci.* **2018**, *9* (35), 7145–7152. DOI: 10.1039/c8sc02411a.

(223) Himmelein, S.; Lewe, V.; Stuart, M. C. A.; Ravoo, B. J. A Carbohydrate-Based Hydrogel Containing Vesicles as Responsive Non-Covalent Cross-Linkers. *Chem. Sci.* **2014**, *5* (3), 1054. DOI: 10.1039/c3sc52964a.

(224) Peng, K.; Tomatsu, I.; Kros, A. Light Controlled Protein Release from a Supramolecular Hydrogel. *Chem. Commun.* **2010**, *46* (23), 4094–4096. DOI: 10.1039/c002565h.

(225) Harada, A.; Kamachi, M. Complex Formation between Poly(Ethylene Glycol) and α -Cyclodextrin. *Macromolecules* **1990**, *23* (10), 2821–2823. DOI: 10.1021/ma00212a039.

(226) Harada, A.; Li, J.; Kamachi, M. Preparation and Properties of Inclusion Complexes of Polyethylene Glycol with α -Cyclodextrin. *Macromolecules* **1993**, *26* (21), 5698–5703. DOI: 10.1021/ma00073a026.

(227) Harada, A.; Takashima, Y.; Yamaguchi, H. Cyclodextrin-Based Supramolecular Polymers. *Chem. Soc. Rev.* **2009**, *38* (4), 875–882. DOI: 10.1039/b705458k.

(228) Topchieva, I. N.; Tonelli, A. E.; Panova, I. G.; Matuchina, E. V.; Kalashnikov, F. A.; Gerasimov, V. I.; Rusa, C. C.; Rusa, M.; Hunt, M. A. Two-Phase Channel Structures Based on α -Cyclodextrin-Polyethylene Glycol Inclusion Complexes. *Langmuir* **2004**, *20* (21), 9036–9043. DOI: 10.1021/la048970d.

(229) Coelho, J. P.; González-Rubio, G.; Delices, A.; Barcina, J. O.; Salgado, C.; Ávila, D.; Peña-Rodríguez, O.; Tardajos, G.; Guerrero-Martínez, A. Polyrotaxane-Mediated Self-Assembly of Gold Nanospheres into Fully Reversible Supercrystals. *Angew. Chem.* **2014**, *126* (47), 12965–12969. DOI: 10.1002/ange.201406323.

(230) Niu, Y.; Yuan, X.; Zhao, Y.; Zhang, W.; Ren, L. Temperature and PH Dual-Responsive Supramolecular Polymer Hydrogels Hybridized with Functional Inorganic Nanoparticles. *Macromol. Chem. Phys.* **2017**, *218* (9), 1600540. DOI: 10.1002/macp.201600540.

(231) Serres-Gómez, M.; González-Gaitano, G.; Kaldybekov, D. B.; Mansfield, E. D. H.; Khutoryanskiy, V. V.; Isasi, J. R.; Dreiss, C. A. Supramolecular Hybrid Structures and Gels from Host-

Guest Interactions between α -Cyclodextrin and PEGylated Organosilica Nanoparticles. *Langmuir* **2018**, *34* (36), 10591–10602. DOI: 10.1021/acs.langmuir.8b01744.

(232) Guo, M.; Jiang, M.; Pispas, S.; Yu, W.; Zhou, C. Supramolecular Hydrogels Made of End-Functionalized Low-Molecular-Weight PEG and α -Cyclodextrin and Their Hybridization with SiO₂ Nanoparticles through Host–Guest Interaction. *Macromolecules* **2008**, *41* (24), 9744–9749. DOI: 10.1021/ma801975s.

(233) Wang, X.; Wang, C.; Zhang, Q.; Cheng, Y. Near Infrared Light-Responsive and Injectable Supramolecular Hydrogels for on-Demand Drug Delivery. *Chem. Commun.* **2016**, *52* (5), 978–981. DOI: 10.1039/c5cc08391e.

(234) Xu, S.; Yin, L.; Xiang, Y.; Deng, H.; Deng, L.; Fan, H.; Tang, H.; Zhang, J.; Dong, A. Supramolecular Hydrogel from Nanoparticles and Cyclodextrins for Local and Sustained Nanoparticle Delivery. *Macromol. Biosci.* **2016**, *16* (8), 1188–1199. DOI: 10.1002/mabi.201600076.

(235) Poudel, A. J.; He, F.; Huang, L.; Xiao, L.; Yang, G. Supramolecular Hydrogels Based on Poly (Ethylene Glycol)-Poly (Lactic Acid) Block Copolymer Micelles and α -Cyclodextrin for Potential Injectable Drug Delivery System. *Carbohydr. Polym.* **2018**, *194*, 69–79. DOI: 10.1016/j.carbpol.2018.04.035.

(236) Ren, L.; He, L.; Sun, T.; Dong, X.; Chen, Y.; Huang, J.; Wang, C. Dual-Responsive Supramolecular Hydrogels from Water-Soluble PEG-Grafted Copolymers and Cyclodextrin. *Macromol. Biosci.* **2009**, *9* (9), 902–910. DOI: 10.1002/mabi.200900021.

(237) Meis, C. M.; Grosskopf, A. K.; Correa, S.; Appel, E. A. Injectable Supramolecular Polymer-Nanoparticle Hydrogels for Cell and Drug Delivery Applications. *J. Vis. Exp.* **2021**, No. 168. DOI: 10.3791/62234.

(238) Stapleton, L. M.; Lucian, H. J.; Grosskopf, A. K.; Smith, A. A. A.; Tothorow, K. P.; Woo, Y. J.; Appel, E. A. Dynamic Hydrogels for Prevention of Post-operative Peritoneal Adhesions. *Adv. Therap.* **2021**, *4* (3), 2000242. DOI: 10.1002/adtp.202000242.

(239) Pryamitsyn, V.; Ganesan, V. Origins of Linear Viscoelastic Behavior of Polymer–nanoparticle Composites. *Macromolecules* **2006**, *39* (2), 844–856. DOI: 10.1021/ma051841z.

(240) Wang, Y.; Wu, X.; Yang, W.; Zhai, Y.; Xie, B.; Yang, M. Aggregate of Nanoparticles: Rheological and Mechanical Properties. *Nanoscale Res. Lett.* **2011**, *6* (1), 114. DOI: 10.1186/1556-276X-6-114.

(241) Franco, S.; Buratti, E.; Nigro, V.; Zaccarelli, E.; Ruzicka, B.; Angelini, R. Glass and Jamming Rheology in Soft Particles Made of PNIPAM and Polyacrylic Acid. *Int. J. Mol. Sci.* **2021**, *22* (8). DOI: 10.3390/ijms22084032.

- (242) Guzzi, E. A.; Tibbitt, M. W. Additive Manufacturing of Precision Biomaterials. *Adv. Mater.* **2020**, *32* (13), e1901994. DOI: 10.1002/adma.201901994.
- (243) Hospodiuk, M.; Dey, M.; Sosnoski, D.; Ozbolat, I. T. The Bioink: A Comprehensive Review on Bioprintable Materials. *Biotechnol. Adv.* **2017**, *35* (2), 217–239. DOI: 10.1016/j.biotechadv.2016.12.006.
- (244) Róka, E.; Ujhelyi, Z.; Deli, M.; Bocsik, A.; Fenyvesi, É.; Szente, L.; Fenyvesi, F.; Vecsernyés, M.; Váradi, J.; Fehér, P.; Gesztelyi, R.; Félix, C.; Perret, F.; Bácskay, I. K. Evaluation of the Cytotoxicity of α -Cyclodextrin Derivatives on the Caco-2 Cell Line and Human Erythrocytes. *Molecules* **2015**, *20* (11), 20269–20285. DOI: 10.3390/molecules201119694.
- (245) Aguado, B. A.; Mulyasmita, W.; Su, J.; Lampe, K. J.; Heilshorn, S. C. Improving Viability of Stem Cells during Syringe Needle Flow through the Design of Hydrogel Cell Carriers. *Tissue Eng. Part A* **2012**, *18* (7–8), 806–815. DOI: 10.1089/ten.TEA.2011.0391.
- (246) Lopez Hernandez, H.; Grosskopf, A. K.; Stapleton, L. M.; Agmon, G.; Appel, E. A. Non-Newtonian Polymer-Nanoparticle Hydrogels Enhance Cell Viability during Injection. *Macromol. Biosci.* **2019**, *19* (1), e1800275. DOI: 10.1002/mabi.201800275.
- (247) Zhao, Y.; Li, Y.; Mao, S.; Sun, W.; Yao, R. The Influence of Printing Parameters on Cell Survival Rate and Printability in Microextrusion-Based 3D Cell Printing Technology. *Biofabrication* **2015**, *7* (4), 045002. DOI: 10.1088/1758-5090/7/4/045002.
- (248) Boularaoui, S.; Al Hussein, G.; Khan, K. A.; Christoforou, N.; Stefanini, C. An Overview of Extrusion-Based Bioprinting with a Focus on Induced Shear Stress and Its Effect on Cell Viability. *Bioprinting* **2020**, *20*, e00093. DOI: 10.1016/j.bprint.2020.e00093.
- (249) Kummer, M. P.; Abbott, J. J.; Kratochvil, B. E.; Borer, R.; Sengul, A.; Nelson, B. J. OctoMag: An Electromagnetic System for 5-DOF Wireless Micromanipulation. *IEEE Trans. Robot.* **2010**, *26* (6), 1006–1017. DOI: 10.1109/TRO.2010.2073030.
- (250) Rahme, K.; Chen, L.; Hobbs, R. G.; Morris, M. A.; O’Driscoll, C.; Holmes, J. D. PEGylated Gold Nanoparticles: Polymer Quantification as a Function of PEG Lengths and Nanoparticle Dimensions. *RSC Adv.* **2013**, *3* (17), 6085. DOI: 10.1039/c3ra22739a.
- (251) Sun, Y.; Ding, X.; Zheng, Z.; Cheng, X.; Hu, X.; Peng, Y. Magnetic Separation of Polymer Hybrid Iron Oxide Nanoparticles Triggered by Temperature. *Chem. Commun.* **2006**, No. 26, 2765–2767. DOI: 10.1039/b604202c.
- (252) Larsen, E. K. U.; Nielsen, T.; Wittenborn, T.; Birkedal, H.; Vorup-Jensen, T.; Jakobsen, M. H.; Ostergaard, L.; Horsman, M. R.; Besenbacher, F.; Howard, K. A.; Kjems, J. Size-Dependent

Accumulation of PEGylated Silane-Coated Magnetic Iron Oxide Nanoparticles in Murine Tumors. *ACS Nano* **2009**, *3* (7), 1947–1951. DOI: 10.1021/nn900330m.

(253) Larsen, E. K. U.; Nielsen, T.; Wittenborn, T.; Rydtoft, L. M.; Lokanathan, A. R.; Hansen, L.; Østergaard, L.; Kingshott, P.; Howard, K. A.; Besenbacher, F.; Nielsen, N. C.; Kjems, J. Accumulation of Magnetic Iron Oxide Nanoparticles Coated with Variably Sized Polyethylene Glycol in Murine Tumors. *Nanoscale* **2012**, *4* (7), 2352–2361. DOI: 10.1039/c2nr11554a.

(254) Majima, E.; Schnabep, W.; Weber, W. Phenyl-2,4,6-Trimethylbenzoylphosphinates as Water-Soluble Photoinitiators. Generation and Reactivity of O=P(C₆H₅)(O⁻) Radical Anions. *Die Makromolekulare Chemie* **1991**, *192* (10), 2307–2315.

(255) Fairbanks, B. D.; Schwartz, M. P.; Bowman, C. N.; Anseth, K. S. Photoinitiated Polymerization of PEG-Diacrylate with Lithium Phenyl-2,4,6-Trimethylbenzoylphosphinate: Polymerization Rate and Cytocompatibility. *Biomaterials* **2009**, *30* (35), 6702–6707. DOI: 10.1016/j.biomaterials.2009.08.055.

(256) Chimene, D.; Kaunas, R.; Gaharwar, A. K. Hydrogel Bioink Reinforcement for Additive Manufacturing: A Focused Review of Emerging Strategies. *Adv. Mater.* **2020**, *32* (1), e1902026. DOI: 10.1002/adma.201902026.

(257) Shen, S.; Zhang, Z.; Huang, H.; Yang, J.; Tao, X.; Meng, Z.; Ren, H.; Li, X. Copper-Induced Injectable Hydrogel with Nitric Oxide for Enhanced Immunotherapy by Amplifying Immunogenic Cell Death and Regulating Cancer Associated Fibroblasts. *Biomater. Res.* **2023**, *27* (1), 44. DOI: 10.1186/s40824-023-00389-4.

(258) Chao, Y.; Chen, Q.; Liu, Z. Smart Injectable Hydrogels for Cancer Immunotherapy. *Adv. Funct. Mater.* **2020**, *30* (2), 1902785. DOI: 10.1002/adfm.201902785.

(259) Tringides, C. M.; Boulingre, M.; Khalil, A.; Lungjangwa, T.; Jaenisch, R.; Mooney, D. J. Tunable Conductive Hydrogel Scaffolds for Neural Cell Differentiation. *Adv. Healthc. Mater.* **2023**, *12* (7), e2202221. DOI: 10.1002/adhm.202202221.

(260) Bertsch, P.; Diba, M.; Mooney, D. J.; Leeuwenburgh, S. C. G. Self-Healing Injectable Hydrogels for Tissue Regeneration. *Chem. Rev.* **2023**, *123* (2), 834–873. DOI: 10.1021/acs.chemrev.2c00179.

(261) Pertici, V.; Pin-Barre, C.; Rivera, C.; Pellegrino, C.; Laurin, J.; Gignes, D.; Trimaille, T. Degradable and Injectable Hydrogel for Drug Delivery in Soft Tissues. *Biomacromolecules* **2019**, *20* (1), 149–163. DOI: 10.1021/acs.biomac.8b01242.

(262) Choi, J.; Kim, S.; Yoo, J.; Choi, S.-H.; Char, K. Self-Healable Antifreeze Hydrogel Based on Dense Quadruple Hydrogen Bonding. *Macromolecules* **2021**, *54* (13), 6389–6399. DOI: 10.1021/acs.macromol.1c00295.

- (263) Madl, A. C.; Madl, C. M.; Myung, D. Injectable Cucurbit[8]Uril-Based Supramolecular Gelatin Hydrogels for Cell Encapsulation. *ACS Macro Lett.* **2020**, *9* (4), 619–626. DOI: 10.1021/acsmacrolett.0c00184.
- (264) Bernhard, S.; Tibbitt, M. W. Supramolecular Engineering of Hydrogels for Drug Delivery. *Adv. Drug Deliv. Rev.* **2021**, *171*, 240–256. DOI: 10.1016/j.addr.2021.02.002.
- (265) Wang, Y. J.; Zhang, X. N.; Song, Y.; Zhao, Y.; Chen, L.; Su, F.; Li, L.; Wu, Z. L.; Zheng, Q. Ultrastiff and Tough Supramolecular Hydrogels with a Dense and Robust Hydrogen Bond Network. *Chem. Mater.* **2019**, *31* (4), 1430–1440. DOI: 10.1021/acs.chemmater.8b05262.
- (266) Okumura, Y.; Ito, K. The Polyrotaxane Gel: A Topological Gel by Figure-of-Eight Cross-Links. *Adv. Mater.* **2001**, *13* (7), 485–487. DOI: 10.1002/1521-4095(200104)13:7<485::AID-ADMA485>3.0.CO;2-T.
- (267) Zhang, X. N.; Wang, Y. J.; Sun, S.; Hou, L.; Wu, P.; Wu, Z. L.; Zheng, Q. A Tough and Stiff Hydrogel with Tunable Water Content and Mechanical Properties Based on the Synergistic Effect of Hydrogen Bonding and Hydrophobic Interaction. *Macromolecules* **2018**, *51* (20), 8136–8146. DOI: 10.1021/acs.macromol.8b01496.
- (268) Grosskopf, A. K.; Roth, G. A.; Smith, A. A. A.; Gale, E. C.; Hernandez, H. L.; Appel, E. A. Injectable Supramolecular Polymer-Nanoparticle Hydrogels Enhance Human Mesenchymal Stem Cell Delivery. *Bioeng. Transl. Med.* **2020**, *5* (1), e10147. DOI: 10.1002/btm2.10147.
- (269) Bovone, G.; Guzzi, E. A.; Bernhard, S.; Weber, T.; Dranseikiene, D.; Tibbitt, M. W. Supramolecular Reinforcement of Polymer-Nanoparticle Hydrogels for Modular Materials Design. *Adv. Mater.* **2022**, *34* (9), e2106941. DOI: 10.1002/adma.202106941.
- (270) Yu, A. C.; Lian, H.; Kong, X.; Lopez Hernandez, H.; Qin, J.; Appel, E. A. Physical Networks from Entropy-Driven Non-Covalent Interactions. *Nat. Commun.* **2021**, *12* (1), 746. DOI: 10.1038/s41467-021-21024-7.
- (271) Chen, G.; Jiang, M. Cyclodextrin-Based Inclusion Complexation Bridging Supramolecular Chemistry and Macromolecular Self-Assembly. *Chem. Soc. Rev.* **2011**, *40* (5), 2254–2266. DOI: 10.1039/c0cs00153h.
- (272) Eftink, M. R.; Andy, M. L.; Bystrom, K.; Perlmutter, H. D.; Kristol, D. S. Cyclodextrin Inclusion Complexes: Studies of the Variation in the Size of Alicyclic Guests. *J. Am. Chem. Soc.* **1989**, *111* (17), 6765–6772. DOI: 10.1021/ja00199a041.
- (273) Okumura, Y.; Ito, K. The Polyrotaxane Gel: A Topological Gel by Figure-of-Eight Cross-Links. *Adv. Mater.* **2001**, *13* (7), 485–487. DOI: 10.1002/1521-4095(200104)13:7<485::AID-ADMA485>3.0.CO;2-T.

- (274) Giubertoni, G.; Burla, F.; Martinez-Torres, C.; Dutta, B.; Pletikapic, G.; Pelan, E.; Rezus, Y. L. A.; Koenderink, G. H.; Bakker, H. J. Molecular Origin of the Elastic State of Aqueous Hyaluronic Acid. *J. Phys. Chem. B* **2019**, *123* (14), 3043–3049. DOI: 10.1021/acs.jpcc.9b00982.
- (275) Scott, J. E.; Heatley, F. Biological Properties of Hyaluronan in Aqueous Solution Are Controlled and Sequestered by Reversible Tertiary Structures, Defined by NMR Spectroscopy. *Biomacromolecules* **2002**, *3* (3), 547–553. DOI: 10.1021/bm010170j.
- (276) Gibbs, D. A.; Merrill, E. W.; Smith, K. A.; Balazs, E. A. Rheology of Hyaluronic Acid. *Biopolymers* **1968**, *6* (6), 777–791. DOI: 10.1002/bip.1968.360060603.
- (277) Falcone, S. J.; Palmeri, D. M.; Berg, R. A. Rheological and Cohesive Properties of Hyaluronic Acid. *J. Biomed. Mater. Res. A* **2006**, *76* (4), 721–728. DOI: 10.1002/jbm.a.30623.
- (278) Harada, A.; Furue, M.; Nozakura, S. Inclusion of Aromatic Compounds by a β -Cyclodextrin–Epichlorohydrin Polymer. *Polym. J.* **1981**, *13* (8), 777–781. DOI: 10.1295/polymj.13.777.
- (279) Taura, D.; Taniguchi, Y.; Hashidzume, A.; Harada, A. Macromolecular Recognition of Cyclodextrin: Inversion of Selectivity of β -Cyclodextrin toward Adamantyl Groups Induced by Macromolecular Chains. *Macromol. Rapid Commun.* **2009**, *30* (20), 1741–1744. DOI: 10.1002/marc.200900283.
- (280) Wenz, G. Recognition of Monomers and Polymers by Cyclodextrins. In *Inclusion Polymers*; Wenz, G., Ed.; Advances in polymer science; Springer Berlin Heidelberg: Berlin, Heidelberg, 2009; Vol. 222, pp 204–254. DOI: 10.1007/12_2008_13.
- (281) Sadrerafi, K.; Moore, E. E.; Lee, M. W. Association Constant of β -Cyclodextrin with Carboranes, Adamantane, and Their Derivatives Using Displacement Binding Technique. *J. Incl. Phenom. Macrocycl. Chem.* **2015**, *83* (1–2), 159–166. DOI: 10.1007/s10847-015-0552-5.
- (282) Poon, K. H.-N.; Cheng, Y.-L. A Quartz Crystal Microbalance Study of β -Cyclodextrin Self Assembly on Gold and Complexation of Immobilized β -Cyclodextrin with Adamantane Derivatives. *J. Incl. Phenom. Macrocycl. Chem.* **2008**, *60* (3–4), 211–222. DOI: 10.1007/s10847-007-9380-6.
- (283) Paolino, M.; Ennen, F.; Lamponi, S.; Cernescu, M.; Voit, B.; Cappelli, A.; Appelhans, D.; Komber, H. Cyclodextrin-Adamantane Host–Guest Interactions on the Surface of Biocompatible Adamantyl-Modified Glycodendrimers. *Macromolecules* **2013**, *46* (9), 3215–3227. DOI: 10.1021/ma400352m.
- (284) Blass, J.; Bozna, B.; Albrecht, M.; Wenz, G.; Bennewitz, R. Molecular Kinetics and Cooperative Effects in Friction and Adhesion of Fast Reversible Bonds. *Phys. Chem. Chem. Phys.* **2019**, *21* (31), 17170–17175. DOI: 10.1039/c9cp03350e.

- (285) Brandl, F.; Sommer, F.; Goepferich, A. Rational Design of Hydrogels for Tissue Engineering: Impact of Physical Factors on Cell Behavior. *Biomaterials* **2007**, *28* (2), 134–146. DOI: 10.1016/j.biomaterials.2006.09.017.
- (286) Akagi, Y.; Gong, J. P.; Chung, U.; Sakai, T. Transition between Phantom and Affine Network Model Observed in Polymer Gels with Controlled Network Structure. *Macromolecules* **2013**, *46* (3), 1035–1040. DOI: 10.1021/ma302270a.
- (287) Wang, R.; Wang, Z.; Guo, Y.; Li, H.; Chen, Z. Design of a RADA16-Based Self-Assembling Peptide Nanofiber Scaffold for Biomedical Applications. *J. Biomater. Sci. Polym. Ed.* **2019**, *30* (9), 713–736. DOI: 10.1080/09205063.2019.1605868.
- (288) Zhang, S.-Q.; Huang, H.; Yang, J.; Kratochvil, H. T.; Lolicato, M.; Liu, Y.; Shu, X.; Liu, L.; DeGrado, W. F. Designed Peptides That Assemble into Cross- α Amyloid-like Structures. *Nat. Chem. Biol.* **2018**, *14* (9), 870–875. DOI: 10.1038/s41589-018-0105-5.
- (289) Holmes, T. C.; de Lacalle, S.; Su, X.; Liu, G.; Rich, A.; Zhang, S. Extensive Neurite Outgrowth and Active Synapse Formation on Self-Assembling Peptide Scaffolds. *Proc Natl Acad Sci USA* **2000**, *97* (12), 6728–6733. DOI: 10.1073/pnas.97.12.6728.
- (290) Yang, J.; Li, Y.; Liu, Y.; Li, D.; Zhang, L.; Wang, Q.; Xiao, Y.; Zhang, X. Influence of Hydrogel Network Microstructures on Mesenchymal Stem Cell Chondrogenesis in Vitro and in Vivo. *Acta Biomater.* **2019**, *91*, 159–172. DOI: 10.1016/j.actbio.2019.04.054.
- (291) Puckert, C.; Tomaskovic-Crook, E.; Gambhir, S.; Wallace, G. G.; Crook, J. M.; Higgins, M. J. Electro-Mechano Responsive Properties of Gelatin Methacrylate (GelMA) Hydrogel on Conducting Polymer Electrodes Quantified Using Atomic Force Microscopy. *Soft Matter* **2017**, *13* (27), 4761–4772. DOI: 10.1039/c7sm00335h.
- (292) Raghuvanshi, V. S.; Garnier, G. Characterisation of Hydrogels: Linking the Nano to the Microscale. *Adv. Colloid Interface Sci.* **2019**, *274*, 102044. DOI: 10.1016/j.cis.2019.102044.
- (293) Kaberova, Z.; Karpushkin, E.; Nevoralová, M.; Vetrík, M.; Šlouf, M.; Dušková-Smrčková, M. Microscopic Structure of Swollen Hydrogels by Scanning Electron and Light Microscopies: Artifacts and Reality. *Polymers (Basel)* **2020**, *12* (3). DOI: 10.3390/polym12030578.
- (294) Shafiei, M.; Balhoff, M.; Hayman, N. W. Chemical and Microstructural Controls on Viscoplasticity in Carbopol Hydrogel. *Polymer* **2018**, *139*, 44–51. DOI: 10.1016/j.polymer.2018.01.080.
- (295) Teng, X.; Li, F.; Lu, C. Visualization of Materials Using the Confocal Laser Scanning Microscopy Technique. *Chem. Soc. Rev.* **2020**, *49* (8), 2408–2425. DOI: 10.1039/c8cs00061a.
- (296) Weiss, S. Shattering the Diffraction Limit of Light: A Revolution in Fluorescence Microscopy? *Proc Natl Acad Sci USA* **2000**, *97* (16), 8747–8749. DOI: 10.1073/pnas.97.16.8747.

- (297) Schermelleh, L.; Ferrand, A.; Huser, T.; Eggeling, C.; Sauer, M.; Biehlmaier, O.; Drummen, G. P. C. Super-Resolution Microscopy Demystified. *Nat. Cell Biol.* **2019**, *21* (1), 72–84. DOI: 10.1038/s41556-018-0251-8.
- (298) Endesfelder, U.; Heilemann, M. Direct Stochastic Optical Reconstruction Microscopy (DSTORM). *Methods Mol. Biol.* **2015**, *1251*, 263–276. DOI: 10.1007/978-1-4939-2080-8_14.
- (299) Rust, M. J.; Bates, M.; Zhuang, X. Sub-Diffraction-Limit Imaging by Stochastic Optical Reconstruction Microscopy (STORM). *Nat. Methods* **2006**, *3* (10), 793–795. DOI: 10.1038/nmeth929.
- (300) Samanta, S.; Gong, W.; Li, W.; Sharma, A.; Shim, I.; Zhang, W.; Das, P.; Pan, W.; Liu, L.; Yang, Z.; Qu, J.; Kim, J. S. Organic Fluorescent Probes for Stochastic Optical Reconstruction Microscopy (STORM): Recent Highlights and Future Possibilities. *Coord. Chem. Rev* **2019**, *380*, 17–34. DOI: 10.1016/j.ccr.2018.08.006.
- (301) Jia, S.; Vaughan, J. C.; Zhuang, X. Isotropic 3D Super-Resolution Imaging with a Self-Bending Point Spread Function. *Nat. Photonics* **2014**, *8*, 302–306. DOI: 10.1038/nphoton.2014.13.
- (302) Gandhimathi, R.; Pinotsi, D.; Köhler, M.; Mansfeld, J.; Ashiono, C.; Kleele, T.; Pawar, S.; Kutay, U. Super-Resolution Microscopy Reveals Focal Organization of ER-Associated Y-Complexes in Mitosis. *EMBO Rep.* **2023**, *24* (9), e56766. DOI: 10.15252/embr.202356766.
- (303) Conley, G. M.; Nöjd, S.; Braibanti, M.; Schurtenberger, P.; Scheffold, F. Superresolution Microscopy of the Volume Phase Transition of PNIPAM Microgels. *Colloids and Surfaces A: Physicochemical and Engineering Aspects* **2016**, *499*, 18–23. DOI: 10.1016/j.colsurfa.2016.03.010.
- (304) Gilbert, T.; Alsop, R. J.; Babi, M.; Moran-Mirabal, J.; Rheinstädter, M. C.; Hoare, T. Nanostructure of Fully Injectable Hydrazone-Thiosuccinimide Interpenetrating Polymer Network Hydrogels Assessed by Small-Angle Neutron Scattering and DSTORM Single-Molecule Fluorescence Microscopy. *ACS Appl. Mater. Interfaces* **2017**, *9* (48), 42179–42191. DOI: 10.1021/acsami.7b11637.
- (305) Albertazzi, L.; van der Zwaag, D.; Leenders, C. M. A.; Fitzner, R.; van der Hofstad, R. W.; Meijer, E. W. Probing Exchange Pathways in One-Dimensional Aggregates with Super-Resolution Microscopy. *Science* **2014**, *344* (6183), 491–495. DOI: 10.1126/science.1250945.
- (306) Adelizzi, B.; Aloï, A.; Van Zee, N. J.; Palmans, A. R. A.; Meijer, E. W.; Voets, I. K. Painting Supramolecular Polymers in Organic Solvents by Super-Resolution Microscopy. *ACS Nano* **2018**, *12* (5), 4431–4439. DOI: 10.1021/acsnano.8b00396.
- (307) Bernhard, S.; Ritter, L.; Müller, M.; Guo, W.; Guzzi, E. A.; Bovone, G.; Tibbitt, M. W. Modular and Photoreversible Polymer–Nanoparticle Hydrogels via Host–Guest Interactions. **2024**.
- (308) Fish, K. N. Total Internal Reflection Fluorescence (TIRF) Microscopy. *Curr. Protoc. Cytom.* **2009**, *Chapter 12*, Unit12.18. DOI: 10.1002/0471142956.cy1218s50.

- (309) Miyake, K.; Yasuda, S.; Harada, A.; Sumaoka, J.; Komiyama, M.; Shigekawa, H. Formation Process of Cyclodextrin Necklace-Analysis of Hydrogen Bonding on a Molecular Level. *J. Am. Chem. Soc.* **2003**, *125* (17), 5080–5085. DOI: 10.1021/ja026224u.
- (310) Ovesný, M.; Křížek, P.; Borkovec, J.; Svindrych, Z.; Hagen, G. M. ThunderSTORM: A Comprehensive ImageJ Plug-in for PALM and STORM Data Analysis and Super-Resolution Imaging. *Bioinformatics* **2014**, *30* (16), 2389–2390. DOI: 10.1093/bioinformatics/btu202.
- (311) Adepu, S.; Ramakrishna, S. Controlled Drug Delivery Systems: Current Status and Future Directions. *Molecules* **2021**, *26* (19). DOI: 10.3390/molecules26195905.
- (312) Danhier, F.; Feron, O.; Pr at, V. To Exploit the Tumor Microenvironment: Passive and Active Tumor Targeting of Nanocarriers for Anti-Cancer Drug Delivery. *J. Control. Release* **2010**, *148* (2), 135–146. DOI: 10.1016/j.jconrel.2010.08.027.
- (313) Su, S.; M Kang, P. Recent Advances in Nanocarrier-Assisted Therapeutics Delivery Systems. *Pharmaceutics* **2020**, *12* (9). DOI: 10.3390/pharmaceutics12090837.
- (314) Ruman, U.; Fakurazi, S.; Masarudin, M. J.; Hussein, M. Z. Nanocarrier-Based Therapeutics and Theranostics Drug Delivery Systems for Next Generation of Liver Cancer Nanodrug Modalities. *IJN* **2020**, *Volume 15*, 1437–1456. DOI: 10.2147/IJN.S236927.
- (315) Gavas, S.; Quazi, S.; Karpiński, T. M. Nanoparticles for Cancer Therapy: Current Progress and Challenges. *Nanoscale Res. Lett.* **2021**, *16* (1), 173. DOI: 10.1186/s11671-021-03628-6.
- (316) Vinogradov, S.; Batrakova, E.; Kabanov, A. Poly(Ethylene Glycol)–Polyethyleneimine NanoGel™ Particles: Novel Drug Delivery Systems for Antisense Oligonucleotides. *Colloids and Surfaces B: Biointerfaces* **1999**, *16* (1–4), 291–304. DOI: 10.1016/S0927-7765(99)00080-6.
- (317) He, C.; Hu, Y.; Yin, L.; Tang, C.; Yin, C. Effects of Particle Size and Surface Charge on Cellular Uptake and Biodistribution of Polymeric Nanoparticles. *Biomaterials* **2010**, *31* (13), 3657–3666. DOI: 10.1016/j.biomaterials.2010.01.065.
- (318) Zhang, W.; Taheri-Ledari, R.; Ganjali, F.; Mirmohammadi, S. S.; Qazi, F. S.; Saeidirad, M.; KashtiAray, A.; Zarei-Shokat, S.; Tian, Y.; Maleki, A. Effects of Morphology and Size of Nanoscale Drug Carriers on Cellular Uptake and Internalization Process: A Review. *RSC Adv.* **2022**, *13* (1), 80–114. DOI: 10.1039/d2ra06888e.
- (319) Cabral, H.; Makino, J.; Matsumoto, Y.; Mi, P.; Wu, H.; Nomoto, T.; Toh, K.; Yamada, N.; Higuchi, Y.; Konishi, S.; Kano, M. R.; Nishihara, H.; Miura, Y.; Nishiyama, N.; Kataoka, K. Systemic Targeting of Lymph Node Metastasis through the Blood Vascular System by Using Size-Controlled Nanocarriers. *ACS Nano* **2015**, *9* (5), 4957–4967. DOI: 10.1021/nn5070259.

- (320) Soni, K. S.; Desale, S. S.; Bronich, T. K. Nanogels: An Overview of Properties, Biomedical Applications and Obstacles to Clinical Translation. *J. Control. Release* **2016**, *240*, 109–126. DOI: 10.1016/j.jconrel.2015.11.009.
- (321) Ahmed, S.; Alhareth, K.; Mignet, N. Advancement in Nanogel Formulations Provides Controlled Drug Release. *Int. J. Pharm.* **2020**, *584*, 119435. DOI: 10.1016/j.ijpharm.2020.119435.
- (322) Fick, A. On Liquid Diffusion. *J. Memb. Sci.* **1995**, *100* (1), 33–38. DOI: 10.1016/0376-7388(94)00230-V.
- (323) Chang, M.; Zhang, F.; Wei, T.; Zuo, T.; Guan, Y.; Lin, G.; Shao, W. Smart Linkers in Polymer-Drug Conjugates for Tumor-Targeted Delivery. *J. Drug Target.* **2016**, *24* (6), 475–491. DOI: 10.3109/1061186X.2015.1108324.
- (324) Ding, Y.; Sun, D.; Wang, G.-L.; Yang, H.-G.; Xu, H.-F.; Chen, J.-H.; Xie, Y.; Wang, Z.-Q. An Efficient PEGylated Liposomal Nanocarrier Containing Cell-Penetrating Peptide and PH-Sensitive Hydrazone Bond for Enhancing Tumor-Targeted Drug Delivery. *Int. J. Nanomedicine* **2015**, *10*, 6199–6214. DOI: 10.2147/IJN.S92519.
- (325) Dutta, K.; Das, R.; Medeiros, J.; Thayumanavan, S. Disulfide Bridging Strategies in Viral and Nonviral Platforms for Nucleic Acid Delivery. *Biochemistry* **2021**, *60* (13), 966–990. DOI: 10.1021/acs.biochem.0c00860.
- (326) Berillo, D.; Yeskendir, A.; Zharkinbekov, Z.; Raziyeva, K.; Saparov, A. Peptide-Based Drug Delivery Systems. *Medicina (Kaunas)* **2021**, *57* (11). DOI: 10.3390/medicina57111209.
- (327) Lee, H.; Park, T. G. Preparation and Characterization of Mono-PEGylated Epidermal Growth Factor: Evaluation of in Vitro Biologic Activity. *Pharm. Res.* **2002**, *19* (6), 845–851. DOI: 10.1023/a:1016113117851.
- (328) Deleavey, G. F.; Watts, J. K.; Damha, M. J. Chemical Modification of siRNA. *Curr. Protoc. Nucleic Acid Chem.* **2009**, *Chapter 16*, Unit 16.3. DOI: 10.1002/0471142700.nc1603s39.
- (329) Gavriel, A. G.; Sambrook, M. R.; Russell, A. T.; Hayes, W. Recent Advances in Self-Immolative Linkers and Their Applications in Polymeric Reporting Systems. *Polym. Chem.* **2022**, *13* (22), 3188–3269. DOI: 10.1039/D2PY00414C.
- (330) Riber, C. F.; Smith, A. A. A.; Zelikin, A. N. Self-Immolative Linkers Literally Bridge Disulfide Chemistry and the Realm of Thiol-Free Drugs. *Adv. Healthc. Mater.* **2015**, *4* (12), 1887–1890. DOI: 10.1002/adhm.201500344.
- (331) Mthembu, S. N.; Sharma, A.; Albericio, F.; de la Torre, B. G. Breaking a Couple: Disulfide Reducing Agents. *Chembiochem* **2020**, *21* (14), 1947–1954. DOI: 10.1002/cbic.202000092.

- (332) Wu, C.; Wang, S.; Brülisauer, L.; Leroux, J.-C.; Gauthier, M. A. Broad Control of Disulfide Stability through Microenvironmental Effects and Analysis in Complex Redox Environments. *Biomacromolecules* **2013**, *14* (7), 2383–2388. DOI: 10.1021/bm400501c.
- (333) Giustarini, D.; Colombo, G.; Garavaglia, M. L.; Astori, E.; Portinaro, N. M.; Reggiani, F.; Badalamenti, S.; Aloisi, A. M.; Santucci, A.; Rossi, R.; Milzani, A.; Dalle-Donne, I. Assessment of Glutathione/Glutathione Disulphide Ratio and S-Glutathionylated Proteins in Human Blood, Solid Tissues, and Cultured Cells. *Free Radic. Biol. Med.* **2017**, *112*, 360–375. DOI: 10.1016/j.freeradbiomed.2017.08.008.
- (334) Gad, S. C. Glutathione. In *Encyclopedia of Toxicology*; Elsevier, 2014; p 751. DOI: 10.1016/B978-0-12-386454-3.00850-2.
- (335) Mauri, E.; Veglianesse, P.; Papa, S.; Mariani, A.; De Paola, M.; Rigamonti, R.; Chincarini, G. M. F.; Rimondo, S.; Sacchetti, A.; Rossi, F. Chemoselective Functionalization of Nanogels for Microglia Treatment. *Eur. Polym. J.* **2017**, *94*, 143–151. DOI: 10.1016/j.eurpolymj.2017.07.003.
- (336) Kolakowski, R. V.; Haelsig, K. T.; Emmerton, K. K.; Leiske, C. I.; Miyamoto, J. B.; Cochran, J. H.; Lyon, R. P.; Senter, P. D.; Jeffrey, S. C. The Methylene Alkoxy Carbamate Self-Immolative Unit: Utilization for the Targeted Delivery of Alcohol-Containing Payloads with Antibody-Drug Conjugates. *Angew. Chem. Int. Ed* **2016**, *55* (28), 7948–7951. DOI: 10.1002/anie.201601506.
- (337) Ghosh, A. K.; Brindisi, M. Organic Carbamates in Drug Design and Medicinal Chemistry. *J. Med. Chem.* **2015**, *58* (7), 2895–2940. DOI: 10.1021/jm501371s.
- (338) Anderson, D. E.; Becktel, W. J.; Dahlquist, F. W. PH-Induced Denaturation of Proteins: A Single Salt Bridge Contributes 3-5 Kcal/Mol to the Free Energy of Folding of T4 Lysozyme. *Biochemistry* **1990**, *29* (9), 2403–2408. DOI: 10.1021/bi00461a025.
- (339) Estey, T.; Kang, J.; Schwendeman, S. P.; Carpenter, J. F. BSA Degradation under Acidic Conditions: A Model for Protein Instability during Release from PLGA Delivery Systems. *J. Pharm. Sci.* **2006**, *95* (7), 1626–1639. DOI: 10.1002/jps.20625.
- (340) Dutta, K.; Hu, D.; Zhao, B.; Ribbe, A. E.; Zhuang, J.; Thayumanavan, S. Templated Self-Assembly of a Covalent Polymer Network for Intracellular Protein Delivery and Traceless Release. *J. Am. Chem. Soc.* **2017**, *139* (16), 5676–5679. DOI: 10.1021/jacs.7b01214.
- (341) Zheng, H.; Shang, G.-Q.; Yang, S.-Y.; Gao, X.; Xu, J.-G. Fluorogenic and Chromogenic Rhodamine Spirolactam Based Probe for Nitric Oxide by Spiro Ring Opening Reaction. *Org. Lett.* **2008**, *10* (12), 2357–2360. DOI: 10.1021/ol800206x.

- (342) Sasaki, H.; Hanaoka, K.; Urano, Y.; Terai, T.; Nagano, T. Design and Synthesis of a Novel Fluorescence Probe for Zn²⁺ Based on the Spirolactam Ring-Opening Process of Rhodamine Derivatives. *Bioorg. Med. Chem.* **2011**, *19* (3), 1072–1078. DOI: 10.1016/j.bmc.2010.05.074.
- (343) Kim, H. N.; Lee, M. H.; Kim, H. J.; Kim, J. S.; Yoon, J. A New Trend in Rhodamine-Based Chemosensors: Application of Spirolactam Ring-Opening to Sensing Ions. *Chem. Soc. Rev.* **2008**, *37* (8), 1465–1472. DOI: 10.1039/b802497a.
- (344) Ansari, M. S.; Raees, K.; Ali Khan, M.; Rafiquee, M. Z. A.; Otero, M. Kinetic Studies on the Catalytic Degradation of Rhodamine B by Hydrogen Peroxide: Effect of Surfactant Coated and Non-Coated Iron (III) Oxide Nanoparticles. *Polymers (Basel)* **2020**, *12* (10). DOI: 10.3390/polym12102246.
- (345) Marco-Dufort, B.; Janczy, J. R.; Hu, T.; Lütolf, M.; Gatti, F.; Wolf, M.; Woods, A.; Tetter, S.; Sridhar, B. V.; Tibbitt, M. W. Thermal Stabilization of Diverse Biologics Using Reversible Hydrogels. *Sci. Adv.* **2022**, *8* (31), eabo0502. DOI: 10.1126/sciadv.abo0502.
- (346) Bogseth, R.; Edgcomb, E.; Jones, C. M.; Chess, E. K.; Hu, P. Acetonitrile Adduct Formation as a Sensitive Means for Simple Alcohol Detection by LC-MS. *J. Am. Soc. Mass Spectrom.* **2014**, *25* (11), 1987–1990. DOI: 10.1007/s13361-014-0975-z.
- (347) Mauri, E.; Veglianese, P.; Papa, S.; Mariani, A.; De Paola, M.; Rigamonti, R.; Chincarini, G. M. F.; Vismara, I.; Rimondo, S.; Sacchetti, A.; Rossi, F. Double Conjugated Nanogels for Selective Intracellular Drug Delivery. *RSC Adv.* **2017**, *7* (48), 30345–30356. DOI: 10.1039/C7RA04584K.

CURRICULUM VITAE

Stéphane BERNHARD

Born in Mulhouse, France

October 23rd, 1996

ACADEMIC EXPERIENCE

- 10/2019 – 05/2024 Doctoral Student (PhD), Department of Mechanical and Process Engineering (Prof. Mark. W. Tibbitt), ETH Zurich, Switzerland.
- 09/2017 – 08/2019 Master of Science in Molecular and Biological Chemistry, EPFL, Switzerland
- 09/2014 – 08/2017 Bachelor of Science in Chemistry and Chemical Engineering, EPFL, Switzerland

LIST OF PUBLICATIONS

First authors underlined.

1. **S. Bernhard**, L. Ritter, M. Müller, W. Guo, E. A. Guzzi, G. Bovone, M. W. Tibbitt*, “Host–guest-based Polymer–Nanoparticle Hydrogels for Modular Materials Design”, *submitted*.
2. **J. Duru**, A. Rüfenacht, J. Löhle, M. Pozzi, C. Forró, L. Ledermann, A. Bernardi, M. Matter, A. Renia, B. Simona, C. M. Tringides, **S. Bernhard**, S. J. Ihle, J. Hengsteler, B. Maurer, X. Zhang, N. Nakatsuka*, “Driving electrochemical reactions at the microscale using CMOS microelectrode arrays”, *Lab on a Chip*, **2023**, 23, 5047-5058.
3. **O. Y. Dudaryeva**, **S. Bernhard**, M. W. Tibbitt*, C. Labouesse*, “Implications of Cellular Mechanical Memory in Bioengineering”, *ACS Biomaterials Science & Engineering*, **2023**, 9, 11, 5985–5998

4. D. Dranseike, Y. Cui, A. S. Ling, F. Donat, **S. Bernhard**, M. Bernero, A. Areeckal, X.-H. Qin, J. S. Oakey, B. Dillenburger, A. R. Studart, M. W. Tibbitt, “Dual carbon sequestration with photosynthetic living materials”, *BioRxiv*, **2023**.
5. T. Komsthöft, G. Bovone, **S. Bernhard**, M. W. Tibbitt*, “Polymer functionalization of inorganic nanoparticles for biomedical applications”, *Current Opinion in Chemical Engineering*, **2022**, 37, 100849.
6. G. Bovone, E. A. Guzzi, **S. Bernhard**, T. Weber, D. Dranseike, M. W. Tibbitt*, “Supramolecular Reinforcement of Polymer-Nanoparticle Hydrogels for Modular”, *Advanced Materials*, **2022**, 34, 2106941.
7. E. A. Guzzi, R. Bischof, D. Dranseike, D. V. Deshmukh, A. Wahlsten, G. Bovone, **S. Bernhard**, M. W. Tibbitt*, “Hierarchical biomaterials via photopatterning-enhanced direct ink writing.”, *Biofabrication*, **2021**, 13, 044105.
8. **S. Bernhard**, M. W. Tibbitt*, “Supramolecular engineering of hydrogels for drug delivery”, *Advanced Drug Delivery Reviews*, **2021**, 171, 240-256.
9. **S. Bernhard**, G. Bovone, E. A. Guzzi, M. W. Tibbitt*, “Polymer-Nanoparticle Hydrogels”, *Chimia*, **2019**, 73, 1034.
10. Oguz, N Candau, **S Bernhard**, C Kosak Soz, O Heinz, G Stochlet, CJG Plummer, E Yilgor, I Yilgor, YZ Menciloglu “Effect of surface modification of colloidal silica nanoparticles on the rigid amorphous fraction and mechanical properties of amorphous polyurethane–urea–silica nanocomposites”, *Journal of Polymer Science Part A: Polymer Chemistry*, **2019**, 57, 2543-2556.

CONFERENCE CONTRIBUTION

1. **S. Bernhard**, L. Ritter, M. Müller, W. Guo, E. A. Guzzi, G. Bovone, M. W. Tibbitt, “Host–guest chemistry for the design of functional polymer–nanoparticle hydrogels”, *MRS Fall Meeting 2023*, Boston, USA, **2023**. Oral contribution.
2. S. Bernhard, C. Söll, G. Bovone, E. Mauri, M. W. Tibbitt, “Redox responsive nanogels for intracellular drug delivery” *ESB 2023*, Davos, Switzerland, **2023**, Poster presentation.
3. **S. Bernhard**, L. Ritter, M. Müller, W. Guo, E. A. Guzzi, G. Bovone, M. W. Tibbitt, “Host–guest-based Polymer–Nanoparticle Hydrogels for Modular Materials Design», *GRC Self-Assembly and Supramolecular Chemistry*, les Diablerets, Switzerland, **2023**, Poster presentation.
4. **S. Bernhard**, G. Bovone, E. A. Guzzi, T. Weber, D. Dranseike, M. W. Tibbitt, “Supramolecular Reinforcement of Polymer–Nanoparticle Hydrogels for Modular Materials Design”, *GRS Self-Assembly and Supramolecular Chemistry*, les Diablerets, Switzerland, **2023**, Oral contribution.
5. **S. Bernhard**, G. Bovone, E. A. Guzzi, M. Müller, N. Petelinsek, W. Guo, M. W. Tibbitt, “Supramolecular design of injectable hydrogels”, *SSB+RM Young Scientist Symposium 2022*, Zürich, Switzerland, 2022, Poster presentation.
6. **S. Bernhard**, M. Müller, E. A. Guzzi, G. Bovone, W. Guo, M. W. Tibbitt, “Host–guest-based Polymer–Nanoparticle Hydrogels for Modular Materials Design”, *Swiss Soft Days*, Zürich, Switzerland, 2022, Poster presentation
7. **S. Bernhard**, G. Bovone, E. A. Guzzi, M. Müller, N. Petelinsek, W. Guo, M. W. Tibbitt, “Supramolecular interactions in the design of polymer–nanoparticle hydrogels”, *SSB+RM*, Zürich, Switzerland, 2021, Poster presentation.

8. **S. Bernhard**, G. Bovone, E. A. Guzzi, T. Weber, D. Dranseike, M. W. Tibbitt, “Supramolecular Reinforcement of Polymer–Nanoparticle Hydrogels for Modular Materials Design”, *Swiss Soft Days*, Villigen PSI, Switzerland, 2021, Oral contribution.

9. **S. Bernhard**, W. Guo, M. W. Tibbitt, “Relating polymer–nanoparticle (PNP) interactions to bulk properties in PNP hydrogel”, *SSB+RM Young Scientist Symposium 2021*, Zürich, Switzerland, 2021, Poster presentation.